Carnegie Mellon University

CARNEGIE INSTITUTE OF TECHNOLOGY

THESIS

SUBMITTED IN PARTIAL FULFILLMENT OF THE REQUIREMENTS

FOR THE DEGREE OF Doctor of Philosophy

TITLE **Evaluation of Air Quality Impacts on Society: Methods and Applications**

PRESENTED BY **Jinhyok Heo**

ACCEPTED BY THE DEPARTMENT OF

Engineering and Public Policy

Peter Adams — February 25, 2015
ADVISOR, MAJOR PROFESSOR — DATE

Douglas Sicker — February 27, 2015
DEPARTMENT HEAD — DATE

APPROVED BY THE COLLEGE COUNCIL

Vijayakumar Bhagavatula — March 11, 2015
DEAN — DATE

Evaluation of Air Quality Impacts on Society: Methods and Application

Submitted in partial fulfillment of the requirements for
the degree of
Doctor of Philosophy
in
Engineering and Public Policy

Jinhyok Heo
B.S., School of Civil, Urban, and Geosystem Engineering, Seoul National University
M.S., Department of Civil and Environmental Engineering, Stanford University

Carnegie Mellon University
Pittsburgh, PA

May, 2015

The views and conclusions contained in this document are those of the author, and should not be interpreted as representing the official policies, either expressed or implied, of any sponsoring institution, the U.S. government, or any other entity.

Keywords: air quality, social cost, public health, $PM_{2.5}$, chemical transport model, carbon capture and storage.

Abstract

Though essential for informed decision-making, it is challenging to estimate the public health impacts of air quality because it must address the complicated atmospheric processes of air pollutants: emissions, dispersion, chemistry, and removal. Employing a chemical transport model (CTM) is the most rigorous way to address these atmospheric processes. The first part of this thesis analyzed the potential risk of ammonia emissions from post-combustion carbon capture and storage (CCS) technology using a CTM. It was found that, if not controlled properly, CCS ammonia may create a serious public health problem, substantially compromising the benefit of reducing carbon dioxide. The results will guide the level of appropriate control for a wide range of future scenarios. CTMs are expensive from a computational standpoint and, therefore, beyond the reach of policy analysis for many types of problems. On the other hand, current tools used for policy analysis fall short of the rigor of CTMs and may lead to biased results. To address this gap, we developed the Estimating Air Pollution Social Impacts Using Regression (EASIUR) method, which builds parameterizations that predict per-tonne social cost and intake fraction at any location in the United States like a CTM with negligible computational costs. With tagged CTM simulations, the EASIUR method builds a dataset of air quality impacts for a large number of representative emissions sources in the United States and then derives parameterizations for those results. We used an "average plume," a generic $PM_{2.5}$ plume generated from CTM results, to describe the exposed population over large receptor areas around an emissions source. The parameterizations have intuitive functional forms with population and common atmospheric variables; their coefficients explain key underlying mechanisms. Out-of-sample evaluations meet the 'excellent' criteria of a common air quality model performance metric in most cases, with

some exceptions meeting the ‘good’ criteria. We found that the average seasonal per-tonne social costs in the United States are $150,000-180,000/t EC, $21,000-34,000/t SO_2, $4,200-15,000/t NO_x, and $29,000-85,000/t NH_3. It is hoped that the EASIUR model will be of great use in policy research that involves changes in air quality.

Acknowledgements

I could enjoy my life at Carnegie Mellon University thanks to a lot of people. Deeply imbued with hospitality and friendship as well as intellectual rigor from those whom I met at CMU, I could grow to accomplish some decent projects. In the interdisciplinary environment carefully nurtured throughout the history of CMU, I could broaden my views and understanding about science, technology, and society from wonderful people.

First and foremost, my study at Carnegie Mellon University would not have been possible had not it been for my advisor Peter Adams. He has been a superb research advisor as well as a life mentor. Peter's advice always intrigued my intellectual curiosity, guided me on a right track throughout good and bad times, and helped me thinking critically as well as writing and speaking clearly and succinctly. I learned from him how to find out what is important and how to focus on it. I will always admire his teaching skills that I witnessed all the time in his classroom, in his public lectures, and in our office meetings; his carefully thought-out simple language that is always to the point never loses his audience. Last but not least, he also got a decent funding for a new set of computer cluster systems, which provided enough computing power for my research!

My thesis committee helped me accomplish the thesis project in a much better shape. Allen Robinson helped me thinking in a broader perspective and guided my research to the right direction. Jeremy Michalek introduced me to different modeling tools and provided valuable advice for model development. I'd like to thank Paulina Jaramillo helped me better understand APEEP model and kind and detailed comment on my research. Shantanu Jathar provided detailed data from his work and helped me understand organic chemistry better; he was also a good friend while he was at CMU.

I also met many wonderful professors. I'd like to thank Liz Casman. I will not be able to forget her kind and warm advice when she had me as her student for a short while. I learned a lot from Jay Apt about the front-end of energy technology and the challenges ahead as well as the history of U.S. energy market and regulation. Thanks to Ed Rubin, I could once spend some time understanding the NEMS model from a technological learning point of view; he also provided valuable advice on my first project on carbon capture and storage technology. While helping to fix some problems of his GNU/Linux machine, I could talk about not only the macroeconomics but also my research with Robert Strauss at Heinz, which helped me thinking my research at a different perspective.

I also received lots of help from folks at the Center for Atmospheric Particle Studies. Ben Murphy helped me start to play with PMCAMx, a little monster at the time. My conversion with Melissa Day and Laura Posner help me further understand the CTM. I learned a lot from Alyssa Mcquilling about ammonia and more immensely from the weekly journal club she organized. I could taste a little bit of global models thanks to Marguerite Marks; she often helped revising my manuscripts, too. Talking to Rawad Saleh was always great. Bonyoung Koo, a CAPS alum, also helped me setting up CAMx and gave valuable advice when I got stuck.

Sharing a big office with fellow EPP doctoral students also made me wonderful friends. I spent quite some time with Alan Jenn talking about silly computer skills. Steve Rose was always nearby for a small talk. Jihoon Min was a friend who I could talk about EPP stuff in my native tongue, which makes me feel a bit smarter. I had some good time with Paul Welle and Clara Santamaría over dinner and beer. I had a joy of meeting and talking quite regularly over a variety of subjects with Makoto Chikaraishi while he was at CMU as a visiting scholar.

Of course, I am greatly in debt to my family. How can I thank you enough to my wife Eunhae. She has been a wonderful wife and mom, taking care of me and my children far away from our families in our home country. Having a great personality, she always made many good friends around her even with the two kids, who also became mine. Eunwoo and Eunjoo, my lovely daughters, have always supported what I do, even though they did not know what I do. It was a great joy to see them grow everyday. I'd like to thank my parents and parents-in-law for supporting our living in Pittsburgh.

I'd like to thank Granger Morgan and Inês Azevedo for supporting my study throughout the entire four and half years under the center for Climate and Energy Decision Making. I had great opportunities to learn about how to frame and solve important challenging questions around energy and climate areas. My thesis work was supported by the center for Climate and Energy Decision Making (SES-0949710), through a cooperative agreement between the National Science Foundation and Carnegie Mellon University. I was also supported by Korean Government Scholarship for Studying Abroad for the first two years.

Contents

List of Figures

List of Tables

Chapter 1. Introduction

1.1 Motivation

It was not long ago when people did not even recognize such a thing as air pollution. Those who survived the infamous 1948 Donora smog remember (Davis, 2002) that a lot of workers and families in Donora did try to carry on their normal routines until people started to get sick and to die during the tragic smog event; for example, a school football team was having a game even though they could hardly see each other. Burning of fossil fuel, the main cause of modern air pollution, had—at least to some people—rather positive connotations, such as making a living and building a new community, as well as technological and economic development. However, after the occurrence of serious air pollution episodes, state and federal governments started to take regulatory actions beginning in early 1960s. Arguably the landmark event was the establishment of the Clean Air Act in 1970, which rolled out the basic structure of air quality regulation in the United States (Ashford and Caldart, 2008).

Now it is common sense that air pollution has adverse effects on human health and the natural environment. If exposed to air pollution, people may get sick or die early. It also affects the natural environment by causing problems such as eutrophication, acidification, agricultural productivity loss, and visibility degradation, which consequently affect associated human welfare. Epidemiological studies found out that fine particulate matter having a diameter of 2.5 μm or less ($PM_{2.5}$) is strongly associated with adverse health impacts such as cardiovascular and respiratory diseases (Pope et al., 2002, 2004; Pope and Dockery, 2006). The $PM_{2.5}$ impacts

on premature death, when monetized, account for more than 90% of the social cost (U.S. EPA, 1999, 2011).

Still, it is challenging to quantify the social costs of air quality. Once emitted, it is not easy to track air pollutants. Air pollutants travel in the atmosphere and usually undergo complex chemical reactions with other pollutants under varying meteorological conditions until they are subsequently removed from the atmosphere by precipitation (though this results in different problems such as eutrophication and acidification), affecting polluters or non-polluters alike along the way with to varying degrees.

A chemical transport model (CTM) is the most realistic tool to model air quality. A CTM, implemented with up-to-date scientific knowledge, can simulate the transport, chemical conversion, and removal process of air pollutants at a detailed spatial and temporal resolution. By its nature, a CTM is computationally burdensome. Employing a CTM requires high computational costs as well as expertise in atmospheric science.

In this work, I explore the potential risk of air quality degradation from an emerging technology using a CTM. Then, a new method of tapping the performance of CTMs without their computational burden was developed. Finally, based on this method, a fully working set of air quality social cost models was built and presented.

1.2 Objectives

This thesis has three main objectives. The first one is to quantify and assess the potential air quality risk of carbon capture and storage technology. It has been worried for a long time that amine scrubbing, one of the most promising CCS technologies, may create an air quality problem (Eide-Haugmo et al., 2009; Koornneef et al., 2010; Rao and Rubin, 2002). It is necessary address the potentially large uncertainty surrounding the performance of emerging

technology and the level of its deployment. Since the future environment would have different emissions and the associated chemical processes in the atmosphere would also change, it would also be necessary to explore uncertainty created by the changing emissions in the future.

The second objective is to develop a method to predict like a CTM without computational burden. A CTM is a superb tool, but it is usually beyond the reach of the policy research community mainly because of the complexity and computational burden of CTMs. There are reduced-form models, which are easy-to-use and fast, some of which are used in many important policy studies such as the Hidden Costs of Energy (National Research Council, 2010). But the current reduced-form models are usually based on an air quality model that is overly simplistic or outdated for important areas. Or, some tools consistent with up-to-date science have a limited spatial or sectoral resolution. Therefore, it would be extremely useful if there were a general purpose social cost tool that could predict like CTMs but in a computationally efficient manner. To develop such a method is the second object of this thesis.

The third objective is to provide a new set of fully working models based on the method that is developed in this thesis. The estimation of air quality social cost involves several components, i.e. not only the air quality simulation but also translating the air quality to public health impacts and associated valuation process. The derived models would need to address each major component so that they work flexibly depending on potential applications.

1.3 Overview

Chapter 2 describes an application of a CTM to explore the potential risk of an emerging technology, post-combustion carbon capture technology. Major sources of uncertainty are addressed so that the results can guide a wide range of future scenarios. In Chapter 3, a new method was developed to derive simple parameterizations from CTM simulation results so that

one can estimate the social cost of air quality quickly and accurately. Based on the accomplishments made in the Chapter 3, Chapter 4 builds a set of new social cost models for four major air pollutants (elemental carbon, sulfur dioxide, nitrogen dioxides, and ammonia). In Chapter 5, the key findings from this work are summarized and recommendations for future work are presented.

1.4 Reference

Ashford, N. A. and Caldart, C. C.: Environmental Law, Policy, and Economics: Reclaiming the Environmental Agenda, First Edition edition., The MIT Press, Cambridge, MA., 2008.

Davis, D.: When Smoke Ran Like Water, 1 edition., Basic Books, New York, NY., 2002.

Eide-Haugmo, I., Brakstad, O. G., Hoff, K. A., Sørheim, K. R., da Silva, E. F. and Svendsen, H. F.: Environmental impact of amines, Energy Procedia, 1(1), 1297–1304, doi:10.1016/j.egypro.2009.01.170, 2009.

Koornneef, J., Ramirez, A., van Harmelen, T., van Horssen, A., Turkenburg, W. and Faaij, A.: The impact of CO2 capture in the power and heat sector on the emission of SO2, NOx, particulate matter, volatile organic compounds and NH3 in the European Union, Atmos. Environ., 44(11), 1369–1385, doi:10.1016/j.atmosenv.2010.01.022, 2010.

Muller, N. Z.: Linking Policy to Statistical Uncertainty in Air Pollution Damages, BE J. Econ. Anal. Policy, 11(1) [online] Available from: http://www.degruyter.com/view/j/bejeap.2011.11.issue-1/bejeap.2011.11.1.2925/bejeap.2011.11.1.2925.xml?format=INT (Accessed 6 February 2013), 2011.

Muller, N. Z. and Mendelsohn, R.: Measuring the damages of air pollution in the United States, J. Environ. Econ. Manag., 54(1), 1–14, doi:10.1016/j.jeem.2006.12.002, 2007.

National Research Council: Hidden Costs of Energy: Unpriced Consequences of Energy Production and Use, The National Academies Press, Washington, DC. [online] Available from: http://www.nap.edu/catalog.php?record_id=12794 (Accessed 19 August 2013), 2010.

Pope, C. A., III, Burnett, R. T., Thun, M. J., Calle, E. E., Krewski, D., Ito, K. and Thurston, G. D.: Lung Cancer, Cardiopulmonary Mortality, and Long-term Exposure to Fine Particulate Air Pollution, J. Am. Med. Assoc., 287(9), 1132 –1141, doi:10.1001/jama.287.9.1132, 2002.

Pope, C. A., III, Burnett, R. T., Thurston, G. D., Thun, M. J., Calle, E. E., Krewski, D. and Godleski, J. J.: Cardiovascular Mortality and Long-Term Exposure to Particulate Air

Pollution Epidemiological Evidence of General Pathophysiological Pathways of Disease, Circulation, 109(1), 71–77, doi:10.1161/01.CIR.0000108927.80044.7F, 2004.

Pope, C. A., III and Dockery, D. W.: Health effects of fine particulate air pollution: lines that connect, J. Air Waste Manag. Assoc., 56(6), 709–742, 2006.

Rao, A. B. and Rubin, E. S.: A Technical, Economic, and Environmental Assessment of Amine-Based CO2 Capture Technology for Power Plant Greenhouse Gas Control, Environ. Sci. Technol., 36(20), 4467–4475, doi:10.1021/es0158861, 2002.

U.S. EPA: The Benefits and Costs of the Clean Air Act, 1990 to 2010, EPA report to Congress, U.S. Environmental Protection Agency. Office of Air and Radiation. Office of Policy, Washington, DC., 1999.

U.S. EPA: The Benefits and Costs of the Clean Air Act from 1990 to 2020, U.S. Environmental Protection Agency. Office of Air and Radiation., Washington, DC., 2011.

U.S. EPA: User's Manual for the Co-Benefits Risk Assessment (COBRA) Screening Model Version: 2.61, U.S. Environmental Protection Agency, Washington, DC., 2013.

Chapter 2

Implications of Ammonia Emissions from Post-Combustion Carbon Capture for Airborne Fine Particulate Matter

Abstract

Post-combustion carbon capture and storage (CCS) technologies could increase ambient concentrations of fine particulate matter ($PM_{2.5}$) due to their ammonia emissions. Deployment of amine scrubbing to capture $2.0\,\mathrm{Gt\,CO_2/year}$, for example, could emit $0.48\,\mathrm{Tg\,NH_3/year}$ in the United States at an ammonia emissions rate typical of current pilot plants. Employing a chemical transport model, we found that this amount of ammonia would cause an increase of $2.0\,\mu\mathrm{g\,PM_{2.5}/m^3}$ in nonattainment areas during wintertime, which would be troublesome for $PM_{2.5}$-burdened areas. In contrast, $PM_{2.5}$ changes were much lower in other seasons as expected from inorganic $PM_{2.5}$ thermodynamics. Wintertime $PM_{2.5}$ increases in nonattainment areas were fairly linear at a rate of $3.4\,\mu\mathrm{g\,PM_{2.5}/m^3}$ per $1\,\mathrm{Tg\,NH_3}$, allowing these results to be applied to other CCS emissions scenarios. The $PM_{2.5}$ impacts are uncertain by 10-20% depending on future emissions of SO_2, NO_x, and NH_3. The public health costs of CCS NH_3 emissions were evaluated to be \$31-68/$\mathrm{t\,CO_2}$, which are similar to the social cost of carbon emissions avoided. Since the costs of solvent loss to CCS operators are lower than the social costs of CCS ammonia, there is a regulatory interest to limit ammonia emissions from CCS.

2.1 Introduction[1]

Carbon capture and storage (CCS) technology is considered an important potential climate change mitigation option (IPCC, 2014; Metz et al., 2005; Bachu, 2008). Amine scrubbing is currently the most mature post-combustion capture technology (Rochelle, 2009). Ammonia-based CO_2 capture, which use aqueous ammonia as a solvent for CO_2 instead of amines, is another promising post-combustion option since it may have energy and cost advantages over the amine-based system (Versteeg and Rubin, 2011a).

There have been various environmental concerns associated with using amines for CCS (Rao et al., 2004). One that is the focus of this study is that amine scrubbing could create an air quality problem associated with its ammonia emissions. Ammonia is a significant precursor of $PM_{2.5}$ (Pinder et al., 2007; Ansari and Pandis, 1998), which refers to particulate matter having a diameter of $2.5\,\mu m$ and smaller. Exposures to $PM_{2.5}$ pollution are strongly associated with increases in mortality and morbidity (Pope and Dockery, 2006).

The other concern is that amine systems produce a hazardous waste. Amines react with acid gas impurities such as SO_2, SO_3, NO_2 and HCl to form corrosive heat-stable salts (HSS). While some amines can be released from HSS for reuse by adding a strong alkali, the remaining HSS must be treated as a hazardous waste. In addition, amines emitted to the atmosphere may react with NO_x to form nitrosamines, which are known carcinogens. Carcinogenic nitrosamine formation is also a concern, though it is not likely since nitrosamines are broken down rapidly by photolysis under sunlight (Ge et al., 2011a) and nitrosamines were not detected in an experimental study on amines emitted by amine-based CO_2 capture technology (Nielsen et al., 2011; Bråten et al., 2009). Lastly, ammonia emissions may also increase nitrogen deposition. Nitrogen burdened ecosystems could suffer from eutrophication and acidification by CCS ammonia (Bouwman et al., 1997).

The role of ammonia in $PM_{2.5}$ formation is largely determined by nonlinear interactions between SO_2, NO_x, NH_3, and their products (Pinder et al., 2007; West et al., 1999; Ansari and

[1] This work is currently under review for publication in *Environmental Science & Technology*.

Pandis, 1998), A unit ammonia emission from CCS may result in highly variable impacts on $PM_{2.5}$ concentrations depending on the ambient concentrations of these species as shown in Figure A-1. Once emitted to the air, ammonia may remain in the gas phase if sulfuric acid and nitric acid are not available, which therefore causes no change in $PM_{2.5}$ concentrations. If unneutralized sulfuric acid exists, ammonia first reacts with it to form PM sulfate ($(NH_4)_2SO_4$). Because unneutralized sulfuric acid already exists overwhelmingly in the particle phase, this reaction increases $PM_{2.5}$ concentrations only marginally by replacing hydrogen with ammonium. If sulfate is neutralized, however, any remaining ammonia may form PM nitrate (NH_4NO_3) by reacting with nitric acid. The formation of ammonium nitrate may be limited either by ammonia or by nitric acid. When ammonia is the limiting reagent, the ammonium nitrate PM can be attributed to its emission, and a unit of ammonia creates much more $PM_{2.5}$ mass by PM nitrate formation than by neutralizing sulfate. Since PM nitrate formation is favored at cold temperatures, ammonia emissions may create a significant amount of $PM_{2.5}$ in winter or at night. Therefore, changes in ammonia emissions will tend to have stronger impacts on $PM_{2.5}$ in regions where ammonia is limiting PM nitrate formation, which has cold temperatures, lower SO_2 emissions, higher NO_x emissions, and intermediate ammonia levels (sufficient to neutralize sulfate but limiting for ammonium nitrate formation). Such conditions occur regularly in the eastern United States in winter (Pinder et al., 2007; West et al., 1999; Ansari and Pandis, 1998).

Since the role of ammonia in $PM_{2.5}$ formation in the atmosphere is sensitive to ambient co-pollutants and atmospheric conditions, it is necessary to employ a chemical transport model to understand the impacts of CCS ammonia on ambient $PM_{2.5}$ concentrations. Though there have been studies looking into the environmental impacts of amine capture systems (Koornneef et al., 2010; Veltman et al., 2010; Eide-Haugmo et al., 2009; Pehnt and Henkel, 2009; Schreiber et al., 2009; Koornneef et al., 2008; Thitakamol et al., 2007; IEA GHG, 2006; Khoo and Tan, 2006; Rao and Rubin, 2002), no study has been done yet to explore the actual physical and chemical interactions of the emitted ammonia in the atmosphere, which determine their consequences to society.

This study focuses on the amine system using monoethanolamine (MEA, C_2H_7NO), an

amine solvent used widely in industrial applications, but the results are readily applied to other post-combustion capture systems such as an ammonia-based process. We focus on ammonia emissions though CCS may reduce SO_2-related $PM_{2.5}$ substantially from forming HSS because, independent of any decision to deploy CCS, the normal processes of air quality regulation (U.S. EPA, 2010; Pinder et al., 2008; Cofala et al., 2006) will continue to reduce SO_2 emissions. Furthermore, once the decision to deploy CCS is made, the SO_2 reductions come "for free" whereas regulators and operators are left with a separate decision about how much to control the associated ammonia emissions, which we seek to inform in our analysis. This study does not consider the potential contribution of amines themselves to $PM_{2.5}$ creation (Ge et al., 2011b; Nielsen et al., 2011) due to the lack of data on emissions and atmospheric chemistry of amines. It has also been suggested that ammonia and/or amines contribute to the number concentration of ultrafine particles by enhancing the rates and frequencies of new particle formation events (Kulmala et al., 2013; Ge et al., 2011a; Smith et al., 2010; Napari et al., 2002), but this chemistry is still highly uncertain and is not considered here. The potential acid-catalyzed oligomerization, a role of sulfate in organic $PM_{2.5}$ formation, is also not considered because it is uncertain, its overall importance to ambient $PM_{2.5}$ is not known (Hallquist et al., 2009), and it has not been adopted in chemical transport models.

This study aims to evaluate the potential changes in $PM_{2.5}$ concentrations and resulting health impacts from amine scrubbing CCS in the United States. We estimated the ammonia emissions under an aggressive amine scrubbing deployment scenario in 2050. Then, we simulated $PM_{2.5}$ concentrations with and without CCS ammonia for 2050. Several additional simulation analyses were carried out to test the sensitivity of our results to major uncertainties. Finally, the health impacts and associated social costs of the $PM_{2.5}$ changes were evaluated. All monetary values in this study were converted to year 2010 US dollars unless otherwise noted.

2.2 Ammonia Emissions from Amine Scrubbing

Ammonia is created from the oxidative degradation of amine in the amine scrubbing process (Rao et al., 2004; Chi and Rochelle, 2002). It was reported that 30-50% of the amine lost in the process oxidizes to ammonia (Rao et al., 2004; Knudsen et al., 2009). Figure 2.1 summarizes the amine loss rates reported in the literature. Current pilot-scale applications show amine loss rates of 0.5-2 kg MEA/t CO_2. Pilot-scale natural gas power plants equipped with the Fluor Daniel Econamine system reported 1.5 kg MEA/t CO_2 (Rubin, 2011; Rao et al., 2004), 1.6 kg MEA/t CO_2 (Chapel et al., 1999) and 0.5-2 kg MEA/t CO_2 (Suda et al., 1992). A pilot-scale coal-fired power plant with an amine system reported losses of 1.4 kg MEA/t CO_2 (Knudsen et al., 2009). However, other studies suggest that the amine loss could be smaller in the future. An expert elicitation study (Rao et al., 2006) reported that experts on amine-based CCS expected losses to be 0.05-2 kg MEA/t CO_2 by 2015 assuming modest R&D. A commercial power plant was able to reduce the solvent loss to 0.35 kg/t CO_2 using the amine solvent called KS-1 and further down to 0.1-0.2 kg/t CO_2 by modifying operational conditions (Mimura et al., 2002). Based on engineering modeling, U.S. NETL (U.S. NETL, 2010) reported a loss rate of 0.1 kg MEA/t CO_2. We could not find a clear difference in ammonia emissions between coal and natural gas plants.

This study selected an ammonia emission rate of 0.24 kg NH_3/t CO_2 based on a supercritical pulverized coal power plant model with amine scrubbing (Rubin et al., 2005), which includes a typical water wash. The performance of the plant model was reported in the IPCC Special Report on Carbon Capture and Storage (Metz et al., 2005). Although amine scrubbing operations may achieve lower emissions, we have deliberately selected this value because it is supported by current operations and we wish to evaluate whether CCS has the potential to create air quality problems. Since amines and ammonia are highly soluble in water, their emissions are technically controllable, and control strategies can be designed depending on the economics of and/or regulations on amine scrubbing.

The other important variable is the level of CCS deployment in 2050, which is difficult to estimate because amine scrubbing systems are only now being demonstrated at the commercial

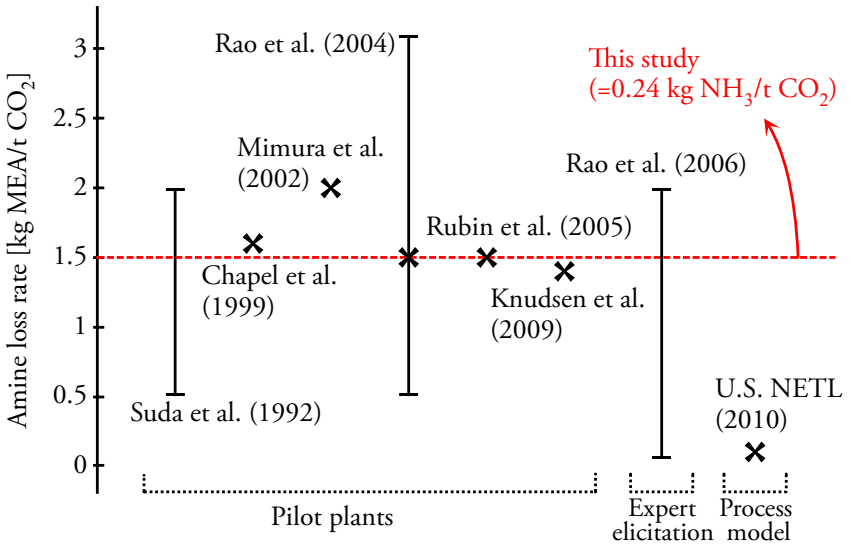

Figure 2.1: Amine loss rates reported or estimated in the literature. An ammonia emissions of $0.24\,\mathrm{kg\,NH_3/t\,CO_2}$ was chosen for this study, which was reported in Rubin et al. (2005) based on a coal power plant model assuming an amine loss rate of $1.5\,\mathrm{kg\,MEA/t\,CO_2}$ (Rao et al., 2004).

scale and carbon mitigation plans are not yet clear in the United States nor in most other nations. Figure 2.2 shows the context for the CCS deployment assumed in this study. Based on the IPCC SRES A2 scenario (Nakićenović et al., 2000), Toth and Rogner (2006) estimated that technical potential of CCS in the United States would be 3.6 Gt CO_2/year in the power sector in 2050 under the A2-IMAGE scenario and 1.8 Gt CO_2 under the A2-AIM scenario. Riahi et al. (2004) reported that OECD90, defined as all members of OECD in 1990, would capture 3.5-5.9 Gt CO_2 in 2050. About 50% of this potential, 1.7-2.9 Gt CO_2, would come from the United States, reflecting coal primary energy consumption in 2000 (Morita). The Energy Modeling Forum 22 study (Fawcett et al., 2009) reported that coal electricity production with CCS ranges from 2.8-6.7 EJ/year among six models for United States transition scenarios targeting 80% emissions reductions below 1990. This would be equivalent to 0.7 Gt CO_2/year to 1.8 Gt CO_2/year if they are captured by the coal power plant model that we assumed for the CCS ammonia emissions above. All these deployment levels are not limited to post-combustion technology or amine scrubbing systems.

To estimate the potential air quality problem from CCS ammonia, we assumed that amine

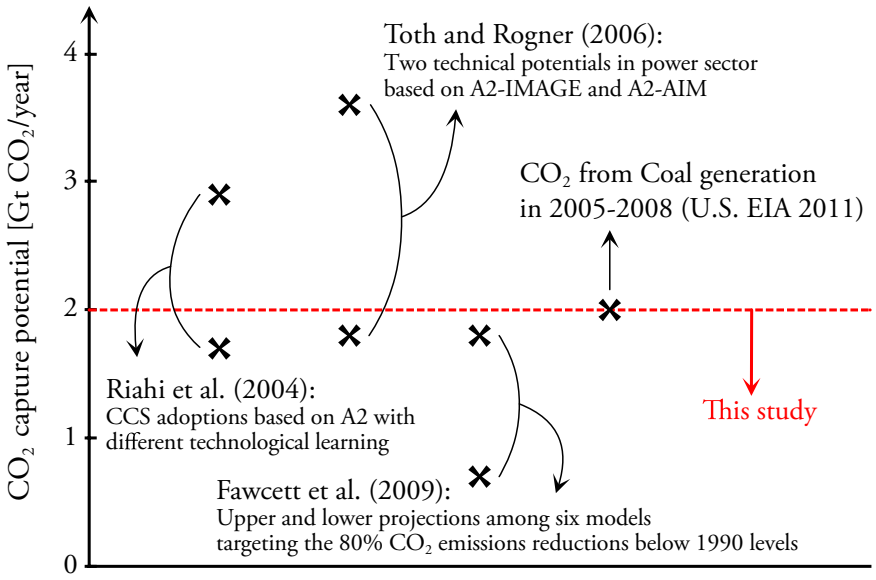

Figure 2.2: CCS potential in the United States. This study assumes that amine scrubbing CCS will capture 2.0 Gt CO_2/year in 2050.

scrubbing in the United States would capture 2.0 Gt CO_2/year from coal-fired power plants and large industrial facilities in 2050. This assumption represents a future with aggressive amine scrubbing deployment since the amount is similar to the CCS deployment levels comprised of all CCS technologies in the scenario studies mentioned above but is realized with only amine scrubbing. The amount of captured CO_2 we assumed is similar to the amount of CO_2 emitted by coal power plants alone annually from 2005-2008 (U.S. EIA, 2011). The CO_2 emissions from natural gas power plants were 320-360 Gt CO_2/year during the same period. Recent shale gas development and new air quality regulations may force old power plants to retire and result in more intensive use of natural gas in electricity generation. Though a natural gas combined cycle (NGCC) emits about half the carbon dioxide to generate a unit of electricity compared to conventional coal plants (U.S. NETL, 2010; Rubin and Zhai, 2012), it would be necessary to equip a portion of the NGCC fleet with CCS to achieve large (~80%) GHG reductions (Fawcett et al., 2009).

From the two factors assumed above, the NH_3 emissions per CO_2 captured, 0.24 kg NH_3/t CO_2, and the amount of CO_2 captured with amine scrubbing, 2.0 Gt CO_2/year, the amount of

ammonia emitted from amine scrubbing CCS was estimated to be 0.48 Tg NH_3/year. This amount of CCS ammonia is ~10% of the current anthropogenic ammonia emissions in the United States, which are 3.5-4.0 Tg NH_3/year (Pinder et al., 2006).

Non-CCS NH_3 emissions are larger in spring and summer than in other seasons since animal husbandry and synthetic fertilizer application are dominant sources of NH_3 (Pinder et al., 2006). Thus the CCS NH_3 emissions would result in a relatively larger increase of NH_3 in winter than in summer, precisely when $PM_{2.5}$ concentrations are most sensitive to ammonia emissions.

2.3 Emissions Scenarios and Sensitivity Simulations

2.3.1 Main Scenarios

We have designed three main scenarios to explore the role of CCS ammonia based on reasonable current and future concentration levels of ambient SO_2, NO_x, and non-CCS NH_3 as shown in Figure A-2. We focused on these three species since the effect of CCS ammonia on ambient $PM_{2.5}$ depends on their relative availability as discussed above.

The first one is *Current*, which corresponds to the current air quality resulting from the emissions database of year 2005 (U.S. EPA, 2011c), which was built for an U.S. EPA's regulatory impact assessment (U.S. EPA, 2010). The database includes emissions from Canada and Mexico and from marine vessels over the oceans. But in the following scenarios we did not change these emissions but only those emitted on the land over the contiguous U.S. domain.

Next, *No-CCS-NH_3 2050* represents a future with significant CCS deployment with no CCS NH_3 emissions. Since the future emissions of SO_2, NO_x and NH_3 would be reduced by CCS or normal air quality regulation (U.S. EPA, 2010; Pinder et al., 2008; Cofala et al., 2006), we assumed that the net impact of these factors is that 85% of SO_2 point emissions relative to 2005, 50% of SO_2 area emissions, 50% of NO_x emissions, and 30% of NH_3 emissions would be reduced by 2050. Amine-based CCS removes almost all SO_2 because SO_2 reacts with amines to form HSS. Therefore, a future with high CCS adoption would easily achieve an 85% reduction of SO_2 point emissions by 2050. Though more difficult than SO_2 point sources, SO_2 area emissions

and NO_x emissions may also achieve significant reductions. Though NH_3 emissions are not currently regulated, a 30% reduction in NH_3 emissions is assumed since NH_3 reduction is a cost-effective $PM_{2.5}$ control measure and regulatory interest in it has increased (Pinder et al., 2007; Aneja et al., 2009; McCubbin et al., 2002).

Lastly, *CCS-NH_3 2050* is the same as the No-CCS-NH_3 2050 scenario just described but with the additional 0.48 Tg NH_3/year of CCS ammonia as estimated above. Assuming large SO_2 sources represent the locations of future CCS plants, either coal plants or other big industrial sources, we added CCS NH_3 to the largest SO_2 point sources, which in total account for the amount of SO_2 emissions by electricity generation in our emissions inventory (U.S. EPA, 2011c). We distributed CCS ammonia to the SO_2 point sources proportionally to their SO_2 emissions on an hourly basis.

2.3.2 Sensitivity to Future Emissions, to CCS Ammonia Emissions and Locations, and to Climate Change

We did sensitivity analyses to address four major uncertainties associated with our main scenarios developed above. One is the future emissions of SO_2, NO_x, and non-CCS NH_3. In order to explore this uncertainty, two more sets of emissions scenarios are developed—High-sensitivity and

Low-sensitivity—as shown in Table A-1. Since it is computationally too expensive to run CAMx with many possible emissions combinations, the two scenarios are developed based on the understanding of inorganic $PM_{2.5}$ thermodynamics discussed above. High-sensitivity represents a future combination of SO_2, NO_x, and non-CCS NH_3 emissions that would result in more $PM_{2.5}$ formation per unit CCS ammonia emissions and Low-sensitivity represents one that would result in less $PM_{2.5}$ formation. SO_2 is assumed to decrease by 95% for High-sensitivity considering a thorough reduction of SO_2 by amine scrubbing and other measures and by 70% for Low-sensitivity considering a future that would capture a substantial amount of CO_2 from natural-gas burning facility while keeping a part of coal generations without CCS. NO_x is assumed to decrease by 70% for Low-sensitivity considering aggressive efforts and by 20% for High-sensitivity considering modest control efforts. And non-CCS NH_3 is assumed to be reduced by 50% for High-sensitivity

considering the cost effectiveness of NH_3 control (Aneja et al., 2009; Pinder et al., 2007; McCubbin et al., 2002) and by 0% for Low-sensitivity considering no action for NH_3 control.

The other major uncertainty is the amount of ammonia emitted from CCS. Despite nonlinearities in the thermodynamics of inorganic $PM_{2.5}$, we assume that the impacts will be approximately proportional to emissions. To test the linearity of impacts on ambient $PM_{2.5}$ concentrations over the range of possible CCS ammonia emissions, CAMx was run for CCS-NH_3 2050, Low-sensitivity, and High-sensitivity scenarios that have 6.25%, 25%, and 200% of the CCS ammonia emissions assumed in CCS-NH_3 2050 scenario.

Thirdly, in order to test the sensitivity of our results to the spatial distribution of CCS NH_3, we performed an additional sensitivity simulation in which we added the CCS ammonia to large NO_x point sources. This also allows us to look at the case of deploying CCS to natural gas power plants and other large natural gas burning facilities as well as coal plants.

Lastly, future temperature increase may affect our results. Under the most warming climate scenario called as Representative Concentration Pathways 8.5, climate models estimate the mean U.S. temperature may increase by 2°C by 2050 on average (mel, 2014). We analyzed a case for an increase of 2°C for the entire simulation domain as a bounding scenario.

2.4 Methods

2.4.1 Air Quality Simulations

We used the Comprehensive Air Quality Model with Extension (CAMx) version 5.41 (ENVIRON, 2012) to simulate the air quality of the scenarios. CAMx is a state-of-the-art CTM that simulates horizontal and vertical advection, dispersion, wet and dry deposition, gas and liquid phase chemistry, and aerosol formation and growth. We used the CAMx air quality modeling platform, which was developed and evaluated in a U.S. EPA's regulatory impact analysis (U.S. EPA, 2010). The platform covers the continental United States with $36\,\mathrm{km}\times36\,\mathrm{km}$ horizontal grid resolution and 14 vertical layers reaching up to $16\,\mathrm{km}$, which is fine enough for $PM_{2.5}$ human health impact analysis (Thompson et al., 2014). The initial and boundary conditions were provided by a global

chemical transport model (U.S. EPA, 2011a). The platform demonstrated the good performance of simulating inorganic species (U.S. EPA, 2011a), which are key pollutants for this study. Figure A-3 presents CAMx results, showing simulated $PM_{2.5}$ concentrations with our 2005 database.

We ran CAMx for the whole year period for the three main scenarios. But due to high computational costs we limited our sensitivity cases to four months (January, April, July, and October). We ran seven days before each simulation period as ramp-up to minimize the effect from initial conditions. Special attention is paid to the $PM_{2.5}$ nonattainment areas designated for 1997 and 2006 standards (U.S. EPA, 2014) (Figure A-4), which are referred to here as $PM_{2.5}$-burdened areas.

2.4.2 Public Health Impacts

The health impacts from CCS-related $PM_{2.5}$ increases were quantified using standard methods adopted by U.S. EPA (U.S. EPA, 2011b, 1999). First, we estimated the changes in mortality rate for the changes in $PM_{2.5}$ concentrations associated with air quality improvements in 2050 (Current to No-CCS-NH_3 2050) and with CCS ammonia impacts (No-CCS-NH_3 2050 to CCS-NH_3 2050). We used the concentration-response relations from the two latest landmark cohort-based PM-mortality studies; for each $PM_{2.5}$ concentration increase of $10\,\mu g\,PM_{2.5}/m^3$, Lepeule et al. (2012) reported that all-cause mortality increases by 14% (95% confidence interval: 7-22%) and Krewski et al. (2009) reported 6% (95% confidence interval: 4-8%). We quantified only at the $PM_{2.5}$ impact on mortality because $PM_{2.5}$ accounts for more than 90% of monetized costs (U.S. EPA, 2011b, 1999; National Research Council, 2010). Second, we estimated the number of premature deaths by multiplying population by the changed mortality rates. We used the year 2040 population forecast provided in the environmental Benefits Mapping and Analysis Program (BenMAP) (Abt Associates, Incorporated, 2012) based on Woods & Poole Economics Inc. (2012), which is 37% larger than the population in 2010. Though our scenarios were developed for 2050, we used the BenMAP population forecast for 2040, the most recent available. Finally, we multiplied the number of premature deaths by the value of a statistical life (VSL), which is people's willingness-to-pay to avoid premature death. We used a Weibull distribution having a mean VSL of $8 million,

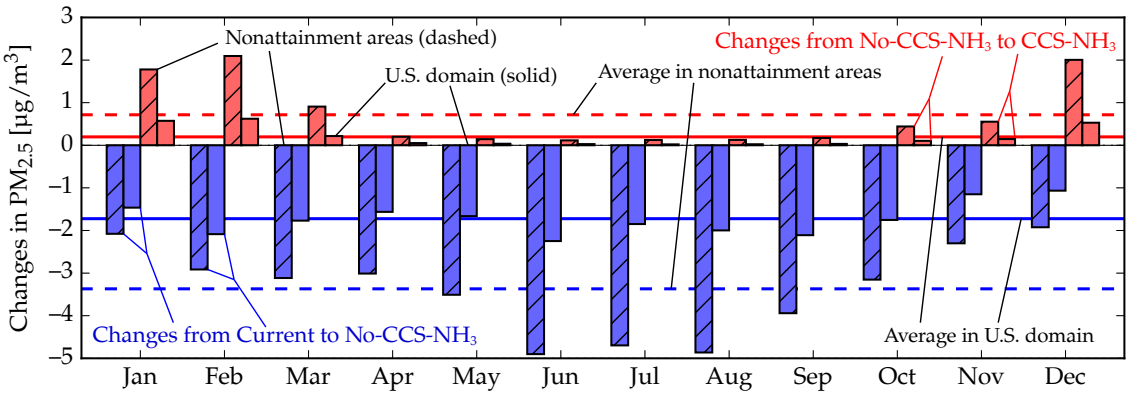

Figure 2.3: Monthly changes in $PM_{2.5}$ concentrations. U.S. domain indicates the concentrations in the continuous U.S. in the simulation grid, not including oceans and other countries like Mexico and Canada.

which is recommened by U.S. EPA (U.S. EPA, 2010). We carried out Monte Carlo simulations, each with 5,000 iterations, to explore uncertainties surrounding concentration-response relation and VSL.

2.5 Results

2.5.1 $PM_{2.5}$ Impacts

The monthly changes in $PM_{2.5}$ concentrations are presented in Figure 2.3. The assumed air quality controls between now and 2050 result in a significant reduction of $3.4\,\mu g/m^3$ in $PM_{2.5}$ (Current to No-CCS-NH_3 2050) on annual average over the nonattainment areas and $1.7\,\mu g/m^3$ over the contiguous United States domain. The annual $PM_{2.5}$ concentrations increase due to CCS (between No-CCS-NH_3 2050 and CCS-NH_3 2050) are smaller but significant: $0.72\,\mu g/m^3$ over nonattainment areas and $0.20\,\mu g/m^3$ over U.S. domain. To better visualize the CTM results, difference maps of $PM_{2.5}$ concentrations are presented in Figures A-5 and 2.4. Summary of the PM concentrations of all scenarios are also presented in Table S2.

Whereas the projected $PM_{2.5}$ reduction is the least in January and the largest in July (Figure A-5), the $PM_{2.5}$ increase from CCS ammonia is the largest in January and the lowest in July (Figure 2.4). This result agrees with the known $PM_{2.5}$ thermodynamics discussed above; wintertime $PM_{2.5}$

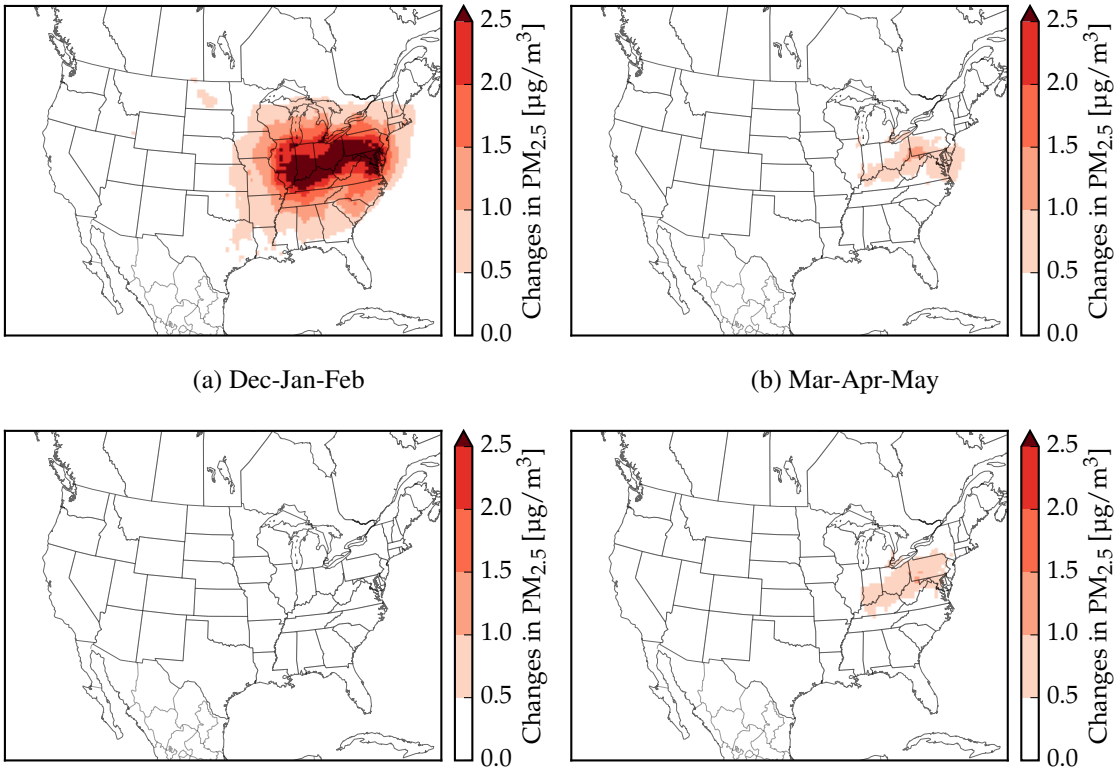

(a) Dec-Jan-Feb

(b) Mar-Apr-May

(c) Jun-Jul-Aug

(d) Sep-Oct-Nov

Figure 2.4: Estimated increase in $PM_{2.5}$ concentrations by CCS ammonia in 2050. $PM_{2.5}$ increase is most sensitive to ammonia emissions during wintertime and relatively insensitive during summertime.

is sensitive to additional ammonia emissions and summertime $PM_{2.5}$ is sensitive to reductions in SO_2 emissions (Pinder et al., 2007; West et al., 1999; Ansari and Pandis, 1998). In winter, the impacts of CCS ammonia offset 86% of the projected future air quality improvements for the nonattainment areas and 38% for the U.S. domain. In summer, by contrast, CCS ammonia offsets 1% for the nonattainment areas and 3% for the U.S. domain. The $PM_{2.5}$ increases in nonattainment areas in spring and fall by CCS ammonia are about 20% of the increase in winter.

$PM_{2.5}$ concentrations increase linearly over a wide range of CCS ammonia for all four months as shown in Figures 2.5 and A-6. The slope in January is $3.4\,\mu g\,PM_{2.5}/m^3$ per Tg NH_3/year for nonattainment areas and $1.1\,\mu g\,PM_{2.5}/m^3$ per Tg NH_3/year for the U.S. domain. The sensitivity of $PM_{2.5}$ increase to CCS ammonia is also linear in other months though the slopes are shallower. Figure A-6 (a) shows that the impact of CCS ammonia on $PM_{2.5}$ shows a modest sensitivity to

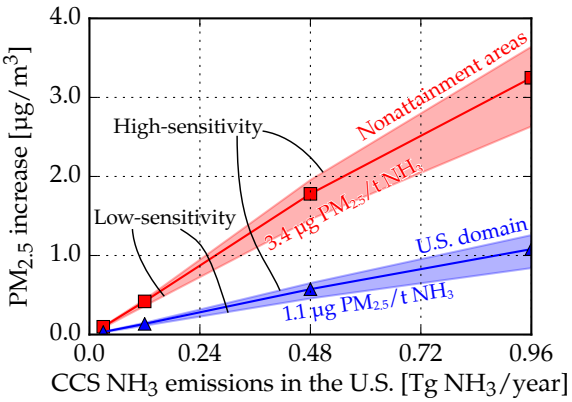

Figure 2.5: Sensitivity analysis of January $PM_{2.5}$ to future levels of co-pollutants (SO_2, NO_x, and non-CCS NH_3) and the amount of ammonia emitted by amine scrubbing.

the mix of other pollutants: SO_2, NO_x, and non-CCS NH_3. In addition, our results are found not to sensitive to the location of CCS ammonia and the temperature increase as shown in Figures A-7 and A-8.

2.5.2 Estimation and Valuation of Premature Deaths

The projected changes in annual premature deaths and their valuations are presented in Figure A-9. Two mean estimates calculated based on the two epidemiological studies are presented as estimated range here. Comparing improved air quality in 2050 without CCS ammonia to the present, the number of annual premature deaths is expected to decrease by 51,000-120,000, which is valued at $410 billion to $930 billion. Under the increased $PM_{2.5}$ from CCS ammonia, the number of annual premature deaths attributed to CCS ammonia is estimated to be 7,600-17,000, valued at -$61 billion to -$140 billion. Given the seasonality of the $PM_{2.5}$ response discussed previously, 68% of the annual-average $PM_{2.5}$ increase resulted from wintertime $PM_{2.5}$ changes with a negligible contribution from summertime changes.

Based on these results, the per unit social health costs of CCS ammonia is calculated to be $130,000-280,000/t NH_3. Wintertime CCS NH_3 are higher at $340,000-770,000/t NH_3. On a basis of CO_2 captured, the costs of CCS ammonia are calculated to be $31-68/t CO_2 per year and $82-186/t CO_2 during the winter.

2.6 Discussion

This paper has explored the air quality and human health impacts that could be imposed by ammonia emissions from amine-based post-combustion CO_2 capture processes. First, we estimated potential ammonia emissions based on current emission factors and analyzed the possible changes in concentrations of fine particulate matter ($PM_{2.5}$), of which ammonia is a major precursor, with a state-of-science chemical transport model, CAMx. Then we estimated the premature mortality associated with the $PM_{2.5}$ formation and monetized the impacts. In this study, we focused on the formation of $PM_{2.5}$ from CCS ammonia but did not look at emissions of amines per se. Though it would be reasonable to assume that amines would have similar impacts per mole of nitrogen emitted, we could not test this due to lack of relevant data. This study also did not consider the effects of ammonia or amines on number concentrations of ultrafine particles via nucleation,Ge et al. (2011a); Kulmala et al. (2013); Smith et al. (2010); Napari et al. (2002) or the concerns over possible formation of carcinogenic nitrosamines by amines in the atmosphere.Ge et al. (2011a); Rao and Rubin (2002); Nielsen et al. (2010) Both processes are poorly understood at the current time.

We found that ammonia emissions from amine-based carbon capture systems at emissions rates typical of current pilot plants would create a significant increase in $PM_{2.5}$ concentrations, resulting in worrisome public health impacts. With an emission factor of 0.24 kg NH_3/t CO_2, a substantial deployment of amine scrubbing to coal power plants to capture 2 Gt CO_2/year would emit 0.48 Tg NH_3/year in the U.S. This amounts to 14% of annual ammonia emissions or 34% of winter emissions of the U.S. in 2005. This scenario is intentionally chosen to result in high ammonia emissions, but sensitivity to differing emissions rates was analyzed. Such emissions would increase the winter $PM_{2.5}$ concentrations in nonattainment areas by $2.0\,\mu g/m^3$ on average and up to $4.3\,\mu g/m^3$ in some locations.

The $PM_{2.5}$ increase for the CCS emissions considered here would significantly compromise air quality. Especially, the winter time $PM_{2.5}$ increase can offset in nonattainment areas 86% of all future air quality improvement including the contribution of CCS to large SO_2 reductions.

An increased $PM_{2.5}$ concentration of $2.0\,\mu g/m^3$ is significant when one considers that current nonattainment areas often seek to cut 1-2 $\mu g/m^3$ to meet the $PM_{2.5}$ National Ambient Air Quality Standards (NAAQS). It may also cause other areas to slip into nonattainment, especially if more stringent NAAQS standards are adopted in the future.

This work has examined the key uncertainties governing the impacts of CCS NH_3, which is summarized in Table A-3. Because CCS ammonia emissions are uncertain and because ammonia impacts depend on the levels of co-pollutants available from other sources, we performed a sensitivity analysis over a wide range of CCS ammonia emissions and potential emissions of co-pollutants (SO_2, NO_x, and non-CCS NH_3) as shown in Figure A-6. We showed that $PM_{2.5}$ impacts are fairly linear with CCS ammonia emissions, and concentrations increase with CCS ammonia at a rate of $3.4\,\mu g/m^3$ per Tg NH_3 in nonattainment areas in January. The $PM_{2.5}$ increase in nonattainment areas in January could vary by -18% to $+10\%$ depending upon the future emissions of the co-pollutants. The approximately linear response is useful; since ammonia emissions from future systems may be lower than current pilot plants, the $PM_{2.5}$ impacts considered here may be scaled accordingly, noting that Figure A-6 shows somewhat higher unit impacts for smaller CCS emissions. In addition, our results are not sensitive to the location of CCS ammonia and the potential temperature increase from climate change (Figures A-7 and A-8). As is always the case with $PM_{2.5}$ health valuations, uncertainties in concentration-response relations and VSL are significant (-90% to $+160\%$).

Our per-tonne costs, \$130,000-280,000/t NH_3, are relatively bigger than those in the literature. This would be mainly because $PM_{2.5}$ formation is more sensitive to ammonia emissions in the atmosphere in 2050 that we assumed and we used 2040 population forecast, which is 37% larger than 2010 population. The following values are converted to 2010 USD and metric tonne from their reported units. With the Response Surface Model,U.S. EPA (2006) an air quality model, Fann et al. (2009) reported social costs per ton of NH_3 emitted from mobile sources was \$120,000/t NH_3 at the national level and \$52,000-170,000/t NH_3 over nine urban areas based on a concentration response relationLaden et al. (2006) similar to Lepeule et al.Lepeule et al. (2012) For area source NH_3, they estimated the social health cost of \$46,000/ton NH_3 at the national level. With a reduced-form

air quality model, Muller et al. (2011) reported the costs of NH_3 for all US counties using a VSL similar to this study and a concentration-response relationPope et al. (2002) similar to Krewski et al.Krewski et al. (2009) They vary from \$2,200/t NH_3 (5th percentile) to \$130,000/t NH_3 (95th percentile) with a mean of \$38,000/t NH_3.

In terms of the social cost in the absence of controls on ammonia emissions, the $PM_{2.5}$ problem resulting from CCS ammonia emissions could be compared to the climate benefits of the avoided CO_2 emissions. Using a standard method of valuing $PM_{2.5}$ mortality, we estimated the social cost of CCS ammonia at \$31-68 per tonne CO_2 captured. Estimates of the social cost of carbon, which includes CO_2 damages on human health, property, and ecosystem services, are uncertain and vary widely, but a U.S. government interagency working group estimated the social cost of carbon in 2050 to be \$28-102/t CO_2.U.S. IAWG (2013) When compared to these estimates, the public health impacts from CCS ammonia emissions are significant in comparison to the climate benefits from CO_2 emissions reductions from CCS and deserve close attention in the future. CCS ammonia impacts could be minimized compared to CO_2 benefits by reducing CCS NH_3 emission factors below those used here.

Operators of CCS facilities have some natural incentives to reduce amine losses. For a solvent loss rate of 1.5 kg MEA/t CO_2 and an assumed amine solvent cost of \$2,250/t MEA,U.S. NETL (2010) the amine consumption costs about \$3.4/t CO_2. However, our analysis shows that the $PM_{2.5}$ social costs are still much higher than the private costs borne by the operators in the form of solvent makeup. Therefore, it makes sense for regulators to impose limits on ammonia and amine emissions from CCS in order to protect the public interest. Since 68% of the burden occurs in winter and virtually none during the summer, it could be considered to enforce more stringent ammonia controls on a seasonal basis.

The concerns noted here suggest a need to proceed cautiously, but the air quality impacts of CCS ammonia are not necessarily prohibitive of the technology. Since ammonia is highly soluble in water, it is not technically difficult to control by installing more or better water wash units. Water wash units are already included in plant design mainly to reduce solvent loss from mechanical entrainment and evaporation.U.S. NETL (2010) Water wash systems could be better

designed to minimize ammonia and amine emissions to the atmosphere in addition to the current purpose of minimizing solvent losses. If CCS ammonia is managed, for example, at the current ammonia control level of the selective catalytic reduction system (2-10 ppm), our estimate for the $PM_{2.5}$ impact from CCS ammonia is reduced by a factor of ten.

We based our analysis on MEA systems because this capture technology is reasonably well understood, but the results are readily applicable to other post-combustion capture systems such as an ammonia-based process. Although little information is currently available about ammonia leakage from such systems, the impacts per unit ammonia emitted could be applied to these systems given such data. Since the material cost of ammonia is much lower than MEA in terms of solvent costs per tonne of CO_2 captured,Versteeg and Rubin (2011b) an ammonia-based CCS power plant may afford to lose more solvent to the atmosphere than an amine-based one. Therefore, there would be an even stronger need for regulatory intervention to protect the public health.

In summary, widespread deployment of CCS technology could result in significant unwanted increases in $PM_{2.5}$ levels and potentially other impacts on air quality as well. There is a need for regulators to be pro-active in considering appropriate emissions-based standards to avoid such an outcome. Currently, there is no federal regulation on ammonia emissions from power plants. Emissions-based standards low enough to prevent significant air quality degradation will incur some cost but should be technically feasible, and the impact assessment performed here provides quantitative guidance for what level of control is appropriate.

2.7 Acknowledgments

This work was supported by the center for Climate and Energy Decision Making (SES-0949710), through a cooperative agreement between the National Science Foundation and Carnegie Mellon University.

2.8 References

Climate Change Impacts in the United States: The Third National Climate Assessment, Tech. rep., U.S. Global Change Research Program, Washington, DC, 2014.

Abt Associates, Incorporated: Environmental Benefits Mapping and Analysis Program (BenMAP) Version 4.0.67, Tech. rep., U.S. Environmental Protection Agency. Office of Air Quality Planning and Standards, Research Triangle Park, NC, 2012.

Aneja, V. P., Schlesinger, W. H., and Erisman, J. W.: Effects of Agriculture upon the Air Quality and Climate: Research, Policy, and Regulations, Environ. Sci. Technol., 43, 4234–4240, doi:10.1021/es8024403, 2009.

Ansari, A. S. and Pandis, S. N.: Response of Inorganic PM to Precursor Concentrations, Environ. Sci. Technol., 32, 2706–2714, doi:10.1021/es971130j, 1998.

Bachu, S.: CO_2 storage in geological media: Role, means, status and barriers to deployment, Prog. Energy Combust. Sci., 34, 254–273, doi:10.1016/j.pecs.2007.10.001, URL `http://www.sciencedirect.com/science/article/pii/S0360128507000494`, 2008.

Bouwman, A. F., Lee, D. S., Asman, W. A. H., Dentener, F. J., van der Hoek, K. W., and Olivier, J. G. J.: A global high-resolution emission inventory for ammonia, Global Biogeochem. Cycles, 11, 561–587, 1997.

Bråten, H. B., Bunkan, A. J., Bache-Andreassen, L., Solimannejad, M., and Nielsen, C. J.: Final report on a theoretical study on the atmospheric degradation of selected amines, Tech. Rep. OR 77/2008, Norwegian Institute for Air Research (NILU), Kjeller, Norway, 2009.

Chapel, D. G., Mariz, C. L., and Ernest, J.: Recovery of CO_2 from Flue Gases: Commercial Trends, in: Canadian Society of Chemical Engineers annual meeting, Saskatoon, Canada, 1999.

Chi, S. and Rochelle, G. T.: Oxidative degradation of monoethanolamine, Ind. Eng. Chem. Res, 41, 4178–4186, 2002.

Cofala, J., Amann, M., and Mechler, R.: Scenarios of world anthropogenic emissions of air pollutants and methane up to 2030, Tech. Rep. IIASA Interim Report, IR-06-023, International Institute for Applied Systems Analysis, Laxenburg, Austria, 2006.

Eide-Haugmo, I., Brakstad, O. G., Hoff, K. A., Sørheim, K. R., da Silva, E. F., and Svendsen, H. F.: Environmental impact of amines, Energy Procedia, 1, 1297–1304, doi:10.1016/j.egypro.2009.01.170, 2009.

ENVIRON: CAMx User's Guide Version 5.41, Tech. rep., Environ International Corporation, Novato, CA, 2012.

Fann, N., Fulcher, C. M., and Hubbell, B. J.: The influence of location, source, and emission type in estimates of the human health benefits of reducing a ton of air pollution, Air Qual., Atmos. Health, 2, 169–176, doi:10.1007/s11869-009-0044-0, 2009.

Fawcett, A., Calvin, K., de la Chesnaye, F., Reilly, J., and Weyant, J.: Overview of EMF 22 US transition scenarios, Energy Economics, 31, S198–S211, 2009.

Ge, X., Wexler, A. S., and Clegg, S. L.: Atmospheric amines – Part I. A review, Atmos. Environ., 45, 524–546, doi:10.1016/j.atmosenv.2010.10.012, 2011a.

Ge, X., Wexler, A. S., and Clegg, S. L.: Atmospheric amines – Part II. Thermodynamic properties and gas/particle partitioning, Atmos. Environ., 45, 561–577, doi:10.1016/j.atmosenv.2010.10.013, 2011b.

Hallquist, M., Wenger, J. C., Baltensperger, U., Rudich, Y., Simpson, D., Claeys, M., Dommen, J., Donahue, N. M., George, C., Goldstein, A. H., Hamilton, J. F., Herrmann, H., Hoffmann, T., Iinuma, Y., Jang, M., Jenkin, M. E., Jimenez, J. L., Kiendler-Scharr, A., Maenhaut, W., McFiggans, G., Mentel, T. F., Monod, A., PrÃl'vÃt't, A. S. H., Seinfeld, J. H., Surratt, J. D., Szmigielski, R., and Wildt, J.: The formation, properties and impact of secondary organic

aerosol: current and emerging issues, Atmos. Chem. Phys., 9, 5155–5236, URL http://www.atmos-chem-phys.net/9/5155/2009/, 2009.

IEA GHG: Environmental impact of solvent scrubbing of CO_2, Tech. Rep. 2006/14, IEA Greenhouse Gas R&D Programme, Orchard Business Centre, Gloucestershire, U.K., 2006.

IPCC: Climate Change 2014, Mitigation of Climate Change. Contribution of Working Group III to the Fifth Assessment Report of the Intergovernmental Panel on Climate Change, Cambridge University Press, Cambridge, United Kingdom and New York, NY, USA, 2014.

Khoo, H. H. and Tan, R. B. H.: Life Cycle Investigation of CO_2 Recovery and Sequestration, Environ. Sci. Technol., 40, 4016–4024, doi:10.1021/es051882a, 2006.

Knudsen, J. N., Jensen, J. N., Vilhelmsen, P., and Biede, O.: Experience with CO_2 capture from coal flue gas in pilot-scale: Testing of different amine solvents, Energy Procedia, 1, 783–790, doi:10.1016/j.egypro.2009.01.104, 2009.

Koornneef, J., van Keulen, T., Faaij, A., and Turkenburg, W.: Life cycle assessment of a pulverized coal power plant with post-combustion capture, transport and storage of CO_2, Int. J. Greenhouse Gas Control, 2, 448–467, doi:10.1016/j.ijggc.2008.06.008, 2008.

Koornneef, J., Ramirez, A., van Harmelen, T., van Horssen, A., Turkenburg, W., and Faaij, A.: The impact of CO_2 capture in the power and heat sector on the emission of SO_2, NO_x, particulate matter, volatile organic compounds and NH_3 in the European Union, Atmos. Environ., 44, 1369–1385, doi:10.1016/j.atmosenv.2010.01.022, 2010.

Krewski, D., Jerrett, M., Burnett, R. T., Ma, R., Hughes, E., Shi, Y., Turner, M. C., Pope, III, C. A., Thurston, G., Calle, E. E., Thun, M. J., Beckerman, B., DeLuca, P., Finkelstein, N., Ito, K., Moore, D. K., Newbold, K. B., Ramsay, T., Ross, Z., Shin, H., and Tempalski, B.: Extended follow-up and spatial analysis of the American Cancer Society study linking particulate air pollution and mortality, Tech. Rep. Research Report 140, Health Effects Institute, Boston, MA, 2009.

Kulmala, M., Kontkanen, J., Junninen, H., Lehtipalo, K., Manninen, H. E., Nieminen, T., Petäjä, T., Sipilä, M., Schobesberger, S., Rantala, P., Franchin, A., Jokinen, T., Järvinen, E., Äijälä, M., Kangasluoma, J., Hakala, J., Aalto, P. P., Paasonen, P., Mikkilä, J., Vanhanen, J., Aalto, J., Hakola, H., Makkonen, U., Ruuskanen, T., Mauldin, R. L., Duplissy, J., Vehkamäki, H., Bäck, J., Kortelainen, A., Riipinen, I., Kurtén, T., Johnston, M. V., Smith, J. N., Ehn, M., Mentel, T. F., Lehtinen, K. E. J., Laaksonen, A., Kerminen, V.-M., and Worsnop, D. R.: Direct Observations of Atmospheric Aerosol Nucleation, Science, 339, 943–946, doi:10.1126/science.1227385, URL `http://www.sciencemag.org/content/339/6122/943`, 2013.

Laden, F., Schwartz, J., Speizer, F. E., and Dockery, D. W.: Reduction in Fine Particulate Air Pollution and Mortality: Extended Follow-up of the Harvard Six Cities Study, Am. J. Respir. Crit. Care Med., 173, 667–672, doi:10.1164/rccm.200503-443OC, 2006.

Lepeule, J., Laden, F., Dockery, D., and Schwartz, J.: Chronic Exposure to Fine Particles and Mortality: An Extended Follow-up of the Harvard Six Cities Study from 1974 to 2009, Environ. Health Perspect., 120, 965–970, doi:10.1289/ehp.1104660, URL `http://www.ncbi.nlm.nih.gov/pmc/articles/PMC3404667/`, 2012.

McCubbin, D. R., Apelberg, B. J., Roe, S., and Divita, F.: Livestock Ammonia Management and Particulate-Related Health Benefits, Environ. Sci. Technol., 36, 1141–1146, doi:10.1021/es010705g, 2002.

Metz, B., Davidson, O., de Coninck, H. C., Loos, M., and Meyer, L. A., eds.: IPCC Special Report on Carbon Dioxide Capture and Storage, Cambridge University Press, Cambridge, U.K. and New York, NY, 2005.

Mimura, T., Nojo, T., Iijima, M., Yoshiyama, T., Tanaka, H., Gale, J., and Kaya, Y.: Recent Developments on Flue Gas CO_2 Recovery Technology, in: Greenhouse Gas Control Technologies - 6th International Conference, vol. II, pp. 1057–1061, Pergamon, Oxford, U.K., 2002.

Morita, T.: Greenhouse Emission Scenario Database Version 5, Center for Global Environmental Research, National Institute for Environmental Studies, Tsukuba, Japan, http://www-cger.nies.go.jp/scenario/index.html (accessed Nov 8, 2010).

Muller, N. Z., Mendelsohn, R., and Nordhaus, W.: Environmental accounting for pollution in the United States economy, Am. Econ. Rev., 101, 1649–1675, 2011.

Nakićenović, N., Alcamo, J., Davis, G., De Vries, B., Fenhann, J., Gaffin, S., Gregory, K., Grübler, A., Jung, T. Y., and Kram, T.: IPCC Special Report on Emissions Scenarios, Cambridge University Press, Cambridge, U.K., 2000.

Napari, I., Noppel, M., Vehkamäki, H., and Kulmala, M.: An improved model for ternary nucleation of sulfuric acid–ammonia–water, J. Chem. Phys., 116, 4221–4227, doi:10.1063/1.1450557, URL http://scitation.aip.org/content/aip/journal/jcp/116/10/10.1063/1.1450557, 2002.

National Research Council: Hidden Costs of Energy: Unpriced Consequences of Energy Production and Use, The National Academies Press, Washington, DC, URL http://www.nap.edu/catalog.php?record_id=12794, 2010.

Nielsen, C. J., D'Anna, B., Dye, C., George, C., Graus, M., Hansel, A., Karl, M., King, S., Musabila, M., Müller, M., Schmidbauer, N., Stenstrøm, Y., and Wisthaler, A.: Atmospheric Degradation of Amines (ADA) Summary Report: Gas phase photo-oxidation of 2-aminoethanol (MEA), Tech. Rep. OR 8/2010, Norwegian Institute for Air Research, Kjeller, Norway, 2010.

Nielsen, C. J., D'Anna, B., Dye, C., Graus, M., Karl, M., King, S., Maguto, M. M., Müller, M., Schmidbauer, N., Stenstrøm, Y., Wisthaler, A., and Pedersen, S.: Atmospheric chemistry of 2-aminoethanol (MEA), Energy Procedia, 4, 2245–2252, doi:16/j.egypro.2011.02.113, 2011.

Pehnt, M. and Henkel, J.: Life cycle assessment of carbon dioxide capture and storage from

lignite power plants, Int. J. Greenhouse Gas Control, 3, 49–66, doi:10.1016/j.ijggc.2008.07.001, 2009.

Pinder, R. W., Adams, P. J., Pandis, S. N., and Gilliland, A. B.: Temporally resolved ammonia emission inventories: Current estimates, evaluation tools, and measurement needs, J. Geophys. Res., 111, D16 310, doi:10.1029/2005JD006603, 2006.

Pinder, R. W., Adams, P. J., and Pandis, S. N.: Ammonia Emission Controls as a Cost-Effective Strategy for Reducing Atmospheric Particulate Matter in the Eastern United States, Environ. Sci. Technol., 41, 380–386, doi:10.1021/es060379a, 2007.

Pinder, R. W., Gilliland, A. B., and Dennis, R. L.: Environmental impact of atmospheric NH_3 emissions under present and future conditions in the eastern United States, Geophys. Res. Lett., 35, L12 808, URL `http://onlinelibrary.wiley.com/doi/10.1029/2008GL033732/abstract`, 2008.

Pope, III, C. A. and Dockery, D. W.: Health effects of fine particulate air pollution: lines that connect, J. Air Waste Manage. Assoc., 56, 709–742, 2006.

Pope, III, C. A., Burnett, R. T., Thun, M. J., Calle, E. E., Krewski, D., Ito, K., and Thurston, G. D.: Lung Cancer, Cardiopulmonary Mortality, and Long-term Exposure to Fine Particulate Air Pollution, JAMA, J. Am. Med. Assoc., 287, 1132–1141, doi:10.1001/jama.287.9.1132, 2002.

Rao, A. B. and Rubin, E. S.: A Technical, Economic, and Environmental Assessment of Amine-Based CO_2 Capture Technology for Power Plant Greenhouse Gas Control, Environ. Sci. Technol., 36, 4467–4475, doi:10.1021/es0158861, 2002.

Rao, A. B., Rubin, E. S., and Berkenpas, M. B.: An integrated modeling framework for carbon management technologies, Tech. rep., Department of Engineering and Public Policy, Carnegie Mellon University, Pittsburgh, PA, 2004.

Rao, A. B., Rubin, E. S., Keith, D. W., and Granger Morgan, M.: Evaluation of potential cost reductions from improved amine-based CO_2 capture systems, Energy Policy, 34, 3765–3772, doi:10.1016/j.enpol.2005.08.004, 2006.

Riahi, K., Rubin, E. S., Taylor, M. R., Schrattenholzer, L., and Hounshell, D.: Technological learning for carbon capture and sequestration technologies, Energy Economics, 26, 539–564, 2004.

Rochelle, G. T.: Amine Scrubbing for CO_2 Capture, Science, 325, 1652–1654, doi:10.1126/science.1176731, 2009.

Rubin, E. S.: Carnegie Mellon University, Pittsburgh, PA. Personal Communication, 2011.

Rubin, E. S. and Zhai, H.: The Cost of Carbon Capture and Storage for Natural Gas Combined Cycle Power Plants, Environ. Sci. Technol., 46, 3076–3084, URL http://dx.doi.org/10.1021/es204514f, 2012.

Rubin, E. S., Rao, A. B., and Chen, C.: Comparative assessments of fossil fuel power plants with CO_2 capture and storage, in: Proceedings of 7th International Conference on Greenhouse Gas Control Technologies, vol. 1, pp. 285–294, 2005.

Schreiber, A., Zapp, P., and Kuckshinrichs, W.: Environmental assessment of German electricity generation from coal-fired power plants with amine-based carbon capture, Int. J. Life Cycle Assess., 14, 547–559, 2009.

Smith, J. N., Barsanti, K. C., Friedli, H. R., Ehn, M., Kulmala, M., Collins, D. R., Scheckman, J. H., Williams, B. J., and McMurry, P. H.: Observations of aminium salts in atmospheric nanoparticles and possible climatic implications, Proc. Natl. Acad. Sci. U. S. A., 107, 6634–6639, doi:10.1073/pnas.0912127107, URL http://www.pnas.org/content/107/15/6634, 2010.

Suda, T., Fujii, M., Yoshida, K., Iijima, M., Seto, T., and Mitsuoka, S.: Development of flue gas

carbon dioxide recovery technology, Energy Convers. Manage., 33, 317–324, doi:10.1016/0196-8904(92)90026-S, 1992.

Thitakamol, B., Veawab, A., and Aroonwilas, A.: Environmental impacts of absorption-based CO_2 capture unit for post-combustion treatment of flue gas from coal-fired power plant, Int. J. Greenhouse Gas Control, 1, 318–342, doi:16/S1750-5836(07)00042-4, 2007.

Thompson, T. M., Saari, R. K., and Selin, N. E.: Air quality resolution for health impact assessment: influence of regional characteristics, Atmos. Chem. Phys., 14, 969–978, doi:10.5194/acp-14-969-2014, URL http://www.atmos-chem-phys.net/14/969/2014/, 2014.

Toth, F. L. and Rogner, H. H.: Carbon dioxide capture: an assessment of plausible ranges, Int. J. Global Energy Issues, 25, 14–59, 2006.

U.S. EIA: Emissions of Greenhouse Gases in the United States 2009, Tech. Rep. DOE/EIA-0573(2009), U.S. Department of Energy, Washington, DC, 2011.

U.S. EPA: The benefits and costs of the Clean Air Act, 1990 to 2010 : EPA report to Congress., Tech. rep., U.S. Environmental Protection Agency. Office of Air and Radiation, Washington DC, 1999.

U.S. EPA: Technical Support Document for the Proposed PM NAAQS Rule, Response Surface Modeling, Tech. rep., U.S. Environmental Protection Agency. Office of Air Quality Planning and Standards., Research Triangle Park, NC, 2006.

U.S. EPA: Guidelines for Preparing Economic Analyses, Tech. rep., National Center for Environmental Economics, Office of Policy, U.S. Environmental Protection Agency, Research Triangle Park, NC, 2010.

U.S. EPA: Regulatory Impact Analysis for the Proposed Federal Transport Rule, Tech. Rep. EPA-HQ-OAR-2009-0491, U.S. Environmental Protection Agency. Office of Air and Radiation, Research Triangle Park, NC, 2010.

U.S. EPA: Air Quality Modeling Final Rule Technical Support Document, Tech. rep., U.S. Environmental Protection Agency. Office of Air Quality Planning and Standards. Air Quality Assessment Division., Research Triangle Park, NC, URL http://www.epa.gov/airquality/transport/pdfs/AQModeling.pdf, 2011a.

U.S. EPA: The Benefits and Costs of the Clean Air Act from 1990 to 2020, Tech. rep., U.S. Environmental Protection Agency. Office of Air and Radiation., Washington DC, 2011b.

U.S. EPA: Emissions Inventory Final Rule TSD, Tech. Rep. EPA-HQ-OAR-2009-0491, U.S. Environmental Protection Agency. Office of Air and Radiation. Office of Air Quality Planning and Standards. Air Quality Assessment Division., Research Triangle Park, NC, 2011c.

U.S. EPA: PM-2.5 (2006 Standard) Area Information, URL http://www.epa.gov/airquality/greenbook/rindex.html, (accessed Aug 27, 2014), 2014.

U.S. IAWG: Technical Support Document: Technical Update of the Social Cost of Carbon for Regulatory Impact Analysis Under Executive Order 12866, Tech. rep., Interagency Working Group on Social Cost of Carbon. United States Government, Washington, DC, 2013.

U.S. NETL: Cost and Performance Baseline for Fossil Energy Plants. Volume 1: Bituminous Coal and Natural Gas to Electricity, Tech. Rep. DOE/NETL-2010/1397, U.S. Department of Energy. National Energy Technology Laboratory, 2010.

Veltman, K., Singh, B., and Hertwich, E. G.: Human and Environmental Impact Assessment of Postcombustion CO_2 Capture Focusing on Emissions from Amine-Based Scrubbing Solvents to Air, Environ. Sci. Technol., 44, 1496–1502, doi:10.1021/es902116r, 2010.

Versteeg, P. and Rubin, E. S.: Technical and economic assessment of ammonia-based post-combustion CO_2 capture, Energy Procedia, 4, 1957–1964, doi:10.1016/j.egypro.2011.02.076, 2011a.

Versteeg, P. and Rubin, E. S.: A technical and economic assessment of ammonia-based

post-combustion CO_2 capture at coal-fired power plants, Int. J. Greenhouse Gas Control, 5, 1596–1605, doi:10.1016/j.ijggc.2011.09.006, 2011b.

West, J. J., Ansari, A. S., and Pandis, S. N.: Marginal $PM_{2.5}$: Nonlinear aerosol mass response to sulfate reductions in the eastern United States, J. Air Waste Manage. Assoc., 49, 1415–1424, 1999.

Woods & Poole Economics Inc.: Complete Demographic Database, Washington, DC, URL `http://www.woodsandpoole.com/`, 2012.

A Appendix: Additional Figures and Tables

						$PM_{2.5}$ mass net increase
Ammonium sulfate PM formation:			SO_2 ↓			
	NH_3 (g)	+	$\frac{1}{2}$ H_2SO_4 (s)	⟶	$\frac{1}{2}$ $(NH_4)_2SO_4$ (s)	
$PM_{2.5}$ [g/mol]:	0		49		66	+17
Ammonium nitrate PM formation:			NOx ↓			
	NH_3 (g)	+	HNO_3 (g)	$\xrightarrow{\text{cold T}}$	NH_4NO_3 (s)	
$PM_{2.5}$ [g/mol]:	0		0		80	+80
Remaining as gas:						
	NH_3 (g)					
$PM_{2.5}$ [g/mol]:	0					0

Figure A-1: Potential reactions of ammonia (NH_3) with sulfuric acid (H_2SO_4) and nitric acid (HNO_3) in the atmosphere. Values below each species indicate the molecular weight of components in the particulate phase, and the right-hand column indicates the very different effect each pathway has on ambient $PM_{2.5}$ concentrations. Ammonia first reacts with sulfuric acid to form ammonium sulfate ($(NH_4)_2SO_4$) PM, and the remaining free ammonia, if any, may react with nitric acid to form ammonium nitrate (NH_4NO_3) PM. Ammonia remains as a gas if there is no SO_2 and NO_x.

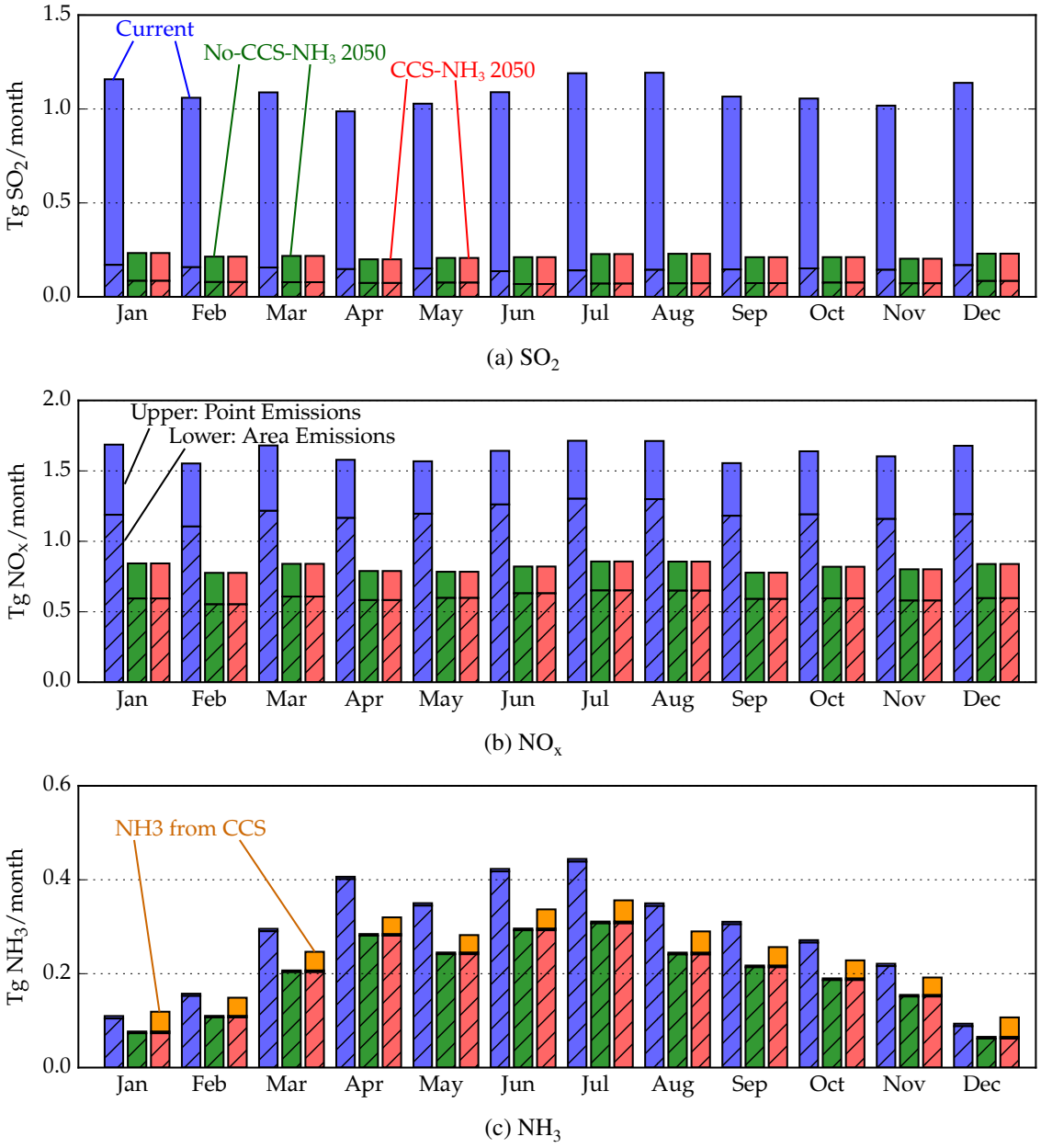

Figure A-2: Emissions assumptions for the three main scenarios. Current represents current emissions as of 2005, No-CCS-NH_3 2050 corresponds to the projected emissions in 2050 assuming an aggressive CCS deployment as well as future air-quality improvement efforts, and CCS-NH_3 2050 assumes that additional NH_3 is emitted by amine scrubbing. The additional ammonia from CCS is 14% of the 2005 ammonia emissions. NH_3, mainly emitted from agricultural sources like livestock and fertilizer, shows a strong seasonal variation. The relative increase is much larger in winter than in summer, which is 34% relative to the 2005 emissions or 48% relative to the 2050 scenario emissions.

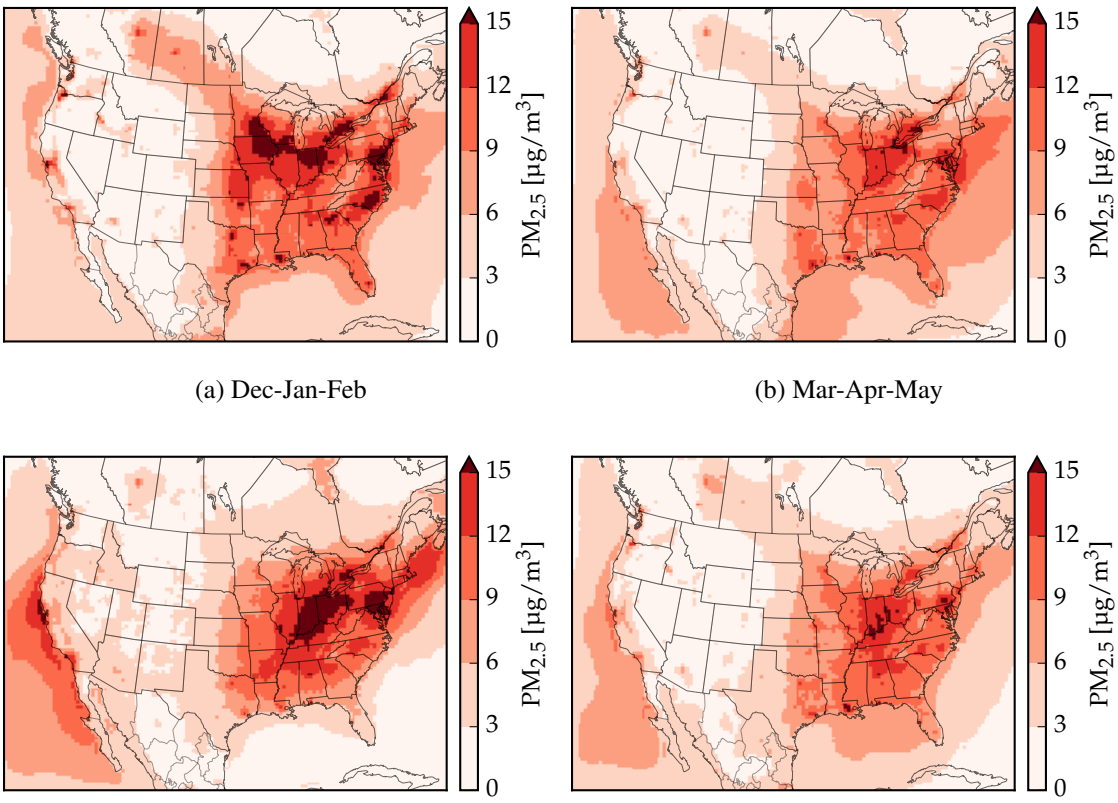

(a) Dec-Jan-Feb

(b) Mar-Apr-May

(c) Jun-Jul-Aug

(d) Sep-Oct-Nov

Figure A-3: Average $PM_{2.5}$ concentrations in 2005 estimated by CAMx.

Table A-1: Emissions assumptions for High-sensitivity and Low-sensitivity scenarios.

Scenario	Emissions reduction relative to Current scenario		
	SO_2	NO_x	Non-CCS NH_3
No-CCS-NH_3 2050	85%[a]	50%	30%
High-sensitivity	95%	20%	50%
Low-sensitivity	70%	70%	0%

[a] No-CCS-NH_3 2050 assumes 85% reduction of SO_2 for point emissions and 50% reduction for area emissions while the point and area emissions of other scenarios are reduced by the same reduction rate of their scenarios.

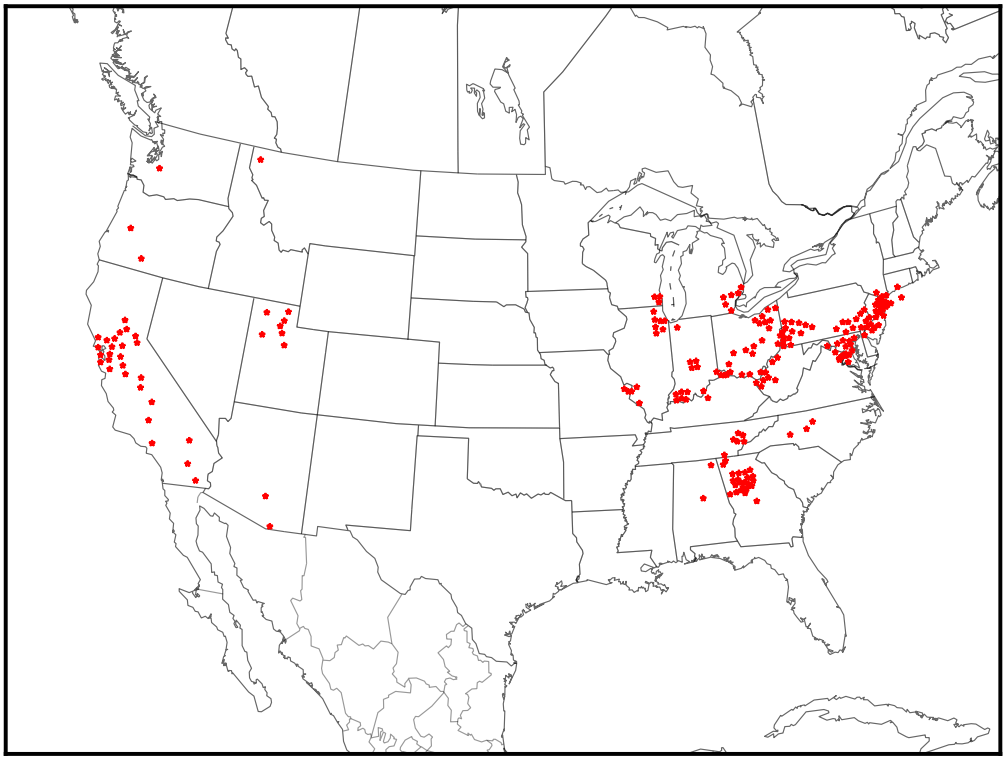

Figure A-4: $PM_{2.5}$ nonattainment areas in the CAMx domain. Red squares show the CAMx grid cells that correspond to $PM_{2.5}$ nonattainment counties designated for 1997 and 2006 standards, representing $PM_{2.5}$-burdened areas. The 1997 annual $PM_{2.5}$ standard required the 3-year average of annual mean PM concentrations under 15 $\mu g/m^3$ and the 3-year average of the annual 98th percentile 24-hour concentrations under 65 $\mu g/m^3$. In 2006, U.S. EPA strengthened the 24-hour standard to 35 $\mu g/m^3$. In 2012, the annual standard was tightened to 12 $\mu g/m^3$.

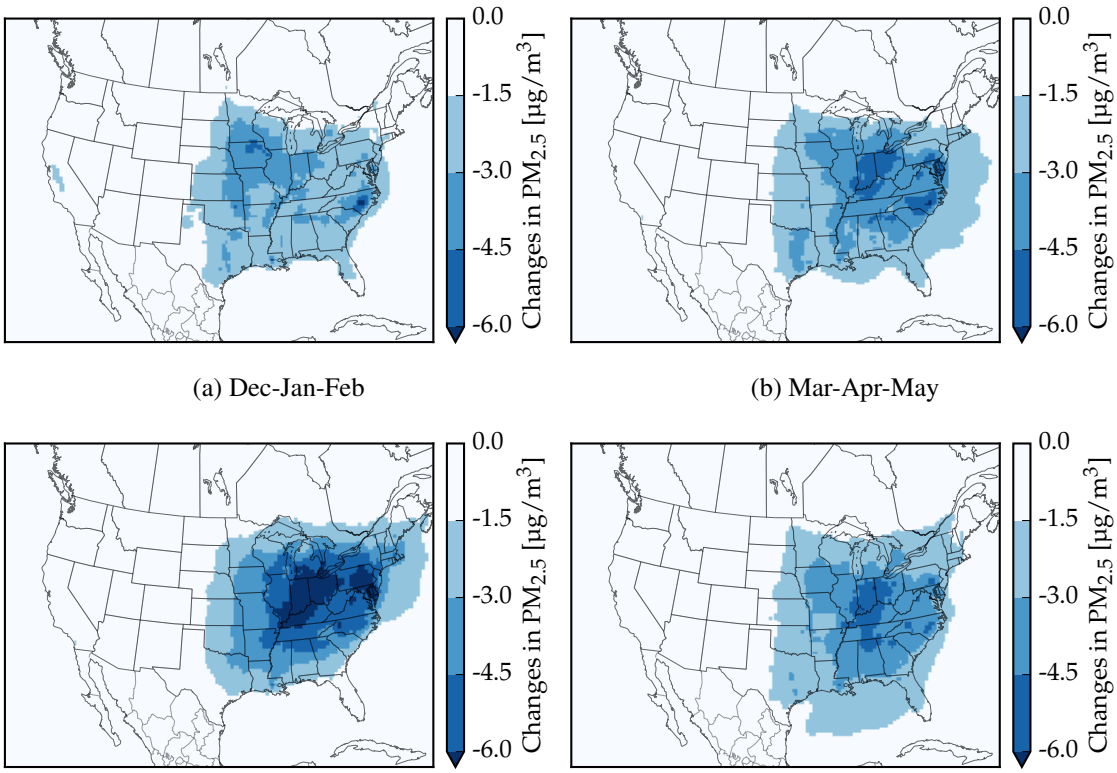

(a) Dec-Jan-Feb

(b) Mar-Apr-May

(c) Jun-Jul-Aug

(d) Sep-Oct-Nov

Figure A-5: Projected air quality improvements in 2050 under No-CCS-NH_3 2050 scenario relative to Current.

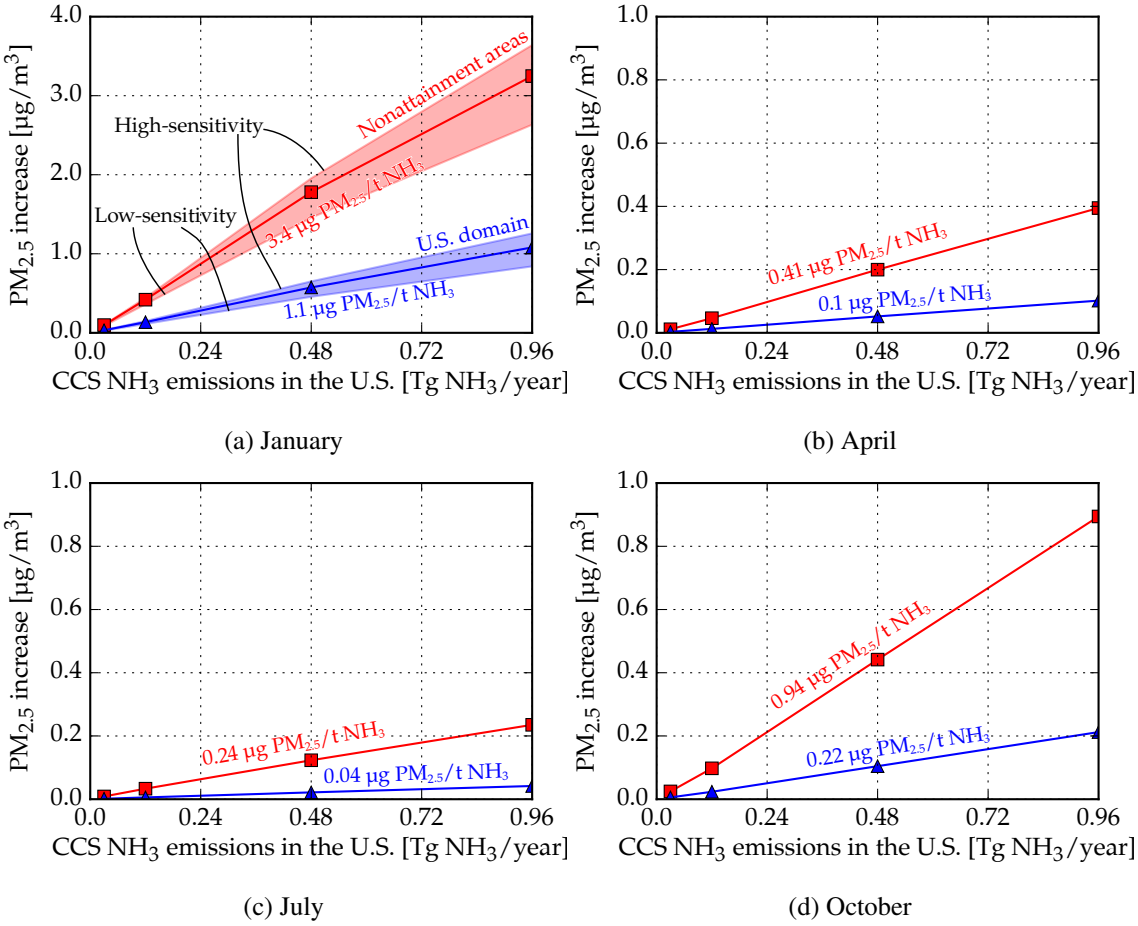

Figure A-6: Sensitivity analysis of $PM_{2.5}$ increase resulting from CCS ammonia to future levels of co-pollutants (SO_2, NO_x, and non-CCS NH_3) and the amount of ammonia emitted by amine scrubbing. Low-sensitivity and High-sensitivity cases were done only for January. $PM_{2.5}$ increase by CCS ammonia is linear over a wide range. (a) is the same as Figure 5 and presented here again for an easy comparison.

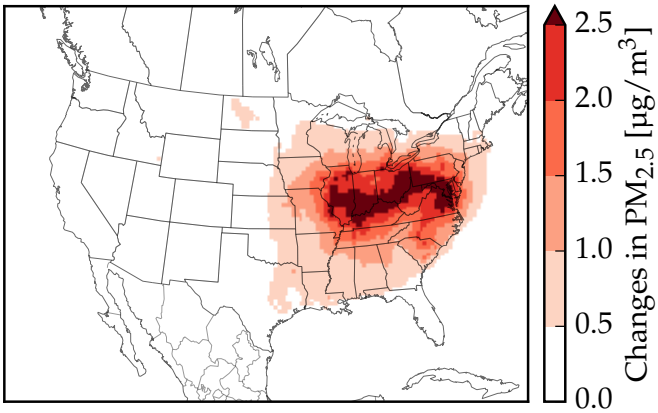

(a) CCS-NH_3 2050 (Basecase)

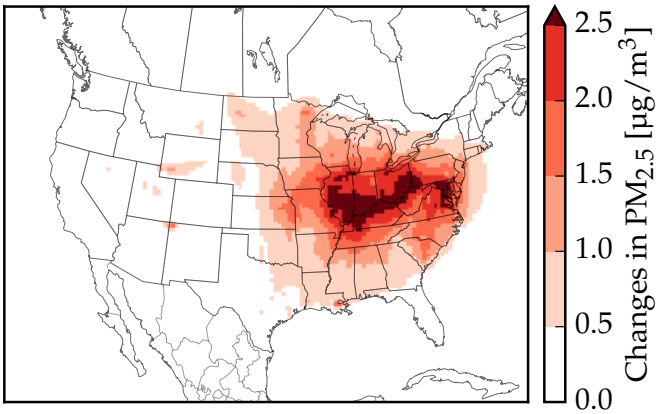

(b) CCS Ammonia added to large NO_x point sources

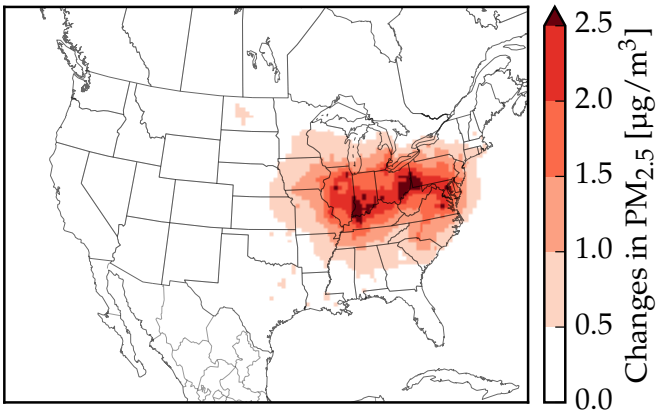

(c) 2°C temperature increase

Figure A-7: $PM_{2.5}$ concentrations increased by CCS ammonia in January. The results of sensitivity cases (b) and (c) do not show a big difference in the magnitude and spatial distribution of the $PM_{2.5}$ increase.

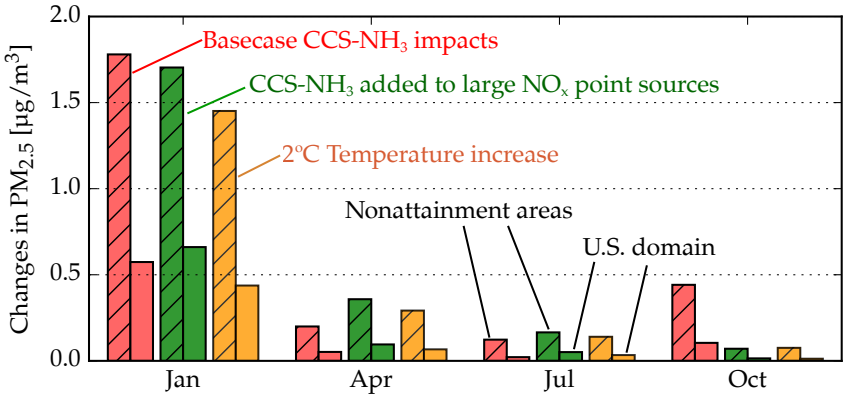

Figure A-8: Sensitivity cases of adding CCS ammonia to large NO_x point sources and of 2°C temperature increase. The results show modest differences in January, when the CCS ammonia impacts are the most important.

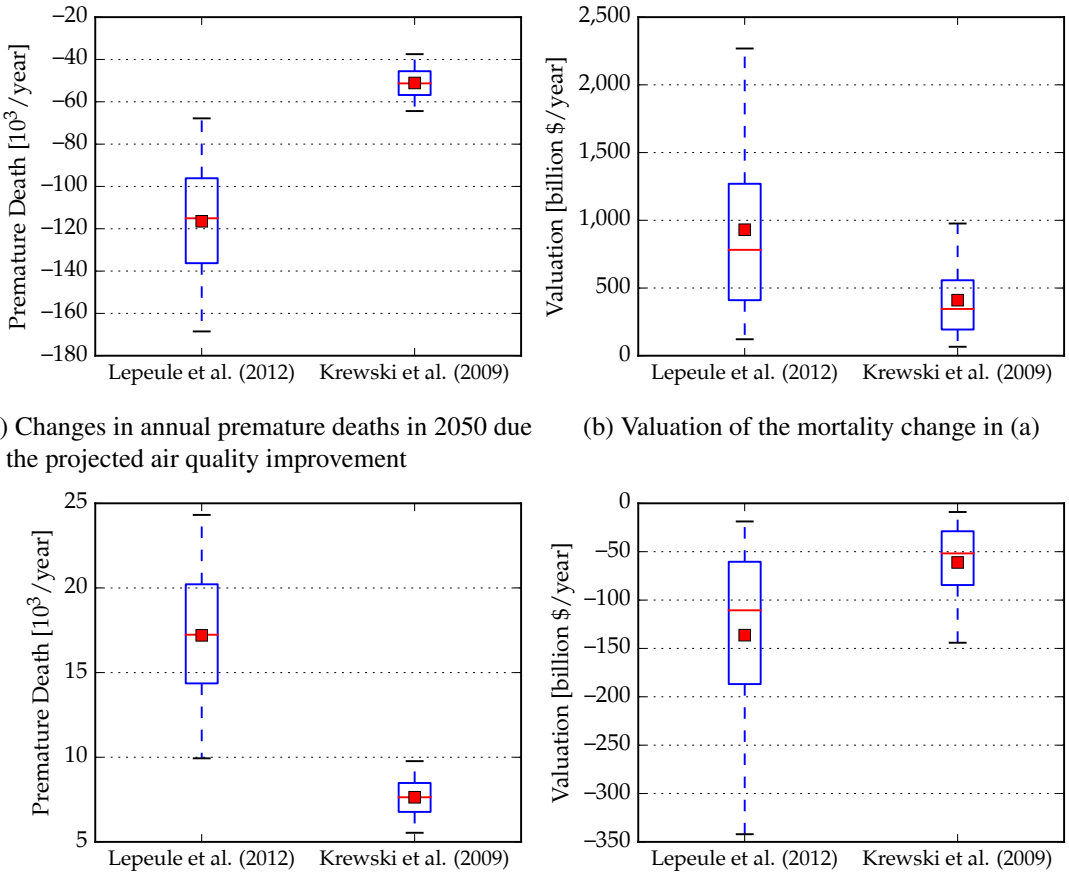

(a) Changes in annual premature deaths in 2050 due to the projected air quality improvement

(b) Valuation of the mortality change in (a)

(c) Changes in annual premature deaths in 2050 due to the ammonia emissions from CCS

(d) Valuation of the mortality change in (c)

Figure A-9: Estimated changes in premature deaths from the $PM_{2.5}$ changes based on two epidemiological studies and their valuations. Box and whiskers represent only the uncertainties surrounding the concentration-response relations and the value of a statistical life. The top and the bottom of a box are 25th and 75th percentiles, and the middle band is the median. The whiskers show 90% confidence intervals and the red squares in the boxes show the means of the estimates.

Table A-2: Summary of simulation results.

Scenario	January		February		March		April		May		June		July		August		September		October		November		December	
	All[a]	NA[b]	All	NA	All	NA	All	NA	All	NA	All	NA	All	NA	All	NA	All	NA	All	NA	All	NA	All	NA
Current	6.98	11.51	8.21	14.88	6.39	11.95	5.40	9.67	5.63	10.43	6.79	12.83	6.61	13.18	7.17	14.17	7.04	12.45	5.96	10.99	4.96	9.65	5.55	11.02
No-CCS-NH_3 2050	5.52	9.43	6.13	11.96	4.62	8.84	3.84	6.66	3.97	6.92	4.54	7.93	4.76	8.48	5.17	9.31	4.93	8.51	4.21	7.84	3.81	7.35	4.48	9.09
CCS-NH_3 2050	6.09	11.21	6.75	14.06	4.83	9.75	3.89	6.86	4.01	7.07	4.57	8.04	4.79	8.60	5.19	9.43	4.97	8.68	4.32	8.28	3.95	7.90	5.01	11.10
No-CCS-NH_3-T[c]	4.87	8.40					3.57	6.13					4.59	8.02					3.96	7.32				
CCS-NH_3-T[c]	5.31	9.85					3.60	6.27					4.60	8.09					4.03	7.61				
CCS-NH_3-N[d]	6.18	11.14					3.89	6.83					4.78	8.55					4.31	8.20				
CCS-NH_3 D0.0625[e]	5.55	9.53					3.84	6.67					4.77	8.49					4.22	7.86				
CCS-NH_3 D0.25[f]	5.65	9.85					3.85	6.71					4.77	8.51					4.24	7.94				
CCS-NH_3 D2.0[g]	6.60	12.68					3.94	7.05					4.81	8.72					4.42	8.73				
No-CCS-NH_3 High[h]	5.21	8.67																						
CCS-NH_3 H0.0625[i]	5.24	8.77																						
CCS-NH_3 H0.25[j]	5.36	9.11																						
CCS-NH_3 H2.0[k]	6.47	12.31																						
No-CCS-NH_3 Low[l]	5.82	10.25																						
CCS-NH_3 L0.0625[m]	5.85	10.34																						
CCS-NH_3 L0.25[n]	5.94	10.61																						
CCS-NH_3 L2.0[o]	6.67	12.88																						

[a] average $PM_{2.5}$ concentrations in contiguous U.S. land areas, [b] average $PM_{2.5}$ concentrations in nonattainment areas, [c] the scenario of 2° temperature increase, [d] the scenario of adding CCS NH_3 at large NO_x sources, [e] the scenario of adding 6.25% NH_3 of CCS-NH_3 2050, [f] the scenario of adding 25% NH_3 of CCS-NH_3 2050, [g] the scenario of adding 200% NH_3 of CCS-NH_3 2050, [h] the High-sensitivity No-CCS-NH_3 scenario, [i] the scenario of adding 6.25% NH_3 of CCS-NH_3 2050 to No-CCS-NH_3 High, [j] the scenario of adding 25% NH_3 of CCS-NH_3 2050 to No-CCS-NH_3 High, [k] the scenario of adding 200% NH_3 of CCS-NH_3 2050 to No-CCS-NH_3 High, [l] the Low-sensitivity No-CCS-NH_3 scenario, [m] the scenario of adding 6.25% NH_3 of CCS-NH_3 2050 to No-CCS-NH_3 Low, [n] the scenario of adding 25% NH_3 of CCS-NH_3 2050 to No-CCS-NH_3 Low, [o] the scenario of adding 200% NH_3 of CCS-NH_3 2050 to No-CCS-NH_3 Low.

Table A-3: Summary of uncertainties

	All domain	Nonattainment Area
Future CCS NH_3 emissions (January)[a]	$1.1\,\mu g/tNH_3$	$3.4\,\mu g/tNH_3$
Future co-pollutants emissions (January)[a]	$-20\,\%$ to $+13\,\%$	$-18\,\%$ to $+10\,\%$
$2\,^{\circ}C$ temperature increase from climate change (January)[a]	$-24\,\%$	$-18\,\%$
CCS NH_3 emitted at NO_x point sources (January)[a]	$-4\,\%$	$+15\,\%$
Concentration-Response (Krewski et al, 2009)[b]	$-33\,\%$ to $+33\,\%$	
Concentration-Response (Lepeule et al, 2012)[b]	$-50\,\%$ to $+57\,\%$	
Value of a Statistical Life[b]	$-90\,\%$ to $+160\,\%$	

[a] based on sensitivity CAMx simulations
[b] based on 95% confidence intervals

Chapter 3. Building Computationally Efficient Models for Air Pollution Social Impacts from Chemical Transport Models

Abstract

Though essential for informed decision-making, it is challenging to estimate the public health impacts of air quality because any analysis must address the complicated atmospheric processes that determine the concentrations of air pollutants: emissions, dispersion, chemistry, and removal. Employing a chemical transport model (CTM), the most rigorous way to address the atmospheric processes, is expensive from a computational standpoint and, therefore, beyond the reach of policy analysis for many types of problems. On the other hand, current reduced-form tools used for policy analysis fall short of the rigor of CTMs and may lead to biased results. To address this gap, we developed the Estimating Air Pollution Impacts Using Regression (EASIUR) method, which builds parameterizations that predict per-tonne social cost and intake fraction at any location in the United States. The prediction performance is similar to a CTM but it requires negligible computation cost. With tagged CTM simulations, the EASIUR method builds a dataset of air quality impacts for a large number of representative emissions sources in the United States and then derives parameterizations for those results. As a proof-of-concept, we performed tagged simulations for elemental carbon and sulfur dioxide emissions from 100 source locations and developed regression models to explain the resulting social costs and intake fractions as a function of exposed population and other key atmospheric variables. We presented two methods of characterizing exposed population: the population ring method and the average plume method. While both methods perform well, the average plume method produced better

parameterizations with the adjusted R^2 of 0.97 for elemental carbon and 0.91 for sulfur dioxide. We also explore the effect of meteorological variability on the proposed impacts and the length of simulations required to average over this variability. Lastly, we also determine the level of emission perturbations to a CTM that may be considered "marginal". The EASIUR method will help tap the latest atmospheric science for application in policy research.

3.1 Introduction

Accurate estimation of the impact of air quality on society is valuable to decision making. Human activities such as generating electricity, heating and cooling, and transportation cause air pollution, imposing burdens on humans and the natural environment. In 2010, ambient particulate matter pollution was the 9th leading burden of disease in 2010 globally (Lim et al., 2012) and the 8th in the United States (US Burden of Disease Collaborators, 2013). Fine particulate matter ($PM_{2.5}$) is strongly related with cardiovascular health effects and cardiopulmonary morbidity and mortality (Pope and Dockery, 2006). Ambient $PM_{2.5}$ is composed of primary (directly emitted) and secondary (chemically produced from gaseous precursors) species. The major precursors for secondary $PM_{2.5}$ include sulfur dioxides (SO_2), nitrogen oxides (NO_x), ammonia (NH_3), and volatile organic compounds (VOCs). Accurate estimation of public health effects from these pollutants would help society better understand the life-cycle costs of human activities, assisting in making decisions on how to control them by weighing associated costs and benefits to society's welfare.

A common metric for the impact on human and natural environment is the monetized social cost of air quality estimated based on the bottom-up assessment that follows the impact pathway of certain emissions to their ultimate consequences (Spadaro and Rabl, 1999). This is a standard method used by U.S. EPA in the benefit-cost analysis reports of the Clean Air Act

(U.S. EPA, 1999, 2011e) and many other regulatory impact analyses. According to the impact pathway analyses (National Research Council, 2010; U.S. EPA, 1999, 2011e), premature mortality associated with $PM_{2.5}$ accounts for more than 90% of the monetized damages of air quality on public health and the environment. The social cost of certain emissions varies substantially largely depending on how the emissions form $PM_{2.5}$ and how many people are exposed to the created $PM_{2.5}$.

Figure 3-1 illustrates the steps involved in the pathway analysis focused on the $PM_{2.5}$ impact on premature death. It starts with estimating the changes in $PM_{2.5}$ concentrations from a given emissions based on an air quality simulation. Epidemiological studies present the so-called concentration-response relations, from which the changes in mortality resulting from the changes in $PM_{2.5}$ concentrations are estimated. Finally, based on the Value of a Statistical Life (VSL), which is people's willingness to pay to avoid the risk of premature death, the health effects are monetized.

Another common metric is the intake fraction, which has been widely used in exposure analysis research (Bennett et al., 2002). For atmospheric emissions, the intake fraction is the fraction of emissions that are inhaled by an exposed population. While the social cost involves the estimation of air pollutant exposure to health effects and the valuation of the effects, the intake fraction is focused on characterizing the emissions-to-intake relationship.

The most rigorous way to perform the air quality simulation step in

Figure 3-1 would be to employ a state-of-the-science chemical transport model (CTM). A CTM is a numerical computer simulation that simulates the emissions, transport, chemical reactions, and removal processes of atmospheric particles and gases with detailed spatial and temporal resolution. Compared to simpler air quality models discussed below, CTMs usually simulate air quality consistent with up-to-date science and with detailed representations of the physical and chemical processes. With CTMs, it is common to use a 'brute-force' method to

estimate the air quality for a technology or policy measure, which runs a CTM twice, once for a base case and again for an alternative case with different input, e.g. changed emissions under a new policy. The CTM results for the two cases are compared to estimate the changes in air quality.

But employing a CTM often involves an high computational cost; for example, simulating the air quality of the United States for one day with a CTM, Comprehensive Air Quality Model with extensions (CAMx), at a spatial resolution used for regulatory impact assessment takes about 8 hours with one CPU on a GNU/Linux workstation (ENVIRON, 2012). Therefore, it is simply infeasible to run a CTM hundreds or more times for uncertainty analysis, optimization, and the like, which are often necessary in technology assessment and policy research.

Due to CTM's computational requirements, several computationally efficient, reduced form models have been developed. The Climatological Regional Dispersion Model (CRDM) (Latimer, 1996) is a widely used one. Popular social cost tools like the Air Pollution Emission Experiments and Policy Analysis Model (APEEP) and AP2 (Muller and Mendelsohn, 2007; Muller, 2011), Co–Benefits Risk Assessment screening model (COBRA) (U.S. EPA, 2013), and regression models for power plants (Levy et al., 2009) are derived from CRDM simulations. Addressing key atmospheric processes, CRDM estimates the contributions of emissions from a given "source" county to annual-average $PM_{2.5}$ concentrations at all other (~3,000) "receptor" counties in the United States. Based on CRDM, APEEP provides in a spreadsheet the social cost estimates, in terms of dollar per ton of emissions, for all counties in the United States for primary $PM_{2.5}$, PM_{10}, sulfur dioxide, nitrogen oxides, ammonia, and VOCs. According to our back-of-the-envelope calculation, assuming 8 CPU-hours per simulation day, it would take about 6,000 CPU-years to generate the APEEP social costs with CAMx in a brute-force way.

Despite their computationally efficiency, however, CRDM's atmospheric algorithms have limitations. First, its time resolution may be overly simple for air quality health impact analysis. Using annual-average meteorological input and emissions, CRDM may not be able to describe the formation of inorganic PM, which involves atmospheric oxidation and sensitive thermodynamic interactions among inorganic species (Ansari and Pandis, 1998; Blanchard et al., 2000; West et al., 1999) as well as the transport and removal processes. All of these processes, notably the thermodynamic interactions that control inorganic $PM_{2.5}$ formation, are nonlinear and depend strongly on seasonal, synoptic, and diurnal variability in the atmosphere. Furthermore, CRDM's treatment of organic PM assumes that it is composed mostly of primary organic PM, which it treats as non-volatile and inert, with a smaller contribution of secondary organic PM formed based on total VOC emissions (Grosjean and Seinfeld, 1989). This treatment is now outdated as of today's understanding. It has been found that a substantial part of primary organic PM evaporates and some of the evaporated organic species return to the particle phase (Robinson et al., 2007). It was also found that, contrary to previous modeling, organic PM is predominantly secondary rather than primary (Goldstein and Galbally, 2007; Zhang et al., 2007) and that intermediate volatile organic compounds, formerly unrecognized source of organic PM, are found to be very potent in forming secondary PM (Robinson et al., 2007), challenging the validity of using the total VOC as a predictor of secondary organic PM. Lastly, CRDM's county-based spatial resolution would be too coarse for big counties. Especially, since the size of counties in the western states of the U.S is much bigger than others, CRDM may not work well for the western states.

There are also reduced-form models built based on CTMs, but the computational limitations of CTMs necessarily limits their spatial and sectoral resolution. The Response Surface Model (RSM) (U.S. EPA, 2006) was developed by applying a multidimensional kriging method to a dataset of $PM_{2.5}$ concentrations, which was estimated by the Community Multi-scale Air

Quality (CMAQ) model (Byun and Schere, 2006) for a comprehensive set of different emissions combinations. However, the RSM can estimate the changes in $PM_{2.5}$ concentrations only for 12 sectors emissions in nine urban areas and the rest continental U.S, though the RSM makes CTM-like predictions. There are also regression models built using 40 CMAQ runs that predict with the size of nearby population $/ton health impacts of power plants in some parts of the U.S. (Buonocore et al., 2014), but their models were not tested outside of its subject power plants and their regions.

Our goal is to overcome these limitations and produce estimates of social cost with the high spatial resolution of APEEP but based on a state-of-the-art CTM. Our new method estimates the per-tonne social cost and the intake fraction with a prediction performance similar to a state-of-the-science CTM but without a high computational requirement. Having the same spatial resolution of its underlying CTM, it produces spatially better estimates than the county-based resolution of CRDM-based models. We also wanted to build a model that is not only simple and easy to use but also intuitive and interpretable, so that it does not work as a black box. We refer to this new method as Estimating Air Pollution Social Impacts Using Regression (EASIUR). The basic approach is to generate a dataset of per-tonne social cost and intake fraction with 'tagged' CTM simulations (further described below) and to parameterize the health impacts using regression.

In this paper, we present the method of building the EASIUR method. Based on a dataset created by running a set of simulations with a state-of-the-science CTM, the EASIUR model is generated by parameterizing the societal impacts of air quality in terms of dollar per tonne of emissions and the intake fraction with population and key atmospheric variables. The model is focused on estimating the societal impacts from a marginal change in emissions because new policy or technology often involves such marginal changes, and this is a commonly used metric. As a proof-of-concept, this study focused on the method development

focused on the health impact of the area emissions of elemental carbon and sulfur dioxide in a July time period. All the monetary values in this paper are reported in year 2010 U.S. dollar unless otherwise noted.

3.2 Method

3.2.1 Overview

We used a regional-scale three-dimensional chemical transport model, the Comprehensive Air Quality Model with extensions (CAMx) (ENVIRON, 2012), to generate a database of air pollution impact measures (per-tonne social cost and intake fraction) for elemental carbon and sulfur dioxide for 100 representative locations in the United States. Then, we sought simple regression approaches that explain the variability in these impacts based on surrounding population as well as atmospheric variables that characterized chemistry and dispersion. We tried two approaches to characterize the $PM_{2.5}$ exposures resulting from a given emissions. The first is based simply on population within certain distances from the given emissions source but does not rigorously account for the lower $PM_{2.5}$ concentrations and exposures further away from a given source. The second approach remedies this limitation by constructing average plumes from simulation results to account for the complex spatial distribution of $PM_{2.5}$ concentrations downwind from a source. In addition, we analysed how the changes in $PM_{2.5}$ concentrations and per-tonne social costs changes over different time periods, which may provide a guideline for the simulation period relevant for public health impact analysis.

3.2.2 The CAMx Chemical Transport Model

We used an air quality modeling platform, CAMx (U.S. EPA, 2011a), developed for a major regulatory impact analysis of U.S. EPA (U.S. EPA, 2011d). CAMx simulates the formation,

chemical transformation, transport and removal processes of primary and secondary $PM_{2.5}$ and their precursors (ENVIRON, 2012). We ran CAMx version 5.41 (ENVIRON, 2012) instead of version 5.3 that was originally used in the platform. Besides a few bug fixes, this version is essentially the same as version 5.3, because we used the same chemistry configuration as in the original platform. The modeling platform has been comprehensively evaluated and showed good performance of estimating the $PM_{2.5}$ concentrations associated with elemental carbon and sulfur dioxides, the species of our interest in this study, as well as other major species (U.S. EPA, 2011a).

The platform domain covers the contiguous United States and adjacent Mexico and Canada with a horizontal grid resolution of 36 km × 36 km and 14 vertical layers reaching up to 100 mb (about 16 km), which is fine enough for $PM_{2.5}$ public health impact analysis (Thompson et al., 2014; Thompson and Selin, 2012). The emission inventory (U.S. EPA, 2011b) represents year 2005 emissions, which also includes emissions from adjacent Mexico and Canada. Meteorological input data for year 2005 were simulated by MM5 (Grell et al., 1995). The initial and boundary conditions were provided by GEOS-Chem (version 7-04-11), a global-scale chemical transport model (http://acmg.seas.harvard.edu/geos/).

In order to maximize our computing resources, we used a CAMx analysis module, the Particulate Matter Source Apportionment Technology (PSAT) (Koo et al., 2009). PSAT is a tagged species method, which "tags" and then tracks the fate of specific emissions to calculate their contributions to $PM_{2.5}$ concentrations at downwind receptor locations. With PSAT, we could simulate the changes in $PM_{2.5}$ concentrations from increased emissions of elemental carbon and sulfur dioxides in many locations in a single CAMx run. PSAT reduced both computation time and disk space by a factor of 10 compared to a common brute-force method.

3.2.3 Calculation of Social Cost and Intake Fraction

3.2.3.1 Social Cost

We used a standard impact pathway method to calculate the per-tonne social cost as shown in Figure 3-1. Once a CTM calculates the changes in $PM_{2.5}$ concentrations on annual average ($\Delta c_{x,y}$, in μg m^{-3}) at each grid cell (x, y) of the simulation domain from given emissions, the changes in mortality ($\Delta y_{x,y}$, in # of premature deaths) can be estimated by a health-impact function, Eq. (1), which has a log-linear functional form derived from epidemiological studies (Hubbell et al., 2009; Abt Associates Inc., 2010, Appendix C).

$$\Delta y_{x,y} = y^0_{x,y} \cdot \left\{1 - \frac{1}{\exp\left(\beta \cdot \Delta c_{x,y}\right)}\right\} \quad (1)$$

where $y^0_{x,y}$ is the baseline mortality at (x, y), which is the product of the baseline mortality rate and the population at (x, y). β is the concentration-response relation defined as follows:

$$\beta = \frac{\ln R}{10} \quad (2)$$

where R is the relative risk reported by epidemiological studies, that is, the changes in mortality rate over a $PM_{2.5}$ increase of 10 $\mu g/m^3$.

As our basis, we used the relative risk of 1.06 (95% confidence interval (CI): 1.04-1.08) reported by Krewski et al. (2009) (The random effects Cox Model for all causes in their Commentary Table 4). However, we parameterized the relative risk in our models to cover the 95% confidence intervals reported by Krewski et al. (2009) as well as Lepeule et al. (2012), which reported the relative risk of 1.14 (95% CI: 1.07-1.22). The two studies are the latest follow-up studies respectively from two landmark cohort-based studies of $PM_{2.5}$ impacts on mortality, the American Cancer Society (ACS) and the Harvard Six Cities (H6C) studies.

The two cohorts have different characteristics (Krewski et al., 2003). The ACS cohort is much larger and cover broader geographical areas than the H6C cohort that were enrolled

from a small number of eastern U.S. cities, which are more SO_2 burdened from coal burning than the west. But the H6C cohort is randomly sampled and, therefore, represents the U.S. population better while the ACS cohort is biased toward better educated and more affluent than average. Because the H6C areas are more focused on eastern U.S., the H6C relative risk may not be good for nationwide estimation, especially producing biased estimates in the west. Conversely, ACS-based estimates may be biased in the east (Fann and Risley, 2013).

The next step is the valuation of the changed mortality using VSL (V, in $). The per-tonne social cost (S, in $/t) is calculated as follows:

$$S = \frac{\sum_{x,y} \Delta y_{x,y} \times V}{E} \quad (3)$$

where E is the amount of emissions in metric ton. We used $8 million for VSL in our analysis. This is the mean of a VSL distribution based on 26 VSL studies, which a U.S. EPA economic analysis guideline recommends (U.S. EPA, 2010). This VSL is based on 1990 income level. For a given year, income growth needs to be accounted for because the elasticity of the willingness-to-pay is positive, or people are willing to pay more to avoid a premature death as their income increases (U.S. EPA, 2010). We provided U.S. EPA's standard income growth adjustment factors together with GDP deflators in Table B-11. We did not discount for delayed timing of premature death after being exposed to $PM_{2.5}$ because Schwartz et al. (2008) showed the effects of $PM_{2.5}$ on mortality occur immediately, within two years.

3.2.3.2 Intake Fraction

The intake fraction (iF, in ppm) is defined as the mass ratio of emissions inhaled by exposed population. iF was calculated as follows:

$$iF = \sum_{x,y} \frac{B \cdot P_{x,y} \cdot \Delta c_{x,y}}{E} \quad (4)$$

where B is the volumetric breathing rate (m^3/person/day), $P_{x,y}$ is the population at (x, y), and $\Delta c_{x,y}$ and E are the same as in Eqs. (1) and (3). For EC, an inert primary species, it is the mass ratio of EC inhaled by population to EC emitted. For SO_2, a precursor to secondary PM, it is the ratio of $PM_{2.5}$ formed from SO_2 and inhaled by population to the amount of SO_2 emitted on a mass basis. We used a population mean breathing rate of 14.6 m^3 /person/day for B, which we derived by weighting U.S. EPA's recommended long-term age-specific breathing rate (U.S. EPA, 2011c) with 2010 US Census population.

3.2.4 Generating a Regression Dataset from Air Quality Simulations

We built a set of social costs and intake fractions for 100 CAMx source grid cells that are randomly selected based on their population. The size of an exposed population would be the largest contributor to the variability of social costs, and the selected locations would represent the different size of population across the domain. We ran CAMx to estimate the per-tonne social costs and intake fractions at the 100 locations as described in Section 3.3.2.3.

First, we mapped the 2010 block-level U.S. Census data to the CAMx spatial grid using the PopGrid software version 4.3 (available at http://www.epa.gov/air/benmap/). We created two population grids that match the ages of the cohorts of the two studies: one has population of 30 year old or older, matching the cohort of the ACS study, and the other has population of 25 year old or older, matching the H6C. Later we analyzed the difference from these two population sets, but the selection of the 100 source grid cells for CAMx simulation was done based on the population of 30 years and older.

Second, we selected two sets of 50 CAMx source cells randomly based on the CAMx population grid as shown in Figure 3-2. One set was used for building regression models and

the other for independent out-of-sample evaluation. In order to evenly spread out sample locations across different population densities, a stratified random sampling method was used; five locations were randomly selected at every 10^{th} percentile of population among non-zero population cells to select 50 locations per set. The same location was not selected for both sets. We simulated one 50-location set in one CAMx PSAT run.

Third, since we are interested in the air quality impacts from marginal emissions, we explored a range of emissions rates to see which would be considered "marginal." Above a certain size of emissions, the $PM_{2.5}$ increase per emissions may change due to nonlinearities in the chemistry (e.g. above a certain size of ammonia emissions where sulfate at a region gets fully neutralized, more PM nitrate may form for the same amount of additional ammonia emissions.) and will not be relevant for marginal emissions. If the size of additional emissions is too small for the numerical precision of CAMx, CAMx results may not be reliable, and the results will be noisy due to numerical round-off error in the computational model. We aggregated area and point source emissions at each grid cell and calculated the annual-average emissions ($\bar{E}$) of EC and SO_2 among non-zero emissions cells. Then, we ran a base case CAMx PSAT simulation for the 50 training sample locations and ran additional simulations with the emissions of $\bar{E}\times 4^k$ $(k = -4, \dots, 0)$ added at each location. Based on this sensitivity results, we chose $\bar{E}\times 4^{-2}$ as the basis of our modeling, which is 6.6 kg/day for EC and 192 kg/day for SO_2.

Then, we also ran CAMx for the test sample set with the same additional emissions of EC and SO_2 and the social costs and intake fractions were calculated for the test set. In the end, we have calculated the per-tonne social costs and the intake fractions of the 100 locations. Later, we explored regression models that best predict the per-tonne social costs and the intake fractions calculated here.

Each simulation was done for a 40-day period of June 21 to July 30, but we discard the first 10 days (June 21-30) of results to avoid the results from being distorted from initial conditions and used only the July 30-day output for our analysis. Since EC is inert, we added the marginal emissions of both EC and SO_2 at the same run. The changes in $PM_{2.5}$ from EC emissions were calculated only with EC concentrations, but the changes in $PM_{2.5}$ from SO_2 were calculated by comparing the sum of CAMx $PM_{2.5}$ species though SO_2 would not actively react with others in summer time (Ansari and Pandis, 1998; Blanchard et al., 2000; West et al., 1999).

In addition, we analyzed how the changes in $PM_{2.5}$ concentrations and social costs change over different lengths of simulation. Even with PSAT, running a CTM is computationally expensive. This analysis will guide the length of CTM simulation that would sufficiently represent the public health impacts.

3.2.5 Model Development with Regression

In the air quality impact estimation, it is crucial to characterize how people would be exposed to $PM_{2.5}$ created by certain emissions. The closer a population to the emission source, the higher the $PM_{2.5}$ concentrations they would usually be exposed to, with the details depending on prevailing wind direction, wind speed, as well as chemical factors governing $PM_{2.5}$ formation. However, because a substantial fraction of $PM_{2.5}$ may be transported over hundreds kilometer or more, we need to include the large number of people in a large downwind region. The degree and shape of $PM_{2.5}$ concentrations will vary by atmospheric conditions and the characteristics of an air pollutant in question.

We built linear regression models with two methods to describe exposed downwind populations. The first, simpler approach uses as explanatory variables population sizes within certain radii from the emissions source. The second, more detailed approach uses an exposed

population metric that is calculated by weighting population around the emissions source based on expected $PM_{2.5}$ concentrations using an "average plume" constructed from CTM outputs.

We also included atmospheric variables in regression for both population methods. Atmospheric variables may explain the conditions associated with $PM_{2.5}$ formation, dilution, and removal. We tried to choose the variables that are commonly available and familiar to potential users.

We used the Akaike information criterion (AIC), a metric of comparing the quality of different regression models, to select a model from a pool of potential model specifications. We present out-of-sample evaluation based on fractional bias and fractional error, which are common performance evaluation metrics for air quality models (Morris et al., 2005). They are good metrics to evaluate a wide range of estimates because the fractional bias and the fractional error are bounded between -200% to +200% and 0-200%, respectively. They are defined as follows:

$$\text{Fractional Bias} = \frac{2}{N}\sum_{i}^{N}\frac{P_i - O_i}{P_i + O_i} \tag{5}$$

$$\text{Fractional Error} = \frac{2}{N}\sum_{i}^{N}\left|\frac{P_i - O_i}{P_i + O_i}\right| \tag{6}$$

where P_i are the social costs or intake fractions predicted from our regression model for the test samples, O_i are those computed directly from the CTM results, and N is the number of training samples. Using the criteria of Morris et al. (2005), a model is considered 'excellent' with fractional bias $\leq 15\%$ and fractional error $\leq 35\%$, 'good' with fractional bias $\leq 30\%$ and fractional error $\leq 50\%$, and 'average' with fractional bias $\leq 60\%$ and fractional error $\leq 75\%$. Additionally, we also report the normalized mean bias and the normalized mean error:

$$\text{Normalized Mean Bias} = \frac{\sum_i^N (P_i - O_i)}{\sum_i^N O_i} \quad (7)$$

$$\text{Normalized Mean Error} = \frac{\sum_i^N |P_i - O_i|}{\sum_i^N O_i} \quad (8)$$

3.2.5.1 Population Ring Method

This method explores whether simple population variables and atmospheric variables can explain the health impacts. The basic regression model has the following log-linear form:

$$\ln S = \alpha + \sum_i \beta_i \ln P_i + \sum_j \gamma_j \ln A_j, \quad i = 1, \dots, n, j = 1, \dots, m, \quad (9)$$

$$\ln iF = \alpha + \sum_i \beta_i \ln P_i + \sum_j \gamma_j \ln A_j, \quad i = 1, \dots, n, j = 1, \dots, m, \quad (10)$$

where α, β_i's, and γ_j's are regression coefficients. S is the per-tonne social cost at a given location, iF is the intake fraction. P_i is a population ring, the size of population between two distances from source, r_{i-1} and r_i, with $r_1 = 0$ (further discussed below). A_j's are atmospheric variables, for which we tried surface atmospheric pressure, temperature, wind speed, precipitation, and humidity. A_j values are from at the surface layer of the CAMx grid at an emission source cell, which are averaged over the simulation period, i.e. 30 days. We assumed that atmospheric conditions at a source cell represent the conditions of area affected by emissions.

We explored the number of population variables P_i from one to three by increasing the size of r_i by a step of 36 km, a unit cell size of the CAMx grid, up to 30×36 km. For one-ring models, we varied r_i from 1 to 30 steps (or 30×36 km). For two-ring, r_1 was varied from 1 to 10 steps and r_2 from r_1 to 30 steps. For three-rings, r_1 was varied from 1 to 10 steps, r_2 from r_1 to 20, and r_3 from r_2 to 30. When calculating population, we used the distance between grid cell centers; the whole population in one cell is counted in or not depending on the

distance between the cell's center and a source cell's center. Fitting each ring model with all the possible combinations of atmospheric variables A_j, we tried to find the number of r_i's and their values and A_j's that produce the best model performance.

3.2.5.2 Average Plume Method

The population ring method just outlined has the obvious limitation that it implicitly assumes that the people within a certain ring around the emissions source are all exposed to the same $PM_{2.5}$ perturbation. In reality, the resulting $PM_{2.5}$ exposure depends strongly on wind direction and decreases with downwind distance. An approach that divides the population ring into several wedges and treating them as separate variables was considered, but regression models quickly become complicated as the number of population variables increases. As a more rigorous alternative, we developed the average plume method.

We constructed an average plume per each pollutant from the $PM_{2.5}$ concentration plumes of the training 50 locations after aligning their average wind directions. The average plume represents the generic shape and varying intensity of $PM_{2.5}$ concentrations. By weighting population around emissions source with this plume, we derived a population variable that capture exposed population with varying degree around the emission source.

To generate the average plume, the spatial distribution of $PM_{2.5}$ concentrations for all 50 training samples were: 1) put on a common grid (a 91×91 array covering 3,276 km × 3,276 km) with the origin as the emissions source; 2) rotated so that the average wind direction is aligned to the same direction; 3) normalized so each had the same net $PM_{2.5}$ impacts. After these procedures, the 50 plumes were averaged to obtain a generic spatial distribution of $PM_{2.5}$ impacts.

When applied to calculate a weighted population, this average plume was placed at a given emissions source on the CAMx source grid and rotated by the average wind direction at the

source. Then, the weighted population was calculated by multiplying the placed average plume with the population array cell by cell.

Using the weighted plume, we fitted the following regression models:

$$\ln S = \alpha + \beta \ln P_w + \sum_j \gamma_j \ln A_j, \quad j=1, ..., m, \tag{11}$$

$$\ln iF = \alpha + \beta \ln P_w + \sum_j \gamma_j \ln A_j, \; j=1, ..., m, \tag{12}$$

where P_w is the sum of population around the emissions source weighted by the average plume, A_j's are the same atmospheric variables as in Eq. (9), and α, β, and γ_j's are the regression coefficients. With weighted population, we fitted Eqs. (11) and (12) with all the subsets of A_j's.

3.3 Results and Discussion

Table B-1 provides the summary statistics of the dataset generated for the 100 sample locations. Figure B-1 presents the correlation matrix plot of selected parameters, which were used for regression. The social costs and the intake fractions of EC and SO_2 vary substantially over about two orders of magnitude depending the location of the emissions source. The atmospheric variables in Table B-1 are the average values for July 1-30 period. They are calculated from the data taken from the lowest model layer from the meteorological fields used as CAMx inputs. Because the meteorological fields report zero humidity for some cells, we added 0.0002 g/m^3, the minimum non-zero value, to all humidity values before the natural log transformation.

As mentioned in Section 3.2.4, we calculated social costs and intake fractions at the 50 training sample locations over a wide range of emissions, 0.41-420 kg/day for EC and 12-12,300 kg/day for SO_2. If the size of perturbation is not marginal, the per-ton social costs or intake fractions will be substantially different for a different size of perturbation. However, as shown in

Figure 3-1 and B-2, the per-tonne social costs and intake fractions of both EC and SO_2 at most places do not vary much for the range except a few locations where SO_2 social cost results show signs of numerical noise for the smallest emissions perturbations. Therefore, the entire range of emissions we explored is small enough to be "marginal." The social costs and intake fractions in Table B-1 were calculated with the fixed amount of emissions, 6.6 kg/day for EC and 192 kg/day for SO_2 as described in Section 3.2.3.

While both population ring and average plume methods produced models that perform very well, regression models derived from the average plume method are better. Many of our analyses show similar results for both social cost and intake fractions because the log-linear equation of Eq. (3) for social cost is virtually linear like Eq. (4) for intake fraction to marginal changes in $PM_{2.5}$ concentrations. We mainly present the results for the social cost models and included the intake fraction results in Appendix.

3.3.1 Population Ring Regression Models

Based on the AIC, we chose the regression models presented in Table 3-1 and 3-2 for social cost models and intake fraction models, respectively. They have two population variables, one near emission source and the other far from the source. Figure 3-4 and B-3 show the goodness of fit and the out-of-sample evaluation. Both EC and SO_2 social cost models perform very well; they have a high goodness of fit as represented by their high adjusted coefficients of determination (Adj. R^2). The social cost models meet the 'excellent' performance criteria. The intake fraction models also meet the 'excellent' criteria except that the fractional error for the EC intake fraction model slightly misses the requirement for 'excellent.' The prediction intervals relative to predicted value are a big bigger than a factor of two for EC and less than a factor of two for SO_2.

The population variables show that both EC and SO_2 have a long-range impact of hundreds of kilometers. The population variables of the SO_2 model are larger than those of the EC model because SO_2 travels farther to forms PM from atmospheric oxidation than EC, which is directly emitted as PM. The radius of the first population ring of EC models for both social cost and intake fraction is 36 km and that of the second ring is 252 km while they are 180 km and 360 km for SO_2 social cost and 252 km and 972 km for SO_2 intake fraction, respectively.

Figure 3-5 and B-4 are tornado diagrams that show the sensitivity of the regression parameters. As expected, population ring variables are strongly correlated with the health impacts. For both EC and SO_2, three atmospheric variables substantially explain the variability of the impacts: atmospheric pressure, temperature, and precipitation. The atmospheric pressure is strongly positively correlated, which turned out to be a proxy of population density. Because the pressure we used is not adjusted for elevation, pressure is strongly correlated with surface elevation. The population density is generally high in the coastal areas but it is generally very low in the mountainous areas and high plains such as the Great Basin and the Great Plains. The temperature variable has a negative coefficient. With a higher surface temperature, air pollutants are mixed higher vertically and, in turn, more diluted, resulting in less population exposure to the pollutants. Precipitation is also negatively correlated because precipitation causes air pollutants to be removed by wet deposition. Humidity did not appear strong in regression, though we suspected it would in SO_2 models because atmospheric water vapor is the source of hydroxyl radical (OH^-), the dominant oxidant converting SO_2 to sulfate PM.

Figure 3-6 and B-5 present the performance of the regression models we have explored. Each point in the figures represents the performance of a model specification with the adjusted R^2 as well as the fractional bias and the fractional error calculated with the test samples. Fitting with two population rings produced better models than one population ring

for EC. For SO_2, though the best two-ring models were better than the best one-ring models, the improvement was small. For both EC and SO_2, the best three-ring models were virtually no better than the best two-ring models. Table B-2 to B-5 present the regression results of the best seven model specifications (i.e. those with lowest AIC), showing the overall composition of parameters and the coefficients of the best candidates.

3.3.2 Average Plume Models

Accounting for varying degree of $PM_{2.5}$ concentrations and dispersion by wind, weighting population with average plumes seem to better describes exposed population than population rings. Figure 3-7 shows the average plume weight for EC and SO_2. Though both plumes affect area large downwind region, the exposure resulting from EC emissions is closer to the source than for SO_2. This is because EC is emitted as PM directly while SO_2 emitted as gas takes time to form sulfate PM by atmospheric oxidation. The cumulative distributions of the average plumes in Figure 3-7 show how EC and SO_2 spread out. For EC, the average plume weight at the emission source cell (36×36 km^2) is 18%, but for SO_2, it is only 1.5%, suggesting the impact of SO_2 is hardly local. The area covering the top 50% of the impact, or the average plume weight, is about $2.9 \cdot 10^3$ km^2 for EC and $8.3 \cdot 10^5$ km^2 for SO_2. For 90%, it is about $1.8 \cdot 10^6$ km^2 for EC and about $5.6 \cdot 10^6$ km^2 for SO_2.

The average plume method further improved model performance. The best average plume models are presented in Table 3-1 and B-2 for the social cost models and intake fraction models, respectively. Figure 3-7. Average plumes constructed with the CTM results of the training samples.

Figure 3-8 and B-6 show the goodness of fit and the out-of-sample evaluation. The performance of both social cost and intake fraction models is better than that of population ring models; they have a higher goodness of fit as represented by their higher adjusted R^2 of

0.97 for EC and 0.91 for SO_2. The average plume models meet the 'excellent' criteria further than population ring models. Figure 3-7. Average plumes constructed with the CTM results of the training samples.

Figure 3-8 and B-6 show that the 95% prediction intervals (orange bars) are mostly within a factor of two for both EC and SO_2, though those of SO_2 models are larger. Figure 3-9 and B-7 show the sensitivity of social cost and intake fraction to regression parameters of average plume models. The population variable produces the widest variability for both EC and SO_2. Atmospheric variables show similar characteristics as in population ring models. Atmospheric pressure is strongly positively correlated as a proxy to population density as in the population ring models. Temperature is negatively correlated, showing its role of governing vertical mixing. Wind speed appears negatively significant in EC models, showing its negative correlation with population parameters shown in Figure B-1; the areas of high altitude are usually windy but less populated. Wind speed may also be related with its role for dispersion; the higher the wind speed, the more $PM_{2.5}$ dispersed to less weighted areas. Wind speed does not appear in SO_2 models, showing the effect of SO_2 is spread out such that local wind speed does not help the regression much. Precipitation is negatively correlated, explaining the removal by wet deposition. Humidity did not appear important for both EC and SO_2.

Each average plume model in Table 3-1 and 3-2 was chosen by AIC among 256 regression specifications per species. The performance of model specifications we explored is presented in Figure 3-10 and B-8. Table B-6 to B-9 present the regression results of the seven lowest AIC model specifications, showing the overall composition of parameters and their coefficients of best candidates.

3.3.3 Relative Risk and Adult Population

Given the uncertainty in the $PM_{2.5}$ relative risk factor, it is convenient to be able to adjust our social cost estimates upward or downward for relative risk values other than the ones we used here. We derived a relative risk adjustment factor (F_R) to adjust for a different relative risk Though the health impact function, Eq. (1), is log-linear, the function is virtually linear for the range of $PM_{2.5}$ concentrations and relative risks relevant for social costs. We calculated the social costs of the 100 sample locations for a range of relative risk (R), 1.04 to 1.22 with a step of 0.02, which covers the 95% confidence intervals for relative risks reported by the two studies, Krewski et al. (2009) and Lepeule et al. (2012). Then, for all R's, we calculated the ratio of the social cost with a relative risk (S_R) to the social cost with the relative risk of the base value ($S_{1.06}$). We found that the ratio ($S_R/S_{1.06}$) for each relative risk was almost identical among samples. As shown in Figure 3-11, we defined the relative risk adjustment factor (F_R) with the ratio, $S_R/S_{1.06}$:

$$F_R = \frac{S_R}{S_{1.06}} = -15.1 + 15.2R. \quad (13)$$

By multiplying F_R, our social cost models can be used to produce estimates for a different relative risk.

Next, we found that the social cost difference between using population of age 30 or older matching the ACS study and population of age 25 or older matching the H6C study is negligible. As shown in Figure 3-12, using the H6C-matching population produced only about 0.9% larger social costs on average than using the ACS. This result is reasonable because the baseline mortality of young adults aged 25-30 would be low and adding this value to social cost estimation would not produce much of an effect. The change stemming from the small difference in population cohort may be ignored.

3.3.4 Social Costs and the Length of the Simulation Period

We compared the 15-day simulation results to the 31-day results and did not discover a large difference between the two. Figure 3-13 presents how the $PM_{2.5}$ formation and social costs change from different simulation lengths from one day to 31 days. Figure 3-13 (a) and (b) show that the changes in $PM_{2.5}$ formation from the marginal emissions of EC and SO_2 become steady state in about 15 days, showing variability of 15% for EC and 20% for SO_2 consistently afterwards. Figure 3-13 (c) to (f) show that the $PM_{2.5}$ concentrations of the 15-day simulation are mostly <20% different from those of 31-day simulations, similar to the variability after 15 day in (a) and (b). The social costs of the 15-day simulation show somewhat bigger difference of 20-40% compared to the 31-day.

In order to analyze how the effects of simulation length on regression, we derived regression models for the 15-day simulation dataset in the same way as the 31-day. The two different periods did not produce a big difference, which is presented in Table B-10. The EC model of the 15-day has the same parameters as that of the 31-day while the SO_2 model has somewhat different parameters. However, they have very similar adjusted R^2 values. Error metrics were also similar, though the 31-day results generally have somewhat smaller errors. In summary, a 15-day simulation would be sufficient to represent the public health impacts of EC and SO_2 of the July period.

3.3.5 Summary

Combining all the results, we present social cost models and intake fraction models for EC and SO_2 here as a summary. Because the average plume method models perform better than the population ring models, we present the average plume models. The social cost models are generalized for VSL and relative risk from the regression results:

$$S_{\mathrm{EC}} = 3.7^{21} \cdot P_w^{0.75} \cdot P^{5.5} \cdot T^{-18} \cdot (C + 0.0002)^{-0.032} \cdot W^{-0.12} \cdot V \cdot F_R \qquad (14)$$

$$S_{\mathrm{SO}_2} = 1.0^{46} \cdot P_w^{0.68} \cdot P^{6.0} \cdot T^{-27} \cdot (C + 0.0002)^{-0.053} \cdot V \cdot F_R \quad (15)$$

where S_{EC} is the social cost of EC [$/t], S_{SO_2} is the social cost of SO2 [$/t], P_w is population weighted by average plume in Figure 3-7. Average plumes constructed with the CTM results of the training samples. [# of people], P is atmospheric pressure [hPa; 1 hPa = 100 Pa = 1 mb], T is temperature [K], C is precipitation [g/m^3], W is wind speed [m/s], V is the value of a statistical life [$/person] that is adjusted for dollar year and income growth (provided in Table B-11), and F_R is the relative risk adjustment factor defined in Eq. (13). Precipitation C [g/m^3] can also be converted from a more common metric of precipitation d [mm/day]: $C = 26.3 \cdot d$.

The intake fraction models are summarized as follows:

$$iF_{\mathrm{EC}} = 1.4^{25} \cdot P_w^{0.81} \cdot P^{4.5} \cdot T^{-17} \cdot (C + 0.0002)^{-0.053} \cdot W^{-0.084} \quad (16)$$

$$iF_{\mathrm{SO}_2} = 2.8^{45} \cdot P_w^{0.74} \cdot P^{5.5} \cdot T^{-25} \cdot (C + 0.0002)^{-0.083} \quad (17)$$

where iF_{EC} is the intake fraction for EC [ppm] and iF_{SO_2} is for SO_2 [ppm].

3.4 Conclusions

We proposed the Estimating Air pollution Social Impacts Using Regression (EASIUR) method that parameterize per-tonne social cost and intake fraction from a dataset generated from a chemical transport model. The treatment of atmospheric processes in current popular reduced form models such as APEEP is overly simplistic, while scientifically rigorous CTMs are computationally too expensive for practical use. By contrast, our methods predict results consistent with CTMs without requiring intensive computation. Moreover, they are easy to update as CTMs evolve with continuing scientific advancements. As a proof-of-concept, we develop impact models (social cost and intake fraction) for summertime emissions of elemental carbon and sulfur dioxide. As part of the development process, we have investigated the appropriate size of the emissions perturbations to derive “marginal” social

costs, the length of the simulations required to average over meteorological variability, and two methods for characterizing exposed populations in the regions surrounding the emissions.

We generated per-tonne social costs and intake fractions with a state-of-the-science CTM, CAMx, for 100 representative locations in the United States. In order to generate the dataset for multiple locations with one CTM run, tagged simulations were used. Next, we built linear regression models to predict the estimated public health effects with population and key atmospheric variables. The derived parameterizations show very good performance. We generalized our parameterizations for a different choice of relative risk over a range relevant to public health impacts and showed a small difference in population cohort can be ignored. In addition, we found that a 15-day CTM simulation produced social costs and parameterizations very similar to a 31-day simulation, which can be a guideline for an appropriate length of simulation for the public health analysis of air quality.

We presented two methods of characterizing exposed populations: the first is the population ring method which uses the size of the population within a certain distance from an emission source; and the second is the average plume method which weights population with a generic plume derived from CTM results. We showed that models derived from the average plume method work better. For example, the adjusted R^2 of EC social cost model improved from 0.91 to 0.97 and the fractional error from 0.35 to 0.18. The average plume models perform very well, showing a high goodness of fit (e.g. the adjusted R^2 of 0.97 for EC social cost model and 0.91 for SO_2 social cost model) and meeting an 'excellent' performance criteria based on fractional bias and fractional error from out-of-sample evaluation (Morris et al., 2005).

The EASIUR method overcomes several limitations of current models. First of all, the EASIUR parameterizations predict like an up-to-date chemical transport model, which is the most rigorous and realistic way of simulating air quality. The EASIUR model, therefore,

overcomes the limited treatment of atmospheric processes in reduced form models. Second, it is not computationally expensive like its underlying CTMs, opening the possibility for application to questions where CTMs are computationally too expensive to employ. For example, the model could be employed for policy research concerned with designing optimal emission strategies among many options, an uncertainty analysis that may require a Monte Carlo simulation over policy or technological options. Third, the EASIUR model can evolve as current understanding of atmospheric science improves because the EASIUR model is relatively easy to re-derive from an up-to-date chemical transport model. Fourth, the spatial resolution of the EASIUR model may produce more consistent estimates than county-based models built based on CRDM because county size varies substantially, something to consider especially with regards to counties in the western U.S. that may be too big to act as a single unit for social cost analysis. As an illustration, we generated with our average plume models the maps for social cost and intake fraction in Figure B-9, which provide more relevant estimates for areas in the west than county-based estimates. Figure B-9 shows our model may provide air pollution impacts on the U.S. population for emissions such as from marine vessels near coastal areas or emissions from neighboring countries. Lastly, the EASIUR model is not presented as a black box. The functional form of the model and its coefficients are intuitive, assisting model users to understand key underlying mechanisms.

As a paper focused on method development, the models presented in this paper have limitations. First, they are based only on a one-month period for July 2005. As the physical and chemical behaviors of air pollutants would change substantially season by season, future work will build models with seasonal or monthly resolution. Second, we currently built models only for EC and SO_2. These species are sufficient to illustrate that the EASIUR method can account for the $PM_{2.5}$ exposures that depend on atmospheric transport, dispersion, removal, and oxidation chemistry such as that which converts SO_2 to PM sulfate. Application

to other species is possible but will require additional work; for example, to model inorganic PM species (sulfur dioxide, nitrogen oxides, and ammonia) one needs to account for nonlinear thermodynamic interactions that control PM formation (Ansari and Pandis, 1998; Blanchard et al., 2000; West et al., 1999). Lastly, the presented models are built based on area emission sources. Since large point sources usually have tall stacks, it would be necessary to explore the role of stack characteristics such as height, flow rate, and temperature. But this is out of the scope of this paper.

In this paper, we have shown that a linear regression on tagged simulation results from a chemical transport model could produce impact models with excellent performance. The models parameterized with exposed population and basic atmospheric variables predict the public health effect of air quality like a CTM without high computational costs. The models can be of great use to policy and technology research efforts that involve air quality.

3.5 Acknowledgements

The authors thank Bonyoung Koo for providing the CAMx database and valuable advice for running CAMx. This work was supported by the center for Climate and Energy Decision Making (SES-0949710), through a cooperative agreement between the National Science Foundation and Carnegie Mellon University.

3.6 References

Abt Associates Inc.: User's Manual Appendices for the Environmental Benefits Mapping and Analysis Program, Prepared for Office of Air Quality Planning and Standards, U.S. Environmental Protection Agency. Research Triangle Park, NC., 2010.

Ansari, A. S. and Pandis, S. N.: Response of Inorganic PM to Precursor Concentrations, Environ. Sci. Technol., 32(18), 2706–2714, doi:10.1021/es971130j, 1998.

Bennett, D. H., McKone, T. E., Evans, J. S., Nazaroff, W. W., Margni, M. D., Jolliet, O. and Smith, K. R.: Defining Intake Fraction, Environ. Sci. Technol., 36(9), 206A–211A, doi:10.1021/es0222770, 2002.

Blanchard, C. L., Roth, P. M., Tanenbaum, S. J., Ziman, S. D. and Seinfeld, J. H.: The Use of Ambient Measurements To Identify which Precursor Species Limit Aerosol Nitrate Formation, J. Air Amp Waste Manag. Assoc., 50(12), 2073–2084, doi:10.1080/10473289.2000.10464239, 2000.

Buonocore, J. J., Dong, X., Spengler, J. D., Fu, J. S. and Levy, J. I.: Using the Community Multiscale Air Quality (CMAQ) model to estimate public health impacts of PM2.5 from individual power plants, Environ. Int., 68, 200–208, doi:10.1016/j.envint.2014.03.031, 2014.

Byun, D. and Schere, K. L.: Review of the Governing Equations, Computational Algorithms, and Other Components of the Models-3 Community Multiscale Air Quality (CMAQ) Modeling System, Appl. Mech. Rev., 59(2), 51–77, doi:10.1115/1.2128636, 2006.

ENVIRON: CAMx User's Guide Version 5.41, Environ International Corporation, Novato, CA., 2012.

Fann, N., Lamson, A. D., Anenberg, S. C., Wesson, K., Risley, D. and Hubbell, B. J.: Estimating the National Public Health Burden Associated with Exposure to Ambient PM2.5 and Ozone, Risk Anal., 32(1), 81–95, doi:10.1111/j.1539-6924.2011.01630.x, 2012.

Fann, N. and Risley, D.: The public health context for PM2.5 and ozone air quality trends, Air Qual. Atmosphere Health, 6(1), 1–11, doi:10.1007/s11869-010-0125-0, 2013.

Goldstein, A. H. and Galbally, I. E.: Known and Unexplored Organic Constituents in the Earth's Atmosphere, Environ. Sci. Technol., 41(5), 1514–1521, doi:10.1021/es072476p, 2007.

Grell, G. A., Dudhia, J. and Stauffer, D. R.: A Description of the Fifth-Generation Penn State/NCAR Mesoscale Model (MM5). [online] Available from: http://nldr.library.ucar.edu/repository/collections/TECH-NOTE-000-000-000-214, 1995.

Grosjean, D. and Seinfeld, J. H.: Parameterization of the formation potential of secondary organic aerosols, Atmospheric Environ. 1967, 23(8), 1733–1747, doi:10.1016/0004-6981(89)90058-9, 1989.

Hubbell, B., Fann, N. and Levy, J. I.: Methodological considerations in developing local-scale health impact assessments: balancing national, regional, and local data, Air Qual. Atmosphere Health, 2(2), 99–110, doi:10.1007/s11869-009-0037-z, 2009.

Jacobson, P. M. Z.: Air Pollution and Global Warming: History, Science, and Solutions, 2 edition., Cambridge University Press, Cambridge ; New York., 2012.

Koo, B., Wilson, G. M., Morris, R. E., Dunker, A. M. and Yarwood, G.: Comparison of source apportionment and sensitivity analysis in a particulate matter air quality model, Environ. Sci. Technol., 43(17), 6669–6675, 2009.

Krewski, D., Burnett, R. T., Goldberg, M. S., Hoover, B. K., Siemiatycki, J., Jerrett, M., Abrahamowicz, M. and White, W. H.: Overview of the reanalysis of the Harvard Six Cities

Study and American Cancer Society Study of Particulate Air Pollution and Mortality, J. Toxicol. Environ. Health A, 66(16-19), 1507–1551, doi:10.1080/15287390306424, 2003.

Krewski, D., Jerrett, M., Burnett, R. T., Ma, R., Hughes, E., Shi, Y., Turner, M. C., Pope, C. A., III, Thurston, G., Calle, E. E., Thun, M. J., Beckerman, B., DeLuca, P., Finkelstein, N., Ito, K., Moore, D. K., Newbold, K. B., Ramsay, T., Ross, Z., Shin, H. and Tempalski, B.: Extended follow-up and spatial analysis of the American Cancer Society study linking particulate air pollution and mortality, Health Effects Institute, Boston, MA., 2009.

Latimer, D. A.: Particulate Matter Source-Receptor Relationships Between All Point and Area Sources in the United States and PSD Class I Area Receptors, prepared for U.S. EPA, OAQPS, Research Triangle Park, NC., 1996.

Lepeule, J., Laden, F., Dockery, D. and Schwartz, J.: Chronic Exposure to Fine Particles and Mortality: An Extended Follow-up of the Harvard Six Cities Study from 1974 to 2009, Environ. Health Perspect., 120(7), 965–970, doi:10.1289/ehp.1104660, 2012.

Levy, J. I., Baxter, L. K. and Schwartz, J.: Uncertainty and Variability in Health-Related Damages from Coal-Fired Power Plants in the United States, Risk Anal., 29(7), 1000–1014, doi:10.1111/j.1539-6924.2009.01227.x, 2009.

Lim, S. S., Vos, T., Flaxman, A. D., Danaei, G., Shibuya, K., Adair-Rohani, H., AlMazroa, M. A., Amann, M., Anderson, H. R., Andrews, K. G., Aryee, M., Atkinson, C., Bacchus, L. J., Bahalim, A. N., Balakrishnan, K., Balmes, J., Barker-Collo, S., Baxter, A., Bell, M. L., Blore, J. D., Blyth, F., Bonner, C., Borges, G., Bourne, R., Boussinesq, M., Brauer, M., Brooks, P., Bruce, N. G., Brunekreef, B., Bryan-Hancock, C., Bucello, C., Buchbinder, R., Bull, F., Burnett, R. T., Byers, T. E., Calabria, B., Carapetis, J., Carnahan, E., Chafe, Z., Charlson, F., Chen, H., Chen, J. S., Cheng, A. T.-A., Child, J. C., Cohen, A., Colson, K. E., Cowie, B. C., Darby, S., Darling, S., Davis, A., Degenhardt, L., Dentener, F., Des Jarlais, D. C., Devries, K., Dherani, M., Ding, E. L., Dorsey, E. R., Driscoll, T., Edmond, K., Ali, S. E., Engell, R. E., Erwin, P. J., Fahimi, S., Falder, G., Farzadfar, F., Ferrari, A., Finucane, M. M., Flaxman, S., Fowkes, F. G. R., Freedman, G., Freeman, M. K., Gakidou, E., Ghosh, S., Giovannucci, E., Gmel, G., Graham, K., Grainger, R., Grant, B., Gunnell, D., Gutierrez, H. R., Hall, W., Hoek, H. W., Hogan, A., Hosgood III, H. D., Hoy, D., Hu, H., Hubbell, B. J., Hutchings, S. J., Ibeanusi, S. E., Jacklyn, G. L., Jasrasaria, R., Jonas, J. B., Kan, H., Kanis, J. A., Kassebaum, N., Kawakami, N., Khang, Y.-H., Khatibzadeh, S., Khoo, J.-P., et al.: A comparative risk assessment of burden of disease and injury attributable to 67 risk factors and risk factor clusters in 21 regions, 1990-2010: a systematic analysis for the Global Burden of Disease Study 2010, The Lancet, 380(9859), 2224–2260, doi:10.1016/S0140-6736(12)61766-8, 2012.

Morris, R. E., McNally, D. E., Tesche, T. W., Tonnesen, G., Boylan, J. W. and Brewer, P.: Preliminary evaluation of the Community Multiscale Air Quality model for 2002 over the southeastern United States, J. Air Waste Manag. Assoc., 55(11), 1694–1708, 2005.

Muller, N. Z.: Linking Policy to Statistical Uncertainty in Air Pollution Damages, BE J. Econ. Anal. Policy, 11(1) [online] Available from: http://www.degruyter.com/view/j/bejeap.2011.11.issue-1/bejeap.2011.11.1.2925/bejeap.2011.11.1.2925.xml?format=INT (Accessed 6 February 2013), 2011.

Muller, N. Z. and Mendelsohn, R.: Measuring the damages of air pollution in the United States, J. Environ. Econ. Manag., 54(1), 1–14, doi:10.1016/j.jeem.2006.12.002, 2007.

National Research Council: Hidden Costs of Energy: Unpriced Consequences of Energy Production and Use, The National Academies Press, Washington, DC. [online] Available from: http://www.nap.edu/catalog.php?record_id=12794 (Accessed 19 August 2013), 2010.

Pope, C. A., III and Dockery, D. W.: Health effects of fine particulate air pollution: lines that connect, J. Air Waste Manag. Assoc., 56(6), 709–742, 2006.

Robinson, A. L., Donahue, N. M., Shrivastava, M. K., Weitkamp, E. A., Sage, A. M., Grieshop, A. P., Lane, T. E., Pierce, J. R. and Pandis, S. N.: Rethinking Organic Aerosols: Semivolatile Emissions and Photochemical Aging, Science, 315(5816), 1259–1262, doi:10.1126/science.1133061, 2007.

Schwartz, J., Coull, B., Laden, F. and Ryan, L.: The Effect of Dose and Timing of Dose on the Association between Airborne Particles and Survival, Environ. Health Perspect., 116(1), 64–69, doi:10.1289/ehp.9955, 2008.

Seabold, J. S. and Perktold, J.: Statsmodels: Econometric and Statistical Modeling with Python, in Proceedings of the 9th Python in Science Conference. [online] Available from: http://statsmodels.sourceforge.net/, 2010.

Spadaro, J. V. and Rabl, A.: Estimates of real damage from air pollution: Site dependence and simple impact indices for LCA, Int. J. Life Cycle Assess., 4(4), 229–243, doi:10.1007/BF02979503, 1999.

Thompson, T. M., Saari, R. K. and Selin, N. E.: Air quality resolution for health impact assessment: influence of regional characteristics, Atmos Chem Phys, 14(2), 969–978, doi:10.5194/acp-14-969-2014, 2014.

Thompson, T. M. and Selin, N. E.: Influence of air quality model resolution on uncertainty associated with health impacts, Atmos Chem Phys, 12(20), 9753–9762, doi:10.5194/acp-12-9753-2012, 2012.

US Burden of Disease Collaborators: The State of US health, 1990-2010: Burden of Diseases, Injuries, and Risk Factors, JAMA, 310(6), 591–606, doi:10.1001/jama.2013.13805, 2013.

U.S. EPA: The Benefits and Costs of the Clean Air Act, 1990 to 2010, EPA report to Congress, U.S. Environmental Protection Agency. Office of Air and Radiation. Office of Policy, Washington, DC., 1999.

U.S. EPA: Technical Support Document for the Proposed PM NAAQS Rule, Response Surface Modeling, Office of Air Quality Planning and Standards, Research Triangle Park, NC., 2006.

U.S. EPA: Guidelines for Preparing Economic Analyses, National Center for Environmental Economics, Office of Policy, U.S. Environmental Protection Agency., 2010.

U.S. EPA: Air Quality Modeling Final Rule Technical Support Document, U.S. Environmental Protection Agency. Office of Air Quality Planning and Standards. Air Quality Assessment Division. [online] Available from: http://www.epa.gov/airquality/transport/pdfs/AQModeling.pdf, 2011a.

U.S. EPA: Emissions Inventory Final Rule TSD, U.S. Environmental Protection Agency. Office of Air and Radiation. Office of Air Quality Planning and Standards. Air Quality Assessment Division., 2011b.

U.S. EPA: Exposure Factors Handbook 2011 Edition, National Center for Environmental Assessment. Office of Research and Development. U.S. Environmental Protection Agency., Washington, DC. [online] Available from: http://cfpub.epa.gov/ncea/risk/recordisplay.cfm?deid=236252 (Accessed 11 August 2014c), 2011.

U.S. EPA: Regulatory Impact Analysis for the Federal Implementation Plans to Reduce Interstate Transport of Fine Particulate Matter and Ozone in 27 States; Correction of SIP Approvals for 22 States, U.S. Environmental Protection Agency, Office of Air and Radiation. [online] Available from: http://www.epa.gov/airtransport/pdfs/FinalRIA.pdf, 2011d.

U.S. EPA: The Benefits and Costs of the Clean Air Act from 1990 to 2020, U.S. Environmental Protection Agency. Office of Air and Radiation., Washington, DC., 2011e.

U.S. EPA: User's Manual for the Co-Benefits Risk Assessment (COBRA) Screening Model Version: 2.61, U.S. Environmental Protection Agency, Washington, DC., 2013.

West, J. J., Ansari, A. S. and Pandis, S. N.: Marginal PM2.5: Nonlinear aerosol mass response to sulfate reductions in the eastern United States, J. Air Waste Manag. Assoc., 49(12), 1415–1424, 1999.

Zhang, Q., Jimenez, J. L., Canagaratna, M. R., Allan, J. D., Coe, H., Ulbrich, I., Alfarra, M. R., Takami, A., Middlebrook, A. M., Sun, Y. L., Dzepina, K., Dunlea, E., Docherty, K., DeCarlo, P. F., Salcedo, D., Onasch, T., Jayne, J. T., Miyoshi, T., Shimono, A., Hatakeyama, S., Takegawa, N., Kondo, Y., Schneider, J., Drewnick, F., Borrmann, S., Weimer, S., Demerjian, K., Williams, P., Bower, K., Bahreini, R., Cottrell, L., Griffin, R. J., Rautiainen, J., Sun, J. Y., Zhang, Y. M. and Worsnop, D. R.: Ubiquity and dominance of oxygenated species in organic aerosols in anthropogenically-influenced Northern Hemisphere midlatitudes, Geophys. Res. Lett., 34(13), L13801, doi:10.1029/2007GL029979, 2007.

Table 3.1: Results for the social cost regression models

Variable	Population Ring Method		Average Plume Method	
	EC	SO_2	EC	SO_2
Intercept	$79^{\star\star}$	$100^{\star\star\star}$	$66^{\star\star\star}$	$110^{\star\star\star}$
	(23)	(19)	(13)	(17)
ln (Population ring 1)[a]	$0.16^{\star\star\star}$	$0.15^{\star\star}$	-	-
[# of people]	(0.024)	(0.049)	-	-
$\{r_1$ [km]$\}$	{36}	{180}	-	-
ln (Population ring 2)[b]	$0.34^{\star\star\star}$	$0.17^{\star\star}$	-	-
[# of people]	(0.049)	(0.061)	-	-
$\{r_2$ [km]$\}$	{252}	{360}	-	-
ln (Weighted population)	-	-	$0.75^{\star\star\star}$	$0.68^{\star\star\star}$
[# of people]	-	-	(0.037)	(0.080)
ln (Temperature)	$-22^{\star\star\star}$	$-25^{\star\star\star}$	$-18^{\star\star\star}$	$-27^{\star\star\star}$
[K]	(4.1)	(3.5)	(2.4)	(3.0)
ln (Pressure)	$7.2^{\star\star\star}$	$6.6^{\star\star\star}$	$5.5^{\star\star\star}$	$6.0^{\star\star\star}$
[hPa]	(0.93)	(0.79)	(0.54)	(0.71)
ln (Ṕrecipitation[c])	$-0.095^{\star\star}$	$-0.056^{\star}$	-0.032^{+}	$-0.053^{\star}$
$[\mathrm{g\,m^{-3}}]$	(0.031)	(0.026)	(0.018)	(0.021)
ln (Wind speed)	-	−0.13	$-0.12^{\star}$	-
$[\mathrm{m\,s^{-1}}]$	-	(0.076)	(0.053)	-
Adj. R^2	0.91	0.89	0.97	0.91
Fractional bias	0.051	0.043	0.052	0.0024
Fractional error	0.35	0.33	0.18	0.26
Normalized mean bias	−0.14	−0.19	0.051	−0.17
Normalized mean error	0.35	0.41	0.16	0.32
95% prediction interval[d]	[0.46, 2.18]	[0.52, 1.93]	[0.64, 1.56]	[0.57, 1.76]
95% confidence interval[d]	[0.78, 1.29]	[0.78, 1.28]	[0.86, 1.17]	[0.83, 1.21]

*** $p < 0.001$, ** $p < 0.001$, * $p < 0.05$, $^{+}$ $p < 0.1$, Standard errors in parentheses, [a] Population (≥ age 30) within r_1 ($r < r_1$), [b] Population (≥ age 30) between r_1 and r_2 ($r_1 \leq r < r_2$), [c] Ṕrecipitation = Precipitation + 0.0002 (shifted for log transformation), [d] Average intervals relative to predicted value.

Table 3.2: Results for the intake fraction regression models

Variable	Population Ring Method		Average Plume Method	
	EC	SO_2	EC	SO_2
Intercept	$69^{\star}$	$89^{\star\star\star}$	$58^{\star\star\star}$	$97^{\star\star\star}$
	(26)	(20)	(13)	(17)
ln (Population ring 1)[a]	$0.17^{\star\star\star}$	$0.23^{\star\star\star}$	-	-
[# of people]	(0.026)	(0.048)	-	-
$\{r_1$ [km]$\}$	{36}	{252}	-	-
ln (Population ring 2)[b]	$0.36^{\star\star\star}$	0.21^{+}	-	-
[# of people]	(0.054)	(0.11)	-	-
$\{r_2$ [km]$\}$	{252}	{972}	-	-
ln (Weighted population)	-	-	$0.81^{\star\star\star}$	$0.74^{\star\star\star}$
[# of people]	-	-	(0.037)	(0.082)
ln (Temperature)	$-21^{\star\star\star}$	$-25^{\star\star\star}$	$-17^{\star\star\star}$	$-25^{\star\star\star}$
[K]	(4.6)	(3.6)	(2.4)	(3.1)
ln (Pressure)	$6.4^{\star\star\star}$	$6.6^{\star\star\star}$	$4.5^{\star\star\star}$	$5.5^{\star\star\star}$
[hPa]	(1.0)	(0.80)	(0.54)	(0.73)
ln (Ṕrecipitation[c])	$-0.13^{\star\star\star}$	$-0.088^{\star\star}$	$-0.053^{\star\star}$	$-0.083^{\star\star\star}$
$[\mathrm{g\,m^{-3}}]$	(0.034)	(0.028)	(0.018)	(0.022)
ln (Wind speed)	-	-	−0.084	-
$[\mathrm{m\,s^{-1}}]$	-	-	(0.053)	-
Adj. R^2	0.89	0.87	0.97	0.91
Fractional bias	0.035	0.042	0.028	−0.0073
Fractional error	0.37	0.31	0.18	0.28
Normalized mean bias	−0.18	−0.21	0.019	−0.16
Normalized mean error	0.39	0.40	0.16	0.32
95% prediction interval[d]	[0.42, 2.37]	[0.50, 1.99]	[0.64, 1.56]	[0.56, 1.79]
95% confidence interval[d]	[0.76, 1.33]	[0.79, 1.28]	[0.86, 1.17]	[0.83, 1.22]

*** $p < 0.001$, ** $p < 0.001$, * $p < 0.05$, $^{+}$ $p < 0.1$, Standard errors in parentheses, [a] Population within r_1 ($r < r_1$), [b] Population between r_1 and r_2 ($r_1 \leq r < r_2$), [c] Ṕrecipitation = Precipitation + 0.0002 (shifted for log transformation), [d] Average intervals relative to predicted value.

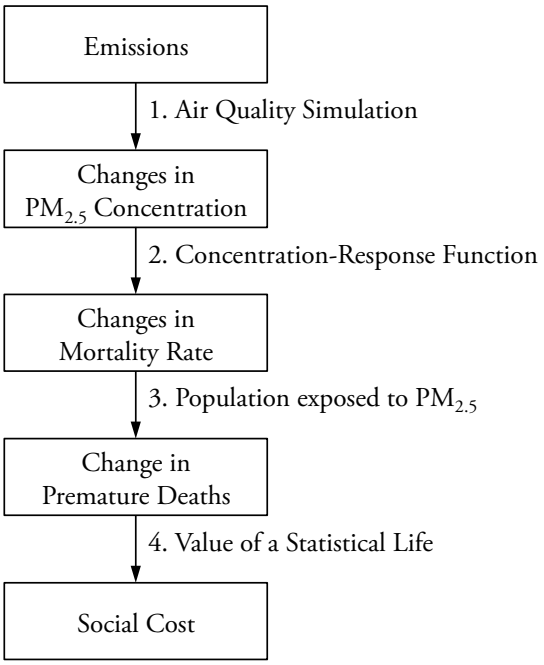

Figure 3.1: The four steps in the impact pathway analysis of air quality social cost.

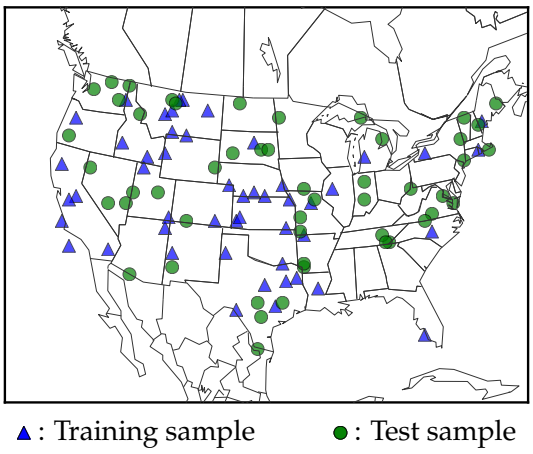

Figure 3.2: The air quality social cost modeling domain and the selected sample locations. CAMx simulated this domain in a 148×112 grid that has a horizontal cell size of 36 km×36 km. The sample locations were selected randomly based on the size of population. The training samples were used to build regression models and the test samples for out-of-sample evaluation.

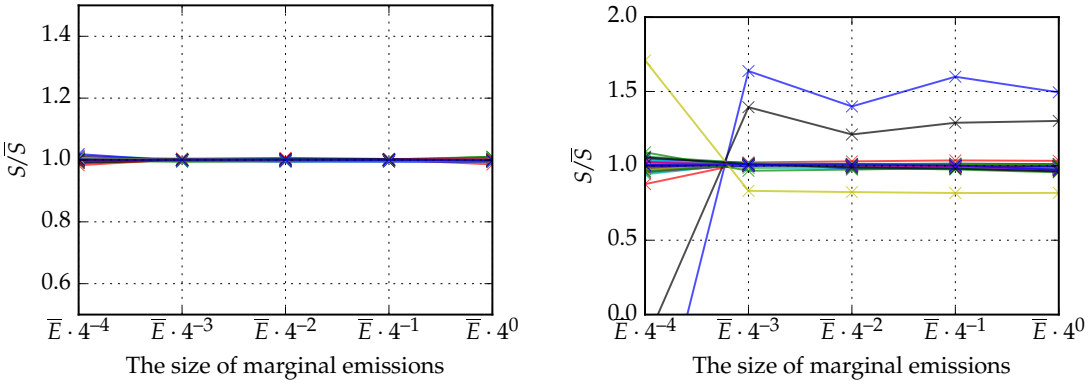

(a) EC

(b) SO_2

Figure 3.3: Social costs over a range of marginal emissions. Each line represents the per-tonne social costs of one sample location. For the 50 training sample locations, the per-tonne social costs were calculated over a range of $\overline{E} \cdot 4^{-k} (k = 0, ..., 4)$, where $\overline{E}$ is the average emissions of area and point sources. The ratios of S, the per-tonne social cost for given emissions at a sample location, over $\overline{S}$, the average of S over all $\overline{E}$ are on the y-axis. The EC social costs mostly stay constant over the range of marginal emissions and start to slightly diverge at the smallest perturbation. The SO_2 social costs also stay largely constant except that a few locations become unstable at the lowest emissions, $\overline{E} \cdot 4^{-4}$. We chose $\overline{E} \cdot 4^{-2}$ as our modeling basis.

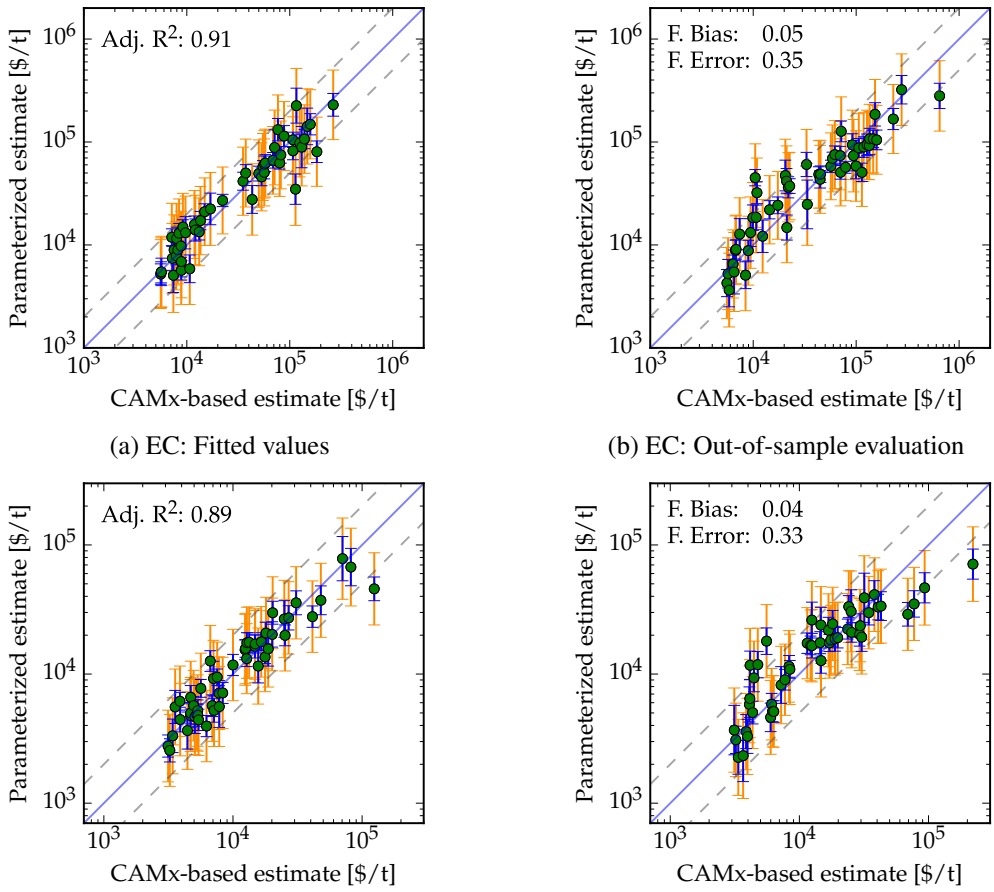

(a) EC: Fitted values

(b) EC: Out-of-sample evaluation

(c) SO_2: Fitted values

(d) SO_2: Out-of-sample evaluation

Figure 3.4: The performance and evaluation of population ring social cost models. On the x-axis are values estimated with CTM results and on the y-axis are values calculated by the regression model. (a) and (c) show the fitted values with 50 training sample locations. (b) and (d) show the out of sample evaluation done with 50 test samples. Yellow error bars present 95% prediction intervals and green error bars 95% confidence intervals.

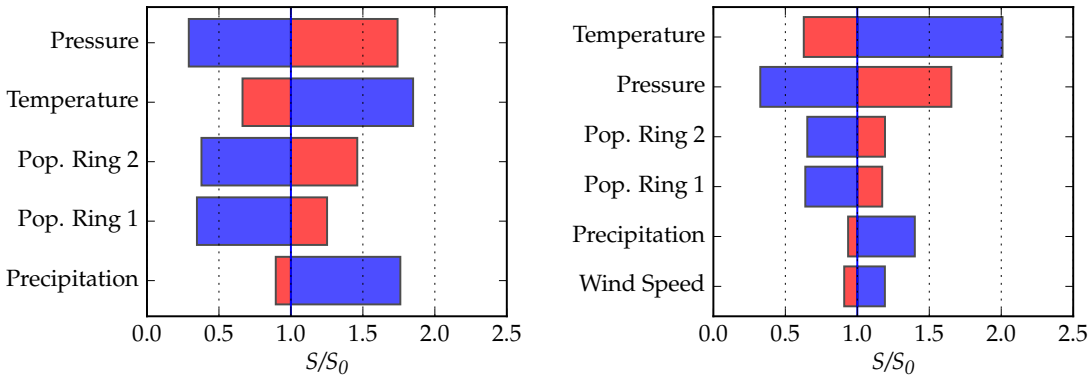

(a) EC

(b) SO_2

Figure 3.5: Sensitivity of social costs to the variables of the population ring social cost models. Each range presents the ratio of social costs calculated with 5th (blue) and 95th (red) percentiles of a variable in the 100 samples to one calculated with its mean, S_0.

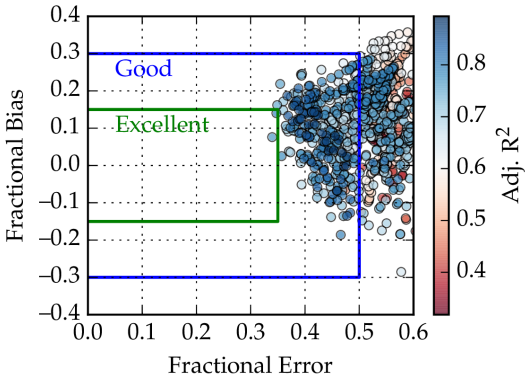

(a) One ring: 928 EC models

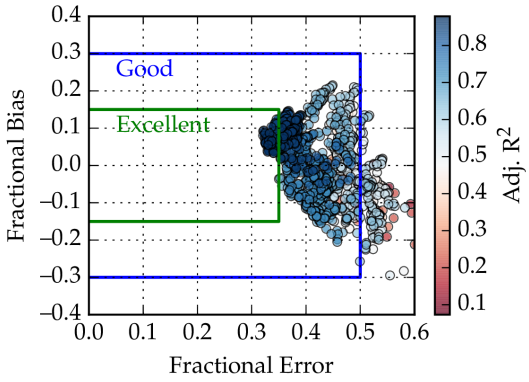

(b) One ring: 928 SO_2 models

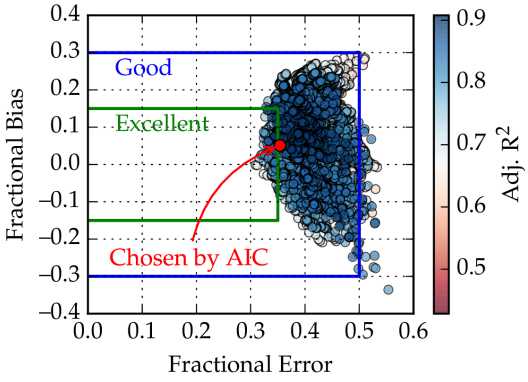

(c) Two rings: 6,912 EC models

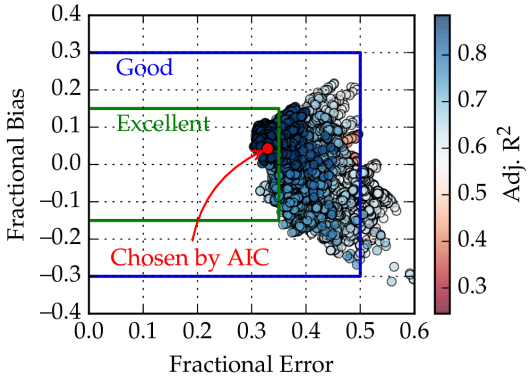

(d) Two rings: 6,912 SO_2 models

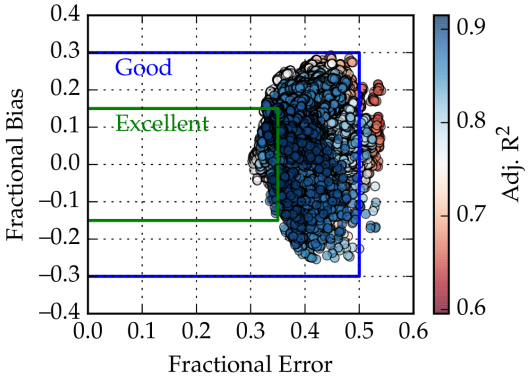

(e) Three rings: 67,488 EC models

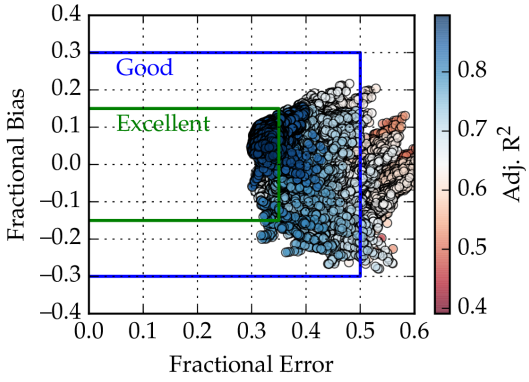

(f) Three rings: 67,488 SO_2 models

Figure 3.6: Evaluation of population ring method social cost models. Each circle shows the adjusted R^2 from regression and the fractional bias and fraction error with the 50 test samples. 'Excellent' and 'Good' evaluation criteria are as defined by Morris et al. (2005).

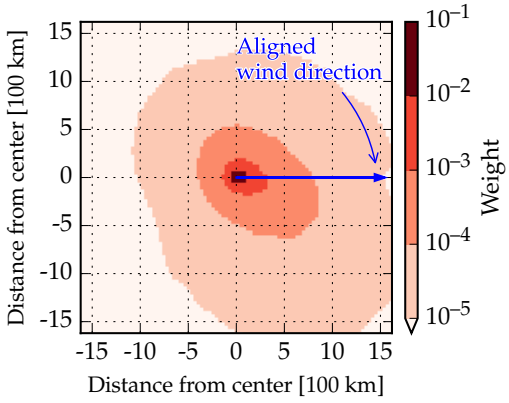

(a) EC: Average plume

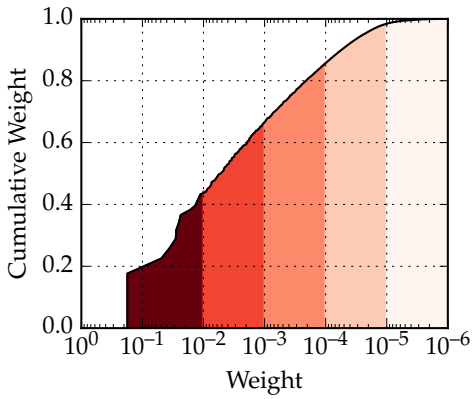

(b) EC: Cumulative distribution

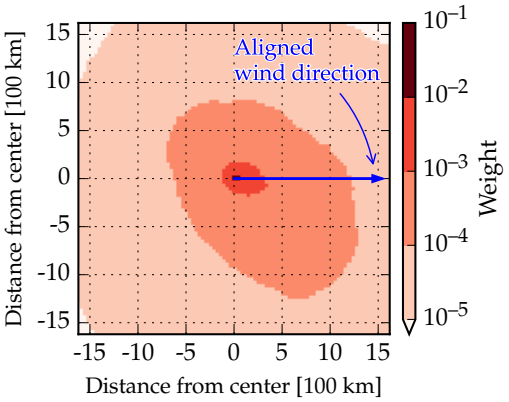

(c) SO_2: Average plume

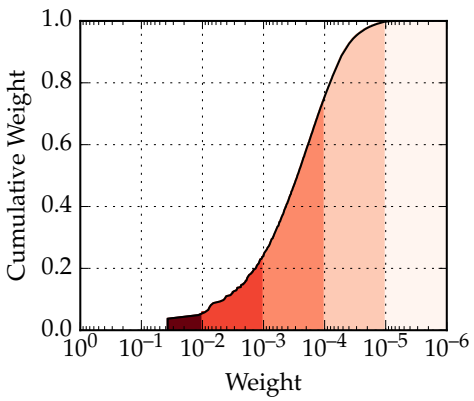

(d) SO_2: Cumulative distribution

Figure 3.7: Average plume weights constructed with the CTM results of the training samples. $PM_{2.5}$ concentrations or plumes of the 50 training samples are aligned to the arrow direction and normalized. This shows both pollutants travel over a large distance, though EC plume is relatively more local than SO_2.

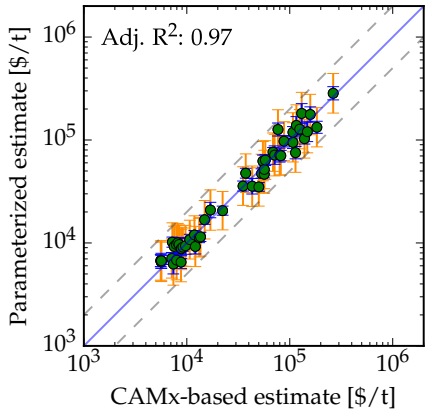

(a) EC: Fitted values

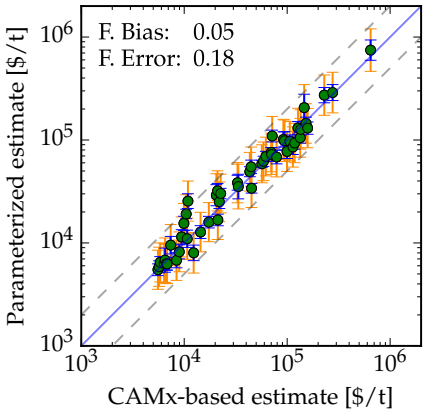

(b) EC: Out-of-sample evaluation

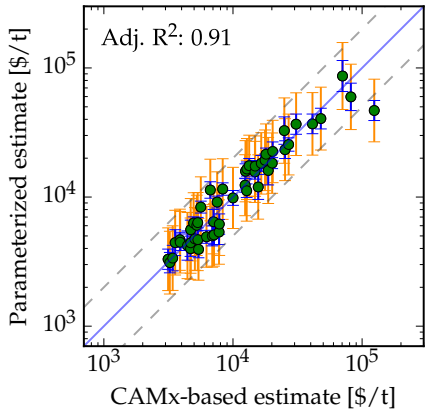

(c) SO_2: Fitted values

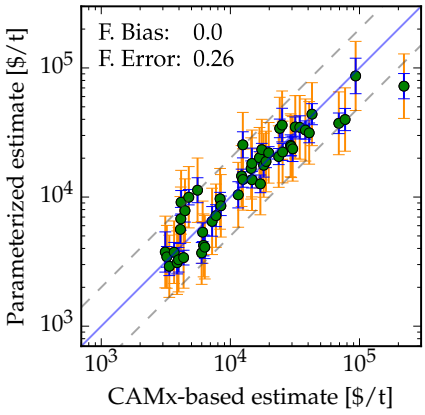

(d) SO_2: Out-of-sample evaluation

Figure 3.8: The performance and evaluation of average plume social cost models. On the x-axis are values estimated with CTM results and on the y-axis are values calculated by the regression model. (a) and (c) show the fitted values with 50 training sample locations. (b) and (d) show the out of sample evaluation done with 50 test samples. Yellow error bars present 95% prediction intervals and green error bars 95% confidence intervals.

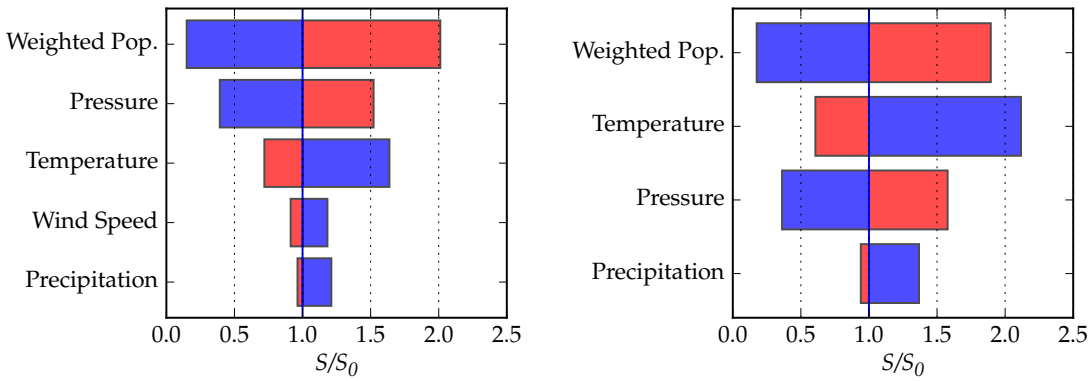

(a) EC (b) SO_2

Figure 3.9: Sensitivity of social costs to the variables of the average plume social cost models. Each range presents the ratio of social costs calculated with 5th (blue) and 95th (red) percentiles of a variable in the 100 samples to one calculated with its mean, S_0.

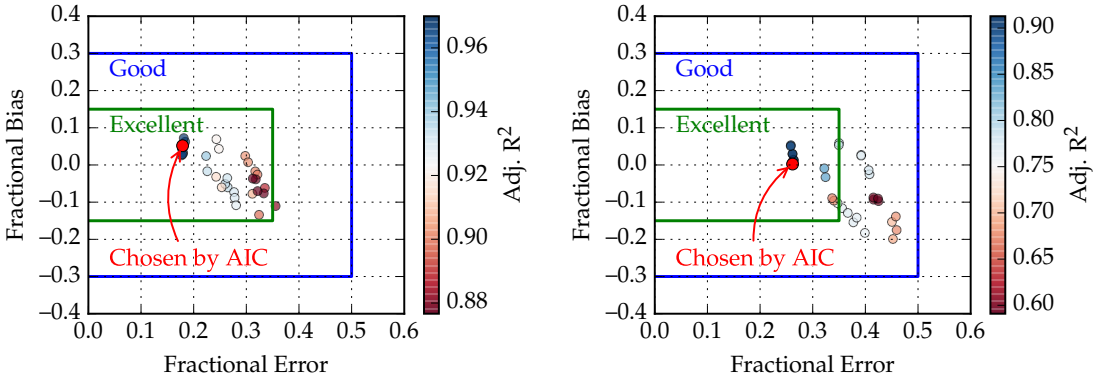

(a) EC (b) SO_2

Figure 3.10: Evaluation of average plume method social cost models. 'Excellent' and 'Good' criteria are as defined by Morris et al. (2005).

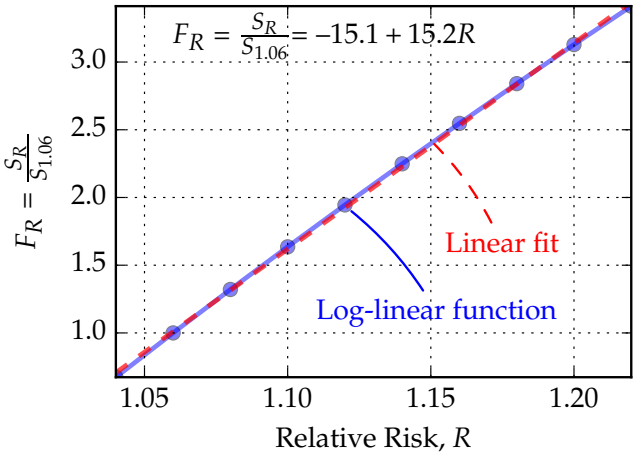

Figure 3.11: Social cost over a range of relative risks. The range covers the 95% confidence intervals of relative risks reported by two land-mark cohort-based epidemiological studies, Krewski et al. (2009) and Lepeule et al. (2012).

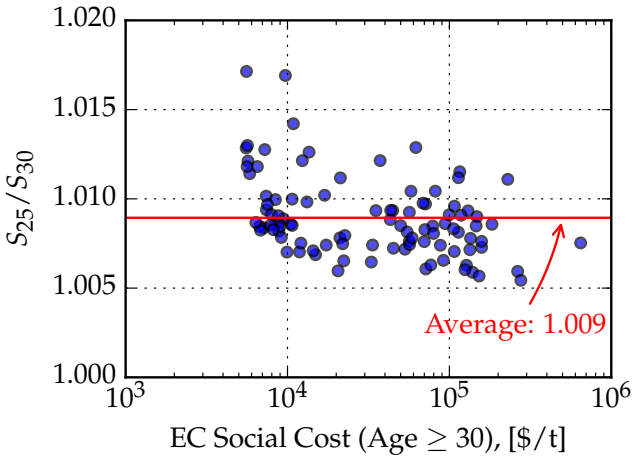

Figure 3.12: Social costs and two population age cohorts. The social costs at the 100 sample locations using population of age 30 or older, S_{30}, were compared those using population of age 25 or older, S_{25}. S_{30} matches the American Cancer Society study cohort (Krewski et al., 2009) and S_{25} the Harvard Six Cities study cohort (Lepeule et al., 2012). X-axis shows the values of S_{30} and y-axis the ratios of S_{25} to S_{30}. At all locations, the difference was only 0.9% on average.

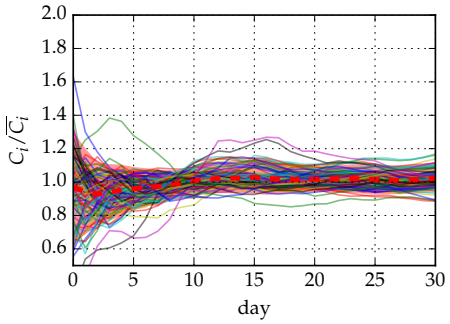

(a) EC: $\Delta PM_{2.5}$ over time

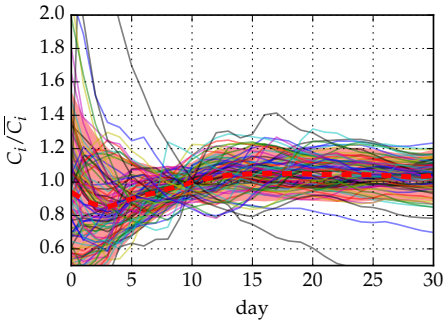

(b) SO_2: $\Delta PM_{2.5}$ over time

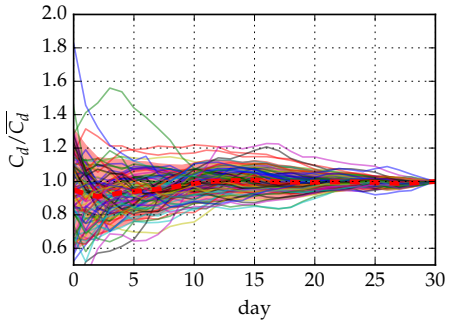

(c) EC: $\Delta PM_{2.5}$ over a different period

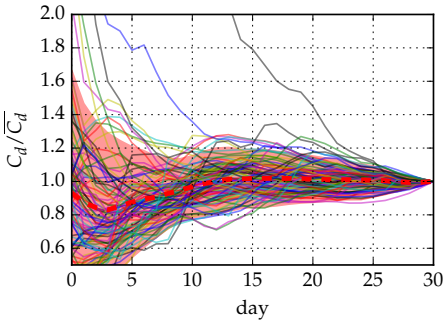

(d) SO_2: $\Delta PM_{2.5}$ over a different period

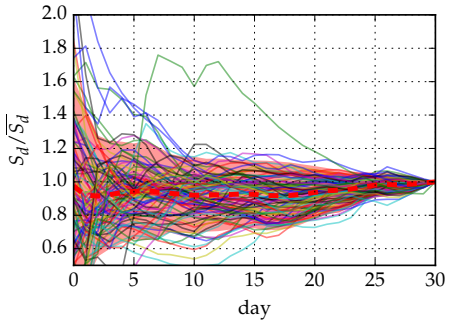

(e) EC: Social cost over a different period

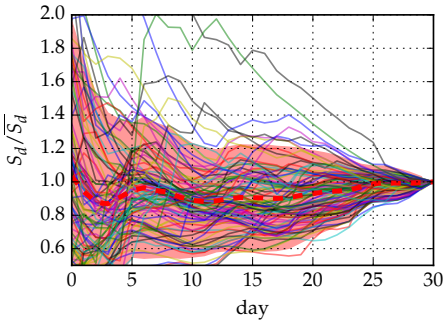

(f) SO_2: Social cost over a different period

Figure 3.13: $PM_{2.5}$ concentrations and social costs over different lengths of simulation. Each line indicates each sample location. C_i is the sum of the CAMx grid of the changes in average $PM_{2.5}$ concentrations for a given day. $\overline{C_i}$ is the average of C_i's over the entire time period. C_d is the sum of the CAMx grid of the average changes in $PM_{2.5}$ concentrations for a given simulation period (e.g. from day one to day d). $\overline{C_d}$ is the sum of the average changes in $PM_{2.5}$ concentrations for the entire period. S is the per-tonne social cost calculated for a given simulation period. $\overline{S}$ is the per-tonne social cost for the entire period. The red dashed line indicates the 2.5% truncated means and the shaded area covers the 95% confidence intervals of the means.

B Appendix: Additional Figures and Tables

Table B-1: Summary of the dataset generated for the 100 sample locations

	Social Cost [$\$\,\mathrm{t}^{-1}$]		Intake Fraction [ppm]		Pressure	Temperature	Precipitation	Wind Speed	Humidity
	EC	SO_2	EC	SO_2	[hPa]	[K]	[$\mathrm{g\,m^{-3}}$]	[$\mathrm{m\,s^{-1}}$]	[ppm]
mean	63,000	18,000	0.93	0.26	965	297	0.077	2.0	18,000
std	84,000	27,000	1.3	0.38	73	4.4	0.086	1.2	6,100
min	5,600	2,900	0.092	0.046	741	286	0.0	0.092	8,400
25%	9,400	4,800	0.13	0.070	929	295	0.016	1.1	11,000
50%	36,000	10,000	0.50	0.14	993	298	0.048	2.0	18,000
75%	92,000	19,000	1.2	0.29	1,020	300	0.11	2.6	22,000
max	650,000	210,000	10	2.7	1,050	307	0.44	6.3	29,000

Table B-2: Evaluations of EC social cost models from the population ring method

Model[†]	(1)[‡]	(2)	(3)	(4)	(5)	(6)	(7)
r_1	36	36	36	36	36	36	36
r_2	252	252	252	252	216	288	216
Intercept	$79^{\star\star}$	$74^{\star\star}$	$77^{\star\star}$	$75^{\star\star}$	$71^{\star\star}$	$78^{\star\star}$	$76^{\star\star}$
ln (Pop_{r_1})	$0.16^{\star\star\star}$	$0.16^{\star\star\star}$	$0.16^{\star\star\star}$	$0.16^{\star\star\star}$	$0.15^{\star\star\star}$	$0.18^{\star\star\star}$	$0.15^{\star\star\star}$
ln (Pop_{r_2})	$0.34^{\star\star\star}$	$0.33^{\star\star\star}$	$0.34^{\star\star\star}$	$0.33^{\star\star\star}$	$0.32^{\star\star\star}$	$0.35^{\star\star\star}$	$0.32^{\star\star\star}$
ln (Pres)	$7.2^{\star\star\star}$	$7.2^{\star\star\star}$	$7.5^{\star\star\star}$	$7.1^{\star\star\star}$	$7.4^{\star\star\star}$	$7.0^{\star\star\star}$	$7.5^{\star\star\star}$
ln (Temp)	$-22^{\star\star\star}$	$-21^{\star\star\star}$	$-22^{\star\star\star}$	$-21^{\star\star\star}$	$-21^{\star\star\star}$	$-21^{\star\star\star}$	$-22^{\star\star\star}$
ln (Prec)	$-0.095^{\star\star}$	$-0.11^{\star\star}$	-0.089^{+}	$-0.11^{\star}$	$-0.10^{\star\star}$	$-0.100^{\star\star}$	$-0.087^{\star}$
ln (Wind)	-	-0.12	-	-0.12	-0.14	-	-
ln (Humid)	-	-	-0.072	0.022	-	-	-
AIC	47	47	49	49	49	49	50
Adj. R^2	0.91	0.91	0.90	0.91	0.90	0.90	0.90
F. Bias	0.051	0.076	0.053	0.076	0.070	0.050	0.040
F. Error	0.35	0.34	0.36	0.34	0.36	0.36	0.37

[†] Seven models with lowest AIC, ordered by AIC, [‡] Chosen by AIC, *** $p < 0.001$, ** $p < 0.001$, * $p < 0.05$, $^{+}$ $p < 0.1$, r_1: the first population ring radius [km], r_2: the second population ring radius [km], Pop_{r_1}: Population ($\geq$ age 30) < r_1 [# of people], Pop_{r_2}: $r_1 \leq$ Population ($\geq$ age 30) < r_2 [# of people], Pres: Pressure [hPa], Temp: Temperature [K], Prec: Precipitation + 0.0002 [$\mathrm{g\,m^{-3}}$] (shifted for log transformation), Wind: Wind speed [$\mathrm{m\,s^{-1}}$], Humid: Humidity [ppm], AIC: Akaike information criterion, Adj. R^2: Adjusted R^2, F. Bias: Fractional bias, F. Error: Fractional error.

Table B-3: Evaluations of EC intake fraction models from the population ring method

Model[†]	(1)[‡]	(2)	(3)	(4)	(5)	(6)	(7)
r_1	36	36	36	36	36	36	36
r_2	252	252	288	252	288	252	216
Intercept	$69^{\star}$	$65^{\star}$	$68^{\star}$	$65^{\star}$	$65^{\star}$	$64^{\star}$	$65^{\star}$
ln (Pop_{r_1})	$0.17^{\star\star\star}$	$0.16^{\star\star\star}$	$0.18^{\star\star\star}$	$0.16^{\star\star\star}$	$0.18^{\star\star\star}$	$0.16^{\star\star\star}$	$0.15^{\star\star\star}$
ln (Pop_{r_2})	$0.36^{\star\star\star}$	$0.36^{\star\star\star}$	$0.38^{\star\star\star}$	$0.37^{\star\star\star}$	$0.38^{\star\star\star}$	$0.36^{\star\star\star}$	$0.35^{\star\star\star}$
ln (Pres)	$6.4^{\star\star\star}$	$6.4^{\star\star\star}$	$6.2^{\star\star\star}$	$6.9^{\star\star\star}$	$6.1^{\star\star\star}$	$6.6^{\star\star\star}$	$6.8^{\star\star\star}$
ln (Temp)	$-21^{\star\star\star}$	$-20^{\star\star\star}$	$-21^{\star\star\star}$	$-21^{\star\star\star}$	$-20^{\star\star\star}$	$-20^{\star\star\star}$	$-21^{\star\star\star}$
ln (Prec)	$-0.13^{\star\star\star}$	$-0.13^{\star\star\star}$	$-0.13^{\star\star\star}$	$-0.11^{\star}$	$-0.14^{\star\star\star}$	$-0.13^{\star}$	$-0.12^{\star\star}$
ln (Wind)	-	-0.088	-	-	-0.083	-0.084	-
ln (Humid)	-	-	-	-0.14	-	-0.072	-
AIC	57	58	58	59	60	60	60
Adj. R^2	0.89	0.88	0.88	0.88	0.88	0.88	0.88
F. Bias	0.035	0.054	0.035	0.039	0.053	0.055	0.025
F. Error	0.37	0.37	0.38	0.38	0.37	0.37	0.39

[†] Seven models with lowest AIC, ordered by AIC, [‡] Chosen by AIC, *** $p < 0.001$, ** $p < 0.001$, * $p < 0.05$, $^{+}$ $p < 0.1$, r_1: the first population ring radius [km], r_2: the second population ring radius [km], Pop_{r_1}: Population < r_1 [# of people], Pop_{r_2}: $r_1 \leq$ Population < r_2 [# of people], Pres: Pressure [hPa], Temp: Temperature [K], Prec: Precipitation + 0.0002 [$\mathrm{g\,m^{-3}}$] (shifted for log transformation), Wind: Wind speed [$\mathrm{m\,s^{-1}}$], Humid: Humidity [ppm], AIC: Akaike information criterion, Adj. R^2: Adjusted R^2, F. Bias: Fractional bias, F. Error: Fractional error.

Table B-4: Evaluations of SO_2 social cost models from the population ring method

Model[†]	(1)[‡]	(2)	(3)	(4)	(5)	(6)	(7)
r_1	180	252	252	252	180	252	252
r_2	360	1,044	972	1,008	612	936	972
Intercept	$100^{\star\star\star}$	$110^{\star\star\star}$	$110^{\star\star\star}$	$110^{\star\star\star}$	$100^{\star\star\star}$	$110^{\star\star\star}$	$100^{\star\star\star}$
ln (Pop_{r_1})	$0.15^{\star\star}$	$0.22^{\star\star\star}$	$0.22^{\star\star\star}$	$0.22^{\star\star\star}$	$0.16^{\star\star}$	$0.22^{\star\star\star}$	$0.21^{\star\star\star}$
ln (Pop_{r_2})	$0.17^{\star\star}$	0.20^{+}	0.19^{+}	0.19^{+}	$0.19^{\star}$	0.17^{+}	0.17
ln (Pres)	$6.6^{\star\star\star}$	$6.9^{\star\star\star}$	$7.0^{\star\star\star}$	$7.0^{\star\star\star}$	$6.6^{\star\star\star}$	$7.0^{\star\star\star}$	$6.9^{\star\star\star}$
ln (Temp)	$-25^{\star\star\star}$	$-26^{\star\star\star}$	$-27^{\star\star\star}$	$-27^{\star\star\star}$	$-25^{\star\star\star}$	$-27^{\star\star\star}$	$-26^{\star\star\star}$
ln (Prec)	$-0.056^{\star}$	$-0.057^{\star}$	$-0.054^{\star}$	$-0.055^{\star}$	$-0.062^{\star}$	-0.051^{+}	$-0.063^{\star}$
ln (Wind)	-0.13	-	-	-	-0.14^{+}	-	-0.095
ln (Humid)	-	-	-	-	-	-	-
AIC	28	29	29	29	29	29	29
Adj. R^2	0.89	0.88	0.88	0.88	0.88	0.88	0.88
F. Bias	0.043	0.048	0.050	0.049	0.058	0.054	0.066
F. Error	0.33	0.32	0.32	0.32	0.33	0.32	0.32

[†] Seven models with lowest AIC and with fractional bias ≤ 0.3, ordered by AIC, [‡] Chosen by AIC, *** $p < 0.001$, ** $p < 0.001$, * $p < 0.05$, $^{+}$ $p < 0.1$, r_1: the first population ring radius [km], r_2: the second population ring radius [km], Pop_{r_1}: Population (≥ age 30) < r_1 [# of people], Pop_{r_2}: r_1 ≤ Population (≥ age 30) < r_2 [# of people], Pres: Pressure [hPa], Temp: Temperature [K], Prec: Precipitation + 0.0002 [$\mathrm{g\,m^{-3}}$] (shifted for log transformation), Wind: Wind speed [$\mathrm{m\,s^{-1}}$], Humid: Humidity [ppm], AIC: Akaike information criterion, Adj. R^2: Adjusted R^2, F. Bias: Fractional bias, F. Error: Fractional error.

Table B-5: Evaluations of SO_2 intake fraction models from the population ring method

Model[†]	(1)[‡]	(2)	(3)	(4)	(5)	(6)	(7)
r_1	252	252	252	252	180	252	252
r_2	972	1,044	936	1,008	360	684	648
Intercept	$89^{\star\star\star}$	$88^{\star\star\star}$	$91^{\star\star\star}$	$88^{\star\star\star}$	$87^{\star\star\star}$	$87^{\star\star\star}$	$88^{\star\star\star}$
ln (Pop_{r_1})	$0.23^{\star\star\star}$	$0.24^{\star\star\star}$	$0.23^{\star\star\star}$	$0.24^{\star\star\star}$	$0.17^{\star\star}$	$0.23^{\star\star\star}$	$0.23^{\star\star\star}$
ln (Pop_{r_2})	0.21^{+}	0.22^{+}	0.20^{+}	0.21^{+}	$0.19^{\star\star}$	0.15^{+}	0.14^{+}
ln (Pres)	$6.6^{\star\star\star}$	$6.6^{\star\star\star}$	$6.6^{\star\star\star}$	$6.6^{\star\star\star}$	$6.4^{\star\star\star}$	$6.4^{\star\star\star}$	$6.4^{\star\star\star}$
ln (Temp)	$-25^{\star\star\star}$	$-25^{\star\star\star}$	$-25^{\star\star\star}$	$-25^{\star\star\star}$	$-24^{\star\star\star}$	$-24^{\star\star\star}$	$-24^{\star\star\star}$
ln (Prec)	$-0.088^{\star\star}$	$-0.091^{\star\star}$	$-0.085^{\star\star}$	$-0.089^{\star\star}$	$-0.075^{\star\star}$	$-0.081^{\star\star}$	$-0.079^{\star\star}$
ln (Wind)	-	-	-	-	-	-	-
ln (Humid)	-	-	-	-	-	-	-
AIC	33	33	33	33	34	34	34
Adj. R^2	0.87	0.87	0.87	0.87	0.87	0.87	0.87
F. Bias	0.042	0.039	0.047	0.040	0.0057	0.050	0.047
F. Error	0.31	0.31	0.31	0.31	0.33	0.33	0.33

[†] Seven models with lowest AIC and with fractional bias ≤ 0.3, ordered by AIC, [‡] Chosen by AIC, *** $p < 0.001$, ** $p < 0.001$, * $p < 0.05$, $^{+}$ $p < 0.1$, r_1: the first population ring radius [km], r_2: the second population ring radius [km], Pop_{r_1}: Population < r_1 [# of people], Pop_{r_2}: r_1 ≤ Population < r_2 [# of people], Pres: Pressure [hPa], Temp: Temperature [K], Prec: Precipitation + 0.0002 [$\mathrm{g\,m^{-3}}$] (shifted for log transformation), Wind: Wind speed [$\mathrm{m\,s^{-1}}$], Humid: Humidity [ppm], AIC: Akaike information criterion, Adj. R^2: Adjusted R^2, F. Bias: Fractional bias, F. Error: Fractional error.

Table B-6: Evaluations of EC social cost models from the average plume method

Model†	(1)‡	(2)	(3)	(4)	(5)	(6)	(7)
Intercept	66^{***}	65^{***}	77^{***}	64^{***}	76^{***}	66^{***}	70^{***}
ln (Pop_w)	0.75^{***}	0.76^{***}	0.76^{***}	0.75^{***}	0.77^{***}	0.77^{***}	0.77^{***}
ln (Pres)	5.5^{***}	6.2^{***}	5.5^{***}	5.7^{***}	5.5^{***}	6.1^{***}	5.6^{***}
ln (Temp)	-18^{***}	-18^{***}	-19^{***}	-17^{***}	-19^{***}	-18^{***}	-18^{***}
ln (Wind)	-0.12^{*}	-0.095^{+}	-0.086^{+}	-0.12^{*}	-	-	-
ln (Prec)	-0.032^{+}	-	-	-0.027	-	-	-0.018
ln (Humid)	-	-0.23	-	-0.058	-	-0.19	-
AIC	-10.0	-8.7	-8.4	-8.0	-7.3	-6.9	-6.5
Adj. R^2	0.97	0.97	0.97	0.97	0.97	0.97	0.97
F. Bias	0.052	0.062	0.072	0.052	0.044	0.033	0.026
F. Error	0.18	0.18	0.18	0.18	0.18	0.18	0.18

† Seven models with lowest AIC ordered by AIC, ‡ Chosen by AIC, *** $p < 0.001$, ** $p < 0.001$, * $p < 0.05$, $^{+}$ $p < 0.1$, Pop_w [# of people]: Populatation (≥ age 30) weighted with average plume, Pres: Pressure [hPa], Temp: Temperature [K], Prec: Precipitation + 0.0002 [$\mathrm{g\,m^{-3}}$] (shifted for log transformation), Wind: Wind speed [$\mathrm{m\,s^{-1}}$], Humid: Humidity [ppm], AIC: Akaike information criterion, Adj. R^2: Adjusted R^2, F. Bias: Fractional bias, F. Error: Fractional error.

Table B-7: Evaluations of EC intake fraction models from the average plume method

Model†	(1)‡	(2)	(3)	(4)	(5)	(6)	(7)
Intercept	58^{***}	61^{***}	55^{***}	54^{***}	55^{***}	55^{***}	76^{***}
ln (Pop_w)	0.81^{***}	0.83^{***}	0.83^{***}	0.82^{***}	0.83^{***}	0.83^{***}	0.83^{***}
ln (Pres)	4.5^{***}	4.6^{***}	5.8^{***}	5.0^{***}	5.3^{***}	5.8^{***}	4.5^{***}
ln (Temp)	-17^{***}	-18^{***}	-18^{***}	-17^{***}	-17^{***}	-17^{***}	-20^{***}
ln (Wind)	-0.084	-	-	-0.077	-	-0.044	-
ln (Prec)	-0.053^{**}	-0.043^{*}	-	-0.040	-0.026	-	-
ln (Humid)	-	-	-0.39^{*}	-0.16	-0.22	-0.41^{*}	-
AIC	-9.9	-9.2	-8.9	-8.5	-8.3	-7.7	-4.4
Adj. R^2	0.97	0.97	0.97	0.97	0.97	0.97	0.97
F. Bias	0.028	0.0095	0.030	0.029	0.014	0.044	0.052
F. Error	0.18	0.18	0.18	0.18	0.18	0.18	0.17

† Seven models with lowest AIC ordered by AIC, ‡ Chosen by AIC, *** $p < 0.001$, ** $p < 0.001$, * $p < 0.05$, $^{+}$ $p < 0.1$, Pop_w [# of people]: Populatation weighted with average plume, Pres: Pressure [hPa], Temp: Temperature [K], Prec: Precipitation + 0.0002 [$\mathrm{g\,m^{-3}}$] (shifted for log transformation), Wind: Wind speed [$\mathrm{m\,s^{-1}}$], Humid: Humidity [ppm], AIC: Akaike information criterion, Adj. R^2: Adjusted R^2, F. Bias: Fractional bias, F. Error: Fractional error.

Table B-8: Evaluations of SO_2 social cost models from the average plume method

Model[†]	(1)[‡]	(2)	(3)	(4)	(5)	(6)	(7)
Intercept	110^{***}	110^{***}	110^{***}	110^{***}	110^{***}	110^{***}	130^{***}
ln (Pop_w)	0.68^{***}	0.71^{***}	0.70^{***}	0.67^{***}	0.68^{***}	0.71^{***}	0.67^{***}
ln (Pres)	6.0^{***}	7.2^{***}	6.5^{***}	5.9^{***}	6.4^{***}	7.2^{***}	6.0^{***}
ln (Temp)	-27^{***}	-27^{***}	-26^{***}	-26^{***}	-26^{***}	-27^{***}	-30^{***}
ln (Wind)	-	-	-	-0.052	-0.041	-0.0023	-
ln (Prec)	$-0.053^{\star}$	-	-0.037	$-0.058^{\star}$	-0.044	-	-
ln (Humid)	-	$-0.45^{\star}$	-0.21	-	-0.17	$-0.46^{\star}$	-
AIC	13	14	14	14	16	16	17
Adj. R^2	0.91	0.91	0.91	0.91	0.91	0.91	0.90
F. Bias	0.0024	0.029	0.0068	0.013	0.014	0.030	0.053
F. Error	0.26	0.26	0.26	0.26	0.26	0.26	0.26

[†] Seven models with lowest AIC ordered by AIC, [‡] Chosen by AIC, *** $p < 0.001$, ** $p < 0.001$, * $p < 0.05$, $^{+}$ $p < 0.1$, Pop_w [# of people]: Populatation (≥ age 30) weighted with average plume, Pres: Pressure [hPa], Temp: Temperature [K], Prec: Precipitation + 0.0002 [$\mathrm{g\,m^{-3}}$] (shifted for log transformation), Wind: Wind speed [$\mathrm{m\,s^{-1}}$], Humid: Humidity [ppm], AIC: Akaike information criterion, Adj. R^2: Adjusted R^2, F. Bias: Fractional bias, F. Error: Fractional error.

Table B-9: Evaluations of SO_2 intake fraction models from the average plume method

Model[†]	(1)[‡]	(2)	(3)	(4)	(5)	(6)	(7)
Intercept	97^{***}	91^{***}	97^{***}	91^{***}	92^{***}	93^{***}	130^{***}
ln (Pop_w)	0.74^{***}	0.76^{***}	0.74^{***}	0.76^{***}	0.78^{***}	0.80^{***}	0.73^{***}
ln (Pres)	5.5^{***}	6.2^{***}	5.5^{***}	6.2^{***}	7.4^{***}	7.4^{***}	5.5^{***}
ln (Temp)	-25^{***}	-25^{***}	-25^{***}	-25^{***}	-26^{***}	-26^{***}	-30^{***}
ln (Wind)	-	-	-0.0098	0.0065	-	0.061	-
ln (Prec)	-0.083^{***}	$-0.063^{\star}$	-0.084^{***}	-0.062^{+}	-	-	-
ln (Humid)	-	-0.26	-	-0.27	-0.68^{**}	-0.67^{**}	-
AIC	16	17	18	19	20	21	28
Adj. R^2	0.91	0.91	0.91	0.91	0.90	0.90	0.88
F. Bias	-0.0073	-0.0019	-0.0054	-0.0030	0.037	0.019	0.073
F. Error	0.28	0.28	0.28	0.27	0.27	0.27	0.28

[†] Seven models with lowest AIC ordered by AIC, [‡] Chosen by AIC, *** $p < 0.001$, ** $p < 0.001$, * $p < 0.05$, $^{+}$ $p < 0.1$, Pop_w [# of people]: Populatation weighted with average plume, Pres: Pressure [hPa], Temp: Temperature [K], Prec: Precipitation + 0.0002 [$\mathrm{g\,m^{-3}}$] (shifted for log transformation), Wind: Wind speed [$\mathrm{m\,s^{-1}}$], Humid: Humidity [ppm], AIC: Akaike information criterion, Adj. R^2: Adjusted R^2, F. Bias: Fractional bias, F. Error: Fractional error.

Table B-10: Comparison of regression results: 31-day simulation v.s. 15-day simulation

Variable	30-day simulation		15-day simulation	
	EC	SO_2	EC	SO_2
Intercept	$66^{\star\star\star}$	$110^{\star\star\star}$	$68^{\star\star\star}$	$110^{\star\star\star}$
	(13)	(17)	(14)	(18)
ln (Weighted population)	$0.75^{\star\star\star}$	$0.68^{\star\star\star}$	$0.78^{\star\star\star}$	$0.75^{\star\star\star}$
[# of people]	(0.037)	(0.080)	(0.046)	(0.085)
ln (Temperature)	$-18^{\star\star\star}$	$-27^{\star\star\star}$	$-18^{\star\star\star}$	$-27^{\star\star\star}$
[K]	(2.4)	(3.0)	(2.6)	(3.1)
ln (Pressure)	$5.5^{\star\star\star}$	$6.0^{\star\star\star}$	$5.7^{\star\star\star}$	$8.0^{\star\star\star}$
[hPa]	(0.54)	(0.71)	(0.66)	(0.99)
ln (Ṕrecipitation[c])	-0.032^{+}	$-0.053^{\star}$	$-0.036^{\star}$	-
$[\mathrm{g\,m^{-3}}]$	(0.018)	(0.021)	(0.016)	-
ln (Wind speed)	$-0.12^{\star}$	-	$-0.13^{\star}$	-
$[\mathrm{m\,s^{-1}}]$	(0.053)	-	(0.062)	-
ln (Humidity)	-	-	-	$-0.50^{\star\star}$
[ppm]	-	-	-	(0.18)
Adj. R^2	0.97	0.91	0.96	0.92
Fractional bias	0.052	0.0024	0.035	−0.038
Fractional error	0.18	0.26	0.21	0.30
Normalized mean bias	0.051	−0.17	0.034	−0.24
Normalized mean error	0.16	0.32	0.20	0.37
95% prediction interval[d]	[0.64, 1.56]	[0.57, 1.76]	[0.59, 1.71]	[0.55, 1.83]
95% confidence interval[d]	[0.86, 1.17]	[0.83, 1.21]	[0.83, 1.20]	[0.82, 1.22]
Mean	63,000	18,000	62,000	20,000
Std	84,000	27,000	82,000	33,000

*** $p < 0.001$, ** $p < 0.001$, * $p < 0.05$, $^{+}$ $p < 0.1$, Standard errors in parentheses, [c] Ṕrecipitation = Precipitation + 0.0002 (shifted for log transformation), [d] Average intervals relative to predicted value.

Table B-11: U.S. EPA standard GDP deflator and income growth adjustment factors (extracted from BenMAP (U.S. EPA, 2014))

Year	GDP Deflator	Income Growth Adj.
1980	0.479	-
1981	0.528	-
1982	0.560	-
1983	0.578	-
1984	0.603	-
1985	0.625	-
1986	0.636	-
1987	0.660	-
1988	0.687	-
1989	0.720	-
1990	0.759	1.000
1991	0.791	0.992
1992	0.815	0.998
1993	0.839	1.003
1994	0.861	1.013
1995	0.885	1.017
1996	0.911	1.024
1997	0.932	1.034
1998	0.947	1.039
1999	0.967	1.043
2000	1.000	1.039
2001	1.028	1.044
2002	1.045	1.050
2003	1.069	1.056
2004	1.097	1.063
2005	1.134	1.069
2006	1.171	1.075
2007	1.204	1.081
2008	1.250	1.087
2009	1.246	1.093
2010	1.266	1.100
2011	-	1.112
2012	-	1.123
2013	-	1.134
2014	-	1.144
2015	-	1.155
2016	-	1.164
2017	-	1.174
2018	-	1.183
2019	-	1.192
2020	-	1.201
2021	-	1.209
2022	-	1.217
2023	-	1.225
2024	-	1.233

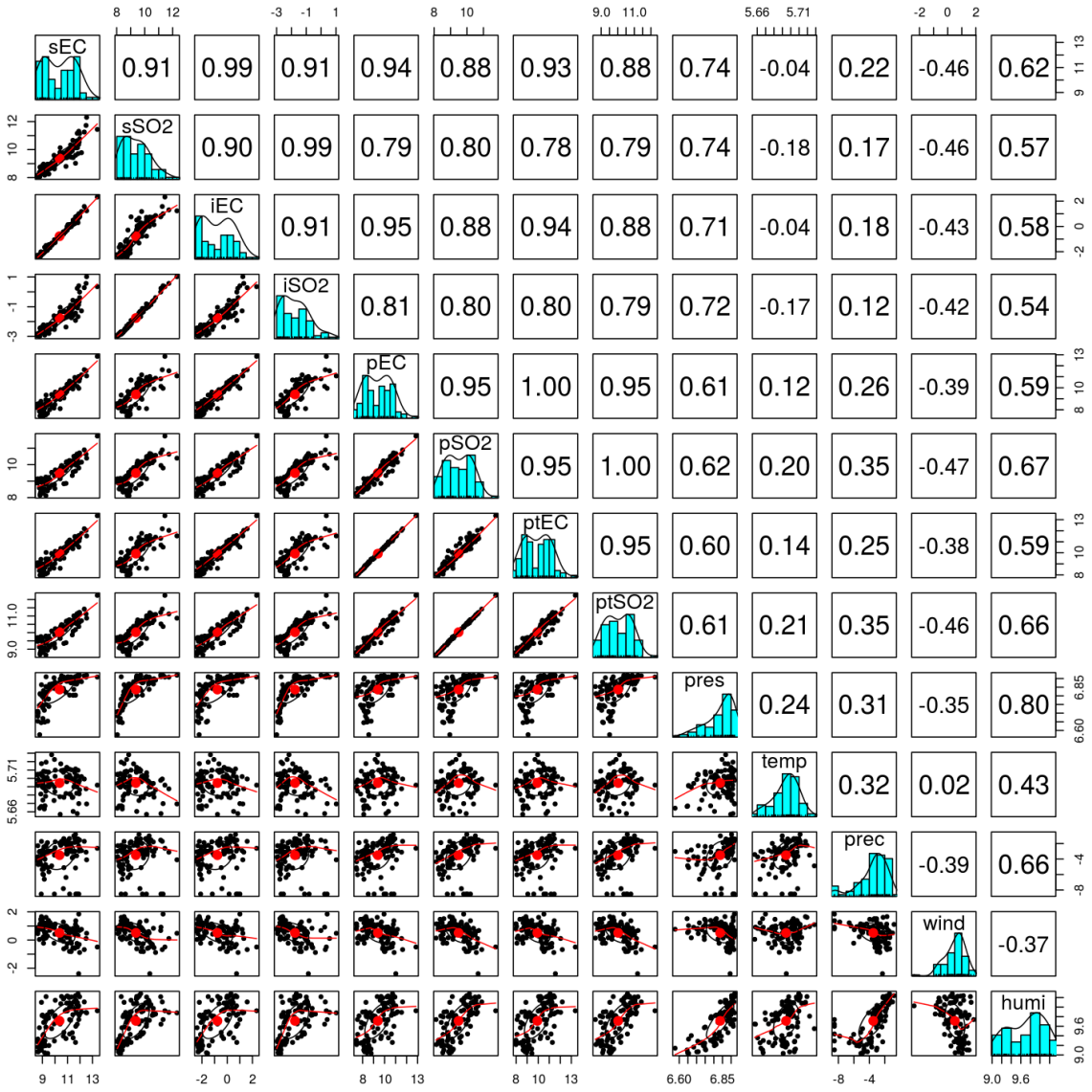

Figure B-1: Correlation matrix plot of selected parameters. All the values are natural log transformed. Pearson's correlation coefficients are on the upper right. sEC and sSO2: social cost [$/t] of EC and SO_2. iEC and iSO2: intake fraction [ppm] of EC and SO_2. pEC and pSO2: population [# of people] weighted for social cost with the average plume of EC and SO_2. ptEC and ptSO2: population [# of people] weighted for intake fraction with the average plume of EC and SO_2. pres: pressure [hPa], temp: temperature [K], prec: precipitation + 0.0002 [$\mathrm{g\,m^{-3}}$] (shifted for log transformation), wind: wind speed [$\mathrm{m\,s^{-1}}$], humi: humidity [ppm].

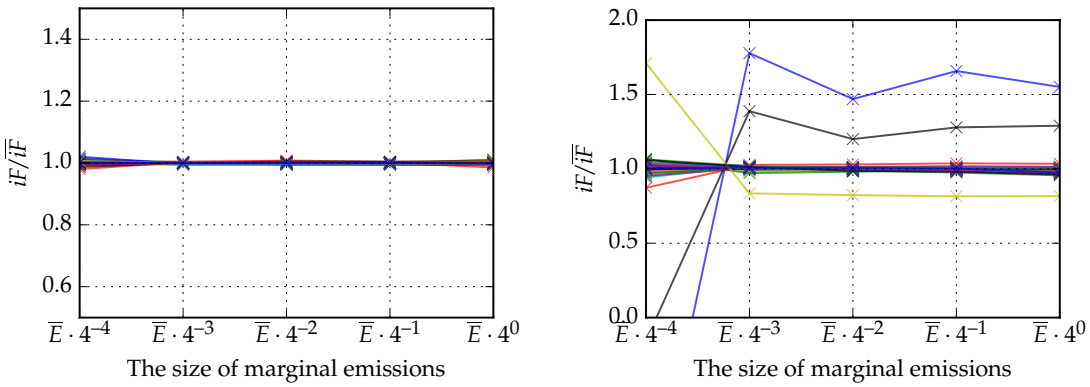

(a) EC

(b) SO_2

Figure B-2: The intake fractions over a range of marginal emissions. Each line represents the per-tonne social costs of one sample location. For the 50 training sample locations, the per-tonne social costs were calculated over a range of $\overline{E} \cdot 4^{-k} (k = 0, ..., 4)$, where $\overline{E}$ is the average emissions of area and point sources. The ratios of iF, the per-tonne social cost for given emissions at a sample location, over $\overline{iF}$, the average of iF over all $\overline{E}$ are on the y-axis. The EC social costs mostly stay constant over the range of marginal emissions and start to slightly diverge at the smallest perturbation. The SO_2 social costs also stay largely constant except that a few locations become unstable at the lowest emissions, $\overline{E} \cdot 4^{-4}$. We chose $\overline{E} \cdot 4^{-2}$ as our modeling basis.

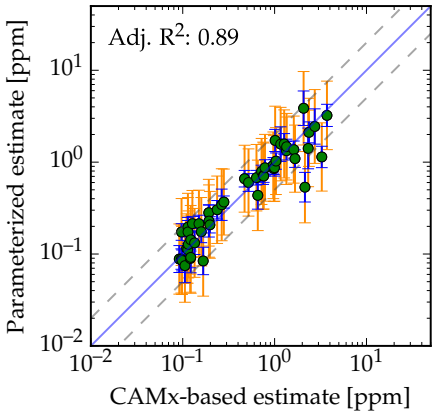

(a) EC: Fitted values

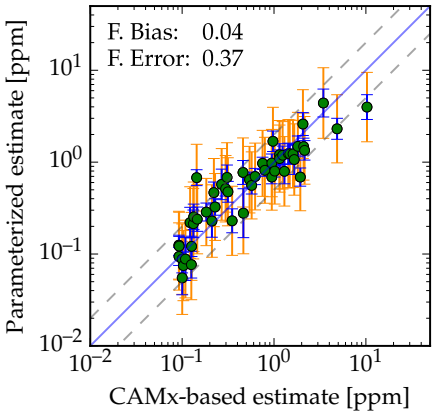

(b) EC: Out-of-sample evaluation

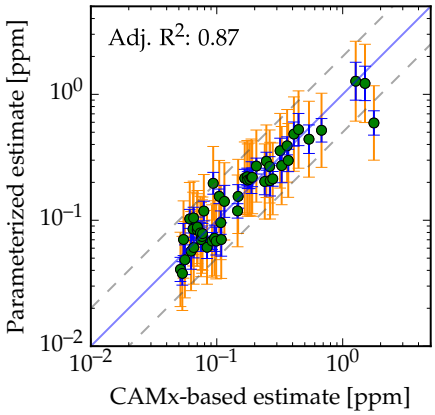

(c) SO_2: Fitted values

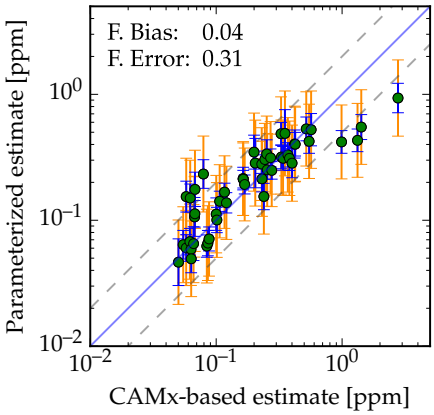

(d) SO_2: Out-of-sample evaluation

Figure B-3: The performance and evaluation of intake fraction population ring method models. On the x-axis are values estimated with CTM results and on the y-axis are values calculated by the regression model. (a) and (c) show the fitted values with 50 training sample locations. (b) and (d) show the out of sample evaluation done with 50 test samples. Yellow error bars present 95% prediction intervals and green error bars 95% confidence intervals.

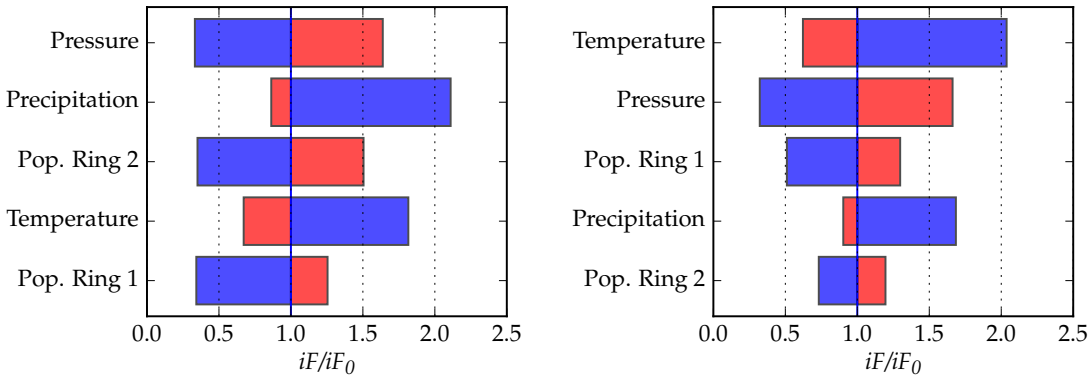

(a) EC

(b) SO_2

Figure B-4: Sensitivity of social costs to the variables of the population ring intake fraction models. Each range presents the ratio of intake fraction calculated with 5th (blue) and 95th (red) percentiles of a variable in the 100 samples to one calculated with its mean, iF_0.

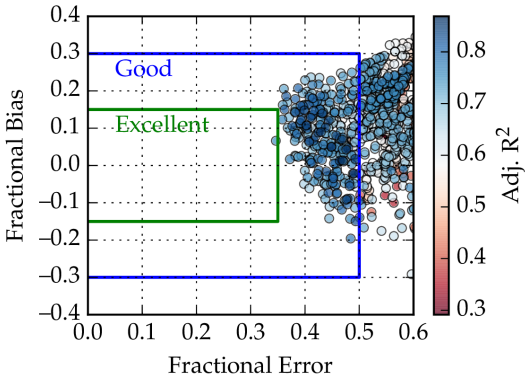

(a) One ring: 928 EC models

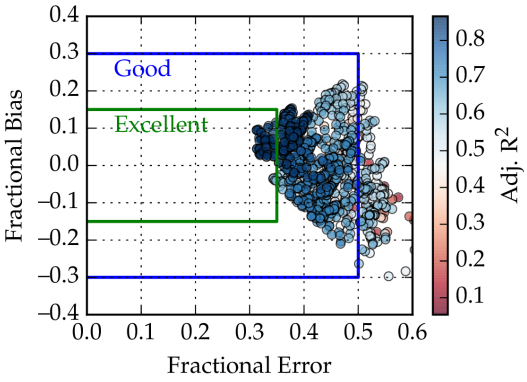

(b) One ring: 928 SO_2 models

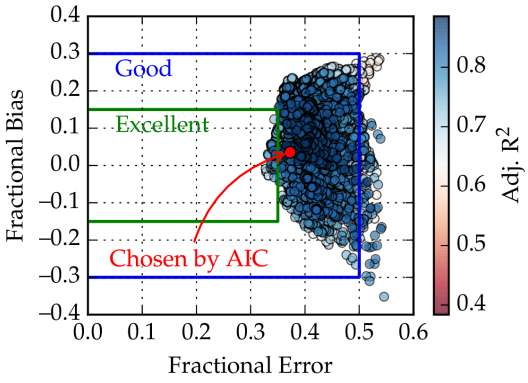

(c) Two rings: 6,912 EC models

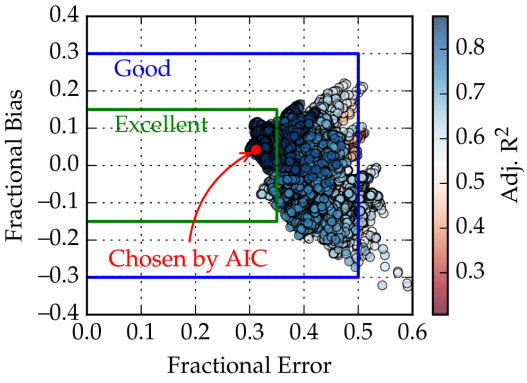

(d) Two rings: 6,912 SO_2 models

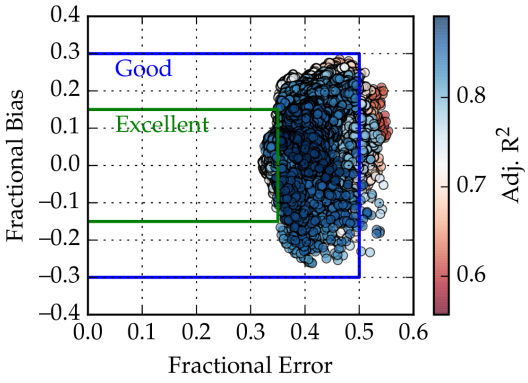

(e) Three rings: 67,488 EC models

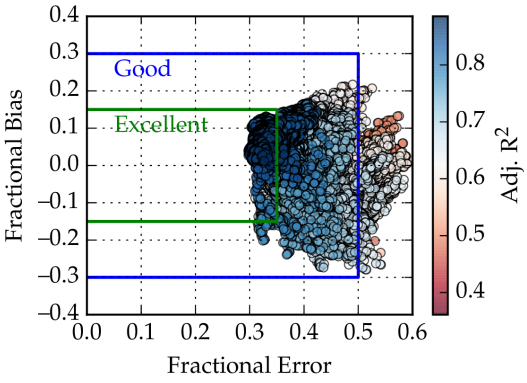

(f) Three rings: 67,488 SO_2 models

Figure B-5: Evaluation of population ring method intake fraction models. Each circle shows the adjusted R^2 from regression and the fractional bias and fraction error with the 50 test samples. 'Excellent' and 'Good' evaluation criteria are as defined by Morris et al. (2005).

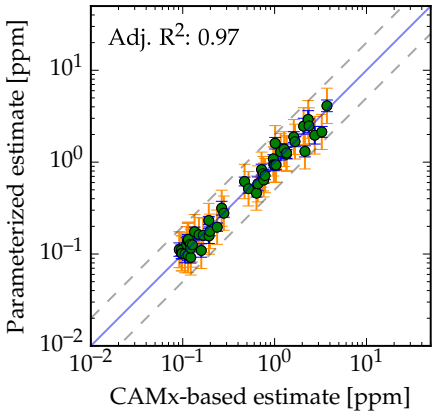

(a) EC: Fitted values

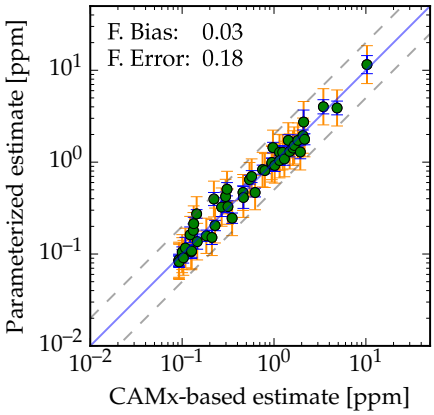

(b) EC: Out-of-sample evaluation

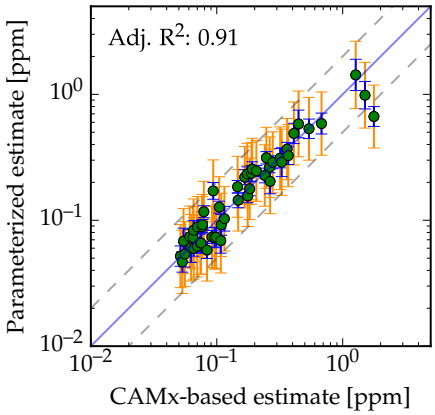

(c) SO_2: Fitted values

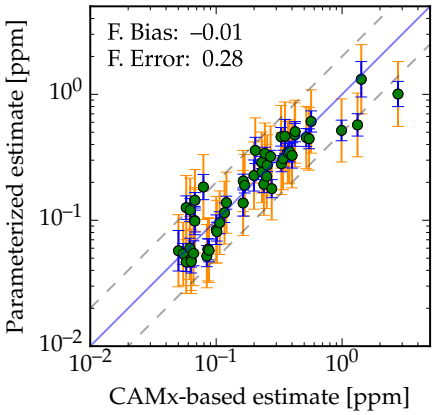

(d) SO_2: Out-of-sample evaluation

Figure B-6: Intake fraction average plume models' performance and evaluation. On the x-axis are values estimated with CTM results and on the y-axis are values calculated by the regression model. (a) and (c) show the fitted values with 50 training sample locations. (b) and (d) show the out of sample evaluation done with 50 test samples. Yellow error bars present 95% prediction intervals and green error bars 95% confidence intervals.

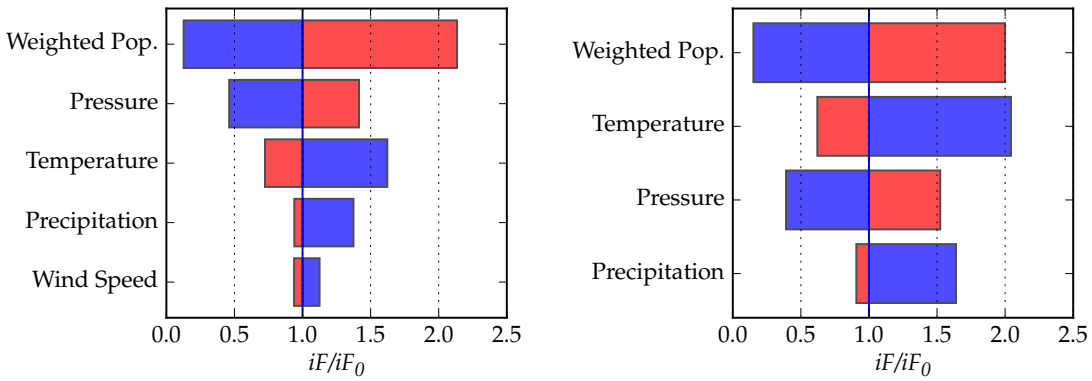

(a) EC (b) SO_2

Figure B-7: Sensitivity of social costs to the variables of the average plume intake fraction models. Each range presents the ratio of intake fraction calculated with 5th (blue) and 95th (red) percentiles of a variable in the 100 samples to one calculated with its mean, iF_0.

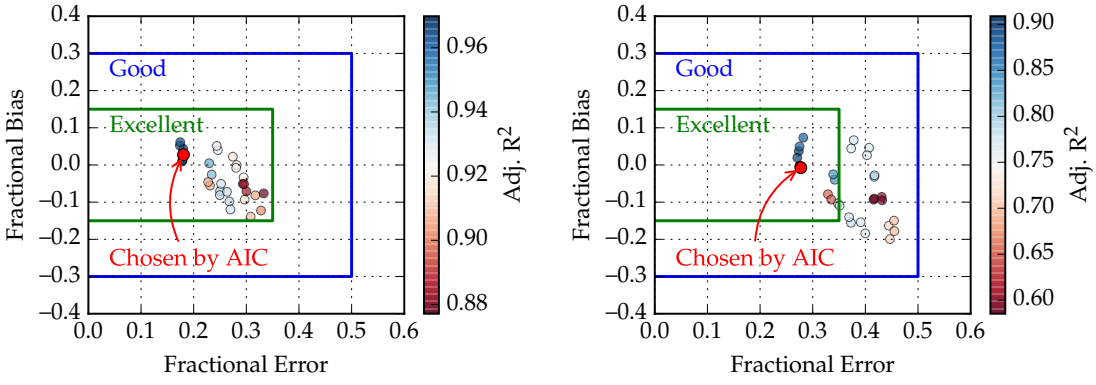

(a) EC (b) SO_2

Figure B-8: Evaluation of average plume method intake fraction models. 'Excellent' and 'Good' criteria are as defined by Morris et al. (2005).

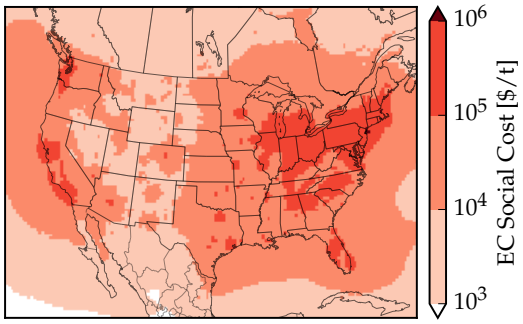

(a) EC social cost map

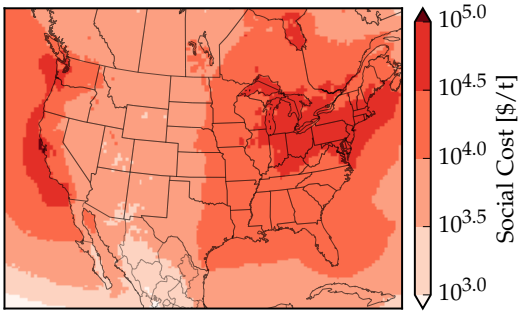

(b) SO_2 social cost map

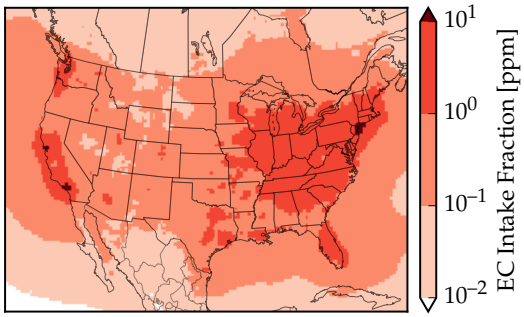

(c) EC intake fraction map

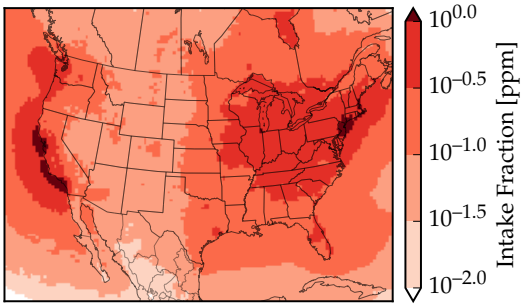

(d) SO_2 intake fraction map

Figure B-9: Air quality health effect maps for EC and SO_2. These maps are estimated by the regression models built using the average plume method. The estimate at a location on the map shows the social cost from the emissions at the location imposed on population nearby areas. The estimates are based on \$8.8M for VSL (adjusted for income level in 2010) and 1.06 for the relative risk.

Chapter 4. Parameterization of Social Costs of Elemental Carbon and Inorganic Particulate Matter Precursors

Abstract

A state-of-the-art chemical transport model (CTM) is too computationally expensive for many policy applications. Current reduced-form models either rely on overly simple atmospheric algorithms or have limited spatial or sectoral resolution. We developed a set of parameterizations for air quality social cost and intake fractions for primary $PM_{2.5}$ and three secondary $PM_{2.5}$ precursors (sulfur dioxide, nitrogen oxides, and ammonia), which give similar predictions like a CTM but are much more computationally efficiently. We used "the Estimating Air pollution Social Impacts Using Regression" (EASIUR) method, which builds parameterizations from running linear regressions on a dataset created for 100 representative locations in the United Stated using "tagged" CTM simulations. We used an "average plume," a generic $PM_{2.5}$ plume generated from CTM results, to describe exposed population over large receptor areas around an emissions source. The parameterizations have intuitive functional forms with population and commonly measured atmospheric variables such as temperature, pressure, precipitation, wind speed, and humidity. The coefficients explain key underlying mechanisms. Including total sulfate, total nitrate, and total ammonia improved the inorganic models further. Out-of-sample evaluations meet the 'excellent' criteria of a common air quality model performance metric (i.e., fractional bias ≤ 0.15 and fractional error ≤ 0.35) in most cases with some exceptions meeting the 'good' criteria (i.e., fractional bias ≤ 0.30 and fractional error ≤ 0.50). We found that the

average seasonal per-tonne social costs in the United States are $150,000-180,000/t EC, $21,000-34,000/t SO_2, $4,200-15,000/t NO_x, and $29,000-85,000/t NH_3. The social cost of EC is much larger than other species. Generally, wintertime social costs are the highest and summertime are the lowest, but for SO_2 it was opposite. The parameterizations presented in this work will be of a great use in policy research that involves changes in air quality.

4.1 Introduction

Estimating the effect of air quality on human health and the natural environment is an essential part of air quality policy assessment and design. Many assessments have sought to quantify these damages, most notably the U.S. EPA's series of the benefit cost analyses of the Clean Air Act (U.S. EPA, 1997, 1999, 2011e) and regulatory impact analyses like one performed for the Cross-State Air Pollution Rule (U.S. EPA, 2011d). $PM_{2.5}$, particulate matter having the diameter of 2.5 μm or less, is strongly associated with premature mortality (Beelen et al., 2014; Crouse et al., 2012; Krewski et al., 2009; Lepeule et al., 2012). Characterizing the $PM_{2.5}$ impacts on mortality is especially important because the impacts account for more than 90% of the monetized cost of worsening air quality (U.S. EPA, 1999, 2011e).

$PM_{2.5}$ could be divided into two categories: primary and secondary species. "Primary" $PM_{2.5}$, such as elemental carbon is directly emitted as particle. However, a substantial fraction of $PM_{2.5}$ consists of secondary species, which are chemically produced in the atmosphere from gaseous precursors. Secondary $PM_{2.5}$ includes inorganic $PM_{2.5}$, which is produced from sulfur dioxide, nitrogen oxides, and ammonia, as well as most organic $PM_{2.5}$ (Zhang et al., 2007). Although active research efforts are underway to find out where the toxicity of $PM_{2.5}$ comes from (e.g. chemical composition or particle size) (Franklin et al., 2008; Harrison et al., 2004), there are not

definitive epidemiological evidences yet to differentiate the effects from different species (Bell, 2012), and $PM_{2.5}$ is currently regulated on a mass concentration basis (U.S. EPA, 2013a).

The social cost and intake fraction are common metric for evaluating the public health impacts of air quality. The social cost of air quality is defined as the monetized damages from air pollution, which is estimated as follows (U.S. EPA, 1999, 2011e). Air quality simulation tracks the emissions of an air pollutant and its physical and chemical processes in the atmosphere and determine $PM_{2.5}$ concentrations exposed to population. Then, the number of premature deaths in exposed population is estimated based on so-called concentration-response relations reported by epidemiological studies. The mortality is monetized with the value of a statistical life, people's willingness-to-pay to avoid the mortality risk. By dividing the monetized value by the amount of emissions, the per-tonne social cost in obtained. Intake fraction (Bennett et al., 2002) is a metric of characterizing the emissions-to-intake relationship, which is defined as the fraction of the amount of air pollutant or its precursors emitted that are inhaled by an exposed population.

Especially, per-tonne social cost and intake fraction for "marginal" emissions are highly convenient for policy research because policy scenarios usually involves "marginal" changes in emissions. Social cost or population intake can be easily evaluated by multiplying marginal social costs or intake fraction by the changes in emissions, assuming that the public health impacts respond linearly to emissions. Per-tonne social cost or intake fraction should be used carefully considering the ranges of emissions that they stay linear.

One of the major technical challenges estimating the per-tonne social cost and intake fraction is to estimate the changes in air quality because, once air pollutants are emitted to the atmosphere, they may affect a large area reaching thousands of kilometers downwind while undergoing complex physical and chemical processes. As computer systems are getting more

powerful and cheap, chemical transport models (CTMs) play a critical role in the social cost analysis (U.S. EPA, 1999, 2011d, 2011e) in determining how emissions changes impact air quality because CTMs are the most sophisticated and realistic models that usually reflect the up-to-date atmospheric science. CTMs divide the atmosphere into a three-dimensional grid of boxes, calculate the atmospheric processes of transport, chemical reactions, and removal in each boxes, and estimate the concentrations of key air pollutants and their precursors at a high temporal resolution typically of 15 minutes or less. Due to detailed characterization of air quality, CTMs require huge computational costs, which inevitably result in compromises in spatial domain covered, time period simulated, and/or spatial resolution.

Therefore, it is not surprising that the existing social cost models based on sophisticated CTMs have a limited spatial or sectoral resolution though they perform like their underlying CTMs. U.S. EPA's Response Surface Model (RSM) (U.S. EPA, 2006) is such a model built with a multidimensional kriging method based on simulation outputs generated by CMAQ (Byun and Schere, 2006), a chemical transport model. The social costs derived from RSM are limited spatially and sectorally, that is, to national and nine urban areas and to emissions changes in 12 sectors. Buonocore et al (2014) provided regression models that parameterized the social cost with populations around a power plant based on a set of CMAQ simulations for about 50 power plants in some parts of the U.S. Their study was limited to 40 CMAQ runs and their models may be probably hard to be applied outside of the power plants in the study region.

Because of the complexity and computational costs of CTMs, policy research often relies on reduced-form models. Perhaps the most widely used tool is the Climatological Regional Dispersion Model (CRDM) (Latimer, 1996), which is a Gaussian-dispersion-based source-receptor air quality model used in popular social cost models (Muller, 2011; Muller and

Mendelsohn, 2007; U.S. EPA, 2013b) as well as in air quality social cost studies (Levy et al., 2009; Shadbegian et al., 2007; U.S. EPA, 2004). CRDM provides the marginal change in annual-average $PM_{2.5}$ concentrations in every U.S. county for an incremental emissions of $PM_{2.5}$ precursor in one county. Based on annual-average meteorology and some seasonal adjustments, CRDM handles dispersion, wet and dry deposition, and first-order chemical conversion for primary and secondary $PM_{2.5}$ species.

However, CRDM's annual time resolution may be overly simple, perhaps producing substantial biases for species with highly nonlinear behaviors. As an example, inorganic $PM_{2.5}$ and its precursors may not work well because they travel a long distance and associated chemical processes vary regionally and are sensitive to meteorological conditions (Ansari and Pandis, 1998; Blanchard et al., 2000; West et al., 1999), which cannot be easily captured by the Gaussian approach that assumes the conditions at the location of emissions stay constant. Furthermore, it was recently found that there are much more secondary organic $PM_{2.5}$ than previously thought (Goldstein and Galbally, 2007; Robinson et al., 2007; Zhang et al., 2007) and that the total volatile organic compounds (VOC) are a bad predictor of organic $PM_{2.5}$ formation (Jathar et al., 2014), which makes CRDM's $PM_{2.5}$ predictions from VOC badly outdated as of today's science. In addition, CRDM's county-based spatial resolution may produce biases for larger and heterogeneous counties, such as those in the western United States.

We previously explored methods of building a model called the Estimating Air Pollution Social Impacts Using Regression (EASIUR) model (Chapter 3), which tries to overcome the limitations of both chemical transport models and current reduced-form models. The basic approach is to derive a regression model from a set of CTM simulations. We ran "tagged" simulations (Koo et al., 2009; Wagstrom et al., 2008), which enabled to create a large dataset

with limited simulation runs, reducing the computational requirement over a factor of 50. A "tagged" simulation tracks emissions from multiple "sources" and calculates their contributions at all "receptor" locations for each "source," which allowed us to simulate the air quality of 50 locations with one CTM run. The EASIUR model predict like CTMs at the computational speed and ease-of-use of reduced-form models. An important merit of the EASIUR model approach is that the model can evolve as the underlying CTMs improve because the EASIUR model can be rebuilt from an improved CTM. This would be especially important for organic $PM_{2.5}$ because the understanding of organic aerosols has changed substantially recently and is expected to improve further in the future.

This paper describes the method of building the EASIUR model and present a complete set of per-tonne social cost and intake fraction parameterizations for the four species that dominate the formation of inorganic $PM_{2.5}$: elemental carbon, sulfur dioxide, nitrogen oxide, and ammonia. We explore the sensitivity of social cost to emissions characteristics and simulation periods and discuss other sources of uncertainty.

4.2 Method

The overall goal of the EASIUR approach is to produce easy-to-use linear regressions for social costs and intake fractions models that are derived from state-of-the-art CTM simulation outputs. To develop a representative set of emissions perturbations, we ran CAMx, a CTM, to calculate per-tonne social costs and intake fractions at 100 locations randomly chosen in the U.S. domain. We ran regression analysis to parameterize the resulting social costs and intake fractions with population and atmospheric variables. We used 'average plumes' (described below) generated from CTM output to characterize the exposed population used in regression. We ran additional several sets of CAMx simulations to explore the sensitivity of air quality impacts to emissions

characteristics and simulation period. All monetary values in this paper are in year 2010 USD unless otherwise noted.

4.2.1 The CAMx Chemical Transport Model

We used the Comprehensive Air Quality Model with extensions (CAMx) version 5.41 (ENVIRON, 2012), a regional-scale three dimensional chemical transport model. CAMx was run with the input database developed for a U.S. EPA's regulatory impact analysis (U.S. EPA, 2011d) and evaluated comprehensively (U.S. EPA, 2011a). The base year of the input database is 2005. The meteorology was generated by MM5 (Grell et al., 1995). Emissions inventory (U.S. EPA, 2011b) was prepared primarily based on the 2005 National Emissions Inventory version 2 (http://www.epa.gov/ttn/chief/net/2005inventory.html). The inventory also includes anthropogenic and biogenic emissions from Mexico and Canada. Using this air quality simulation platform, we simulated the United States domain in a 148×112 grid (shown in Figure 4.1) with a horizontal resolution of 36×36 km^2 and 14 vertical layers reaching up to about 16 km, which is an appropriate resolution for $PM_{2.5}$ public health effects (Thompson and Selin, 2012).

The Particulate Source Apportionment Technology (PSAT) (Koo et al., 2007) is a CAMx extension that substantially reduces the computational burden associated with the large number of emissions perturbations simulations required here. PSAT is a "tagging" algorithm that tracks the contributions of emissions separately from multiple designated cells to $PM_{2.5}$ concentrations in the CAMx grid. With PSAT, we tracked such contributions from emissions at 50 locations in one CAMx simulation, only requiring about a tenth of computation time and disk space compared to a common brute force simulation.

4.2.2 Generating the Social Cost and Intake Fraction Modeling Dataset

We generated a dataset of social cost and intake fractions for emissions stemming from 100 sample CAMx grid cells using the tagged CAMx PSAT simulations. We divided these 100 locations into two sets of 50, one for training the regression models and the other for out-of-sample testing. These locations are shown in Figure 4.1. We anticipate that most of the variability in social costs results from the number of people exposed, so the training sets should include emissions in both densely and sparsely populated regions. To accomplish this, five locations for each sample set were randomly selected at every 10^{th} population percentile among CAMx cells where population is not zero.

We calculated the changes in $PM_{2.5}$ concentrations from "marginal" emissions by comparing a simulation with base case emissions and a simulation with the "marginal" emissions. The choice of the size of "marginal" emissions is important because CAMx may not simulate properly for too small values due to its numerical precision limit or the $PM_{2.5}$ impacts may not be linear above large emissions due to nonlinear atmospheric processes. After we explored the sensitivity to the size of perturbation over a wide range (See Chapter 3.3 and Chapter 4.3.3), we added for perturbation cases one sixteenth (or about 6.25%) of annual average emissions ($\bar{E}$) for each species (EC: 6.6 kg/day, SO_2: 190 kg/day, NO_x: 270 kg/day, and NH_3: 69 kg/day) to each sample location. Even though each emissions perturbation is relatively small, perturbation experiments for each inorganic species (SO_2, NO_x, and NH_3) were run in separate sets from each other to avoid nonlinear interactions. EC perturbation cases were included in SO_2 perturbation cases because EC does not react chemically in the atmosphere. The changes in $PM_{2.5}$ concentrations were calculated by comparing the sum of inorganic $PM_{2.5}$ concentrations between base case and perturbation case for SO_2, NO_x, and NH_3 and by comparing just EC concentrations for EC. Each

CAMx simulation was run for the entire 2005 year in a set of four separate seasonal simulations. We refer winter season defined here as January, February, and March; spring as April, May, and June; summer as July, August, and September; and fall as October, November, and December. Each simulation period includes 10 days from the prior month for model spin-up to prevent distorted results from initial conditions, and these 10 days are not included in the analysis.

We calculated the social cost of air quality with a standard method used in U.S. EPA's regulatory impact analyses (U.S. EPA, 1999, 2011e) (see Chapter 3.2.3). From CAMx simulations, we calculated the changes in $PM_{2.5}$ resulting from emissions at the 100 sample grid-cell locations by comparing $PM_{2.5}$ concentrations from a base case and a perturbations case. We compared only EC concentrations for EC emissions perturbations but, for SO_2, NO_x, and NH_3 emissions, we examined all CAMx $PM_{2.5}$ species to account for interactions between these species. Then, the changes in premature death from the changes in $PM_{2.5}$ concentrations were calculated based on cohort-based $PM_{2.5}$ epidemiological studies. We used concentration-response relations from each latest follow-up studies from the two landmark studies; we used Krewski et al. (2009) as our basis but also generalized our results to Lepeule et al. (2012). The estimated changes in premature mortality were monetized by using $8M for the value of a statistical life (VSL), which U.S. EPA recommends based on 26 value-of-life studies (U.S. EPA, 2010). Later, our results are also generalized for the choice of VSL. Finally, by dividing the monetized value by the added marginal emissions, per-tonne social cost at each sample location is calculated per species as well as per season.

The intake fraction (Bennett et al., 2002) is defined as the mass ratio of the $PM_{2.5}$ inhaled by population to the emissions of its precursor:

$$iF = \sum_{x,y} \frac{B \cdot P_{x,y} \cdot \Delta c_{x,y}}{E} \quad (1)$$

where B is the volumetric breathing rate (m^3/person/day), $P_{x,y}$ is the population at a grid cell (x, y), $\Delta c_{x,y}$ is the change in $PM_{2.5}$ concentration at that grid cell, and E is the emissions perturbation from the upwind cell. We used a population mean value, 14.6 m^3/person/day, for B, which was derived by weighting U.S. EPA's recommended long-term age-specific breathing rate (U.S. EPA, 2011c) with 2010 US Census population.

4.2.3 The Parameterization Approach of the EASIUR Method

Our parameterization is based on a log linear functional form as follows:

$$\ln S = \alpha + \beta \cdot \ln P_w + \sum_i \gamma_i \cdot \ln A_i \,, i = 1, \dots, k \quad (2)$$

$$\ln iF = \alpha + \beta \cdot \ln P_w + \sum_j \gamma_j \cdot \ln A_j \,, j = 1, \dots, l \quad (3)$$

where S is the per-tonne social cost [$/t], iF is intake fraction [ppm], P_w is population weighted with an average plume (described below), and A_i and A_j are atmospheric variables. $\alpha, \beta,$ and γ_i are regression coefficients. For A_j, we tried temperature [K], surface atmospheric pressure [hPa], wind speed [m/s], humidity [ppm], daily average precipitation [g/m^3], cloud optical depth (dimensionless), and vertical diffusivity [m/s^2]. The daily average precipitation (A_p), which is the precipitation water content [g/m^3] in the CAMx surface layer of 38 m depth, can be converted from a common precipitation metric (d) [mm]: $A_p = 26.3 \cdot d$. We used daily average value for each season for all A_j's. Each season's dataset was separately fitted per species.

It is crucial and challenging to precisely describe an exposed population in a simple way. In general, $PM_{2.5}$ and its precursors are transported hundreds of kilometers or more, so population

density in the source grid cell is insufficient by itself to characterize the exposed population. Population near the emissions source will be exposed to higher levels of pollutants than those further from the source. But the size of exposed population increases as air pollutants travel farther from the source though they may be exposed to lower concentrations. Since different species undergo different chemical processes, they also differ in how far downwind their impacts are felt, which make it more complicated to characterize the population exposure. Therefore, a successful approach for dealing with this should weight population nearer a source more heavily and should also differ by pollutant type. We developed two methods in Chapter 3: the population ring method and the average plume method. Though both methods worked well, the latter worked better and, therefore, we used the average plume method.

An average plume resulting from a $PM_{2.5}$ precursor describes the spatial distribution of $PM_{2.5}$ impacts around a generic emissions source, which accounts for transport, dispersion, chemical conversions, and removal over affected area. An average plume is computed for each precursor and season. To generate the average plume, the spatial distribution of $PM_{2.5}$ impacts for all 50 training samples were: 1) put on a common grid with the origin as the emissions source; 2) rotated so that the prevailing wind direction was in the x-direction; 3) normalized so each had the same net $PM_{2.5}$ impacts. After these procedures, the 50 plumes are averaged to obtain a generic spatial distribution of $PM_{2.5}$ impacts in a season for a given source. A weighted population, P_w in Eqs. 2 and 3, is calculated by placing an average plume to a source location of interest after aligning dominant wind direction and summing the product a plume value with corresponding population cell by cell.

We expected that it would be challenging to parameterize social cost and intake fraction when the inorganic species (SO_2, NO_x, and NH_3) interact with each other through nonlinear acid-base

neutralization (Ansari and Pandis, 1998; Blanchard et al., 2000). For example, when ammonia, an important atmospheric base, is emitted, it may remain as a gas if sulfuric acid or nitric acid does not exist, forming no $PM_{2.5}$. But if unneutralized sulfuric acid exists, ammonia neutralizes sulfuric acids, forming ammonium sulfate PM ($(NH_4)_2SO_4$). If excess ammonia exists after neutralizing sulfuric acid, it forms ammonium nitrate PM (NH_4NO_3), which is enhanced by low temperature and high relative humidity. What complicates the estimation of $PM_{2.5}$ formation is that one mol of ammonia adds about 5 times more $PM_{2.5}$ mass by forming ammonium nitrate PM than ammonium sulfate PM. Therefore, the same amount of emissions may form different amount of $PM_{2.5}$ depending on the availability of ambient sulfur dioxide, nitrogen oxide, and ammonia. PM nitrate formation is common during wintertime in the eastern United States. In California, PM nitrate formation is common all the time because of NO_x emissions from urban mobile sources mixed with ammonia emissions from large agricultural areas (Hand et al., 2012; Pitchford et al., 2009; Chow et al., 1994). Though the inorganic system is well understood (Ansari and Pandis, 1998; Blanchard et al., 2000; West et al., 1999), the $PM_{2.5}$ formation is not easy to predict because of its nonlinear nature.

Considering the complexity of inorganic $PM_{2.5}$, we also tried as an atmospheric parameter (A_i in Eqs. 2-3) total sulfate ($TS \equiv SO_4^{2-}$ [mol/m^3]), total nitrate ($TN \equiv HNO_3 + NO_3^-$ [mol/m^3]), and total ammonia ($TA \equiv NH_3 + NH_4^+$ [mol/m^3]). Two more parameters, the gas ratio (GR) and the adjusted gas ratio (adjGR), were also considered. GR(Ansari and Pandis, 1998) is an effective indicator describing the thermodynamic regime of the inorganic PM system as defined as follows:

$$GR = \frac{\text{free ammonia}}{\text{total nitrate}} = \frac{TA - 2 \cdot TS}{TN} \quad (4)$$

And, adjGR (Pinder et al., 2008a) is an indicator that is similar but better to describe conditions where sulfate is not fully neutralized.

$$\text{adjGR} = \frac{\text{TA} - \text{DSN} \cdot \text{TS}}{\text{TN}} \tag{5}$$

where DSN is the degree of sulfate neutralization (DSN $\equiv ([\text{NH}_4^+] - [\text{NO}_3^-])/[\text{SO}_4^{2-}]$). When sulfate is fully neutralized, DSN = 2.

We fitted Eqs. (2) and (3) with all the possible combinations of selected parameters. We used the Akaike information criterion (AIC) to select the best models. AIC, a measure of the relative regression performance, favors the goodness of fit but also penalizes for the number of parameters to discourage overfitting (Akaike, 1974). With the test 50 samples, we evaluated the chosen models with the model performance criteria suggested by Morris et al., (2005), which are commonly used to evaluate air quality models. The criteria are based on fractional bias and fractional error, which are defined as follows:

$$\text{Fractional bias} = \frac{2}{N}\sum_{\text{i}}^{\text{N}} \frac{P_i - O_i}{P_i + O_i} \tag{6}$$

$$\text{Fractional error} = \frac{2}{N}\sum_{\text{i}}^{\text{N}} \left|\frac{P_i - O_i}{P_i + O_i}\right| \tag{7}$$

where P_i is prediction, O_i is CAMx-based estimate, and N is the number of test samples. Performance is considered 'excellent' for fractional bias $\leq \pm 0.15$ and fractional error ≤ 0.35, 'good' for fractional bias $\leq \pm 0.3$ and fractional error ≤ 0.5, and 'average' for fractional bias $\leq \pm 0.6$ and fractional error ≤ 0.75. We also report normalized mean bias and normalized mean error as defined below:

$$\text{Normalized Mean Bias} = \frac{\sum_i^N (P_i - O_i)}{\sum_i^N O_i} \tag{8}$$

$$\text{Normalized Mean Error} = \frac{\sum_i^N |P_i - O_i|}{\sum_i^N O_i} \quad (9)$$

4.2.4 Sensitivity of Air Quality Impacts to Emission Characteristics and Simulation Period

We explored the sensitivities of public health impacts to several factors. First, how per-tonne social cost and intake fraction change over a range of emissions was explored to analyze the range where our results would remain valid because they may not remain linear above a certain range due to nonlinear atmospheric responses. Compared to what we have done in Chapter 3, we here analyzed more species for more time periods over a wider range of emissions. We ran simulations to include all inorganic species (EC, SO_2, NO_x, and NH_3) for one month period per season by changing the perturbation size over a range of $\bar{E}\times 4^i$ for $i = -4, \dots, 1$, where $\bar{E}$ is the annual average emissions of non-zero emissions CAMx grid cells.

The other sensitivity analysis was done for the length of simulation time periods. We explored how social cost estimates at the 100 sample locations vary with the length of the CTM simulation to see how social cost and intake fraction converge over the time period. This can inform the variability of $PM_{2.5}$ formation and associated health impacts over different time periods. In addition, it would provide a guideline for the appropriate length of CTM simulations relevant for public health impact analysis, showing what simulation length could represent a certain season or month.

Lastly, the social costs of point sources are compared to those of area sources since point emissions are usually emitted at an elevated height and would have different consequences than area emissions. It is likely that emissions made at an elevated stack may result in lower marginal

damages compared to the same amount of emissions made at the ground level if emissions occur nearby densely populated areas since more $PM_{2.5}$ may travel farther to less populated areas. Conversely, elevated emissions at less populated areas may results in higher marginal damages because $PM_{2.5}$ may travel farther to reach more population downwind. CAMx point sources have various information such as location, stack height, stack diameter, stack exit temperature, and flow rate. Since it is not easy to evaluate how all these factors affect our results, we chose one case of having a median stack. The hypothetical stack has a height of 20 m, a diameter of 0.8 m, an exit temperature of 555 K, a flow rate of 45,000 m^3/h. We ran additional simulations by adding this hypothetical stack at the training sample locations with the same additional emissions ($\bar{E}/16$) as in area emissions cases. We compared the social costs of point emissions to those of area emissions.

4.3 Results and Discussion

4.3.1 Average Plumes

Figure 4.2 shows the average plumes of the four species for summer season. To give a sense of scale, they were put on a map with their center on Pittsburgh. A complete set of average plumes for all seasons together with cumulative distributions are presented in Figures C-18 to C-21. The average plumes show the general characteristics of an air pollutant's dispersion and chemical conversion. The impacts of elemental carbon and ammonia emissions are nearer to the sources than sulfur dioxide and nitrogen oxides (i.e. 50% of EC and NH_3 weights covers about 200-300 km from source while 50% of SO_2 and NO_x covers 700-1000 km). Emitted directly as particle, EC travels less than the other gaseous PM precursors. Ammonia has a higher impact near the emissions source because ammonia gas partitions to the aqueous phase much more readily than

SO_2 and NO_x and, therefore, affects nearby source location more with dry depositions. The impact of sulfur dioxide and nitrogen oxides is more widely spread out because they need to undergo atmospheric oxidation to form $PM_{2.5}$. All the plumes are skewed to the right from the aligned wind direction, which is caused by the rotation of the Earth, that is, the Coriolis effect.

However, even the weight of elemental carbon and ammonia at the source cell (36 km × 36 km) is less than 20% and a substantial fraction covers a large area. For example, the area covering 80% of the EC weight reaches about 700-1,000 km from source. The weight of NO_x and SO_2 at the source grid cell is only 1-3% and 80% of the weights reach about 2,000 km from source. Average plumes show that it is important to address the exposure $PM_{2.5}$ levels that change over a large area. A little caveat is that average plumes are not directly translated to health damages. It still needs to account for where the population lies for a given source location as well as for regional differences in $PM_{2.5}$ formation (i.e. $PM_{2.5}$ formation would be different depending on atmospheric conditions).

4.3.2 Generated Dataset of Social Cost and Intake Fraction

Social costs and intake fractions calculated from CAMx simulations are presented in Figures 4.3 and C-1. The summary statistics of social costs, intake fractions, and associated parameters of the sample locations are presented in Tables C-1 to C-8. The social costs and intake fractions show the seasonal and chemical characteristics of the species. The public health impacts of elemental carbon are much higher than those of others because EC is emitted directly as PM while others form PM chemically in the atmosphere. In winter, all the species show higher impacts as well as narrower variability, showing the role of low temperature in reducing the vertical mixing height, which makes air pollutants less diluted vertically in winter. Such a trend

is even stronger for NO_x and NH_3, which is due to more PM nitrate formation from cold temperature in wintertime.

Correlation matrix plots of selected variables are presented in Figures C-2 to C-9. The maps of meteorological variables we used in parameterization—pressure, temperature, precipitation, wind speed, humidity, total sulfate, total nitrate, and total ammonia—are presented in Figures C-10 to C17. Note that there was one negative social cost and one negative intake fraction for NO_x in spring and summer. Because the number is small, we did not include them for simplicity in our regression as well as in the summary statistics.

4.3.3 The EASIUR Model

In Tables 4.1-4.8, we present one set of the EASIUR model for elemental carbon but two sets for inorganic species. One regression model set is 'simple,' having fewer parameters with more intuitive coefficients. With TS, TN, and TA as additional parameters, the other set has a 'better-fit', having a better prediction performance but their coefficients are not intuitive because the additional parameters are correlated with other parameters. Though simpler models may be easier to use and better to understand the key mechanisms behind estimates, the better prediction would be more valuable in application. However, since the emissions of sulfur dioxide and nitrogen oxides are decreasing in recent years and expected to decrease substantially further in the future (Pinder et al., 2008b; U.S. EPA, 2011d), the "better-fit" models may not be used with input data from a different year because the presented models are tuned with TS, TN, and TA estimated from emissions in 2005.

EC parameterizations for both social cost and intake fraction have a high goodness of fit as represented by the high adjusted R^2 of mostly about 0.9 or higher as shown in Table 4.1 and 4.2. The scatter plot of out-of-sample evaluations for EC social cost models presented in Figure 4.4

shows the comparison between social costs estimated by regression models and those directly estimated from CAMx results for the 50 test sample locations. The independent test shows that the simple one-equation models predict the computationally expensive CTM-based estimates very well with tight prediction intervals less than a factor of two. The out-of-sample tests of all EC models meet the 'excellent' criteria. Additional scatter plots of out-of-sample evaluations together with those of comparing fitted values to CTM estimates are presented in Figure C-22 and C-23.

Parameterizations of SO_2, NO_x, and NH_3 also show good performance in general. The high adjusted R^2 values are mostly about 0.8 or higher, with the exception of winter and fall SO_2 and NO_x models, which were expected to be difficult due to their nonlinear nature. As shown in Figure 4.5, adding TS, TN, and TA improves the adjusted R^2 for SO_2 and NO_x in winter and fall, which are the worst cases, as well as NH_3 in spring and summer. Figure 4.6 and 4.7 present the out-of-sample evaluations for 'simple' and 'better-fit' models. The out-of-sample tests also show that the model performance improves with the additional parameters in the 'better-fit' models. Even with additional parameters, summer NO_x models produce relatively high fractional errors, meeting the 'good' criteria. Note that social costs of NO_x in summer tend to be low (i.e. the median value is just \$690/t NO_x) and, therefore, the high variability of NO_x social cost estimates may not be a problem in policy analysis. In addition, the out-of-sample test figure also shows that the worst cases are not unacceptable. Despite the lowest adjusted R^2, the winter SO_2 models predictions are mostly within a factor of two compared to CTM-based estimates and their prediction intervals are also tight, about a factor of two, comparable to other seasons. In spring and summer, when the nonlinear chemistry is weak, SO_2 models perform better than NO_x and NH_3. As summarized in Figure 4.8, all the "better-fit" models meet the 'excellent' criteria except

that the NO_x models in summer and fall meet the 'good' criteria. All the "simple" models are 'excellent' or 'good' except for the summer NO_x model. Additional scatter plots of out-of-sample evaluations together with those of comparing fitted values to CTM estimates are presented in Figure C-24 and C-35.

In most models, weighted population, temperature, and pressure appeared as very significant parameters. As expected, weighted population is positively correlated, representing the size of exposed population, which is shown in the correlation matrix plots in Figure C-2 to C-9. Exceptions are NO_x and SO_2 models in January (further discussed below). Temperature is strongly negatively correlated in all models except winter SO_2 'simple' model. This would be because the higher temperature the higher boundary mixing layer height, which results in more vertical dilution of $PM_{2.5}$. Surface atmospheric pressure is positively correlated. The pressure values we used are not sea level adjusted and strongly correlated with surface elevation as can be seen in Figure C-10. This means that pressure is a proxy variable for population because population density is low not only in the mountainous areas such as the Rocky Mountains and the Appalachian Mountains but also in the high plateaus such as the Great Basin and the Great Plains while many densely populated urban areas are in coastal areas. The correlation plots show that pressure is correlated with weighted population.

Precipitation, wind speed, and humidity appear in many parameterizations, though they are often not statistically significant. Precipitation generally has negative coefficients, indicating its role in wet deposition, the dominant $PM_{2.5}$ removal mechanism. An exception is summer NH_3 models, which may be because precipitation keeps NH_3 in the aqueous phase by suppressing active summertime NH_3 volatilization from high temperature. Wind speed generally has negative coefficients. Though it may be related with the role of wind in dispersion, wind speed

seems to be more negatively correlated with population density, as shown the consistent negative correlations with population variables in correlation plots. Figure C-13 also shows that the windy areas are located along the Rocky Mountains as well as some under-populated part of the Midwest. Humidity is generally positively correlated. This would also be related with population because coastal areas are more humid than mountainous areas, which is similar to pressure. However, humidity has a negative coefficient in all summer models, which would be because humidity is more positively related to precipitation rather than population and, therefore, indicates the PM removal from precipitation. Correlation plots show that humidity is positively correlated with pressure as well as weighted population and that humidity is most strongly positively correlated with precipitation in summer. Though not shown in results, we tried cloud optical depth for its potential role in photochemical processes but it did not appear statistically significant. We also tried interaction terms among variables, but the improvement was limited and they were not included.

In 'better fit' models, total sulfate, total nitrate, and total ammonia are found to be significant parameters in many models. But their coefficients are difficult to interpret because they are correlated with each other as well as with weighted population, pressure, and humidity, as shown in the correlation matrix plots. The correlated parameters describe exposed population better as a whole. However, some of their signs remain reasonable. Their role looks partly correlated with atmospheric chemistry. TS has positive coefficients in NH_3 models. Since ammonia neutralizes sulfate to form ammonium sulfate $PM_{2.5}$, ammonia may form $PM_{2.5}$ more easily if more sulfate is available. TS has negative coefficients in NO_x models, which would be because sulfate would more readily react with ammonia, which would limit PM nitrate formation.

Adjusted R^2 values of SO_2 and NO_x winter models are lower than those of others, though they meet the 'excellent' and 'good' criteria. This was expected due to the nonlinear thermodynamic system of inorganic species as discussed above. We tried the gas ratio, the adjusted gas ratio, and the degree of sulfate neutralization as parameter, but they did not substantially improve those model as well as others. Because SO_2 and NO_x affects a large span of area as can be seen in the shape of their average plumes, it may not be easy to estimate their $PM_{2.5}$ formation with the gas ratio or the adjusted gas ratio at the source. We did not include them for simplicity and because the associated chemistry is also partly represented by TS, TN, and TA.

We used the Akaike information criterion (AIC) as a measure to select a model specification from the combinations of selected parameters. As a summary, we presented the adjusted R^2, fractional bias, and fractional error of each model candidates in Figures C-36 to C-43. Tables C-9 to C-64 show seven model specifications having the lowest AIC for each parameterization. The figures and tables show the performance space where models vary over and how regressions improve with the inclusion of TS, TN, and TA.

4.3.4 The Effect of the Size of Marginal Emissions

Figure C-44 shows the results of our sensitivity simulations for the size of additional emissions, showing the range of "marginal" emissions, where estimates from our parameterizations remain constant. The results show that per-tonne social cost and intake fraction are not sensitive to the size of perturbation over a wide range. Elemental carbon did not change much for the entire range we tested, which is expected because elemental carbon is inert. For SO_2, NO_x, and NH_3, they did not change much for the entire range of $\bar{E} \cdot 4^{-3}$ or larger. Note that most values of $S/\bar{S}$ deviated from one in Figure C-44 are caused by the big numerical noise at the lowest emissions size and, therefore, all the species have only one or two places that are not stable over the range.

For the smallest perturbation, $\bar{E} \cdot 4^{-4}$, they become unstable, with the exception of EC. This is because the size is small enough to go beyond the numerical precision of CAMx. Because social cost and intake fraction are not sensitive to the perturbation size, our parameterizations would work well for the range we have explored. Though the sensitivity test was done only for January and July, the result would be similar for April and October, which are meteorologically between January and July.

4.3.5 Uncertainty and Variability within a Simulation Period

Figures C-45 shows the relative $PM_{2.5}$ level of each day throughout the simulation period, which presents what the variability of $PM_{2.5}$ level created by the marginal emissions ($\bar{E} \cdot 4^{-4}$) becomes. Figure C-46 and C-47 shows the $PM_{2.5}$ levels and social costs relative to those at the end of each season. The figures show that EC and SO_2 social costs mostly stay the same throughout each season with a variability of less than 30% or up to 50% in about 15 day of simulation. $PM_{2.5}$ levels from NO_x and NH_3 changes from 30% to 50% within a season time period. This would be because even within a season the sensitivity of PM nitrate formation changes. The change is most noticeable in spring for NO_x and fall for NO_x and NH_3; in spring, PM nitrate formation become less common at the end of the season than the beginning, and in fall, vice versa. The variability of $PM_{2.5}$ level from NO_x and NH_3 is generally larger when PM nitrate formation is common. The figures would be useful to find the uncertainty of our parameterizations for emissions at a specific time; for example, NO_x estimates from the same NOx winter parameterization can be in fact different by a factor of two. In order to reduce the uncertainty, parameterizations can be derived in a finer time period, e.g. monthly instead of seasonal. The same analysis was done for intake fraction, but they showed essentially the same results and are not presented.

4.3.6 The Effect of Point Emissions Compared to Area Emissions

We found that marginal damages from point sources with a common stack height (20 m) are very similar to those from area sources. Figure C-49 shows the comparison of social costs from area and point emissions (the intake fractions show the essentially same results and are not presented). EC estimates of point sources are about 6-9% less than those of area emissions. But point source estimates were virtually the same as area source estimates for other species. This is an expected result because once emitted or created $PM_{2.5}$ spread out over a large area as shown in the shape of average plumes in Figure 4.2 and C-18 to C21. Therefore, point emissions would generally result in health effects similar to area emissions.

However, our results may not be applicable to large emitters with tall stacks because the 20 m-high hypothetical stack we added is just one typical case. Even though the stack represents a majority, 64%, of point sources in our emissions database by number, it accounts for only 5% of SO_2 and 15% of NO_x emissions in terms of the amount of emissions. In addition, those large emitters have much higher stack heights, which ranges from 90 m to 370 m. In order to evaluate the effect of stack characteristics of large point emitters such as power plants and industrial facilities, a more systematic sensitivity analysis for stack characteristics would be necessary.

4.3.7 Generalization for VSL and Relative Risk

Our analysis is based on the relative risk of 1.06, that is, 6% increase in mortality per 10-$\mu g/m^3$ increase of $PM_{2.5}$ concentrations, which was reported by Krewski et al. (2009) (Random effects Cox Model for all causes in Commentary Table 4). But Chapter 3.3.3 showed that for the range of the relative risk from 1.02 to 1.22, which covers the 95% confidence intervals of the relative risks reported by both Krewski et al. (2009) and Lepeule et al. (2012). The social cost can be adjusted by the following factor, F_R:

$$F_R = \frac{S_R}{S_{1.06}} = -15.1 + 15.2R, \quad (10)$$

where R is a relative risk of interest, S_R is the social cost estimated with the relative risk R, and $S_{1.06}$ is the social cost estimated with the relative risk of 1.06. This is because the log-linear relation between $PM_{2.5}$ and mortality is almost linear for a range of $PM_{2.5}$ relevant to its effect on mortality. By multiplying F_R to the social cost models presented above, social cost can be estimated for a wide range of relative risks.

In addition, while the cohort of Krewski et al. (2009) is taken from the adult population aged 30 or older, Lepeule et al. (2012) is based on the adult population of age 25 or older. But we previously also showed in Chapter 3.3.3 that the five-year age difference makes less than a 1% difference. The difference caused by the small difference in population cohort may be small enough to be ignored.

Our analysis is based on $8M for the Value of a Statistical Life. Since VSL is just a multiplier, it is straightforward to generalize our parameterizations. It would need to multiply a factor, F_v, defined in the following:

$$F_v = \frac{V}{\$8\text{M}} \quad (11)$$

U.S. EPA recommends the social cost be adjusted not only for inflation but also for income level (U.S. EPA, 2010). That is because as people get richer, they are willing to pay more to avoid of a premature death. For reference, we included US EPA's standard GDP deflator and income growth adjustment factors in Table B-11. Our parameterizations are based on 1990 income level. The social cost would need to be adjusted for income accordingly if necessary.

4.3.8 Major Sources of Uncertainty in EASIUR marginal damages

There are five major sources of uncertainty or error affecting social cost and intake fraction estimated by our parameterizations: the quality of the chemical transport model, CAMx, itself; the uncertainty and errors introduced by the EASIUR regressions to capture CAMx results; the concentration-response relation; the value of a statistical life; and breathing rate. We discuss how these factors would affect our parameterizations here. Naturally, the concentration-response relationship and value of a statistical life affect the social costs whereas breathing rate affects the intake fraction.

Air quality simulation is a complicated process that involves many uncertainties such as those associated with emissions inventory, meteorology input, and chemical and physical algorithms. Because of the computational burden of running CTMs, it is very difficult to quantify uncertainties using some of the systematic and rigorous approaches often applied (e.g. with the Monte Carlo method) and, therefore, the uncertainty of CTMs is usually reported by comparing CTM's predictions against observations. According to the evaluation of our air quality modeling platform with monitoring network (U.S. EPA, 2011a), for sulfate and nitrate, the bias averaged over subregions (Northeast, Midwest, Southeast, and Central) between observation and prediction is 5-30% and, in some cases, up to 60%. For ammonium, the bias is 10-20%. For elemental carbon, there are over-predictions up to 100%, which is largely, however, due to the different definition of EC in CAMx and observations as well as emissions inventory (U.S. EPA, 2011a). In addition, we use the CTM results in a relative manner, that is, comparing a base case and a perturbed case, which may sometimes reduce the bias introduced by CTMs when compared to comparisons between predictions and observations in absolute values (National Research Council, 2002). However, in general, a cautious approach would be to use the biases

and error of the CTM compared to observations as indicators of uncertainty in the CTM's simulation of marginal changes in air quality. The 95% prediction intervals of EASIUR marginal estimates are generally about a factor of two or three depending on species and season, which is similar or larger than the size of differences between CAMx's predictions and observations. (Prediction intervals presented in the regression results indicate the uncertainty range that a predicted value may lie within while confidence intervals show the uncertainty range of the mean of predicted values; prediction intervals are always larger than confidence intervals.) Therefore, the 95% prediction intervals of EASIUR marginal estimates would sufficiently represent the uncertainty introduced by air quality simulations.

The concentration-response relation is also an important source of uncertainty for social cost estimates. Since we are relying on $PM_{2.5}$ epidemiological studies on mortality, associated uncertainty could be explored by the confidence intervals of relative risks reported by the original studies. For example, Krewski et al. (2009) reported 0.04-0.08 for the 95% confidence intervals of the mean estimate of the relative risk, 0.06. Lepeule et al. (2012) reported the confidence intervals of 0.07-0.22 for the mean, 1.14. Using the linear relationship of Eq. (10), the range of uncertainty from the concentration response relation could be quantified.

The value of a statistical life also needs to be addressed for social cost uncertainty. U.S. EPA (U.S. EPA, 2010) recommends using $8M VSL for benefit analysis, which is the central estimate from a Weibull distribution fitted with 26 value-of-life studies. A standard way of exploring VSL uncertainty would be a Monte Carlo method with the original Weibull distribution, parameters of which are location=0, scale=$5.32 \cdot 10^6$, and shape=1.51, for VSL in 1990 USD.

Breathing rate is an important factor for quantifying intake fraction. Apte et al. (2012) showed that intake fraction varied 10-16% under a range of reasonable breathing rate assumptions

including a rate very similar to our chosen value. This range of uncertainty would also be relevant to our intake fraction models. In addition, U.S. EPA (2011c) provides detailed uncertainty ranges for breathing rate for different population subgroups, which could be used to quantify the uncertainty in detail.

These uncertainties will play out differently in different applications, and users of these estimates should consider the following factors. First, how spatially distributed are the emissions in question? As discussed above, national average social costs will tend to have lower uncertainties than those for a single source at a specific location. Second, what are the key species driving social costs? Uncertainties in some species (e.g. NO_x) will be larger than others. Third, do uncertainties in concentration-response and value of statistical life matter or do they cancel out? When ranking $PM_{2.5}$ health damages from two different emissions scenarios, these factors and their uncertainties will cancel. When evaluating emissions control costs or other economic costs versus monetized health damages, these relatively large uncertainties matter.

4.4 Applications and Comparisons

4.4.1 The Burden of Air Quality Social Cost and Intake Fraction of the United States

Using EASIUR, we have generated the map of annual per-tonne social cost and intake fraction in Figures 4.9 and 4.10 and seasonal maps in Figures C-50 to C-57. The social costs were calculated based on the relative risk of 1.06 and the VSL of $8.8M, which is obtained from adjusting the VSL of $8M for 2010 income level. The social costs and intake fractions in Canada and Mexico include the public health impact on U.S. population only. Note that the high social costs and intake estimates for NO_x and SO_2 in the maps may not be accurate because the size of

emissions from large NO_x and SO_2 point sources are beyond the range of "marginal" emissions we tested above.

We compared the EASIUR estimates with APEEP, a commonly used database of social costs. Based on CRDM, a reduced-form air quality model, APEEP provides a per-ton social cost for every U.S. county. We generated the EASIUR estimates for each county and compared with their corresponding APEEP values, which is presented in Figure 4.11. We used the most recent APEEP values for area sources reported in Muller et al. (2011), which were adjusted for dollar year, metric tonne, and VSL. Note that AP2 (Muller, 2011) is a stochastic version of APEEP and that the mean values of AP2 estimates are similar to APEEP estimates. For EC, EASIUR and APEEP produce similar variability, though the EASIUR estimates are generally about two times higher than the APEEP. For other species, the spatial correlation between the two models is lower; especially, they were the most different for NO_x. Since we have controlled for concentration-response function and valuation, the differences between APEEP and EASIUR are primarily attributable to their underlying air quality modeling systems.

U.S. EPA estimates for area sources are shown in Figure 4-11, using data from Fann et al., (2012), which estimated per-ton social costs for 17 emissions sectors using CAMx PSAT. To compare to the EPA's national-average values, we compute average social costs by averaging our spatially resolved results, weighted by emissions in each grid cell. U.S. EPA's estimates are about two times bigger than the EASIUR averages for EC; 40% bigger for SO_2; and 40% smaller for NO_x. As both the EASIUR and Fann et al. (2012) values are derived from CTMs, both may be considered state-of-the-art. Therefore, even for nationally averaged social costs, we assign an uncertainty of approximately a factor of two.

We also analyzed the difference between EASIUR and APEEP spatially, as shown in Figure C-58. EASIUR generally produces larger estimates for EC except some parts of southern California. For SO_2, EASIUR's estimates are larger in the substantial part of the Midwest and the Southwest but smaller in many densely populated areas. For NO_x, EASIUR produces larger values for the east but the smaller values for the west except near the coast. NH_3 shows a trend similar to SO_2, but the differences are generally larger.

4.4.2 Application of EASIUR to Estimate the Social Costs of Emissions from Electricity Generation

As an example application of EASIUR, the life cycle social costs of emissions from electricity generation were estimated. For comparison, they were also estimated with a recent version of APEEP (Muller et al., 2011) and compared with those estimated by EASIUR. The emissions of direct $PM_{2.5}$, SO_2, NO_x, and NH_3 from five categories associated with the life cycle of electricity generation were taken from the 2005 National Emissions Inventory (http://www.epa.gov/ttnchie1/net/2005inventory.html). The categories are power generation, energy pipelines, oil & gas extraction, coal mining, and petroleum refineries. Table C-65 shows the summary of emissions and Figures C-59 to C-63 shows the geographical distribution of emissions of four species (EC, SO_2, NO_x, and NH_3) for each category.

Since EASIUR's marginal damages are provided on a 148x112 grid that covers the U.S., the location of each emission source from the inventory was matched to the corresponding EASIUR grid location. For APEEP, the location was matched to the corresponding APEEP county since APEEP's marginal damages are provided on a county basis. The social costs were calculated by multiplying marginal damages from EASIUR and APEEP by the amount of each emission. Note that, strictly speaking, it is inaccurate to apply marginal damages from both EASIUR and

APEEP to a large total amount of emissions (i.e. entire emissions from a sector), but this is a rough approximation made elsewhere (National Research Council, 2010), and we adopt it here as well. The social costs from both models were adjusted to use the same VSL ($8.8M). Because EASIUR currently provides marginal damages only for area sources while APEEP provides marginal damages for point sources of three different height levels (0-250m, 250-500m, and >500m) in addition to area source, two estimates are made with APEEP: one with area source marginal damages for all emission categories and the other with 250-500m point source damages for power generation and petroleum refineries and area source damages for others. The first one is a fairer comparison between EASIUR and APEEP since it relies on area source damages from both models while the second one would produce more accurate damages of electricity generation for APEEP.

Figure 4.12 summarizes the aggregate social costs of the life cycle of electricity generation. EASIUR produced generally larger estimates than APEEP. In Figure 4.12, APEEP Area is an estimate made based on area source marginal damages for all sectors and APEEP Point/Area is based on point source marginal damages for power generation and petroleum refineries and area source marginal damages for the other three sectors. EASIUR and APEEP produced similar estimates, $480B with EASIUR and $450B with APEEP Area, for the social cost of electricity generation. Power generation dominates the social costs, accounting for ~95% of the total values. The similarity of the two estimates is probably in part fortuitous. We saw earlier (Section 4.3.9 and Figure 4.11) that EASIUR and APEEP produced very similar social cost estimates for SO_2 on average compared to other species. Since SO_2 from power generation dominates the social costs in both cases (accounting for 68% and 81% of total damages estimated by EASIUR and

APEEP Area, respectively), the totals largely reflect their agreement for SO_2. However, estimates for other species are more different.

Comparisons of aggregate social cost by species and sector are summarized in and Tables 4.10 and 4.11. Both tables contain the same estimates for EASIUR while Table 4.11 is based on APEEP point source estimates for power generation and petroleum refineries. In Table 4.10, while APEEP produced only 10% bigger estimates for SO_2 than EASIUR, it produced 51% less for EC, 47% less for NO_X, and 55% larger for NH_3. In Table 4.11, where APEEP's point source estimates are used for power generation and petroleum refineries, APEEP produced a substantially lower estimate of social costs: $290B for the aggregate damages. APEEP produced 26% less estimates for SO_2 than EASIUR, but 78% less for EC, 57% less for NO_X, and 47% less for NH_3. Future work will have to investigate whether EASIUR social costs decrease by a similar amount when elevated sources are accounted for.

The results suggest that differences between EASIUR and APEEP are likely around a factor of two even when averaged over emissions in each category. However, the difference would be substantially bigger when comparisons are made at a subregional level. Figures C-64 to C-70 compares the social costs of EASIUR and APEEP at emission locations for each category. The figures show EASIUR produces systematically higher estimates for EC than APEEP in most locations. However, EASIUR and APEEP compare differently depending on regions for other species.

Depending on geographical distribution of emissions, the comparisons between the two models vary substantially. Despite the different marginal damages from the two models, SO_2 emissions are made across the domain as shown in Figure C-68, canceling out the spatial differences when averaged. However, emissions from limited geographical areas produce

substantially different results. The large aggregate difference for NH_3 from oil and gas extraction, APEEP's being 750% higher than EASIUR, is found because emissions are concentrated in California as (Figure C-61), where APEEP provides much bigger marginal damages than EASIUR (Figure C-66). The social costs of NOx from oil & gas extraction is also quite different those of other sector NO_x emissions. While APEEP generally produced 61-37% smaller social costs for NO_x than EASIUR, APEEP produced 30% larger social costs for NO_x from the oil and gas extraction. This is because the majority of emissions are made in areas like South Central regions (Figure C-61). Therefore, while national average social cost estimates probably have an overall uncertainty of approximately a factor of two, more specialized applications for problematic species (e.g. NH_3) over limited regions may be uncertain by a factor of 6-8.

APEEP's estimates based on point source estimates suggest that EASIUR needs to address the elevation of point sources more rigorously. The sensitivity simulations in this work (Section 4.3.6) showed that 20 m-high point sources produced virtually the same social costs as area sources. However, the difference may be substantial for a higher elevation (e.g. 200 m or higher, which is relevant for power plants and industrial facilities). At a location that is closer to densely populated areas and, therefore, has high marginal social costs, marginal damages for a high point source would be lower because elevated emissions may transport $PM_{2.5}$ farther and population exposure nearby the location would be lower than area emissions. Conversely, elevated emissions where nearby population is not big may result in causing more damages farther from the source. In short, in a future work, EASIUR would need to address the effect of emission height more rigorously.

4.5 Conclusions

We presented a set of parameterizations for estimating the public health impacts of air quality, which was derived by the Estimating Air pollution Social Impacts Using Regression (EASIUR) method. The parameterizations can estimate the per-tonne social costs and intake fractions for four inorganic species (elemental carbon, sulfur dioxide, nitrogen oxides, and ammonia) anywhere in the United States. The predictions are similar to a chemical transport model (CTM), but do not have the associated high computational burdens. The EASIUR method derives the parameterizations by (1) generating per-tonne social costs and intake fractions at 100 representative sample locations from a set of "tagged" CTM simulations; (2) building a normalized average plume per species for each season from CTM results, which is a generic shape of $PM_{2.5}$ plume created by the "marginal" emissions of $PM_{2.5}$ precursors; and (3) deriving parameterizations from linear regressions on social costs and intake fractions with population weighted by the average plume and common atmospheric variables. Regression models show a high goodness of fit, 0.9 or higher in most cases, and the predictions intervals of estimates are tight, generally within a factor of two or smaller.

We provided two sets of parameterizations: 'simple' and 'better-fit.' The 'simple' models are parameterized with weighted population, temperature, pressure, precipitation, wind speed, and humidity. Weighted population using an average plume of a specific $PM_{2.5}$ precursor and season characterizes well the dispersion and chemical conversions of air pollutants. Temperature explains the role of governing the vertical mixing height. Precipitation explains the $PM_{2.5}$ removal by precipitation. However, though there are some exceptions such as humidity in summer models, pressure, wind speed, and humidity represent the population density rather than atmospheric chemistry, as shown in their correlation with population variables. The 'better-fit'

models additionally have the parameters of total sulfate (TS), total nitrogen (TN), and total ammonia (TA). While 'better-fit' models predict better than 'simple' models, plugging-in data from a different year may produce biased results because they are tuned to the TS, TN, and TA of year 2005, which are expected to change substantially in future years in the United States (Pinder et al., 2008b; U.S. EPA, 2011d).

It was shown that marginal damages from EASIUR are substantially different (i.e. a factor of two or much more) from those from APEEP, a current popular tool, depending on species and location. Though the two models may produce similar aggregate social cost estimates for emissions made over a geographically large region (e.g. a national level), they may result in different policy implications for emissions made at a sub-regional level (e.g. a state level or smaller).

The EASIUR models showed that the performance of state-of-the-science chemical transport models could be tapped to policy analysis without computational burdens. Moreover, model users would not have to treat the parameterizations as a black box because the coefficients of model parameters are intuitive, describing underlying key mechanisms. We hope that the parameterizations in this work will be of a great use in policy research that involves changes in air quality. We included a User's Guide for the EASIUR model in Appendix D.

4.6 Acknowledgments

The authors thank Bonyoung Koo for providing the CAMx database and valuable advice for running CAMx. This work was supported by the center for Climate and Energy Decision Making (SES-0949710), through a cooperative agreement between the National Science Foundation and Carnegie Mellon University.

4.7 References

Akaike, H.: A new look at the statistical model identification, IEEE Trans. Autom. Control, 19(6), 716–723, doi:10.1109/TAC.1974.1100705, 1974.

Ansari, A. S. and Pandis, S. N.: Response of Inorganic PM to Precursor Concentrations, Environ. Sci. Technol., 32(18), 2706–2714, doi:10.1021/es971130j, 1998.

Apte, J. S., Bombrun, E., Marshall, J. D. and Nazaroff, W. W.: Global Intraurban Intake Fractions for Primary Air Pollutants from Vehicles and Other Distributed Sources, Environ. Sci. Technol., 46(6), 3415–3423, doi:10.1021/es204021h, 2012.

Beelen, R., Raaschou-Nielsen, O., Stafoggia, M., Andersen, Z. J., Weinmayr, G., Hoffmann, B., Wolf, K., Samoli, E., Fischer, P., Nieuwenhuijsen, M., Vineis, P., Xun, W. W., Katsouyanni, K., Dimakopoulou, K., Oudin, A., Forsberg, B., Modig, L., Havulinna, A. S., Lanki, T., Turunen, A., Oftedal, B., Nystad, W., Nafstad, P., De Faire, U., Pedersen, N. L., Östenson, C.-G., Fratiglioni, L., Penell, J., Korek, M., Pershagen, G., Eriksen, K. T., Overvad, K., Ellermann, T., Eeftens, M., Peeters, P. H., Meliefste, K., Wang, M., Bueno-de-Mesquita, B., Sugiri, D., Krämer, U., Heinrich, J., de Hoogh, K., Key, T., Peters, A., Hampel, R., Concin, H., Nagel, G., Ineichen, A., Schaffner, E., Probst-Hensch, N., Künzli, N., Schindler, C., Schikowski, T., Adam, M., Phuleria, H., Vilier, A., Clavel-Chapelon, F., Declercq, C., Grioni, S., Krogh, V., Tsai, M.-Y., Ricceri, F., Sacerdote, C., Galassi, C., Migliore, E., Ranzi, A., Cesaroni, G., Badaloni, C., Forastiere, F., Tamayo, I., Amiano, P., Dorronsoro, M., Katsoulis, M., Trichopoulou, A., Brunekreef, B. and Hoek, G.: Effects of long-term exposure to air pollution on natural-cause mortality: an analysis of 22 European cohorts within the multicentre ESCAPE project, The Lancet, 383(9919), 785–795, doi:10.1016/S0140-6736(13)62158-3, 2014.

Bell, M. L.: Assessment of the health impacts of particulate matter characteristics, Health Effects Institute, Boston, MA., 2012.

Bennett, D. H., McKone, T. E., Evans, J. S., Nazaroff, W. W., Margni, M. D., Jolliet, O. and Smith, K. R.: Defining Intake Fraction, Environ. Sci. Technol., 36(9), 206A–211A, doi:10.1021/es0222770, 2002.

Blanchard, C. L., Roth, P. M., Tanenbaum, S. J., Ziman, S. D. and Seinfeld, J. H.: The Use of Ambient Measurements To Identify which Precursor Species Limit Aerosol Nitrate Formation, J. Air Amp Waste Manag. Assoc., 50(12), 2073–2084, doi:10.1080/10473289.2000.10464239, 2000.

Buonocore, J. J., Dong, X., Spengler, J. D., Fu, J. S. and Levy, J. I.: Using the Community Multiscale Air Quality (CMAQ) model to estimate public health impacts of PM2.5 from individual power plants, Environ. Int., 68, 200–208, doi:10.1016/j.envint.2014.03.031, 2014.

Byun, D. and Schere, K. L.: Review of the Governing Equations, Computational Algorithms, and Other Components of the Models-3 Community Multiscale Air Quality (CMAQ) Modeling System, Appl. Mech. Rev., 59(2), 51–77, doi:10.1115/1.2128636, 2006.

Chow, J. C., Watson, J. G., Fujita, E. M., Lu, Z., Lawson, D. R. and Ashbaugh, L. L.: Temporal and spatial variations of PM2.5 and PM10 aerosol in the Southern California air quality study, Atmos. Environ., 28(12), 2061–2080, doi:10.1016/1352-2310(94)90474-X, 1994.

Crouse, D. L., Peters, P. A., van Donkelaar, A., Goldberg, M. S., Villeneuve, P. J., Brion, O., Khan, S., Atari, D. O., Jerrett, M., Pope, C. A., Brauer, M., Brook, J. R., Martin, R. V., Stieb, D. and Burnett, R. T.: Risk of Nonaccidental and Cardiovascular Mortality in Relation to Long-term Exposure to Low Concentrations of Fine Particulate Matter: A Canadian National-Level Cohort Study, Environ. Health Perspect., 120(5), 708–714, doi:10.1289/ehp.1104049, 2012.

ENVIRON: CAMx User's Guide Version 5.41, Environ International Corporation, Novato, CA., 2012.

Fann, N., Baker, K. R. and Fulcher, C. M.: Characterizing the PM2.5-related health benefits of emission reductions for 17 industrial, area and mobile emission sectors across the U.S., Environ. Int., 49, 141–151, doi:10.1016/j.envint.2012.08.017, 2012.

Franklin, M., Koutrakis, P. and Schwartz, J.: The Role of Particle Composition on the Association Between PM2.5 and Mortality, Epidemiol. Camb. Mass, 19(5), 680–689, 2008.

Goldstein, A. H. and Galbally, I. E.: Known and Unexplored Organic Constituents in the Earth's Atmosphere, Environ. Sci. Technol., 41(5), 1514–1521, doi:10.1021/es072476p, 2007.

Grell, G. A., Dudhia, J. and Stauffer, D. R.: A Description of the Fifth-Generation Penn State/NCAR Mesoscale Model (MM5). [online] Available from: http://nldr.library.ucar.edu/repository/collections/TECH-NOTE-000-000-000-214, 1995.

Hand, J. L., Schichtel, B. A., Pitchford, M., Malm, W. C. and Frank, N. H.: Seasonal composition of remote and urban fine particulate matter in the United States, J. Geophys. Res. Atmospheres, 117(D5), D05209, doi:10.1029/2011JD017122, 2012.

Harrison, R., Smith, D. and Kibble, A.: What is responsible for the carcinogenicity of PM2.5?, Occup. Environ. Med., 61(10), 799–805, doi:10.1136/oem.2003.010504, 2004.

Jathar, S. H., Gordon, T. D., Hennigan, C. J., Pye, H. O. T., Pouliot, G., Adams, P. J., Donahue, N. M. and Robinson, A. L.: Unspeciated organic emissions from combustion sources and their influence on the secondary organic aerosol budget in the United States, Proc. Natl. Acad. Sci., 201323740, doi:10.1073/pnas.1323740111, 2014.

Koo, B., Dunker, A. M. and Yarwood, G.: Implementing the Decoupled Direct Method for Sensitivity Analysis in a Particulate Matter Air Quality Model, Environ. Sci. Technol., 41(8), 2847–2854, doi:10.1021/es0619962, 2007.

Koo, B., Wilson, G. M., Morris, R. E., Dunker, A. M. and Yarwood, G.: Comparison of source apportionment and sensitivity analysis in a particulate matter air quality model, Environ. Sci. Technol., 43(17), 6669–6675, 2009.

Krewski, D., Jerrett, M., Burnett, R. T., Ma, R., Hughes, E., Shi, Y., Turner, M. C., Pope, C. A., III, Thurston, G., Calle, E. E., Thun, M. J., Beckerman, B., DeLuca, P., Finkelstein, N., Ito, K., Moore, D. K., Newbold, K. B., Ramsay, T., Ross, Z., Shin, H. and Tempalski, B.: Extended follow-up and spatial analysis of the American Cancer Society study linking particulate air pollution and mortality, Health Effects Institute, Boston, MA., 2009.

Latimer, D. A.: Particulate Matter Source-Receptor Relationships Between All Point and Area Sources in the United States and PSD Class I Area Receptors, prepared for U.S. EPA, OAQPS, Research Triangle Park, NC., 1996.

Lepeule, J., Laden, F., Dockery, D. and Schwartz, J.: Chronic Exposure to Fine Particles and Mortality: An Extended Follow-up of the Harvard Six Cities Study from 1974 to 2009, Environ. Health Perspect., 120(7), 965–970, doi:10.1289/ehp.1104660, 2012.

Levy, J. I., Baxter, L. K. and Schwartz, J.: Uncertainty and Variability in Health-Related Damages from Coal-Fired Power Plants in the United States, Risk Anal., 29(7), 1000–1014, doi:10.1111/j.1539-6924.2009.01227.x, 2009.

Morris, R. E., McNally, D. E., Tesche, T. W., Tonnesen, G., Boylan, J. W. and Brewer, P.: Preliminary evaluation of the Community Multiscale Air Quality model for 2002 over the southeastern United States, J. Air Waste Manag. Assoc., 55(11), 1694–1708, 2005.

Muller, N. Z.: Linking Policy to Statistical Uncertainty in Air Pollution Damages, BE J. Econ. Anal. Policy, 11(1) [online] Available from: http://www.degruyter.com/view/j/bejeap.2011.11.issue-1/bejeap.2011.11.1.2925/bejeap.2011.11.1.2925.xml?format=INT (Accessed 6 February 2013), 2011.

Muller, N. Z. and Mendelsohn, R.: Measuring the damages of air pollution in the United States, J. Environ. Econ. Manag., 54(1), 1–14, doi:10.1016/j.jeem.2006.12.002, 2007.

Muller, N. Z., Mendelsohn, R. and Nordhaus, W.: Environmental accounting for pollution in the United States economy, Am. Econ. Rev., 101(5), 1649–1675, 2011.

National Research Council: Estimating The Public Health Benefits Of Proposed Air Pollution Regulations, Committee on Estimating the Health-Risk-Reduction Benefits of Proposed Air Pollution Regulations. National Research Council of the National Academies., Washington, DC. [online] Available from: http://www.nap.edu/catalog.php?record_id=10511 (Accessed 9 January 2014), 2002.

National Research Council: Hidden Costs of Energy: Unpriced Consequences of Energy Production and Use, The National Academies Press, Washington, DC. [online] Available from: http://www.nap.edu/catalog.php?record_id=12794 (Accessed 19 August 2013), 2010.

Pinder, R. W., Dennis, R. L. and Bhave, P. V.: Observable indicators of the sensitivity of PM2.5 nitrate to emission reductions--Part I: Derivation of the adjusted gas ratio and applicability at regulatory-relevant time scales, Atmos. Environ., 42(6), 1275–1286, doi:10.1016/j.atmosenv.2007.10.039, 2008a.

Pinder, R. W., Gilliland, A. B. and Dennis, R. L.: Environmental impact of atmospheric NH3 emissions under present and future conditions in the eastern United States, Geophys. Res. Lett., 35(12), L12808, doi:10.1029/2008GL033732, 2008b.

Pitchford, M. L., Poirot, R. L., Schichtel, B. A. and Malm, W. C.: Characterization of the Winter Midwestern Particulate Nitrate Bulge, J. Air Waste Manag. Assoc., 59(9), 1061–1069, doi:10.3155/1047-3289.59.9.1061, 2009.

Robinson, A. L., Donahue, N. M., Shrivastava, M. K., Weitkamp, E. A., Sage, A. M., Grieshop, A. P., Lane, T. E., Pierce, J. R. and Pandis, S. N.: Rethinking Organic Aerosols: Semivolatile Emissions and Photochemical Aging, Science, 315(5816), 1259–1262, doi:10.1126/science.1133061, 2007.

Shadbegian, R. J., Gray, W. and Morgan, C.: Benefits and Costs From Sulfur Dioxide Trading: A Distributional Analysis, in Acid in the Environment, edited by G. R. Visgilio and D. M. Whitelaw, pp. 241–259, Springer US. [online] Available from: http://link.springer.com/chapter/10.1007/978-0-387-37562-5_13 (Accessed 10 November 2014), 2007.

Thompson, T. M. and Selin, N. E.: Influence of air quality model resolution on uncertainty associated with health impacts, Atmos Chem Phys, 12(20), 9753–9762, doi:10.5194/acp-12-9753-2012, 2012.

U.S. EPA: The Benefits and Costs of the Clean Air Act, 1970 to 1990, U.S. Environmental Protection Agency, Washington, DC., 1997.

U.S. EPA: The Benefits and Costs of the Clean Air Act, 1990 to 2010, EPA report to Congress, U.S. Environmental Protection Agency. Office of Air and Radiation. Office of Policy, Washington, DC., 1999.

U.S. EPA: Regulatory Impact Analysis for the Industrial Boilers and Process Heaters NESHAP, U.S. Environmental Protection Agency. Office of Air Quality Planning and Standards. Air Quality Strategies and Standards Division., Research Triangle Park, NC. [online] Available from: http://cfpub.epa.gov/ols/catalog/advanced_full_record.cfm?&FIELD1=SUBJECT&INPUT1=Environmental%20factors&TYPE1=EXACT&LOGIC1=AND&COLL=&SORT_TYPE=MTIC&item_count=48 (Accessed 22 February 2013), 2004.

U.S. EPA: Technical Support Document for the Proposed PM NAAQS Rule, Response Surface Modeling, Office of Air Quality Planning and Standards, Research Triangle Park, NC., 2006.

U.S. EPA: Guidelines for Preparing Economic Analyses, National Center for Environmental Economics, Office of Policy, U.S. Environmental Protection Agency., 2010.

U.S. EPA: Air Quality Modeling Final Rule Technical Support Document, U.S. Environmental Protection Agency. Office of Air Quality Planning and Standards. Air Quality Assessment Division. [online] Available from: http://www.epa.gov/airquality/transport/pdfs/AQModeling.pdf, 2011a.

U.S. EPA: Emissions Inventory Final Rule TSD, U.S. Environmental Protection Agency. Office of Air and Radiation. Office of Air Quality Planning and Standards. Air Quality Assessment Division., 2011b.

U.S. EPA: Exposure Factors Handbook 2011 Edition, National Center for Environmental Assessment. Office of Research and Development. U.S. Environmental Protection Agency., Washington, DC. [online] Available from: http://cfpub.epa.gov/ncea/risk/recordisplay.cfm?deid=236252 (Accessed 11 August 2014c), 2011.

U.S. EPA: Regulatory Impact Analysis for the Federal Implementation Plans to Reduce Interstate Transport of Fine Particulate Matter and Ozone in 27 States; Correction of SIP Approvals for 22 States, U.S. Environmental Protection Agency, Office of Air and Radiation. [online] Available from: http://www.epa.gov/airtransport/pdfs/FinalRIA.pdf, 2011d.

U.S. EPA: The Benefits and Costs of the Clean Air Act from 1990 to 2020, U.S. Environmental Protection Agency. Office of Air and Radiation., Washington, DC., 2011e.

U.S. EPA: National Ambient Air Quality Standards for Particulate Matter; Final Rule, Fed. Regist., 78(10), 2013a.

U.S. EPA: User's Manual for the Co-Benefits Risk Assessment (COBRA) Screening Model Version: 2.61, U.S. Environmental Protection Agency, Washington, DC., 2013b.

Wagstrom, K. M., Pandis, S. N., Yarwood, G., Wilson, G. M. and Morris, R. E.: Development and application of a computationally efficient particulate matter apportionment algorithm in a three-dimensional chemical transport model, Atmos. Environ., 42(22), 5650–5659, doi:10.1016/j.atmosenv.2008.03.012, 2008.

West, J. J., Ansari, A. S. and Pandis, S. N.: Marginal PM2.5: Nonlinear aerosol mass response to sulfate reductions in the eastern United States, J. Air Waste Manag. Assoc., 49(12), 1415–1424, 1999.

Zhang, Q., Jimenez, J. L., Canagaratna, M. R., Allan, J. D., Coe, H., Ulbrich, I., Alfarra, M. R., Takami, A., Middlebrook, A. M., Sun, Y. L., Dzepina, K., Dunlea, E., Docherty, K., DeCarlo, P. F., Salcedo, D., Onasch, T., Jayne, J. T., Miyoshi, T., Shimono, A., Hatakeyama, S., Takegawa, N., Kondo, Y., Schneider, J., Drewnick, F., Borrmann, S., Weimer, S., Demerjian, K., Williams, P., Bower, K., Bahreini, R., Cottrell, L., Griffin, R. J., Rautiainen, J., Sun, J. Y., Zhang, Y. M. and Worsnop, D. R.: Ubiquity and dominance of oxygenated species in organic aerosols in anthropogenically-influenced Northern Hemisphere midlatitudes, Geophys. Res. Lett., 34(13), L13801, doi:10.1029/2007GL029979, 2007.

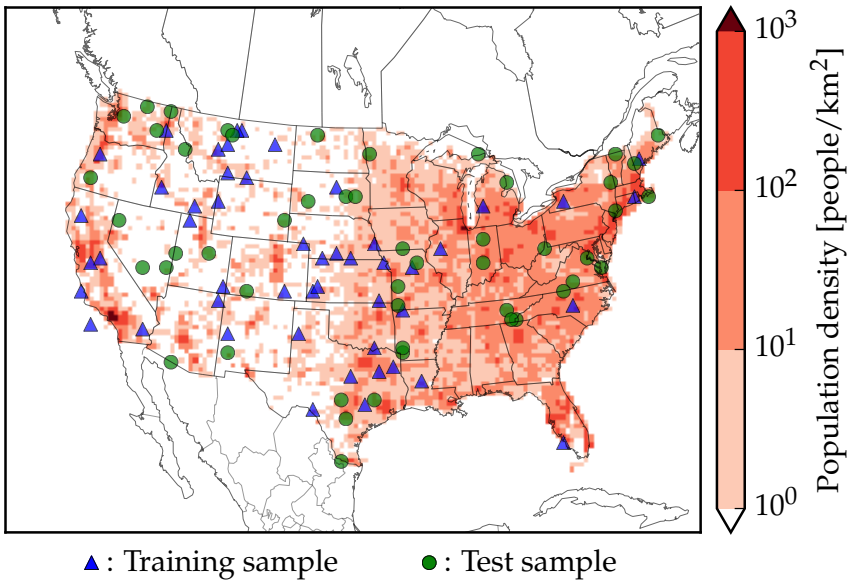

Figure 4.1: The domain of air quality simulation and the selected sample locations. CAMx simulated this domain in a 148×112 grid that has a horizontal cell size of 36 km×36 km. The sample locations were randomly selected based on the size of population where population is not zero. The training samples were used to build regression models and the test samples for out-of-sample evaluation.

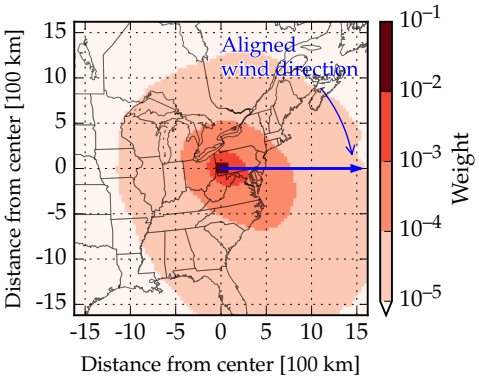

(a) EC: average plume weight

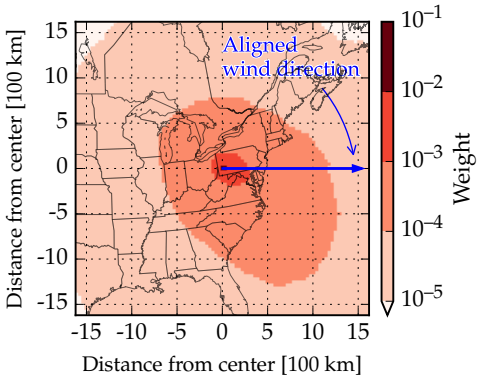

(b) SO_2: average plume weight

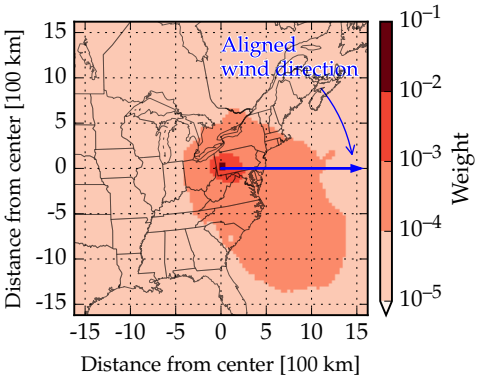

(c) NO_x: average plume weight

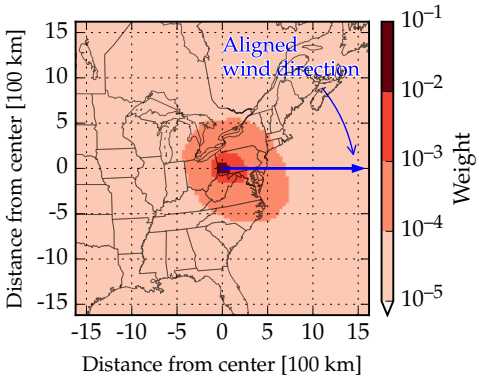

(d) NH_3: average plume weight

Figure 4.2: Average plumes for summer. $PM_{2.5}$ concentrations or plumes of the training samples were aligned by wind direction to the same direction (the arrow in the figure) and normalized so that they sum to one. To give a sense of scale, the center of a plume is put on Pittsburgh.

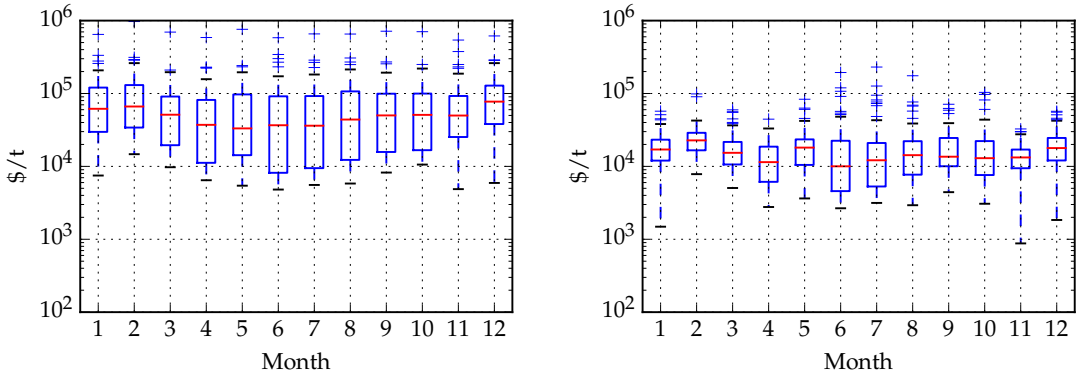

(a) EC (b) SO_2

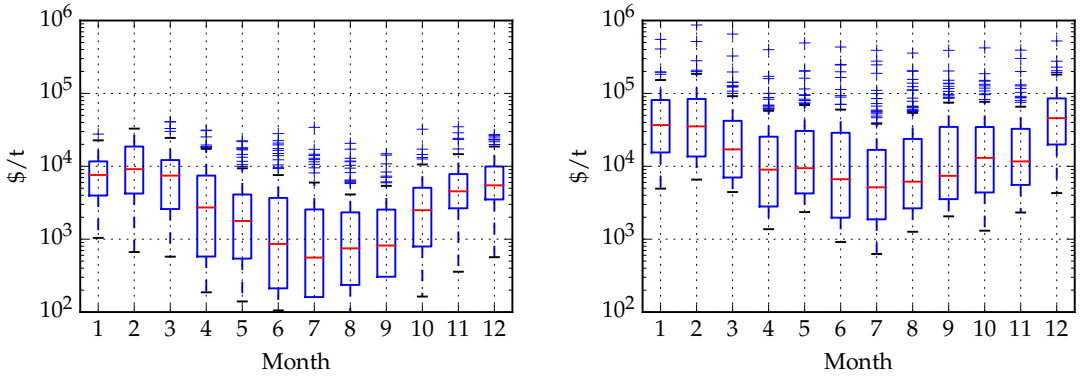

(c) NO_x (d) NH_3

Figure 4.3: Social costs at the 100 sample locations. The bottom and top of the box are the first and third quartile, and the red band inside the box indicates median. Whiskers show 1.5 × IQR (interquartile range) below the first quartile and beyond the third quartile.

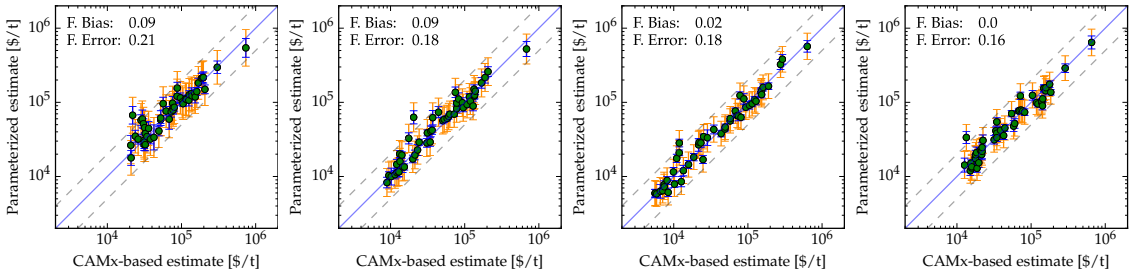

(a) EC: Winter (b) EC: Spring (c) EC: Summer (d) EC: Fall

Figure 4.4: Out-of-sample evaluation of EC social cost models. Dashed lines indicate a factor of two and solid line indicates unbiased prediction. Orange bars show 95% prediction intervals and blue bars show 95% confidence intervals.

Table 4.1: EC social cost model regression results.

Variable	Winter	Spring	Summer	Fall
Intercept	$86^{\star\star}$	$72^{\star\star\star}$	$73^{\star\star\star}$	$72^{\star\star\star}$
	(25)	(13)	(10)	(20)
ln (Weighted Population)	$0.61^{\star\star\star}$	$0.72^{\star\star\star}$	$0.74^{\star\star\star}$	$0.60^{\star\star\star}$
[# of people]	(0.047)	(0.035)	(0.034)	(0.052)
ln (Temperature)	$-20^{\star\star\star}$	$-19^{\star\star\star}$	$-19^{\star\star\star}$	$-17^{\star\star\star}$
[K]	(5.0)	(2.4)	(2.0)	(3.8)
ln (Pressure)	$3.7^{\star\star\star}$	$5.4^{\star\star\star}$	$6.0^{\star\star\star}$	$3.1^{\star\star\star}$
[hPa]	(0.64)	(0.65)	(0.52)	(0.78)
ln (Humidity)	$0.70^{\star}$	$0.37^{\star}$	-	$0.64^{\star}$
[ppm]	(0.30)	(0.15)	-	(0.30)
Adj. R^2	0.92	0.97	0.97	0.90
Fractional Bias	0.11	0.057	0.0034	0.10
Fractional Error	0.19	0.19	0.16	0.21
Normalized Mean Bias	0.052	−0.0066	−0.039	0.025
Normailzed Mean Error	0.19	0.16	0.13	0.17
95% PI[a]	[0.61, 1.64]	[0.67, 1.49]	[0.67, 1.49]	[0.60, 1.68]
95% CI[a]	[0.86, 1.17]	[0.88, 1.14]	[0.89, 1.12]	[0.85, 1.17]

*** $p < 0.001$, ** $p < 0.001$, * $p < 0.05$, $^{+}$ $p < 0.1$, Standard errors in parentheses, Weighted Population: population (≥ age 30) weighted by average plume, Ṕrecipitation = precipitation + 0.0002 (shifted for log transformation), Winter ≡ Januanry + February + March, Spring ≡ April + May + June, Summer ≡ July + August + September, Winter ≡ October + November + December, [a] Average intervals relative to predicted value.

Table 4.2: EC intake fraction model regression results.

Variable	Winter	Spring	Summer	Fall
Intercept	$74^{\star\star}$	$46^{\star\star\star}$	$54^{\star\star\star}$	$25^{\star}$
	(26)	(9.9)	(13)	(12)
ln (Weighted Population)	$0.65^{\star\star\star}$	$0.76^{\star\star\star}$	$0.80^{\star\star\star}$	$0.66^{\star\star\star}$
[# of people]	(0.048)	(0.036)	(0.032)	(0.057)
ln (Temperature)	$-19^{\star\star\star}$	$-16^{\star\star\star}$	$-17^{\star\star\star}$	$-9.2^{\star\star\star}$
[K]	(5.2)	(2.0)	(2.3)	(2.5)
ln (Pressure)	$2.9^{\star\star\star}$	$5.5^{\star\star\star}$	$5.8^{\star\star\star}$	$2.9^{\star\star\star}$
[hPa]	(0.65)	(0.57)	(0.57)	(0.79)
ln (Humidity)	$0.70^{\star}$	-	$-0.30^{\star}$	-
[ppm]	(0.31)	-	(0.13)	-
Adj. R^2	0.91	0.97	0.97	0.88
Fractional Bias	0.10	0.064	−0.0036	0.085
Fractional Error	0.19	0.19	0.16	0.21
Normalized Mean Bias	0.029	−0.014	−0.056	−0.011
Normailzed Mean Error	0.21	0.16	0.14	0.20
95% PI[a]	[0.60, 1.66]	[0.66, 1.51]	[0.68, 1.46]	[0.57, 1.76]
95% CI[a]	[0.85, 1.17]	[0.89, 1.13]	[0.89, 1.13]	[0.85, 1.18]

*** $p < 0.001$, ** $p < 0.001$, * $p < 0.05$, $^{+}$ $p < 0.1$, Standard errors in parentheses, Weighted Population: population weighted by average plume, Ṕrecipitation = precipitation + 0.0002 (shifted for log transformation), Winter ≡ Januanry + February + March, Spring ≡ April + May + June, Summer ≡ July + August + September, Winter ≡ October + November + December, [a] Average intervals relative to predicted value.

Table 4.3: SO_2 social cost model regression results.

Variable	Simple				Better-fit			
	Winter	Spring	Summer	Fall	Winter	Spring	Summer	Fall
Intercept	$86^{\star}$	$120^{\star\star\star}$	$110^{\star\star\star}$	$92^{\star\star\star}$	$77^{\star}$	$89^{\star\star\star}$	$76^{\star\star\star}$	$150^{\star\star\star}$
	(38)	(12)	(11)	(20)	(34)	(12)	(13)	(19)
ln (Pop_w)	-	$0.40^{\star\star\star}$	$0.54^{\star\star\star}$	$0.19^{\star}$	-	$0.34^{\star\star\star}$	$0.45^{\star\star\star}$	$0.54^{\star\star\star}$
[# of people]	-	(0.050)	(0.059)	(0.089)	-	(0.060)	(0.076)	(0.099)
ln (Temp)	$-19^{\star}$	$-28^{\star\star\star}$	$-26^{\star\star\star}$	$-21^{\star\star\star}$	$-14^{\star}$	$-23^{\star\star\star}$	$-19^{\star\star\star}$	$-35^{\star\star\star}$
[K]	(7.5)	(2.2)	(2.0)	(3.8)	(6.8)	(2.4)	(2.8)	(4.0)
ln (Pres)	$3.0^{\star\star\star}$	$6.3^{\star\star\star}$	$6.3^{\star\star\star}$	$3.9^{\star\star\star}$	-	$6.2^{\star\star\star}$	$6.8^{\star\star\star}$	$5.1^{\star\star\star}$
[hPa]	(0.79)	(0.54)	(0.51)	(0.79)	-	(0.58)	(0.55)	(0.67)
ln (Prec)	-	$-0.052^{\star}$	$-0.064^{\star\star}$	-	-	-	-	$-0.10^{\star}$
[g/m^3]	-	(0.025)	(0.022)	-	-	-	-	(0.041)
ln (Wind)	-0.14^{+}	$-0.070^{\star}$	-	0.10	$-0.15^{\star}$	$-0.074^{\star}$	-	-
[m/s]	(0.069)	(0.030)	-	(0.069)	(0.071)	(0.029)	-	-
ln (Humi)	$0.96^{\star}$	$0.50^{\star\star\star}$	-	$0.85^{\star\star}$	$1.0^{\star}$	$0.30^{\star}$	$-0.71^{\star\star}$	$1.9^{\star\star\star}$
[ppm]	(0.45)	(0.14)	-	(0.29)	(0.43)	(0.13)	(0.22)	(0.30)
ln (TS)	-	-	-	-	$-0.25^{\star}$	-	$0.32^{\star}$	$-0.58^{\star\star\star}$
[$\mu mol/m^3$]	-	-	-	-	(0.11)	-	(0.13)	(0.11)
ln (TN)	-	-	-	-	$0.47^{\star\star\star}$	0.094^{+}	-	-
[$\mu mol/m^3$]	-	-	-	-	(0.090)	(0.049)	-	-
ln (TA)	-	-	-	-	$-0.24^{\star}$	$-0.092^{\star\star}$	$-0.10^{\star\star}$	-
[$\mu mol/m^3$]	-	-	-	-	(0.11)	(0.033)	(0.031)	-
Adj. R^2	0.38	0.95	0.93	0.69	0.54	0.96	0.95	0.81
F. Bias	0.10	0.13	0.0051	0.083	0.00087	0.13	0.063	−0.0084
F. Error	0.28	0.24	0.21	0.24	0.26	0.24	0.21	0.25
N. Bias	0.016	0.12	−0.11	0.023	−0.081	0.10	−0.034	−0.081
N. Error	0.30	0.30	0.26	0.26	0.28	0.30	0.25	0.27
95% PI[a]	[0.48, 2.08]	[0.72, 1.38]	[0.68, 1.48]	[0.60, 1.66]	[0.53, 1.90]	[0.73, 1.38]	[0.69, 1.44]	[0.67, 1.50]
95% CI[a]	[0.80, 1.26]	[0.89, 1.13]	[0.89, 1.13]	[0.83, 1.20]	[0.79, 1.26]	[0.88, 1.13]	[0.87, 1.15]	[0.86, 1.17]

*** $p < 0.001$, ** $p < 0.001$, * $p < 0.05$, $^{+}$ $p < 0.1$, Standard errors in parentheses, Pop_w: population (≥ age 30) weighted by average plume, Pres: pressure, Temp: temperature, Prec = precipitation + 0.0002 (shifted for log transformation), Wind: wind speed, Humi: humidity, TS: total sulfate (≡ [SO_4^{2-}]) [$\mu mol/m^3$], TN: total nitrate (≡ [HNO_3] + [NO_3^-]) [$\mu mol/m^3$], TA: total ammonia (≡ [NH_3] + [NH_4^+]) [$\mu mol/m^3$], F. Bias: fractional bias, F. Error: fractional error, N. Bias: normalized mean bias, N. Error: normalized mean error, Winter ≡ Januanry + February + March, Spring ≡ April + May + June, Summer ≡ July + August + September, Winter ≡ October + November + December.

Table 4.4: NO_x social cost model regression results.

Variable	Simple				Better-fit			
	Winter	Spring	Summer	Fall	Winter	Spring	Summer	Fall
Intercept	$55^{\star\star}$	$150^{\star\star\star}$	$200^{\star\star\star}$	$100^{\star\star\star}$	$99^{\star}$	$76^{\star\star\star}$	$180^{\star\star\star}$	$170^{\star\star\star}$
	(17)	(24)	(30)	(25)	(40)	(16)	(28)	(36)
ln (Pop_w)	$0.37^{\star\star}$	$0.98^{\star\star\star}$	$1.1^{\star\star\star}$	$0.59^{\star\star}$	$0.36^{\star\star}$	$0.63^{\star\star\star}$	$0.65^{\star\star}$	$0.95^{\star\star\star}$
[# of people]	(0.13)	(0.10)	(0.19)	(0.18)	(0.11)	(0.094)	(0.21)	(0.17)
ln (Temp)	$-19^{\star\star\star}$	$-40^{\star\star\star}$	$-51^{\star\star\star}$	$-29^{\star\star\star}$	$-23^{\star\star}$	$-21^{\star\star\star}$	$-41^{\star\star\star}$	$-45^{\star\star\star}$
[K]	(3.4)	(4.5)	(5.7)	(5.1)	(8.0)	(3.3)	(5.9)	(7.3)
ln (Pres)	$8.1^{\star\star\star}$	$9.6^{\star\star\star}$	$12^{\star\star\star}$	$8.8^{\star\star\star}$	$4.1^{\star\star}$	$6.9^{\star\star\star}$	$7.1^{\star\star\star}$	$8.1^{\star\star\star}$
[hPa]	(1.3)	(1.2)	(1.5)	(1.5)	(1.5)	(1.0)	(1.9)	(1.6)
ln (Prec)	-	-	-0.12^{+}	-	-	0.079^{+}	$-0.17^{\star\star}$	-
[g/m^3]	-	-	(0.066)	-	-	(0.040)	(0.063)	-
ln (Wind)	-	-0.084	-	0.24	-	-0.088	$-0.24^{\star}$	0.21^{+}
[m/s]	-	(0.062)	-	(0.15)	-	(0.053)	(0.12)	(0.12)
ln (Humi)	-	$0.85^{\star\star}$	-	-	0.88^{+}	-	-	$1.9^{\star\star}$
[ppm]	-	(0.27)	-	-	(0.50)	-	-	(0.56)
ln (TS)	-	-	-	-	$-0.48^{\star\star\star}$	-	-	$-0.95^{\star\star\star}$
[$\mu mol/m^3$]	-	-	-	-	(0.13)	-	-	(0.19)
ln (TN)	-	-	-	-	$0.50^{\star\star\star}$	$0.55^{\star\star\star}$	$0.38^{\star\star}$	-
[$\mu mol/m^3$]	-	-	-	-	(0.097)	(0.080)	(0.11)	-
ln (TA)	-	-	-	-	-	$-0.20^{\star\star}$	-	$0.31^{\star\star}$
[$\mu mol/m^3$]	-	-	-	-	-	(0.064)	-	(0.092)
Adj. R^2	0.72	0.94	0.86	0.65	0.82	0.96	0.88	0.79
F. Bias	0.25	0.17	0.11	0.22	0.061	0.12	0.068	-0.020
F. Error	0.36	0.33	0.49	0.36	0.27	0.28	0.47	0.38
N. Bias	0.25	0.25	-0.068	0.23	-0.016	0.14	-0.20	-0.063
N. Error	0.38	0.50	0.69	0.42	0.23	0.37	0.51	0.41
95% PI[a]	[0.38, 2.63]	[0.48, 2.09]	[0.32, 3.13]	[0.33, 3.05]	[0.45, 2.23]	[0.57, 1.77]	[0.35, 2.86]	[0.41, 2.42]
95% CI[a]	[0.75, 1.35]	[0.78, 1.30]	[0.70, 1.44]	[0.69, 1.48]	[0.74, 1.36]	[0.81, 1.24]	[0.68, 1.49]	[0.70, 1.45]

*** $p < 0.001$, ** $p < 0.001$, * $p < 0.05$, $^{+}$ $p < 0.1$, Standard errors in parentheses, Pop_w: population (≥ age 30) weighted by average plume, Pres: pressure, Temp: temperature, Prec = precipitation + 0.0002 (shifted for log transformation), Wind: wind speed, Humi: humidity, TS: total sulfate (≡ [SO_4^{2-}]) [$\mu mol/m^3$], TN: total nitrate (≡ [HNO_3] + [NO_3^-]) [$\mu mol/m^3$], TA: total ammonia (≡ [NH_3] + [NH_4^+]) [$\mu mol/m^3$], F. Bias: fractional bias, F. Error: fractional error, N. Bias: normalized mean bias, N. Error: normalized mean error, Winter ≡ Januanry + February + March, Spring ≡ April + May + June, Summer ≡ July + August + September, Winter ≡ October + November + December.

Table 4.5: NH_3 social cost model regression results.

Variable	Simple				Better-fit			
	Winter	Spring	Summer	Fall	Winter	Spring	Summer	Fall
Intercept	190^{***}	99^{**}	54^{*}	210^{***}	160^{***}	89^{***}	75^{**}	160^{***}
	(32)	(35)	(27)	(31)	(30)	(16)	(23)	(25)
ln (Pop_w)	0.81^{***}	0.90^{***}	0.78^{***}	0.64^{***}	0.77^{***}	0.81^{***}	0.81^{***}	0.50^{***}
[# of people]	(0.077)	(0.10)	(0.10)	(0.075)	(0.075)	(0.058)	(0.085)	(0.069)
ln (Temp)	-41^{***}	-22^{**}	-15^{**}	-43^{***}	-34^{***}	-18^{***}	-18^{***}	-31^{***}
[K]	(6.5)	(6.5)	(5.1)	(5.8)	(6.1)	(3.2)	(4.4)	(4.9)
ln (Pres)	4.0^{***}	2.4	4.8^{***}	3.5^{**}	3.4^{***}	2.7^{*}	4.5^{**}	2.0^{+}
[hPa]	(0.88)	(1.7)	(1.3)	(0.99)	(0.89)	(1.0)	(1.4)	(1.0)
ln (Prec)	-0.26^{*}	-	0.21^{**}	-0.14^{*}	-0.19^{+}	-	0.16^{**}	-
[g/m^3]	(0.10)	-	(0.061)	(0.064)	(0.099)	-	(0.055)	-
ln (Wind)	-0.11^{+}	-0.13	-0.31^{**}	-0.21^{*}	-	-0.13^{*}	-0.17^{*}	-0.12
[m/s]	(0.059)	(0.090)	(0.11)	(0.086)	-	(0.050)	(0.085)	(0.083)
ln (Humi)	1.7^{***}	0.93^{*}	-	1.9^{***}	1.2^{**}	-	-	1.2^{**}
[ppm]	(0.40)	(0.39)	-	(0.41)	(0.39)	-	-	(0.37)
ln (TS)	-	-	-	-	0.37^{***}	1.3^{***}	0.84^{***}	0.44^{***}
[µmol/m^3]	-	-	-	-	(0.097)	(0.12)	(0.20)	(0.12)
ln (TN)	-	-	-	-	-	-0.24^{**}	-0.24^{*}	-
[µmol/m^3]	-	-	-	-	-	(0.077)	(0.097)	-
ln (TA)	-	-	-	-	-0.12^{+}	-0.33^{***}	-0.32^{***}	-
[µmol/m^3]	-	-	-	-	(0.068)	(0.058)	(0.064)	-
Adj. R^2	0.90	0.83	0.85	0.88	0.92	0.95	0.92	0.90
F. Bias	-0.030	-0.25	-0.23	-0.0039	0.037	0.075	-0.048	0.081
F. Error	0.33	0.35	0.40	0.39	0.25	0.21	0.21	0.31
N. Bias	-0.22	-0.45	-0.45	-0.26	-0.11	0.013	-0.14	-0.14
N. Error	0.34	0.46	0.48	0.41	0.24	0.17	0.19	0.31
95% PI[a]	[0.53, 1.89]	[0.35, 2.90]	[0.36, 2.76]	[0.52, 1.93]	[0.56, 1.79]	[0.57, 1.75]	[0.46, 2.19]	[0.54, 1.84]
95% CI[a]	[0.79, 1.27]	[0.70, 1.44]	[0.72, 1.40]	[0.79, 1.27]	[0.80, 1.26]	[0.81, 1.24]	[0.73, 1.39]	[0.79, 1.27]

*** $p < 0.001$, ** $p < 0.001$, * $p < 0.05$, $^{+}$ $p < 0.1$, Standard errors in parentheses, Pop_w: population (≥ age 30) weighted by average plume, Pres: pressure, Temp: temperature, Prec = precipitation + 0.0002 (shifted for log transformation), Wind: wind speed, Humi: humidity, TS: total sulfate (≡ $[SO_4{}^{2-}]$) [µmol/m^3], TN: total nitrate (≡ $[HNO_3]$ + $[NO_3{}^-]$) [µmol/m^3], TA: total ammonia (≡ $[NH_3]$ + $[NH_4{}^+]$) [µmol/m^3], F. Bias: fractional bias, F. Error: fractional error, N. Bias: normalized mean bias, N. Error: normalized mean error, Winter ≡ Januanry + February + March, Spring ≡ April + May + June, Summer ≡ July + August + September, Winter ≡ October + November + December.

Table 4.6: SO_2 intake fraction model regression results.

Variable	Simple				Better-fit			
	Winter	Spring	Summer	Fall	Winter	Spring	Summer	Fall
Intercept	$-20^{\star\star\star}$	$110^{\star\star\star}$	$100^{\star\star\star}$	$64^{\star}$	59	$88^{\star\star\star}$	$66^{\star\star\star}$	$59^{\star\star}$
	(5.3)	(14)	(11)	(25)	(43)	(18)	(15)	(21)
ln (Pop_w)	-	$0.44^{\star\star\star}$	$0.60^{\star\star\star}$	0.20^{+}	-	$0.46^{\star\star\star}$	$0.56^{\star\star\star}$	$0.44^{\star\star\star}$
[# of people]	-	(0.057)	(0.062)	(0.11)	-	(0.084)	(0.079)	(0.11)
ln (Temp)	-	$-28^{\star\star\star}$	$-26^{\star\star\star}$	$-18^{\star\star\star}$	-13	$-25^{\star\star\star}$	$-19^{\star\star\star}$	$-17^{\star\star\star}$
[K]	-	(2.5)	(2.1)	(4.6)	(8.5)	(3.6)	(3.0)	(4.8)
ln (Pres)	$2.7^{\star\star}$	$6.4^{\star\star\star}$	$5.9^{\star\star\star}$	$3.9^{\star\star\star}$	-	$6.3^{\star\star\star}$	$6.5^{\star\star\star}$	$2.9^{\star\star}$
[hPa]	(0.78)	(0.61)	(0.53)	(0.94)	-	(0.63)	(0.65)	(1.0)
ln (Prec)	-	$-0.082^{\star\star}$	$-0.11^{\star\star\star}$	-	-	-0.050	-0.044	-
[g/m^3]	-	(0.028)	(0.024)	-	-	(0.032)	(0.033)	-
ln (Wind)	-	-0.047	-	0.12	$-0.20^{\star}$	$-0.068^{\star}$	0.070^{+}	-
[m/s]	-	(0.033)	-	(0.083)	(0.089)	(0.033)	(0.041)	-
ln (Humi)	-	$0.39^{\star}$	-	0.67^{+}	1.0^{+}	0.41^{+}	$-0.71^{\star}$	$1.1^{\star\star}$
[ppm]	-	(0.15)	-	(0.35)	(0.55)	(0.21)	(0.27)	(0.32)
ln (TS)	-	-	-	-	$-0.42^{\star\star}$	-0.17^{+}	$0.30^{\star}$	$-0.55^{\star\star\star}$
[μmol/m^3]	-	-	-	-	(0.14)	(0.093)	(0.13)	(0.11)
ln (TN)	-	-	-	-	$0.51^{\star\star\star}$	0.096	-	$0.28^{\star\star}$
[μmol/m^3]	-	-	-	-	(0.11)	(0.063)	-	(0.089)
ln (TA)	-	-	-	-	-0.26^{+}	-0.079^{+}	$-0.11^{\star\star}$	$-0.15^{\star}$
[μmol/m^3]	-	-	-	-	(0.14)	(0.042)	(0.032)	(0.071)
Adj. R^2	0.19	0.94	0.93	0.58	0.41	0.95	0.95	0.77
F. Bias	0.049	0.14	0.0085	0.083	-0.030	0.11	0.052	-0.039
F. Error	0.26	0.23	0.21	0.25	0.29	0.24	0.22	0.26
N. Bias	-0.046	0.16	-0.085	0.024	-0.11	0.10	-0.026	-0.10
N. Error	0.30	0.31	0.25	0.27	0.32	0.29	0.26	0.27
95% PI[a]	[0.40, 2.47]	[0.69, 1.44]	[0.66, 1.51]	[0.55, 1.83]	[0.44, 2.25]	[0.70, 1.42]	[0.69, 1.46]	[0.64, 1.57]
95% CI[a]	[0.84, 1.19]	[0.88, 1.14]	[0.88, 1.14]	[0.81, 1.25]	[0.75, 1.34]	[0.86, 1.16]	[0.86, 1.17]	[0.84, 1.20]

*** $p < 0.001$, ** $p < 0.001$, * $p < 0.05$, $^{+}$ $p < 0.1$, Standard errors in parentheses, Pop_w: population weighted by average plume, Pres: pressure, Temp: temperature, Prec = precipitation + 0.0002 (shifted for log transformation), Wind: wind speed, Humi: humidity, TS: total sulfate (≡ [SO_4^{2-}]) [μmol/m^3], TN: total nitrate (≡ [HNO_3] + [NO_3^-]) [μmol/m^3], TA: total ammonia (≡ [NH_3] + [NH_4^+]) [μmol/m^3], F. Bias: fractional bias, F. Error: fractional error, N. Bias: normalized mean bias, N. Error: normalized mean error, Winter ≡ Januanry + February + March, Spring ≡ April + May + June, Summer ≡ July + August + September, Winter ≡ October + November + December.

Table 4.7: NO_x intake fraction model regression results.

Variable	Simple				Better-fit			
	Winter	Spring	Summer	Fall	Winter	Spring	Summer	Fall
Intercept	$38^{\star}$	$140^{\star\star\star}$	$200^{\star\star\star}$	$83^{\star\star}$	$86^{\star}$	$77^{\star\star\star}$	$180^{\star\star\star}$	$130^{\star\star}$
	(18)	(25)	(34)	(27)	(40)	(16)	(32)	(38)
ln (Pop_w)	$0.39^{\star\star}$	$1.1^{\star\star\star}$	$1.1^{\star\star\star}$	$0.61^{\star\star}$	$0.40^{\star\star\star}$	$0.71^{\star\star\star}$	$0.61^{\star}$	$0.89^{\star\star\star}$
[# of people]	(0.14)	(0.11)	(0.21)	(0.20)	(0.11)	(0.100)	(0.24)	(0.18)
ln (Temp)	$-17^{\star\star\star}$	$-39^{\star\star\star}$	$-52^{\star\star\star}$	$-27^{\star\star\star}$	$-23^{\star\star}$	$-23^{\star\star\star}$	$-40^{\star\star\star}$	$-36^{\star\star\star}$
[K]	(3.6)	(4.6)	(6.4)	(5.4)	(8.1)	(3.4)	(6.7)	(8.3)
ln (Pres)	$7.4^{\star\star\star}$	$9.7^{\star\star\star}$	$11^{\star\star\star}$	$8.4^{\star\star\star}$	$3.8^{\star}$	$6.6^{\star\star\star}$	$6.3^{\star\star}$	$6.4^{\star\star}$
[hPa]	(1.3)	(1.3)	(1.7)	(1.6)	(1.5)	(1.1)	(2.1)	(1.9)
ln (Prec)	-	-	$-0.16^{\star}$	-	-	-	$-0.22^{\star\star}$	-
[g/m^3]	-	-	(0.074)	-	-	-	(0.071)	-
ln (Wind)	-	-	-	0.26	-	-0.086	-0.25^{+}	-
[m/s]	-	-	-	(0.16)	-	(0.054)	(0.13)	-
ln (Humi)	-	$0.67^{\star}$	-	-	$1.0^{\star}$	-	-	$1.6^{\star\star}$
[ppm]	-	(0.29)	-	-	(0.50)	-	-	(0.56)
ln (TS)	-	-	-	-	$-0.62^{\star\star\star}$	-	-	$-1.1^{\star\star\star}$
[$\mu mol/m^3$]	-	-	-	-	(0.13)	-	-	(0.19)
ln (TN)	-	-	-	-	$0.53^{\star\star\star}$	$0.53^{\star\star\star}$	$0.43^{\star\star}$	$0.35^{\star\star}$
[$\mu mol/m^3$]	-	-	-	-	(0.098)	(0.084)	(0.13)	(0.11)
ln (TA)	-	-	-	-	-	$-0.19^{\star\star}$	-	-
[$\mu mol/m^3$]	-	-	-	-	-	(0.065)	-	-
Adj. R^2	0.68	0.93	0.82	0.61	0.81	0.96	0.85	0.79
F. Bias	0.24	0.17	0.090	0.21	0.028	0.14	0.040	-0.038
F. Error	0.34	0.34	0.52	0.38	0.27	0.29	0.48	0.40
N. Bias	0.24	0.29	-0.100	0.23	-0.047	0.21	-0.23	-0.099
N. Error	0.37	0.55	0.72	0.45	0.24	0.40	0.52	0.43
95% PI[a]	[0.36, 2.77]	[0.46, 2.16]	[0.28, 3.60]	[0.31, 3.25]	[0.44, 2.25]	[0.55, 1.83]	[0.31, 3.27]	[0.42, 2.40]
95% CI[a]	[0.74, 1.37]	[0.78, 1.29]	[0.67, 1.51]	[0.67, 1.51]	[0.74, 1.36]	[0.80, 1.25]	[0.65, 1.56]	[0.72, 1.41]

*** $p < 0.001$, ** $p < 0.001$, * $p < 0.05$, $^{+}$ $p < 0.1$, Standard errors in parentheses, Pop_w: population weighted by average plume, Pres: pressure, Temp: temperature, Prec = precipitation + 0.0002 (shifted for log transformation), Wind: wind speed, Humi: humidity, TS: total sulfate (≡ $[SO_4{}^{2-}]$) [$\mu mol/m^3$], TN: total nitrate (≡ $[HNO_3]$ + $[NO_3{}^-]$) [$\mu mol/m^3$], TA: total ammonia (≡ $[NH_3]$ + $[NH_4{}^+]$) [$\mu mol/m^3$], F. Bias: fractional bias, F. Error: fractional error, N. Bias: normalized mean bias, N. Error: normalized mean error, Winter ≡ Januanry + February + March, Spring ≡ April + May + June, Summer ≡ July + August + September, Winter ≡ October + November + December.

Table 4.8: NH_3 intake fraction model regression results.

Variable	Simple				Better-fit			
	Winter	Spring	Summer	Fall	Winter	Spring	Summer	Fall
Intercept	180^{***} (29)	110^{**} (34)	50^{+} (26)	190^{***} (27)	150^{***} (28)	80^{***} (17)	23 (30)	170^{***} (27)
ln (Pop_w) [# of people]	0.83^{***} (0.068)	1.0^{***} (0.083)	0.84^{***} (0.10)	0.67^{***} (0.065)	0.81^{***} (0.070)	0.86^{***} (0.062)	0.83^{***} (0.080)	0.60^{***} (0.068)
ln (Temp) [K]	-41^{***} (5.7)	-23^{***} (6.3)	-16^{**} (4.9)	-42^{***} (5.0)	-35^{***} (5.7)	-18^{***} (3.3)	-8.8 (6.0)	-36^{***} (5.5)
ln (Pres) [hPa]	3.5^{***} (0.77)	- -	4.1^{**} (1.3)	3.0^{**} (0.85)	3.1^{***} (0.82)	1.9^{+} (1.1)	4.2^{**} (1.3)	2.0^{*} (0.91)
ln (Prec) [g/m^3]	-0.25^{**} (0.088)	- -	0.21^{**} (0.059)	-0.15^{**} (0.055)	-0.21^{*} (0.092)	- -	0.24^{***} (0.063)	-0.099^{+} (0.057)
ln (Wind) [m/s]	-0.094^{+} (0.052)	- -	-0.27^{*} (0.10)	-0.21^{**} (0.075)	- -	-0.11^{+} (0.053)	-0.12 (0.080)	-0.15^{*} (0.075)
ln (Humi) [ppm]	1.8^{***} (0.35)	1.1^{**} (0.33)	- -	1.8^{***} (0.35)	1.4^{***} (0.36)	- -	-0.95^{+} (0.50)	1.4^{***} (0.38)
ln (TS) [$\mu mol/m^3$]	- -	- -	- -	- -	0.28^{**} (0.090)	1.2^{***} (0.12)	1.0^{***} (0.23)	0.27^{*} (0.12)
ln (TN) [$\mu mol/m^3$]	- -	- -	- -	- -	- -	-0.18^{*} (0.082)	-0.17^{+} (0.090)	- -
ln (TA) [$\mu mol/m^3$]	- -	- -	- -	- -	-0.098 (0.064)	-0.35^{***} (0.061)	-0.36^{***} (0.060)	- -
Adj. R^2	0.92	0.82	0.85	0.90	0.93	0.95	0.93	0.91
F. Bias	-0.030	-0.28	-0.23	-0.0064	0.022	0.066	-0.036	0.044
F. Error	0.31	0.36	0.39	0.37	0.25	0.22	0.22	0.32
N. Bias	-0.25	-0.48	-0.46	-0.29	-0.16	-0.048	-0.14	-0.22
N. Error	0.35	0.49	0.48	0.41	0.28	0.18	0.22	0.36
95% PI[a]	[0.57, 1.76]	[0.36, 2.80]	[0.37, 2.68]	[0.56, 1.77]	[0.58, 1.72]	[0.55, 1.80]	[0.48, 2.07]	[0.57, 1.74]
95% CI[a]	[0.81, 1.23]	[0.76, 1.33]	[0.73, 1.38]	[0.81, 1.23]	[0.81, 1.24]	[0.80, 1.26]	[0.73, 1.38]	[0.80, 1.25]

$^{***}\ p < 0.001$, $^{**}\ p < 0.001$, $^{*}\ p < 0.05$, $^{+}\ p < 0.1$, Standard errors in parentheses, Pop_w: population weighted by average plume, Pres: pressure, Temp: temperature, Prec = precipitation + 0.0002 (shifted for log transformation), Wind: wind speed, Humi: humidity, TS: total sulfate (≡ $[SO_4{}^{2-}]$) [$\mu mol/m^3$], TN: total nitrate (≡ $[HNO_3]$ + $[NO_3{}^{-}]$) [$\mu mol/m^3$], TA: total ammonia (≡ $[NH_3]$ + $[NH_4{}^{+}]$) [$\mu mol/m^3$], F. Bias: fractional bias, F. Error: fractional error, N. Bias: normalized mean bias, N. Error: normalized mean error, Winter ≡ Januanry + February + March, Spring ≡ April + May + June, Summer ≡ July + August + September, Winter ≡ October + November + December.

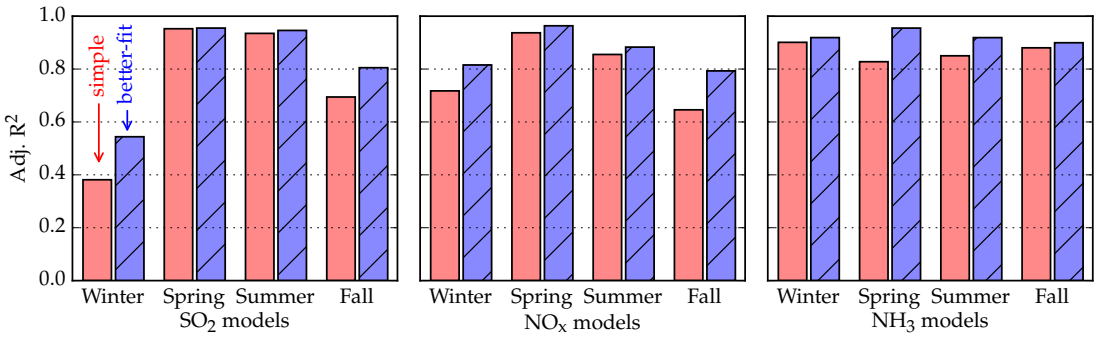

Figure 4.5: Comparison of 'simple' and 'better-fit' models. Adding TS, TN, and TA parameters substantially improves the winter and fall models of SO_2 and NO_x as well as the spring and summer models of NH_3.

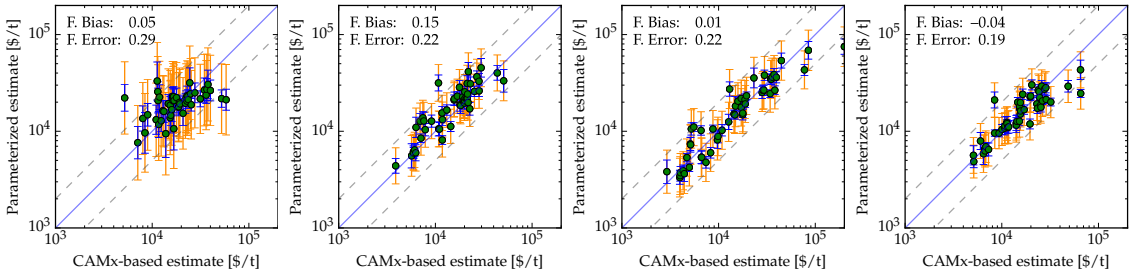

(a) SO_2: Winter (b) SO_2: Spring (c) SO_2: Summer (d) SO_2: Fall

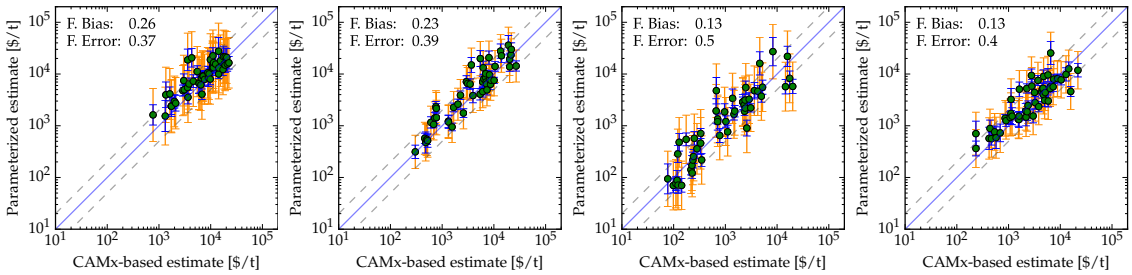

(e) NO_x: Winter (f) NO_x: Spring (g) NO_x: Summer (h) NO_x: Fall

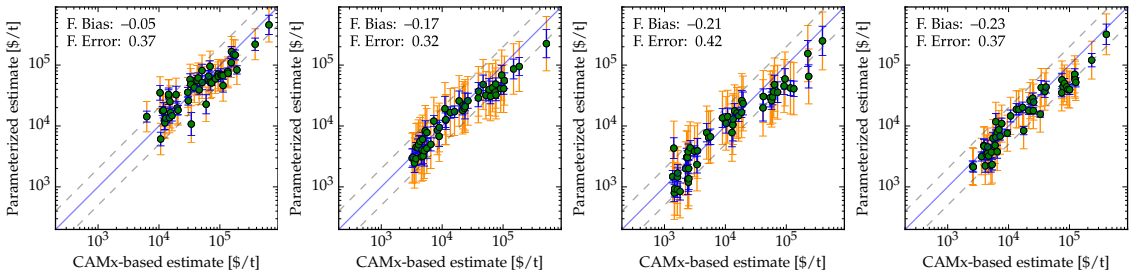

(i) NH_3: Winter (j) NH_3: Spring (k) NH_3: Summer (l) NH_3: Fall

Figure 4.6: Out-of-sample evaluation of 'simple' social cost models. Dashed lines indicate a factor of two and solid line indicates unbiased prediction. Orange bars show 95% prediction intervals and blue bars show 95% confidence intervals.

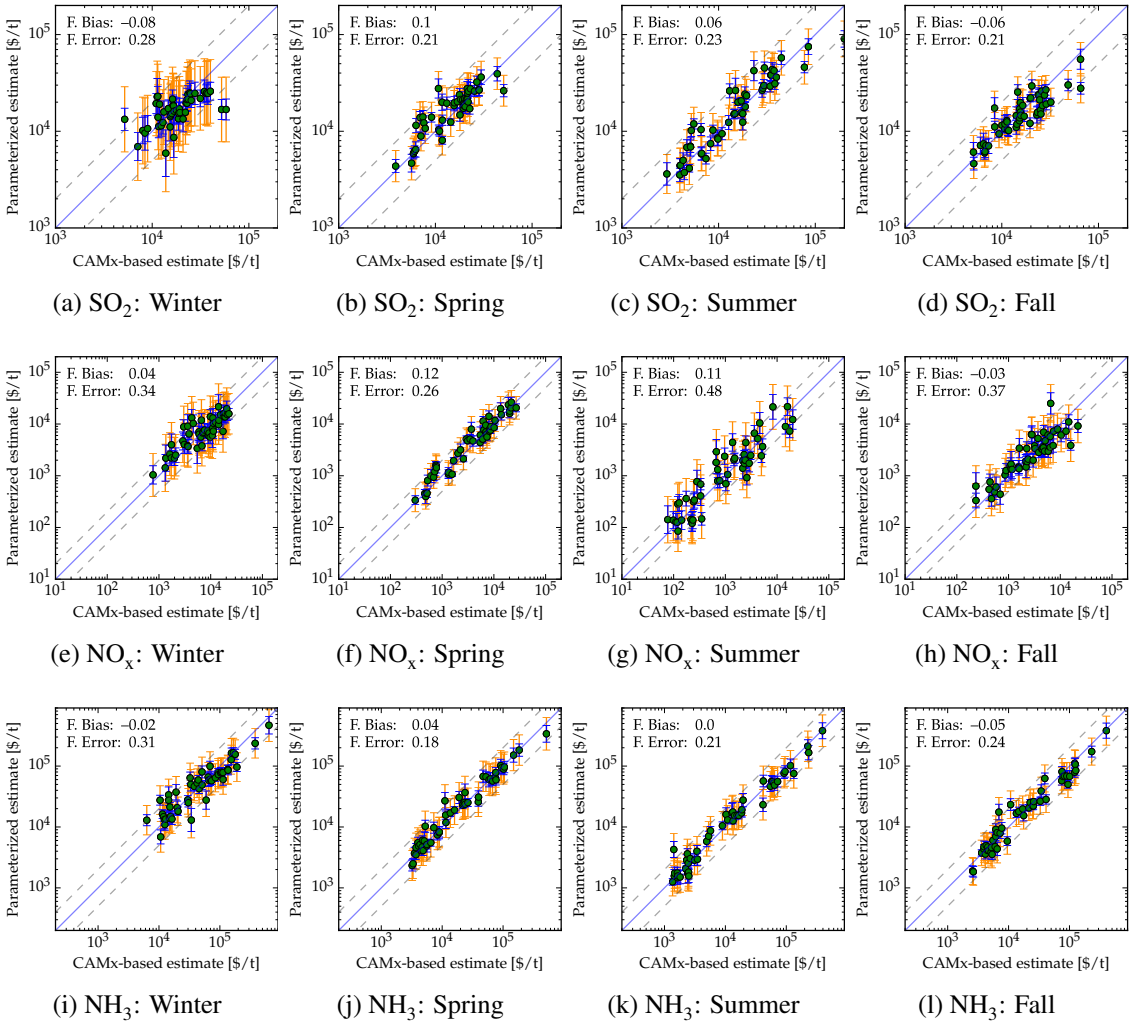

(a) SO_2: Winter (b) SO_2: Spring (c) SO_2: Summer (d) SO_2: Fall

(e) NO_x: Winter (f) NO_x: Spring (g) NO_x: Summer (h) NO_x: Fall

(i) NH_3: Winter (j) NH_3: Spring (k) NH_3: Summer (l) NH_3: Fall

Figure 4.7: Out-of-sample evaluation of 'better-fit' social cost models. Dashed lines indicate a factor of two and solid line indicates unbiased prediction. Orange bars show 95% prediction intervals and blue bars show 95% confidence intervals.

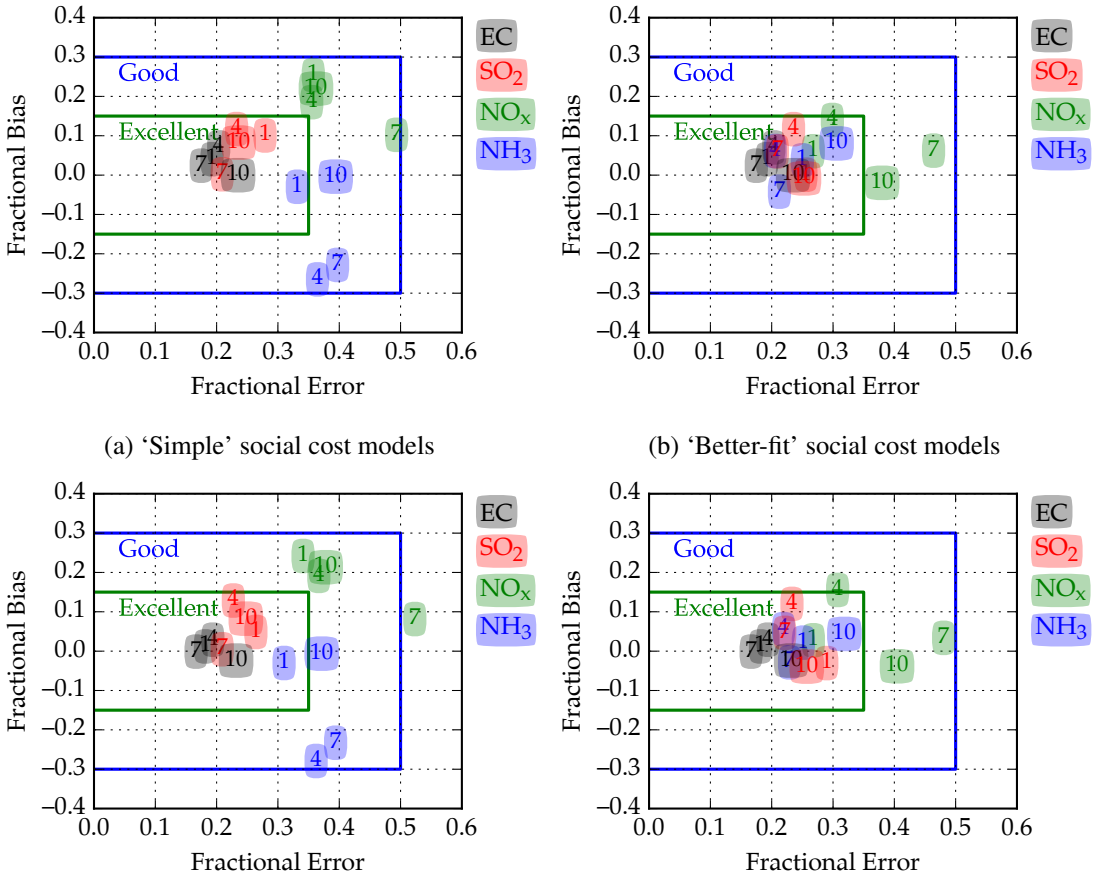

(a) 'Simple' social cost models

(b) 'Better-fit' social cost models

(c) 'Simple' intake fraction models

(d) 'Better-fit' intake fraction models

Figure 4.8: Summary of model evaluations. Numbers (1, 4, 7, and 10) indicate corresponding season models (winter, spring, summer, and fall). 'Excellent' and 'Good' model performance criteria are shown as suggested by Morris et al. (2005). 'Better-fit' SO_2, NO_x, and NH_3 models have TS, TN, and TA as additional parameters. Same EC models are presented on both sides. With the additional parameters, model performance improves.

Table 4.9: Average social costs and intake fractions in the United States.

	Social cost [$/t]				Intake Fraction [ppm]			
	EC	SO_2	NO_x	NH_3	EC	SO_2	NO_x	NH_3
Winter	180,000	23,000	15,000	85,000	2.8	0.30	0.21	1.2
Spring	150,000	31,000	10,000	33,000	2.3	0.44	0.15	0.46
Summer	150,000	34,000	4,200	29,000	2.4	0.47	0.057	0.43
Fall	170,000	21,000	9,700	64,000	2.6	0.29	0.13	0.87
Annual	170,000	27,000	9,700	46,000	2.5	0.38	0.14	0.64

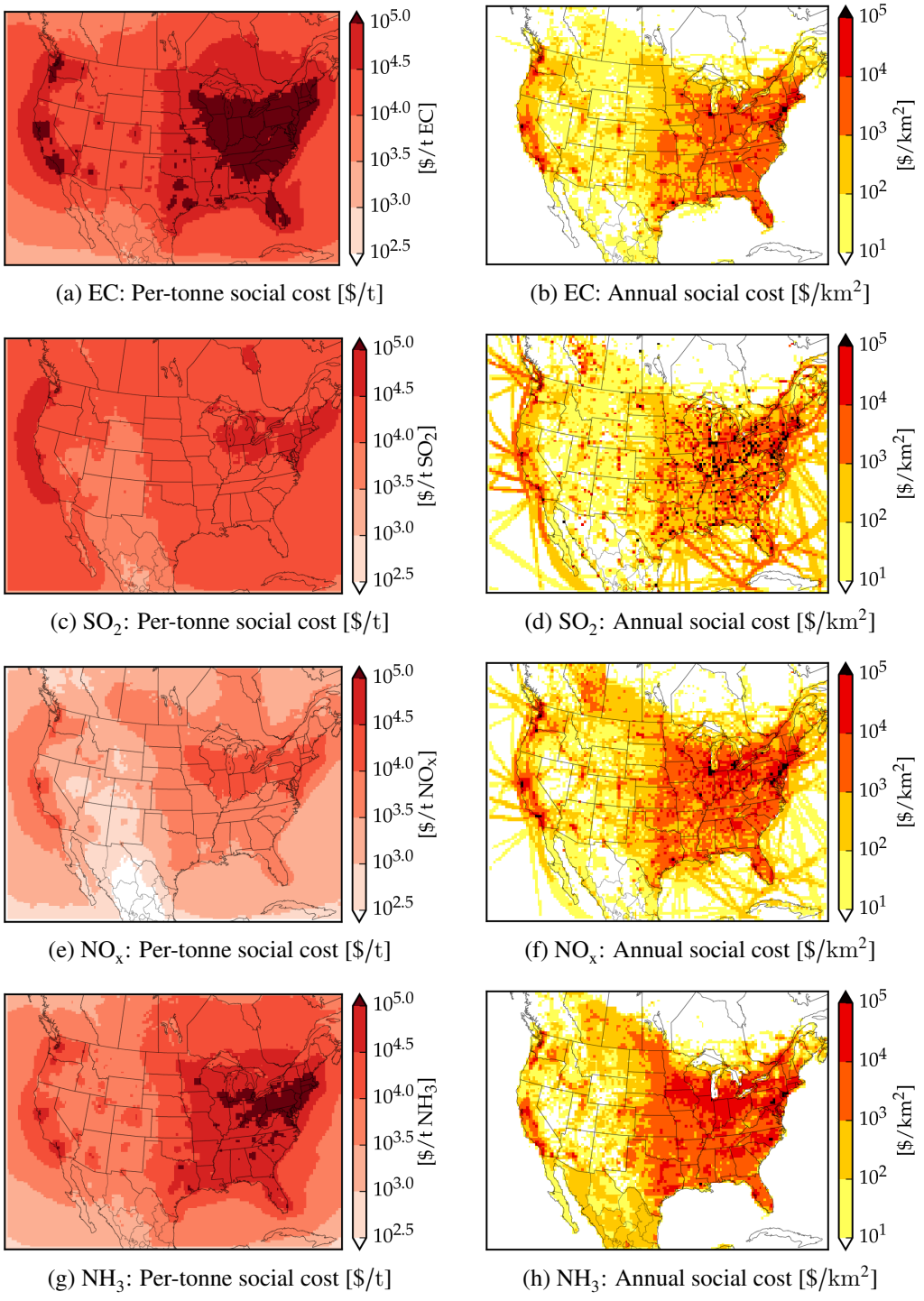

(a) EC: Per-tonne social cost [$/t]

(b) EC: Annual social cost [$/km^2]

(c) SO_2: Per-tonne social cost [$/t]

(d) SO_2: Annual social cost [$/km^2]

(e) NO_x: Per-tonne social cost [$/t]

(f) NO_x: Annual social cost [$/km^2]

(g) NH_3: Per-tonne social cost [$/t]

(h) NH_3: Annual social cost [$/km^2]

Figure 4.9: Map of social costs at the point of emissions estimated using the relative risk of 1.06 and the VSL of $8.8M. The left-hand figures show the average per-tonne social costs estimated with corresponding season models. The right-hand side figures show the annual intake values calculated by multiplying the intake fraction of each season with its corresponding seasonal emissions.

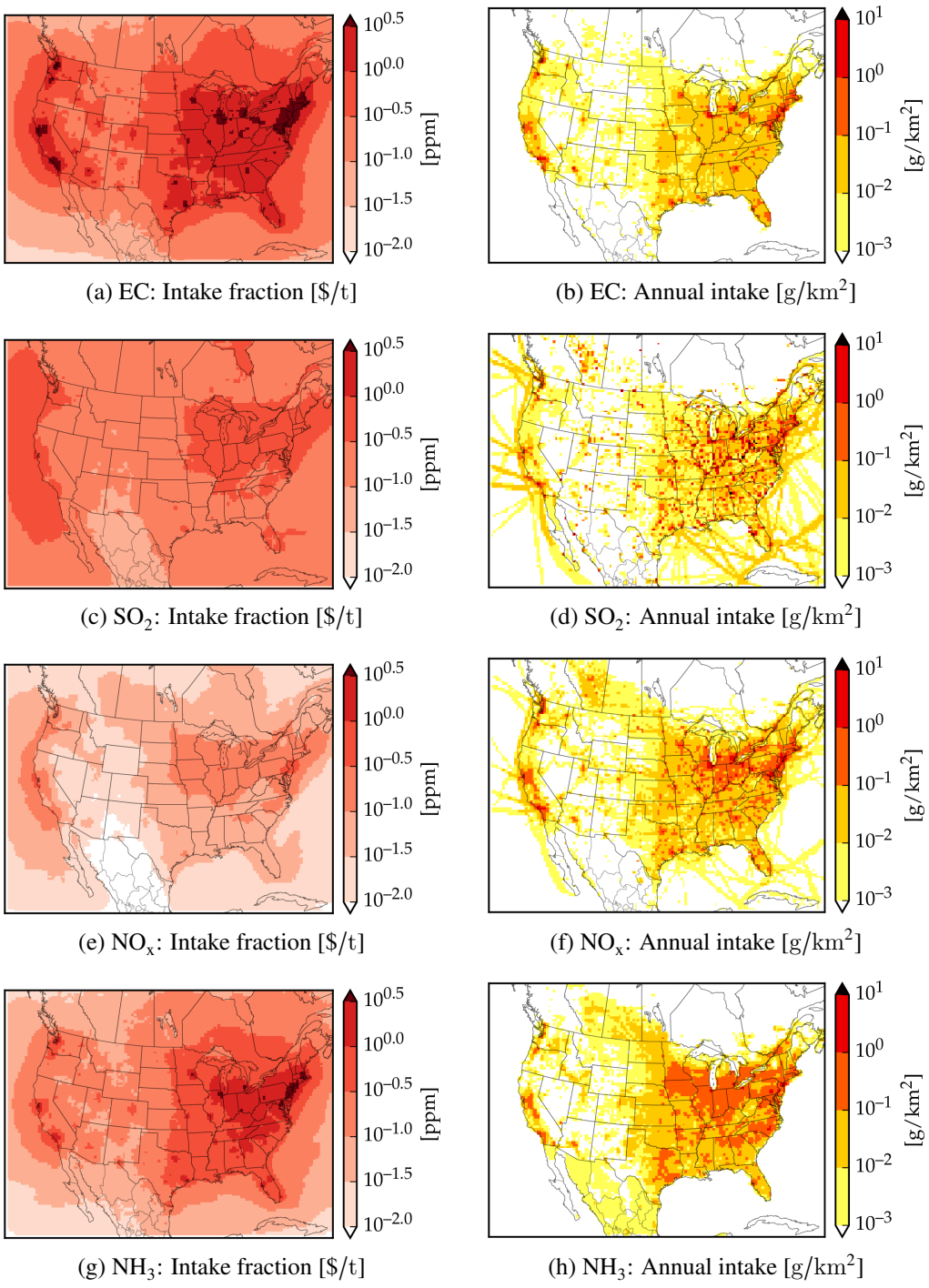

(a) EC: Intake fraction [\$/t]

(b) EC: Annual intake [g/km^2]

(c) SO_2: Intake fraction [\$/t]

(d) SO_2: Annual intake [g/km^2]

(e) NO_x: Intake fraction [\$/t]

(f) NO_x: Annual intake [g/km^2]

(g) NH_3: Intake fraction [\$/t]

(h) NH_3: Annual intake [g/km^2]

Figure 4.10: Map of intake fractions at the point of emissions. The left-hand figures show the average intake fractions of four estimates estimated with corresponding season models. The right-hand side figures show the annual intake values calculated by multiplying the intake fraction of each season with its corresponding seasonal emissions.

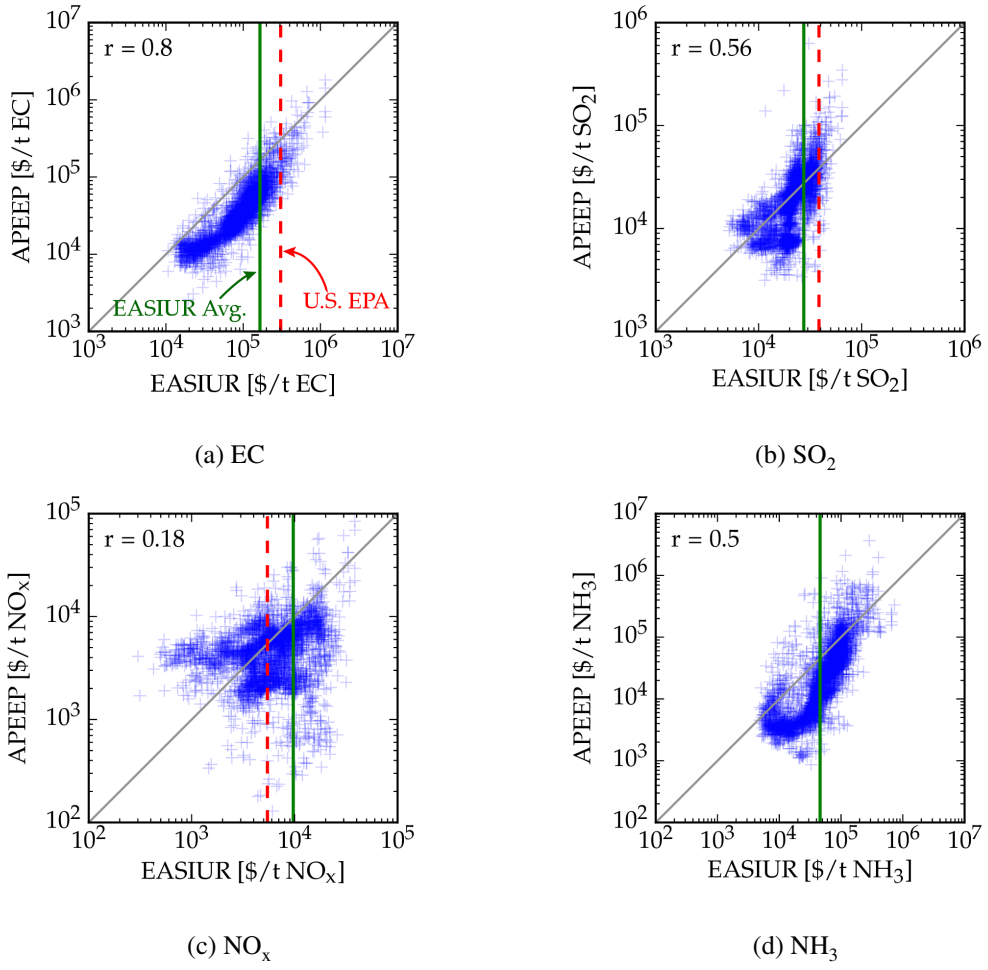

(a) EC (b) SO_2

(c) NO_x (d) NH_3

Figure 4.11: Comparison of EASIUR with others. The APEEP values are based on Muller et al (2011). The dotted red lines are reported by Fann et al (2012) for area sources. All the values are further adjusted to match dollar year, income growth, VSL, and tonne unit with the EASIUR estimates. Solid green lines indicate emission-weighted average EASIUR values for U.S. emissions (not including those from ocean, Canada, and Mexico).

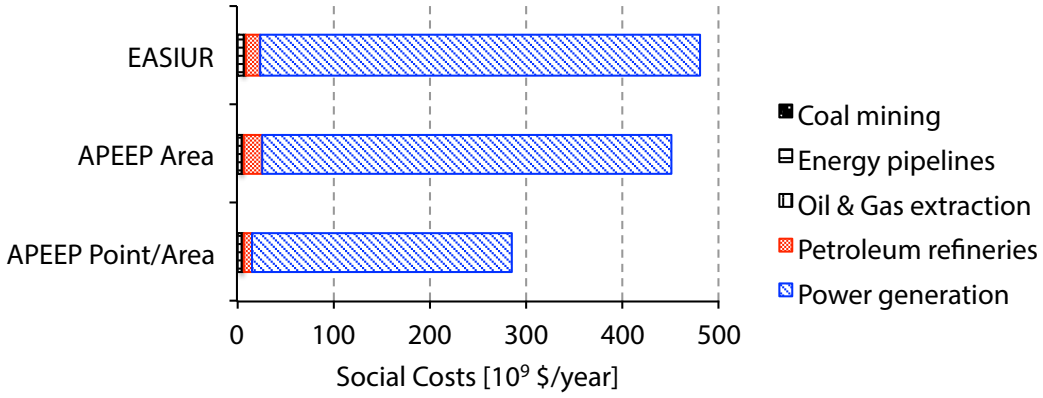

Figure 4.12: Social costs from the life cycle of electricity generation. APEEP Area is based on marginal damages for area sources from APEEP for all sectors. APEEP Area/Point is based on marginal damages for mid-height (250-500 m) point sources from APEEP for petroleum refineries and power generation and marginal damages for area sources for all other sectors.

Table 4.10: Social costs [$] from the life cycle of electricity generation. For APEEP, marginal damages for area sources were used for all sector emissions.

		Coal mining	Energy Pipelines	Oil & Gas extraction	Petroleum refineries	Power generation	Total
EC	EASIUR	5.7E+08	1.4E+09	3.9E+08	6.6E+09	1.0E+11	1.1E+11
	APEEP	2.3E+08	6.5E+08	2.1E+08	4.2E+09	4.8E+10	5.3E+10
	A/E[a]	0.41	0.48	0.54	0.64	0.48	0.49
SO_2	EASIUR	5.8E+07	1.1E+09	1.2E+09	7.7E+09	3.2E+11	3.3E+11
	APEEP	6.2E+07	1.2E+09	9.4E+08	1.2E+10	3.5E+11	3.7E+11
	A/E	1.07	1.02	0.78	1.55	1.11	1.12
NO_x	EASIUR	1.6E+07	2.9E+09	9.0E+08	1.7E+09	3.6E+10	4.1E+10
	APEEP	6.4E+06	1.8E+09	1.2E+09	9.0E+08	2.2E+10	2.6E+10
	A/E	0.39	0.62	1.30	0.54	0.62	0.63
NH_3	EASIUR	4.6E+07	1.0E+08	3.6E+06	4.4E+08	2.5E+09	3.1E+09
	APEEP	4.4E+07	1.1E+08	2.7E+07	2.4E+09	2.2E+09	4.8E+09
	A/E	0.95	1.13	7.48	5.43	0.89	1.55
Total	EASIUR	6.9E+08	5.5E+09	2.5E+09	1.6E+10	4.5E+11	4.8E+11
	APEEP	3.5E+08	3.7E+09	2.3E+09	1.9E+10	4.2E+11	4.5E+11
	A/E	0.50	0.68	0.94	1.19	0.93	0.94

[a] A ratio of APEEP-based estimates to EASIUR-based estimates.

Table 4.11: Social costs [$] from the life cycle of electricity generation. For APEEP, marginal damages for medium height (250-500m) point sources were used for petroleum refineries and power generation but marginal damages for area sources were used for the other sectors.

		Coal mining	Energy Pipelines	Oil & Gas extraction	Petroleum refineries	Power generation	Total
EC	EASIUR	5.7E+08	1.4E+09	3.9E+08	6.6E+09	1.0E+11	1.1E+11
	APEEP	2.3E+08	6.5E+08	2.1E+08	1.4E+09	2.2E+10	2.4E+10
	A/E[a]	0.41	0.48	0.54	0.21	0.22	0.22
SO_2	EASIUR	5.8E+07	1.1E+09	1.2E+09	7.7E+09	3.2E+11	3.3E+11
	APEEP	6.2E+07	1.2E+09	9.4E+08	5.7E+09	2.3E+11	2.4E+11
	A/E	1.07	1.02	0.78	0.74	0.74	0.74
NO_x	EASIUR	1.6E+07	2.9E+09	9.0E+08	1.7E+09	3.6E+10	4.1E+10
	APEEP	6.4E+06	1.8E+09	1.2E+09	5.4E+08	1.4E+10	1.8E+10
	A/E	0.39	0.62	1.30	0.32	0.40	0.43
NH_3	EASIUR	4.6E+07	1.0E+08	3.6E+06	4.4E+08	2.5E+09	3.1E+09
	APEEP	4.4E+07	1.1E+08	2.7E+07	6.1E+08	8.4E+08	1.6E+09
	A/E	0.95	1.13	7.48	1.39	0.34	0.53
Total	EASIUR	6.9E+08	5.5E+09	2.5E+09	1.6E+10	4.5E+11	4.8E+11
	APEEP	3.5E+08	3.7E+09	2.3E+09	8.2E+09	2.7E+11	2.9E+11
	A/E	0.50	0.68	0.94	0.50	0.60	0.60

[a] A ratio of APEEP-based estimates to EASIUR-based estimates.

C Appendix I: Additional Figures and Tables

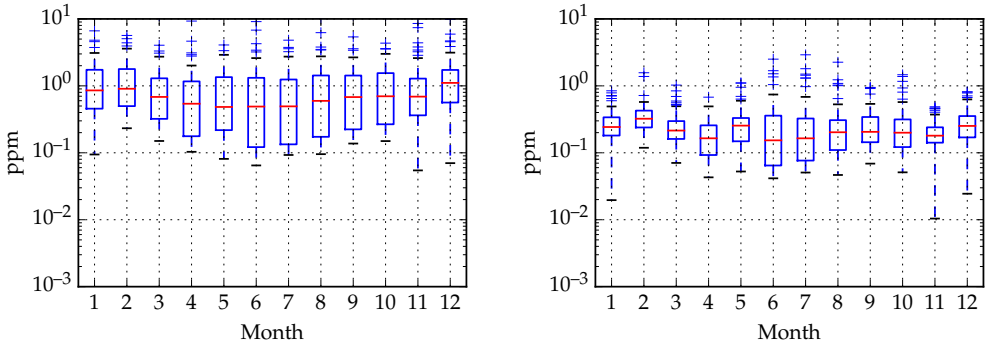

(a) EC

(b) SO_2

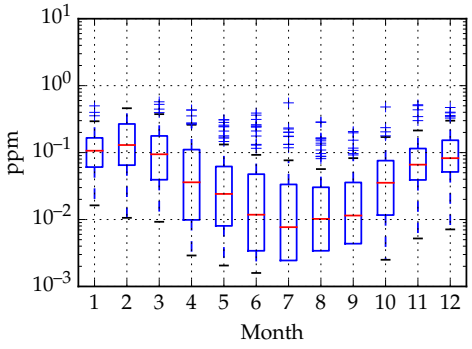

(c) NO_x

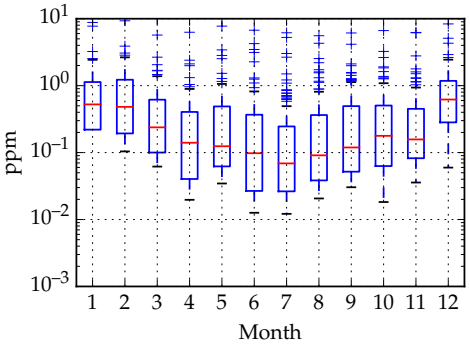

(d) NH_3

Figure C-1: Intake fractions at the 100 sample locations. The bottom and top of the box are the first and third quartile, and the red band inside the box indicates median. Whiskers show 1.5 × IQR (interquartile range) below the first quartile and beyond the third quartile.

Table C-1: Summary of social costs and selected parameters for winter.

	sEC	sSO2	sNOX	sNH3	pEC	pSO2	pNOX	pNH3	pres	temp	prec	wind	humi	ta	tn	ts
count	100	100	100	100	100	100	100	100	100	100	100	100	100	100	100	100
mean	85,000	20,000	9,400	58,000	23,000	18,000	19,000	22,000	935	276	0.074	1.6	6,300	0.080	0.90	0.022
std	91,000	10,000	6,700	86,000	31,000	14,000	17,000	30,000	73.9	6.3	0.040	1.1	2,700	0.063	0.74	0.014
min	16,000	5,400	770	6,600	2,000	3,400	2,800	2,200	707	264	0.014	0.15	3,200	0.0064	0.024	0.0054
25%	27,000	13,000	4,000	12,000	5,800	8,100	7,600	6,100	897	271	0.042	0.69	4,500	0.022	0.23	0.0075
50%	59,000	19,000	7,700	32,000	14,000	13,000	13,000	13,000	963	275	0.071	1.3	5,400	0.070	0.75	0.019
75%	110,000	24,000	14,000	69,000	31,000	22,000	24,000	31,000	993	280	0.10	2.2	7,000	0.14	1.4	0.035
max	760,000	64,000	26,000	680,000	270,000	100,000	120,000	260,000	1,020	293	0.24	6.0	17,000	0.29	3.2	0.051

* sEC, sSO2, sNOX, and sNH3: per-tonne social cost (using \$8M VSL and the relative risk of 1.06 per $10\,\mu g\,PM_{2.5}/m^3$) [\$/t] of EC, SO_2, NO_x, and NH_3. pEC, pSO2, pNOX, and pNH3: population (of ≥ age 30) [# of people] weighted with the average plume of EC, SO_2, NO_x, and NH_3, pres: pressure [hPa], temp: temperature [K], prec: precipitation + 0.0002 [g/m^3] (shifted for log transformation), wind: wind speed [m/s], humi: humidity [ppm], ta: total ammonia [$\mu mol/m^3$], tn: total nitrate [$\mu mol/m^3$], ts: total sulfate [$\mu mol/m^3$].

Table C-2: Summary of social costs and selected parameters for spring.

	sEC	sSO2	sNOX	sNH3	pEC	pSO2	pNOX	pNH3	pres	temp	prec	wind	humi	ta	tn	ts
count	100	100	99	100	100	100	100	100	100	100	100	100	100	100	100	100
mean	63,000	17,000	4,000	28,000	24,000	18,000	19,000	22,000	932	289	0.083	1.7	11,000	0.095	0.35	0.024
std	82,000	15,000	5,500	56,000	36,000	14,000	18,000	33,000	72.5	5.1	0.041	1.2	4,000	0.077	0.38	0.016
min	5,900	3,100	150	2,000	1,800	3,900	3,400	2,300	710	276	0.0002	0.045	5,700	0.011	0.022	0.0068
25%	11,000	7,400	420	3,000	4,800	8,100	7,300	5,300	896	286	0.059	0.84	8,000	0.029	0.056	0.0089
50%	36,000	14,000	1,900	8,800	14,000	14,000	14,000	14,000	959	289	0.082	1.3	11,000	0.082	0.25	0.020
75%	87,000	21,000	5,000	30,000	34,000	25,000	27,000	32,000	990	292	0.11	2.2	14,000	0.15	0.45	0.036
max	640,000	100,000	26,000	440,000	310,000	110,000	140,000	280,000	1,010	302	0.24	7.0	23,000	0.39	1.9	0.059

* Look at Table C-1 for parameter definitions.

Table C-3: Summary of social costs and selected parameters for summer.

	sEC	sSO2	sNOX	sNH3	pEC	pSO2	pNOX	pNH3	pres	temp	prec	wind	humi	ta	tn	ts
count	100	100	99	100	100	100	100	100	100	100	100	100	100	100	100	100
mean	68,000	19,000	2,200	28,000	23,000	18,000	17,000	22,000	934	296	0.066	1.9	17,000	0.097	0.20	0.025
std	86,000	21,000	3,700	54,000	37,000	14,000	15,000	33,000	71.2	4.5	0.046	1.1	5,500	0.080	0.29	0.019
min	6,600	3,500	89	1,500	1,800	3,600	3,600	2,200	717	286	0.0003	0.12	8,300	0.011	0.0091	0.0051
25%	12,000	7,600	270	2,800	4,500	7,400	7,300	5,500	899	293	0.033	1.2	12,000	0.027	0.030	0.0080
50%	44,000	14,000	690	6,000	14,000	13,000	12,000	13,000	961	296	0.056	1.9	18,000	0.085	0.10	0.018
75%	98,000	24,000	2,500	24,000	31,000	25,000	23,000	29,000	992	298	0.093	2.5	22,000	0.15	0.26	0.035
max	680,000	160,000	22,000	380,000	320,000	100,000	120,000	290,000	1,010	306	0.28	6.0	28,000	0.43	1.7	0.080

* Look at Table C-1 for parameter definitions.

Table C-4: Summary of social costs and selected parameters for fall.

	sEC	sSO2	sNOX	sNH3	pEC	pSO2	pNOX	pNH3	pres	temp	prec	wind	humi	ta	tn	ts
count	100	100	100	100	100	100	100	100	100	100	100	100	100	100	100	100
mean	80,000	17,000	5,900	44,000	22,000	17,000	17,000	22,000	935	281	0.076	2.0	8,200	0.067	0.50	0.016
std	80,000	8,700	4,400	59,000	30,000	13,000	13,000	29,000	72.6	5.6	0.066	1.2	2,700	0.057	0.44	0.011
min	8,400	4,800	390	3,600	2,100	3,500	3,400	2,400	710	271	0.0057	0.19	5,100	0.0063	0.023	0.0038
25%	27,000	12,000	2,500	9,800	5,900	8,700	7,200	5,700	897	276	0.036	1.2	6,200	0.023	0.15	0.0057
50%	58,000	16,000	4,800	24,000	13,000	14,000	14,000	13,000	961	280	0.049	1.7	7,400	0.061	0.40	0.015
75%	110,000	21,000	8,000	51,000	31,000	23,000	24,000	30,000	990	284	0.10	2.5	9,600	0.10	0.74	0.024
max	620,000	58,000	18,000	450,000	250,000	88,000	91,000	240,000	1,010	295	0.34	6.9	21,000	0.40	2.0	0.043

* Look at Table C-1 for parameter definitions.

Table C-5: Summary of intake fractions and selected parameters for winter.

	iEC	iSO2	iNOX	iNH3	pEC	pSO2	pNOX	pNH3	pres	temp	prec	wind	humi	ta	tn	ts
count	100	100	100	100	100	100	100	100	100	100	100	100	100	100	100	100
mean	1.2	0.29	0.14	0.84	38,000	30,000	32,000	37,000	935	276	0.074	1.6	6,300	0.080	0.90	0.022
std	1.5	0.15	0.096	1.4	52,000	23,000	27,000	50,000	73.9	6.3	0.040	1.1	2,700	0.063	0.74	0.014
min	0.25	0.036	0.012	0.11	3,400	5,900	4,900	3,700	707	264	0.014	0.15	3,200	0.0064	0.024	0.0054
25%	0.42	0.19	0.056	0.17	10,000	14,000	13,000	11,000	897	271	0.042	0.69	4,500	0.022	0.23	0.0075
50%	0.84	0.25	0.11	0.46	23,000	23,000	23,000	23,000	963	275	0.071	1.3	5,400	0.070	0.75	0.019
75%	1.6	0.33	0.20	0.96	54,000	38,000	42,000	54,000	993	280	0.10	2.2	7,000	0.14	1.4	0.035
max	12	1.0	0.37	11	440,000	170,000	200,000	430,000	1,020	293	0.24	6.0	17,000	0.29	3.2	0.051

* iEC, iSO2, iNOX, and iNH3: intake fraction [ppm] of EC, SO_2, NO_x, and NH_3. pEC, pSO2, pNOX, and pNH3: population [# of people] weighted with the average plume of EC, SO_2, NO_x, and NH_3, pres: pressure [hPa], temp: temperature [K], prec: precipitation + 0.0002 [g/m^3] (shifted for log transformation), wind: wind speed [m/s], humi: humidity [ppm], ta: total ammonia [$\mu mol/m^3$], tn: total nitrate [$\mu mol/m^3$], ts: total sulfate [$\mu mol/m^3$].

Table C-6: Summary of intake fractions and selected parameters for spring.

	iEC	iSO2	iNOX	iNH3	pEC	pSO2	pNOX	pNH3	pres	temp	prec	wind	humi	ta	tn	ts
count	100	100	99	100	100	100	100	100	100	100	100	100	100	100	100	100
mean	0.92	0.25	0.058	0.41	40,000	30,000	32,000	38,000	932	289	0.083	1.7	11,000	0.095	0.35	0.024
std	1.3	0.21	0.078	0.86	60,000	24,000	29,000	54,000	72.5	5.1	0.041	1.2	4,000	0.077	0.38	0.016
min	0.090	0.046	0.0023	0.028	3,000	6,700	5,700	3,900	710	276	0.0002	0.045	5,700	0.011	0.022	0.0068
25%	0.16	0.11	0.0067	0.044	8,400	14,000	13,000	9,100	896	286	0.059	0.84	8,000	0.029	0.056	0.0089
50%	0.54	0.20	0.029	0.12	24,000	24,000	24,000	23,000	959	289	0.082	1.3	11,000	0.082	0.25	0.020
75%	1.3	0.32	0.073	0.46	57,000	42,000	44,000	54,000	990	292	0.11	2.2	14,000	0.15	0.45	0.036
max	10	1.3	0.36	6.9	510,000	180,000	230,000	470,000	1,010	302	0.24	7.0	23,000	0.39	1.9	0.059

* Look at Table C-5 for parameter definitions.

Table C-7: Summary of intake fractions and selected parameters for summer.

	iEC	iSO2	iNOX	iNH3	pEC	pSO2	pNOX	pNH3	pres	temp	prec	wind	humi	ta	tn	ts
count	100	100	99	100	100	100	100	100	100	100	100	100	100	100	100	100
mean	1.00	0.28	0.032	0.40	39,000	30,000	28,000	37,000	934	296	0.066	1.9	17,000	0.097	0.20	0.025
std	1.4	0.29	0.054	0.84	61,000	24,000	25,000	55,000	71.2	4.5	0.046	1.1	5,500	0.080	0.29	0.019
min	0.11	0.056	0.0012	0.024	3,200	6,200	6,200	3,800	717	286	0.0003	0.12	8,300	0.011	0.0091	0.0051
25%	0.17	0.11	0.0040	0.039	7,900	13,000	13,000	9,300	899	293	0.033	1.2	12,000	0.027	0.030	0.0080
50%	0.61	0.19	0.0090	0.091	23,000	22,000	20,000	22,000	961	296	0.056	1.9	18,000	0.085	0.10	0.018
75%	1.3	0.34	0.033	0.36	54,000	42,000	40,000	50,000	992	298	0.093	2.5	22,000	0.15	0.26	0.035
max	11	2.0	0.35	6.0	540,000	170,000	200,000	490,000	1,010	306	0.28	6.0	28,000	0.43	1.7	0.080

* Look at Table C-5 for parameter definitions.

Table C-8: Summary of intake fractions and selected parameters for fall.

	iEC	iSO2	iNOX	iNH3	pEC	pSO2	pNOX	pNH3	pres	temp	prec	wind	humi	ta	tn	ts
count	100	100	100	100	100	100	100	100	100	100	100	100	100	100	100	100
mean	1.2	0.25	0.087	0.63	37,000	29,000	30,000	36,000	935	281	0.076	2.0	8,200	0.067	0.50	0.016
std	1.3	0.13	0.066	0.94	49,000	21,000	22,000	48,000	72.6	5.6	0.066	1.2	2,700	0.057	0.44	0.011
min	0.11	0.066	0.0060	0.056	3,700	5,900	5,700	4,200	710	271	0.0057	0.19	5,100	0.0063	0.023	0.0038
25%	0.41	0.17	0.037	0.14	10,000	15,000	13,000	10,000	897	276	0.036	1.2	6,200	0.023	0.15	0.0057
50%	0.82	0.22	0.071	0.33	23,000	23,000	24,000	22,000	961	280	0.049	1.7	7,400	0.061	0.40	0.015
75%	1.6	0.30	0.12	0.71	52,000	40,000	41,000	50,000	990	284	0.10	2.5	9,600	0.10	0.74	0.024
max	9.9	0.90	0.33	7.1	410,000	150,000	150,000	400,000	1,010	295	0.34	6.9	21,000	0.40	2.0	0.043

* Look at Table C-5 for parameter definitions.

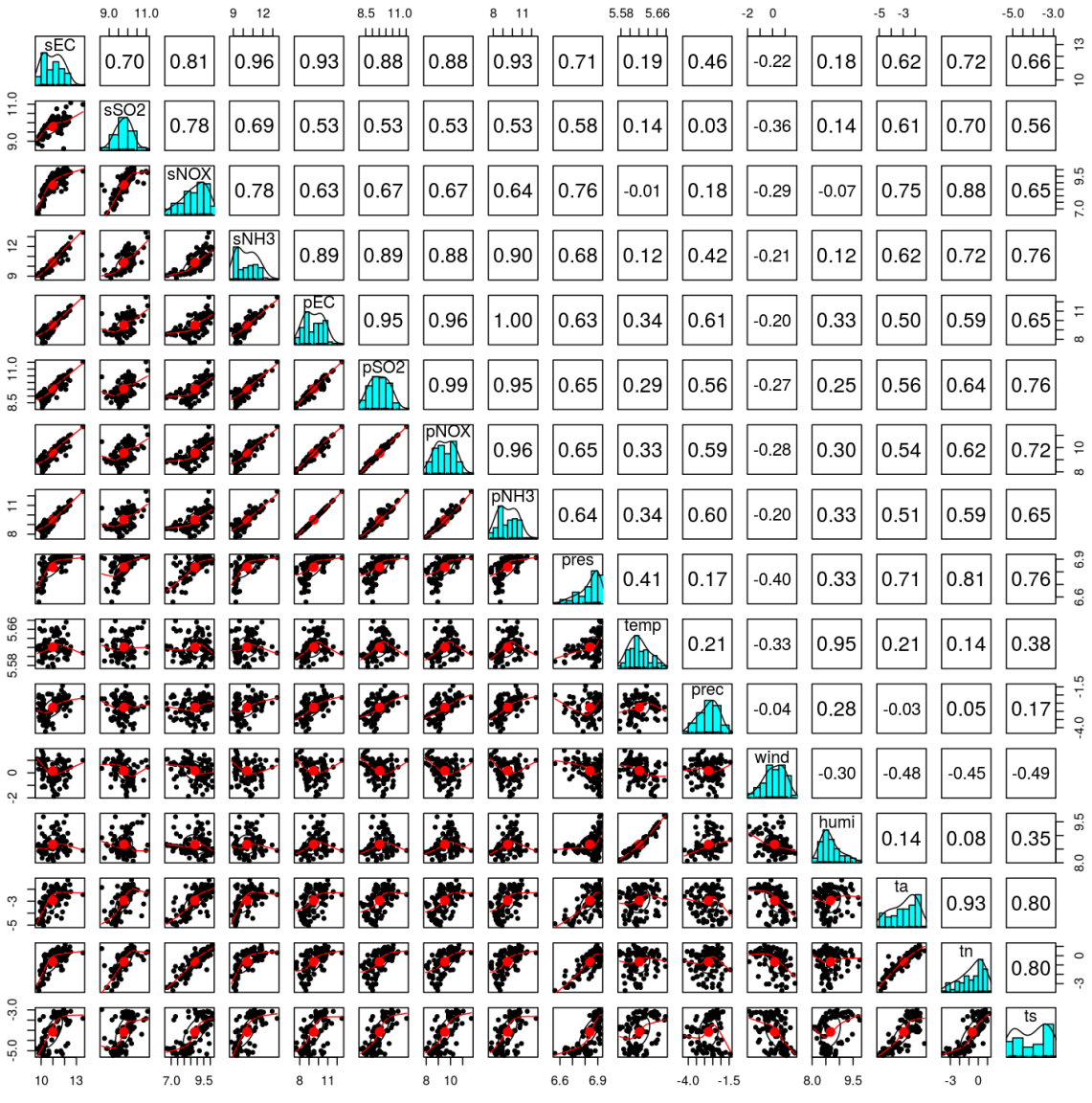

Figure C-2: Correlation matrix plot of selected parameters for winter social cost dataset. All the values are natural log transformed. Pearson's correlation coefficients are on the upper right. Look at Table C-1 for parameter definitions.

Figure C-3: Correlation matrix plot of selected parameters for spring social cost dataset. All the values are natural log transformed. Pearson's correlation coefficients are on the upper right. Look at Table C-1 for parameter definitions.

Figure C-4: Correlation matrix plot of selected parameters for summer social cost dataset. All the values are natural log transformed. Pearson's correlation coefficients are on the upper right. Look at Table C-1 for parameter definitions.

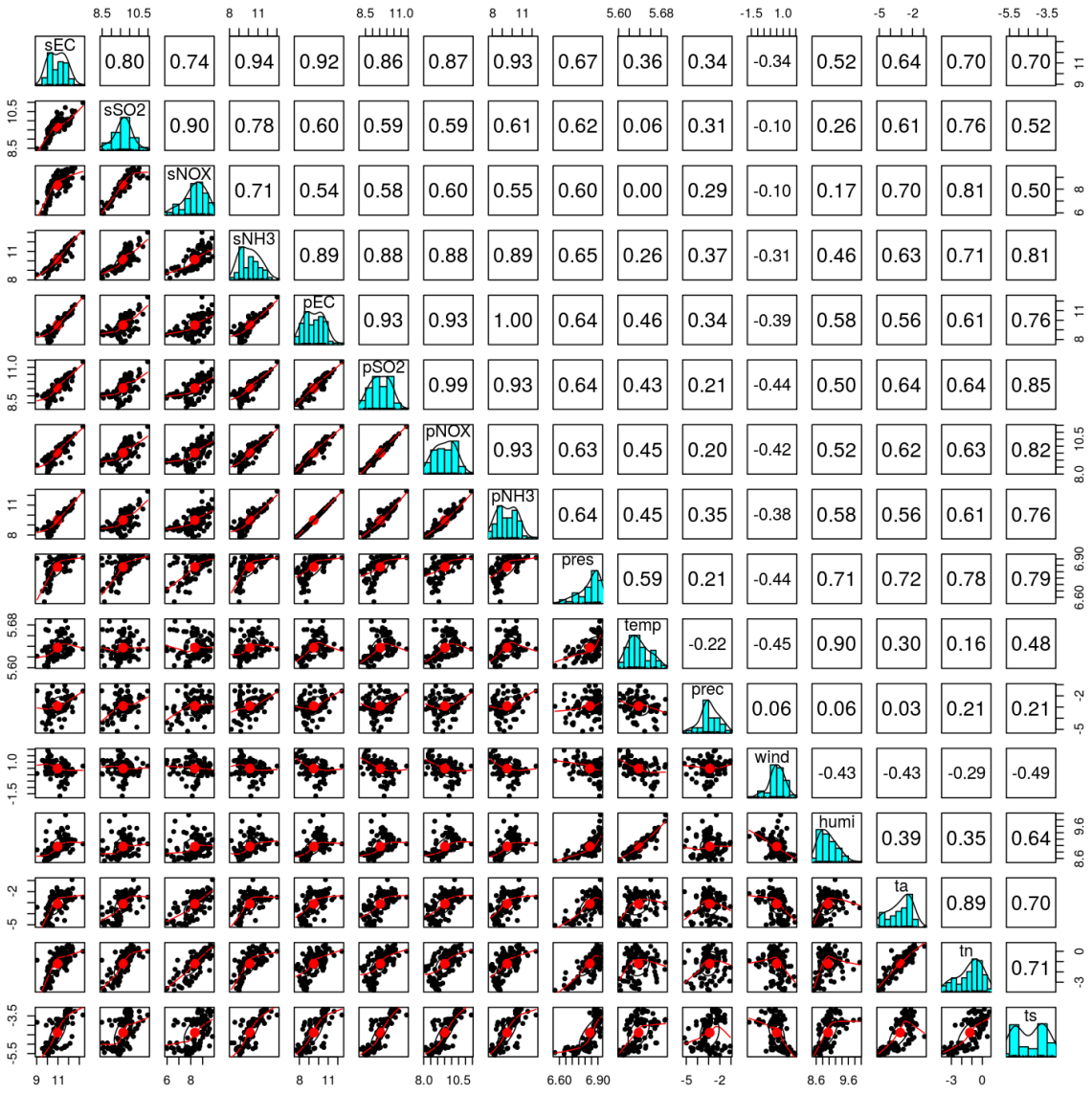

Figure C-5: Correlation matrix plot of selected parameters for fall social cost dataset. All the values are natural log transformed. Pearson's correlation coefficients are on the upper right. Look at Table C-1 for parameter definitions.

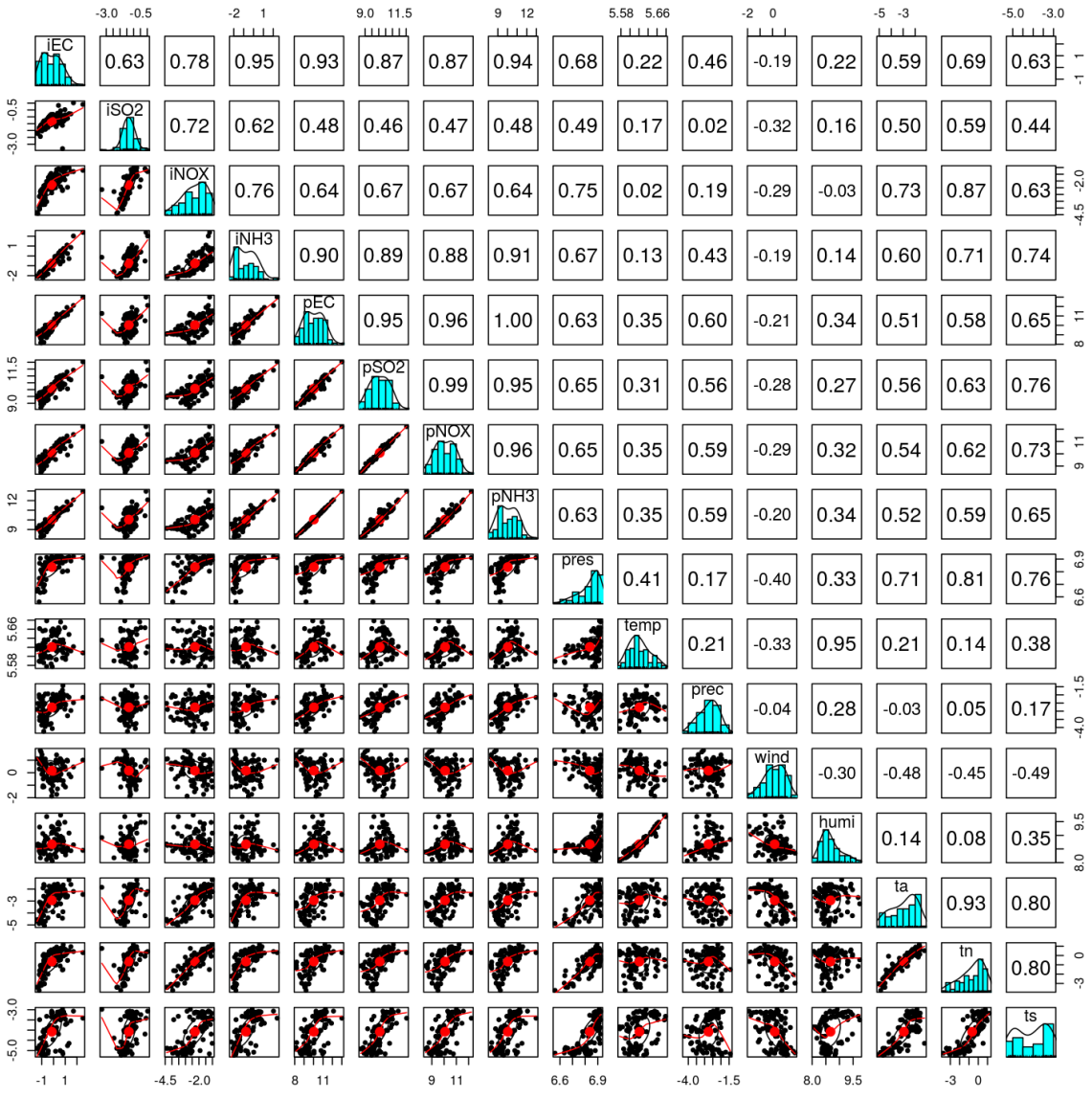

Figure C-6: Correlation matrix plot of selected parameters for winter intake fraction dataset. All the values are natural log transformed. Pearson's correlation coefficients are on the upper right. Look at Table C-5 for parameter definitions.

Figure C-7: Correlation matrix plot of selected parameters for spring intake fraction dataset. All the values are natural log transformed. Pearson's correlation coefficients are on the upper right. Look at Table C-5 for parameter definitions.

Figure C-8: Correlation matrix plot of selected parameters for summer intake fraction dataset. All the values are natural log transformed. Pearson's correlation coefficients are on the upper right. Look at Table C-5 for parameter definitions.

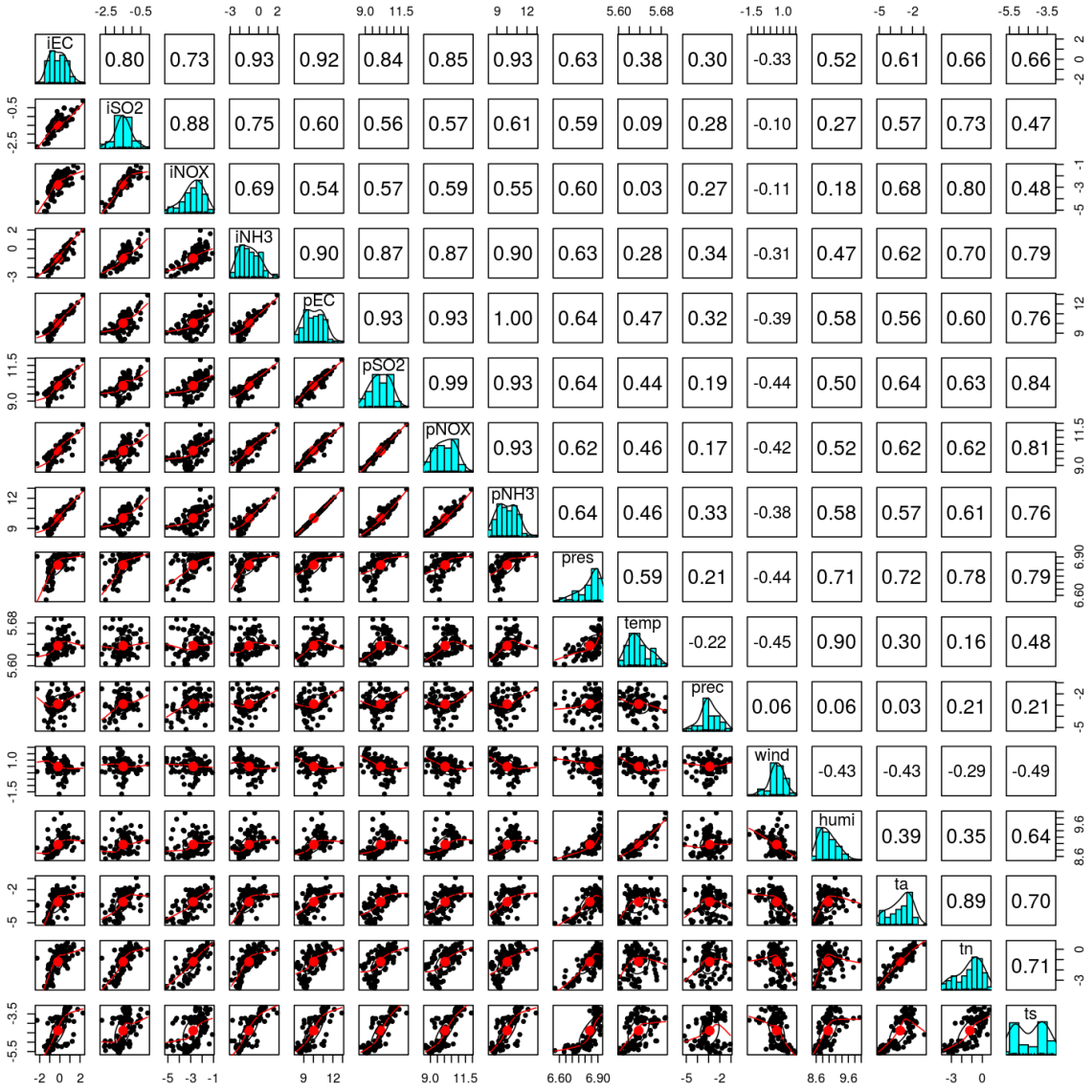

Figure C-9: Correlation matrix plot of selected parameters for fall intake fraction dataset. All the values are natural log transformed. Pearson's correlation coefficients are on the upper right. Look at Table C-5 for parameter definitions.

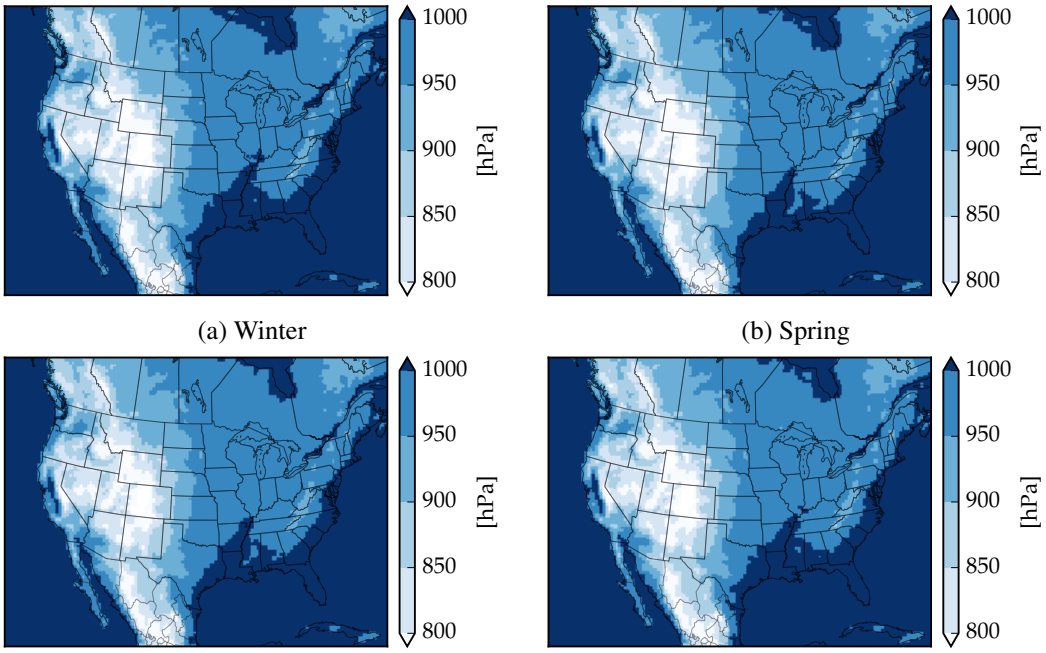

(a) Winter (b) Spring

(c) Summer (d) Fall

Figure C-10: Pressure of the United States in 2005. Daily mean values are presented.

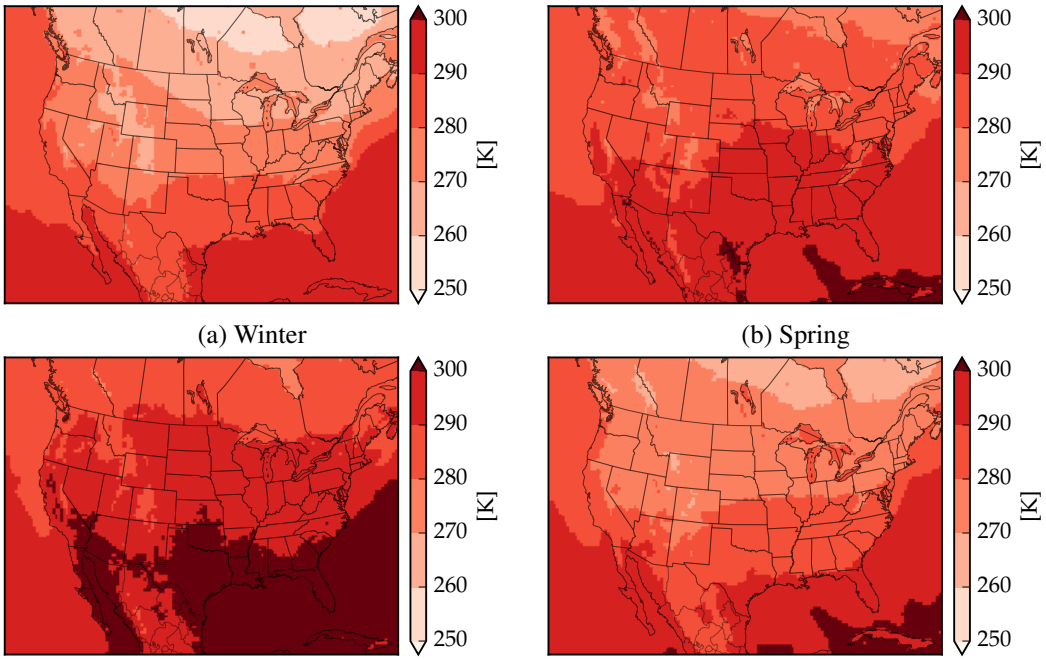

(a) Winter (b) Spring

(c) Summer (d) Fall

Figure C-11: Temperature of the United States in 2005. Daily mean values are presented.

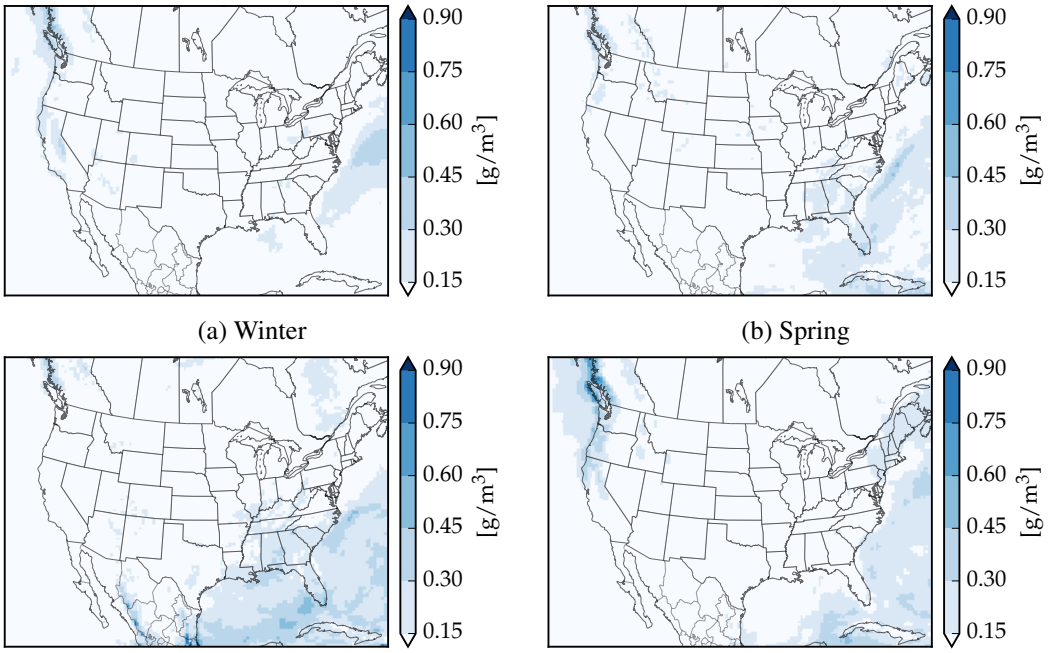

(a) Winter (b) Spring

(c) Summer (d) Fall

Figure C-12: Precipitation of the United States in 2005. Daily mean values are presented.

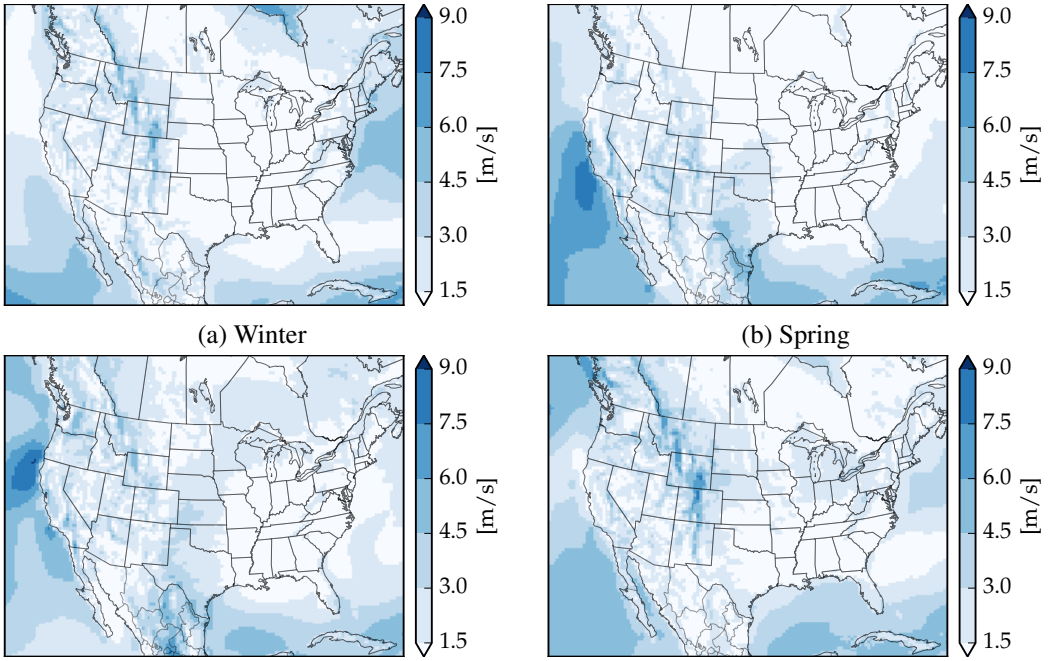

(a) Winter (b) Spring

(c) Summer (d) Fall

Figure C-13: Wind speed of the United States in 2005. Daily mean values are presented.

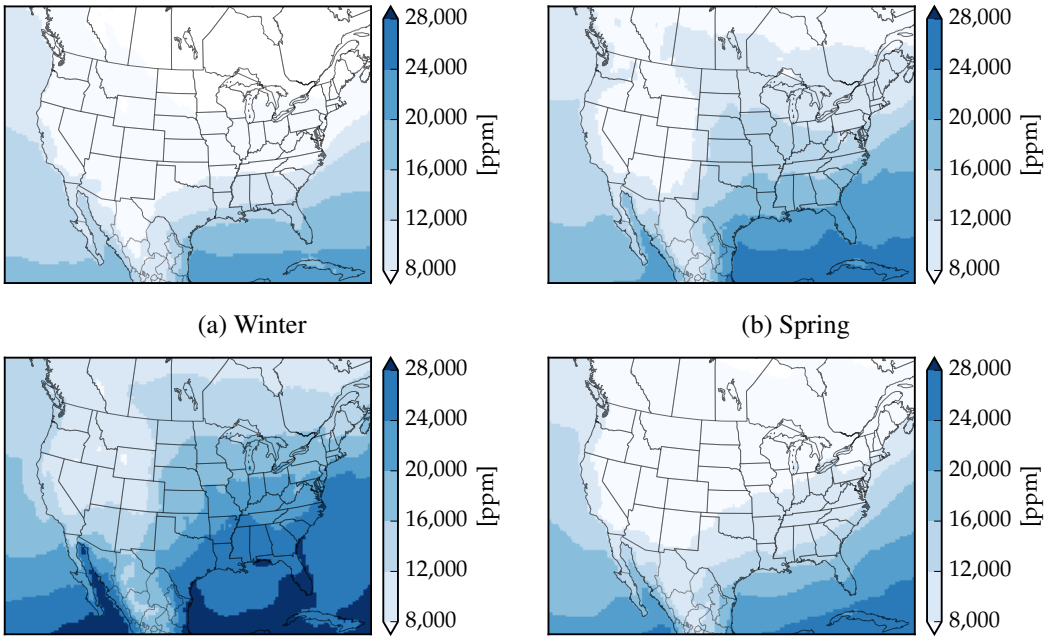

(a) Winter (b) Spring

(c) Summer (d) Fall

Figure C-14: Humidity of the United States in 2005. Daily mean values are presented.

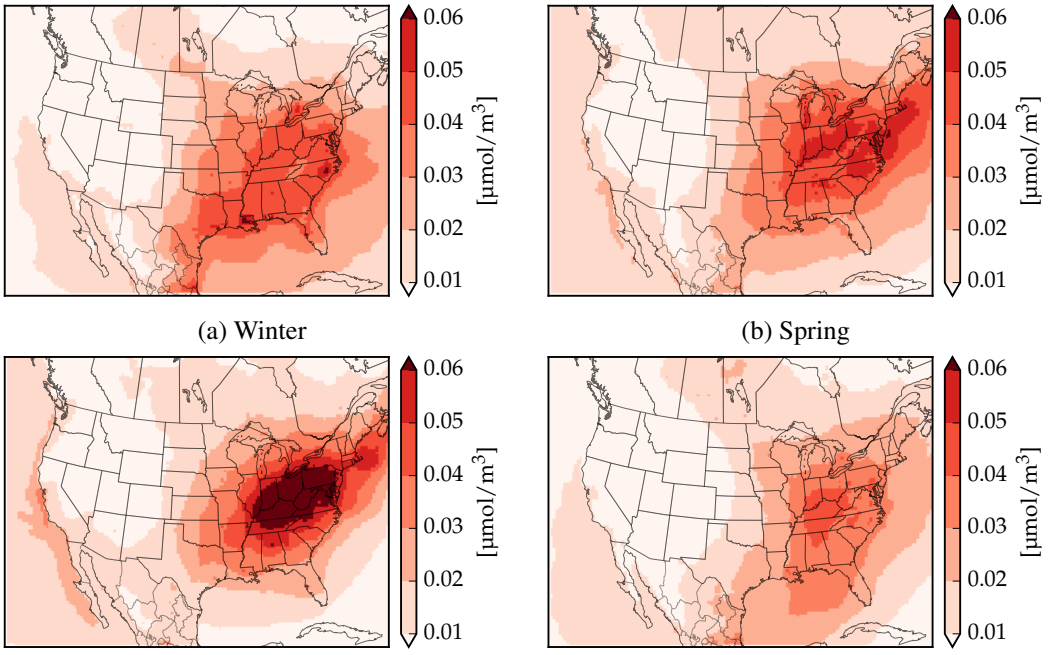

(a) Winter (b) Spring

(c) Summer (d) Fall

Figure C-15: Total sulfate of the United States in 2005. Daily mean values are presented.

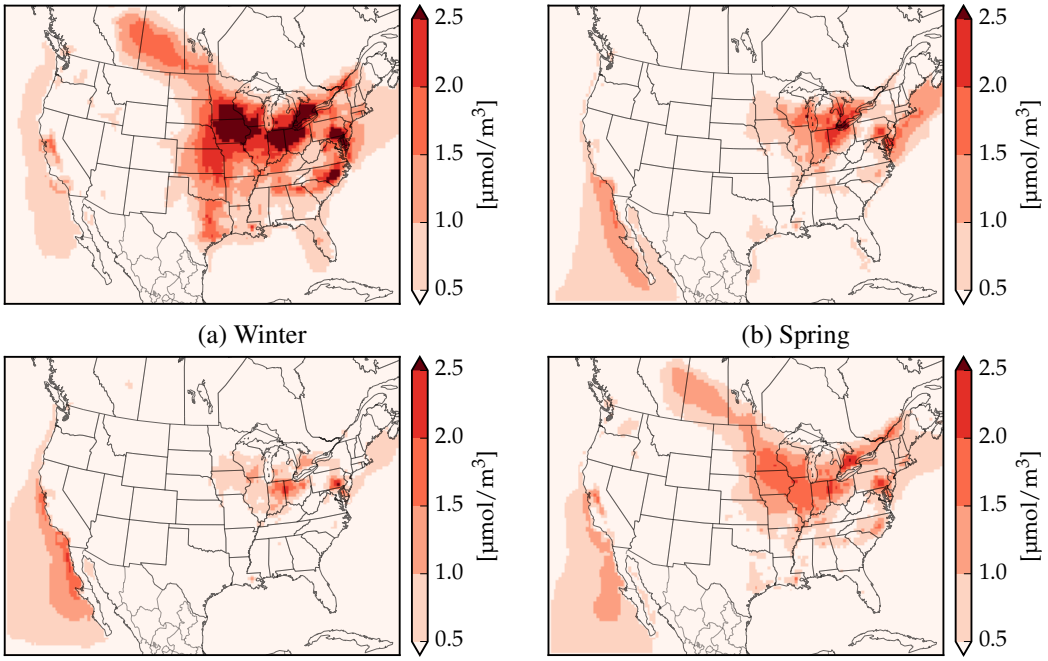

(a) Winter (b) Spring

(c) Summer (d) Fall

Figure C-16: Total nitrate of the United States in 2005. Daily mean values are presented.

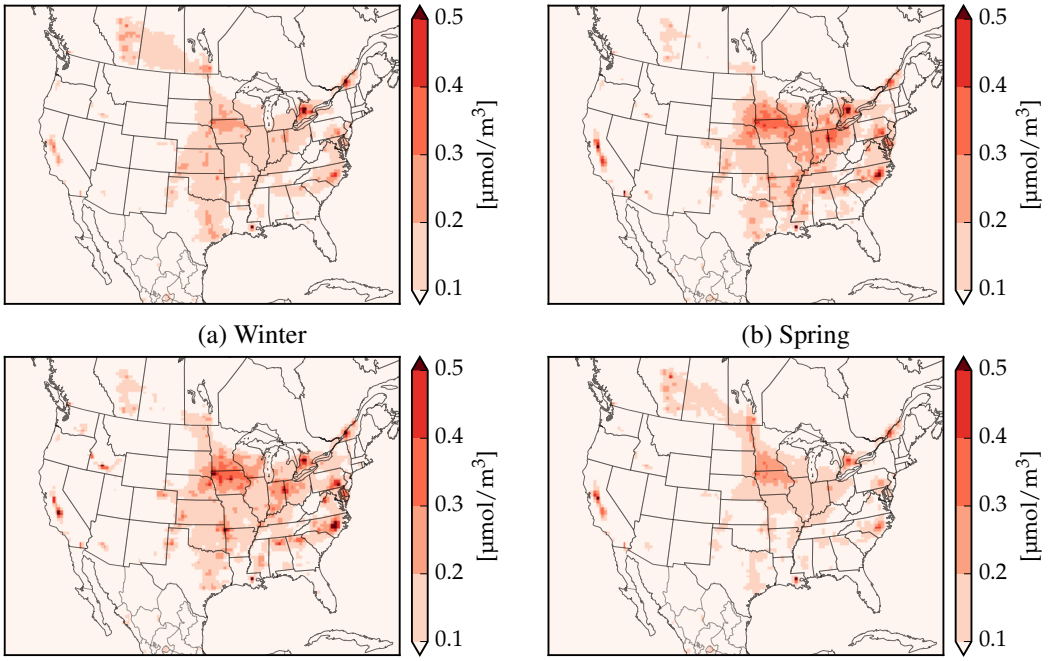

(a) Winter (b) Spring

(c) Summer (d) Fall

Figure C-17: Total ammonia of the United States in 2005. Daily mean values are presented.

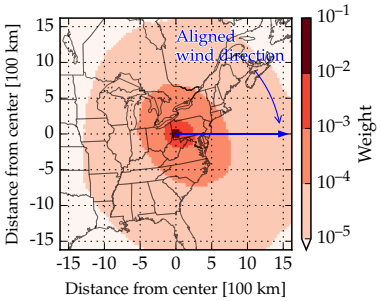

(a) Winter: average plume weight

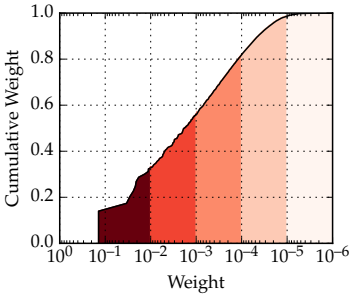

(b) Winter: cumulative distribution

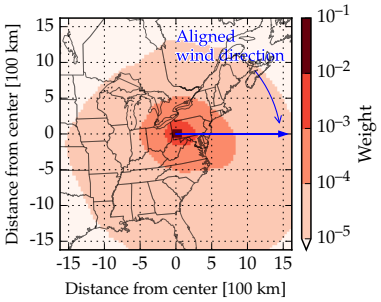

(c) Spring: average plume weight

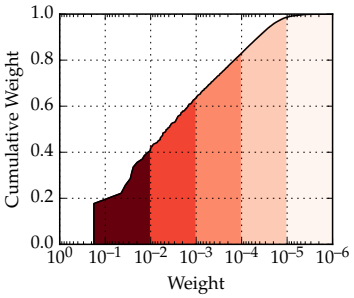

(d) Spring: cumulative distribution

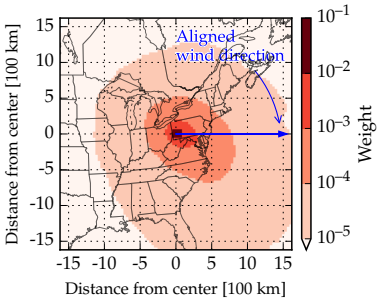

(e) Summer: average plume weight

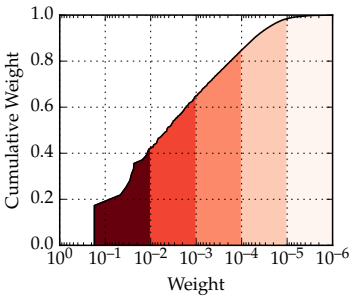

(f) Summer: cumulative distribution

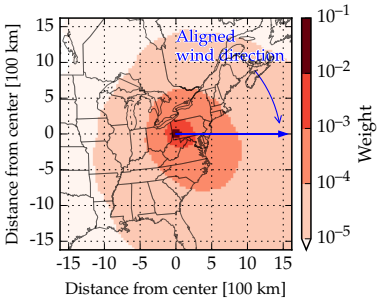

(g) Fall: average plume weight

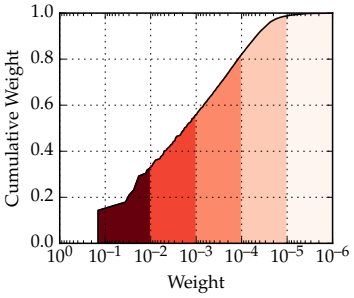

(h) Fall: cumulative distribution

Figure C-18: EC average plume weights constructed with the CTM results of the 50 training samples. $PM_{2.5}$ concentrations or plumes of the training samples were aligned by wind direction to the same direction (the arrow in the figure) and normalized so that they sum to one. To give a sense of scale, the center of a plume is put on Pittsburgh.

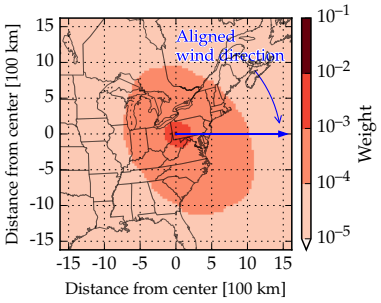

(a) Winter: average plume weight

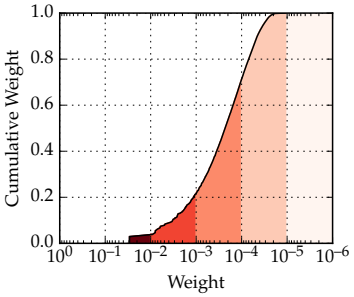

(b) Winter: cumulative distribution

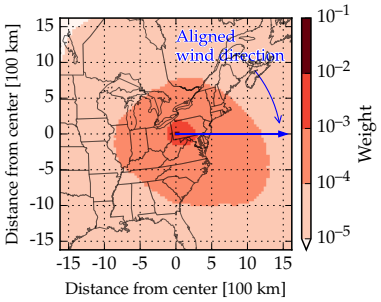

(c) Spring: average plume weight

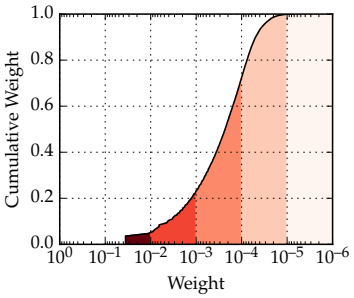

(d) Spring: cumulative distribution

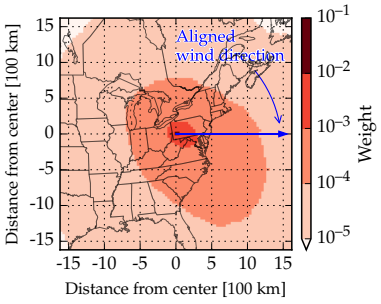

(e) Summer: average plume weight

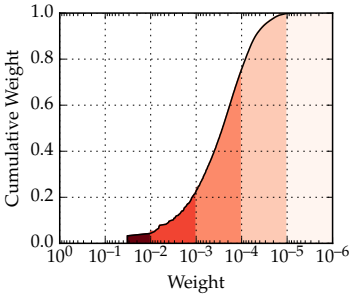

(f) Summer: cumulative distribution

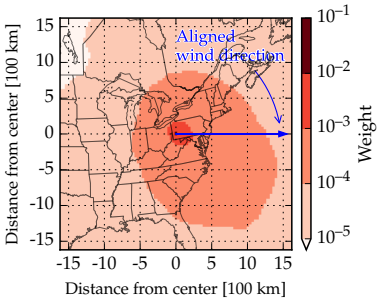

(g) Fall: average plume weight

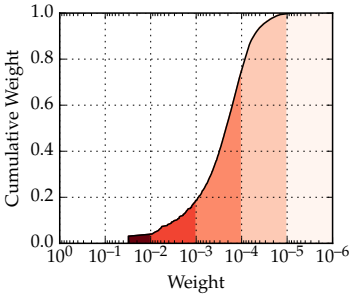

(h) Fall: cumulative distribution

Figure C-19: SO_2 average plume weights constructed with the CTM results of the 50 training samples. $PM_{2.5}$ concentrations or plumes of the training samples were aligned by wind direction to the same direction (the arrow in the figure) and normalized so that they sum to one. To give a sense of scale, the center of a plume is put on Pittsburgh.

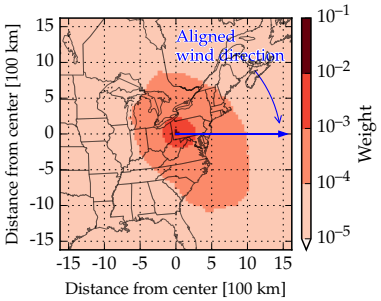

(a) Winter: average plume weight

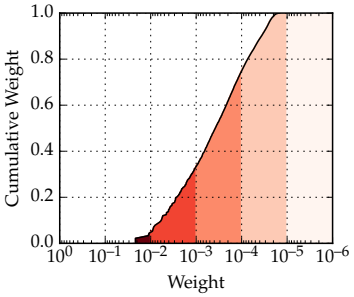

(b) Winter: cumulative distribution

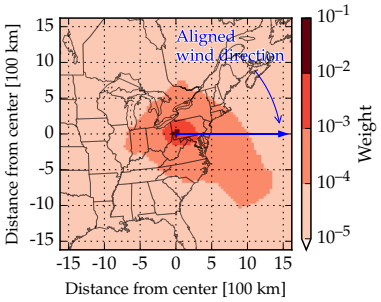

(c) Spring: average plume weight

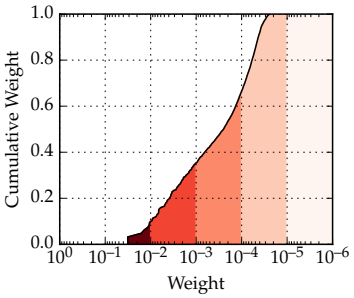

(d) Spring: cumulative distribution

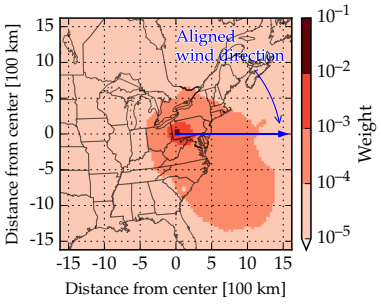

(e) Summer: average plume weight

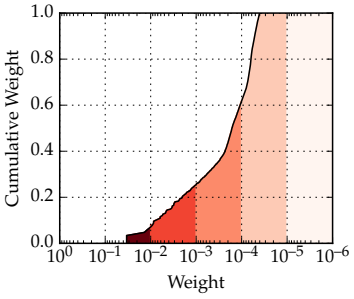

(f) Summer: cumulative distribution

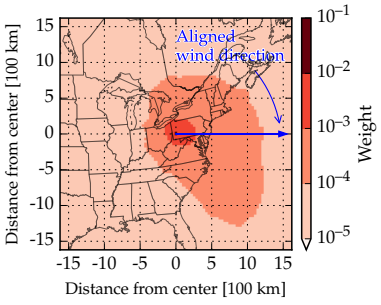

(g) Fall: average plume weight

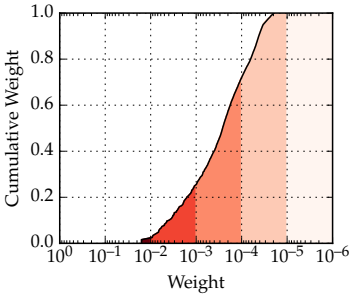

(h) Fall: cumulative distribution

Figure C-20: NO_x average plume weights constructed with the CTM results of the 50 training samples. $PM_{2.5}$ concentrations or plumes of the training samples were aligned by wind direction to the same direction (the arrow in the figure) and normalized so that they sum to one. To give a sense of scale, the center of a plume is put on Pittsburgh.

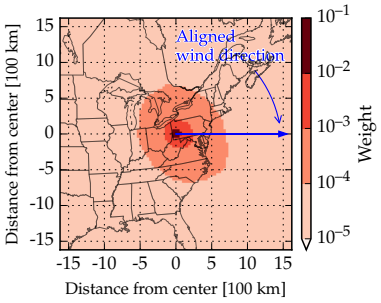

(a) Winter: average plume weight

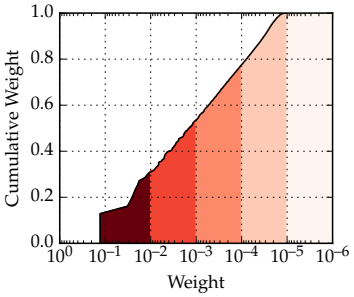

(b) Winter: cumulative distribution

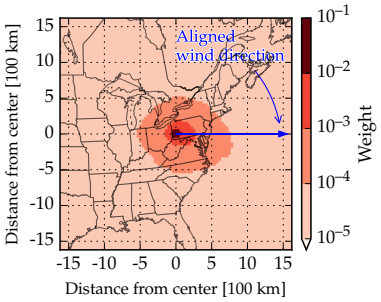

(c) Spring: average plume weight

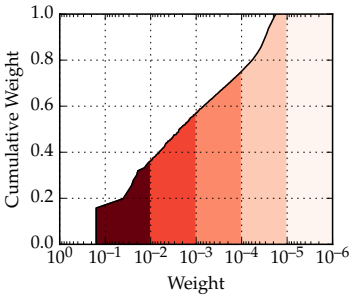

(d) Spring: cumulative distribution

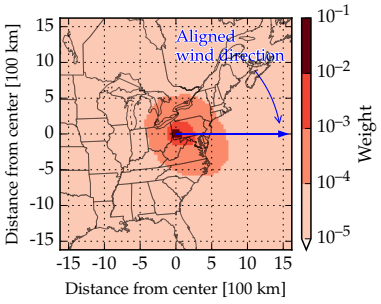

(e) Summer: average plume weight

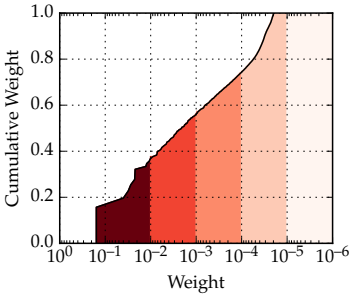

(f) Summer: cumulative distribution

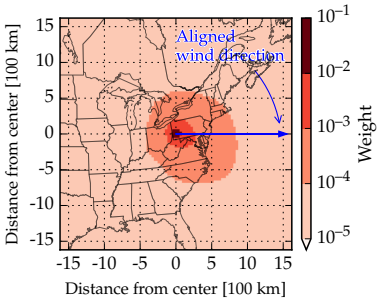

(g) Fall: average plume weight

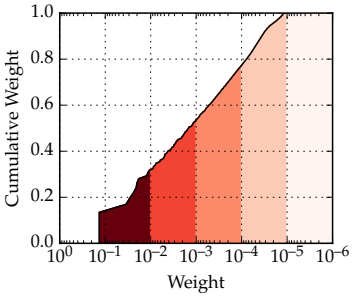

(h) Fall: cumulative distribution

Figure C-21: NH_3 average plume weights constructed with the CTM results of the 50 training samples. $PM_{2.5}$ concentrations or plumes of the training samples were aligned by wind direction to the same direction (the arrow in the figure) and normalized so that they sum to one. To give a sense of scale, the center of a plume is put on Pittsburgh.

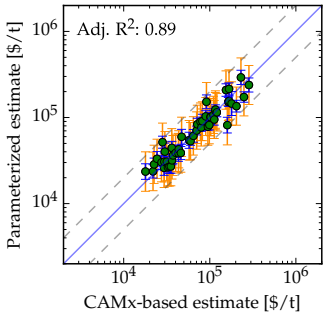

(a) Winter: Fitted values

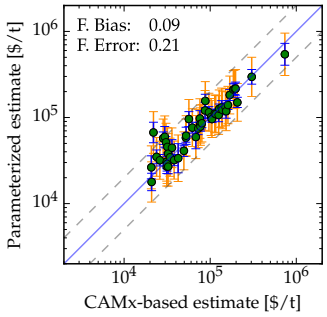

(b) Winter: Out-of-sample test

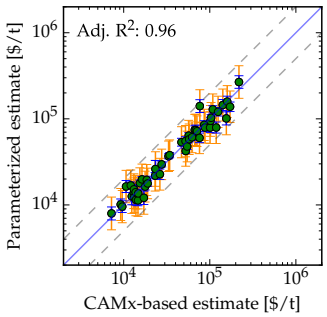

(c) Spring: Fitted values

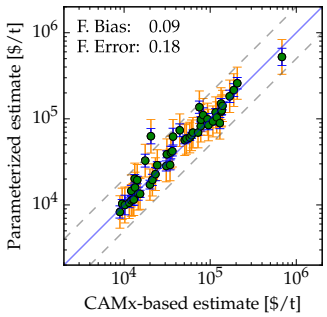

(d) Spring: Out-of-sample test

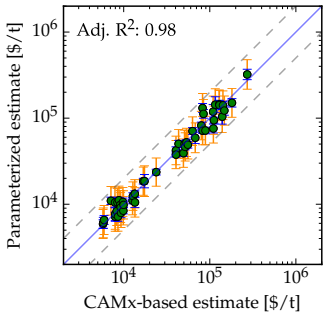

(e) Summer: Fitted values

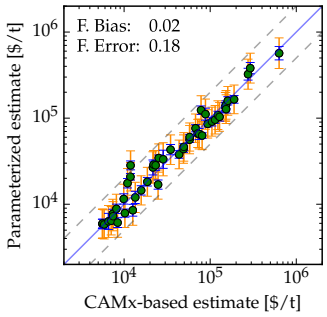

(f) Summer: Out-of-sample test

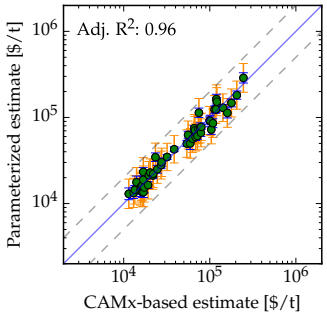

(g) Fall: Fitted values

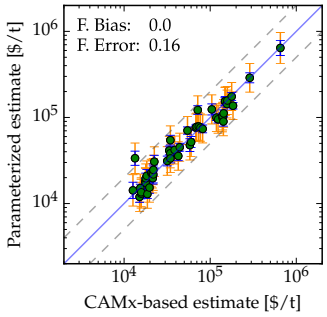

(h) Fall: Out-of-sample test

Figure C-22: Performance of EC social cost model. Dashed lines indicate a factor of two and solid line indicates unbiased prediction. Orange bars show 95% prediction intervals and blue bars show 95% confidence intervals. The right-hand side figures are also presented in Figure 4.4.

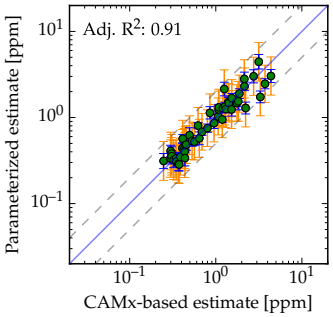

(a) Winter: Fitted values

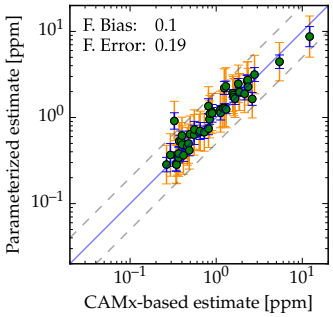

(b) Winter: Out-of-sample test

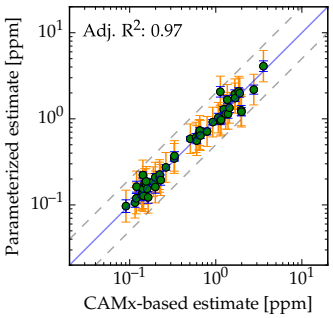

(c) Spring: Fitted values

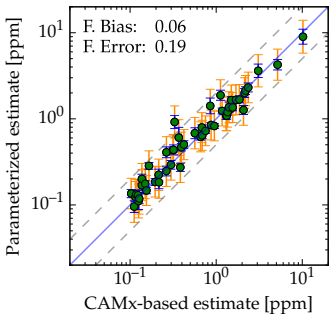

(d) Spring: Out-of-sample test

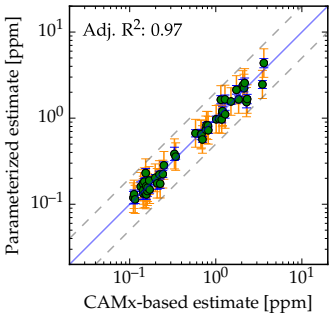

(e) Summer: Fitted values

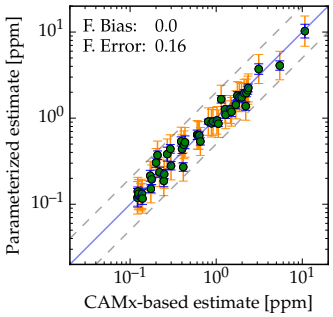

(f) Summer: Out-of-sample test

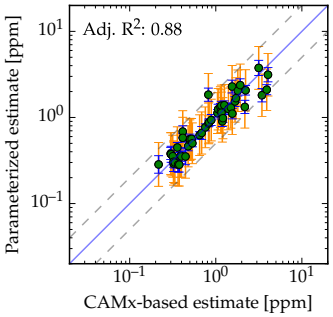

(g) Fall: Fitted values

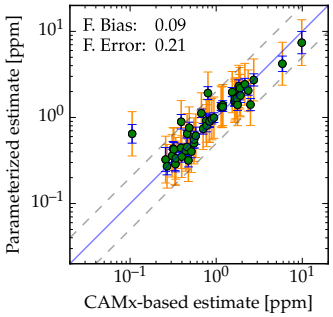

(h) Fall: Out-of-sample test

Figure C-23: Performance of EC intake fraction model. Dashed lines indicate a factor of two and solid line indicates unbiased prediction. Orange bars show 95% prediction intervals and blue bars show 95% confidence intervals.

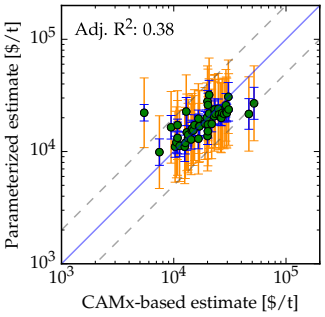

(a) Winter: Fitted values

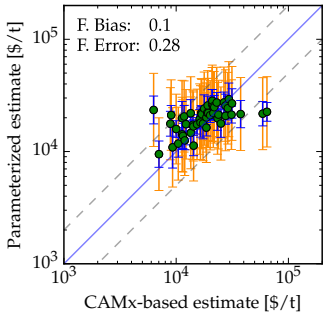

(b) Winter: Out-of-sample test

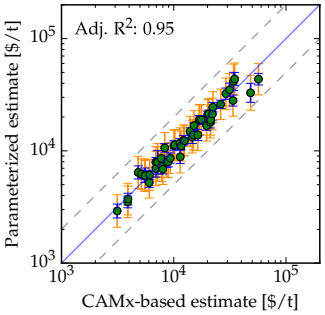

(c) Spring: Fitted values

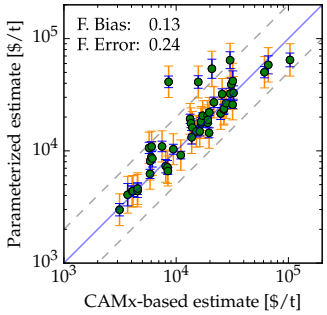

(d) Spring: Out-of-sample test

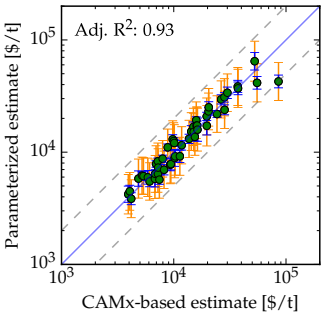

(e) Summer: Fitted values

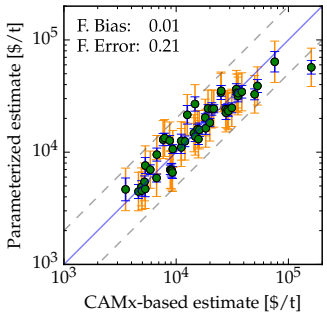

(f) Summer: Out-of-sample test

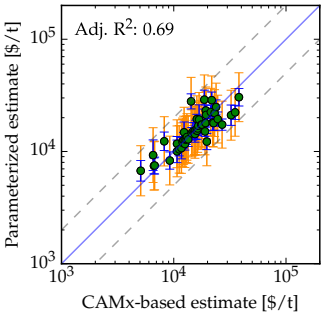

(g) Fall: Fitted values

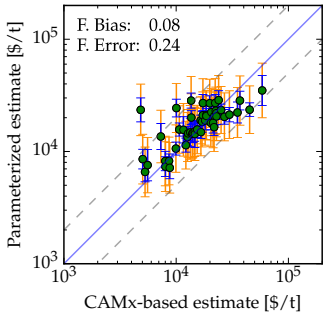

(h) Fall: Out-of-sample test

Figure C-24: Performance of SO_2 social cost 'simple' model. Dashed lines indicate a factor of two and solid line indicates unbiased prediction. Orange bars show 95% prediction intervals and blue bars show 95% confidence intervals.

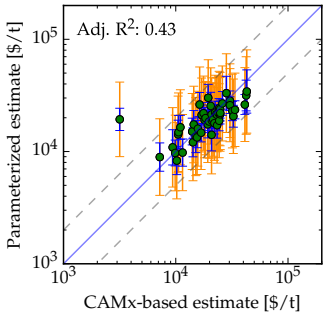

(a) Winter: Fitted values

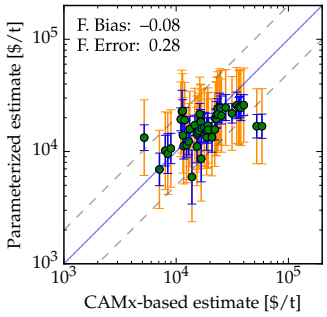

(b) Winter: Out-of-sample test

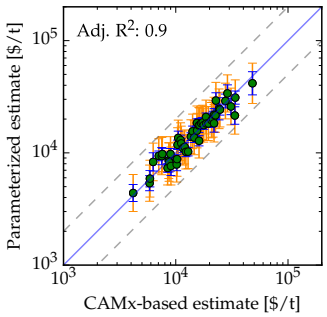

(c) Spring: Fitted values

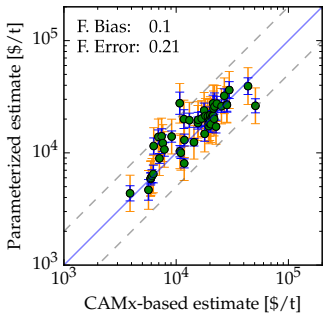

(d) Spring: Out-of-sample test

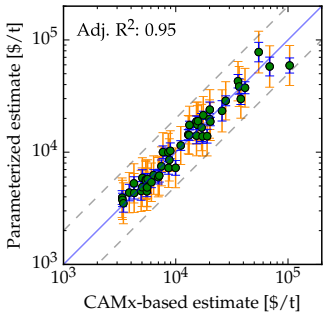

(e) Summer: Fitted values

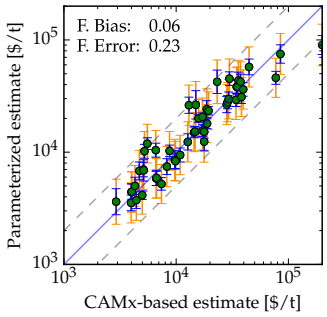

(f) Summer: Out-of-sample test

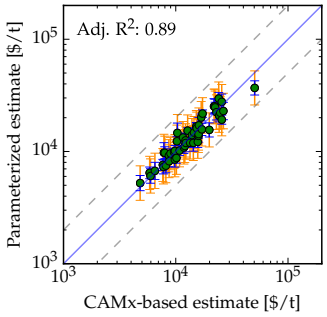

(g) Fall: Fitted values

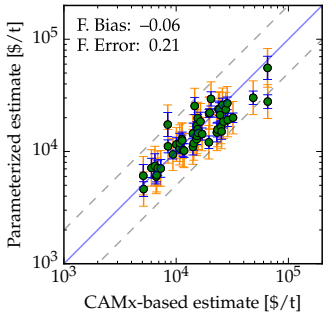

(h) Fall: Out-of-sample test

Figure C-25: Performance of SO_2 social cost 'better-fit' model. Dashed lines indicate a factor of two and solid line indicates unbiased prediction. Orange bars show 95% prediction intervals and blue bars show 95% confidence intervals.

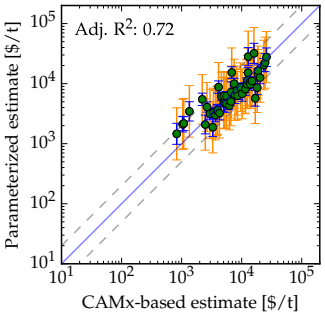

(a) Winter: Fitted values

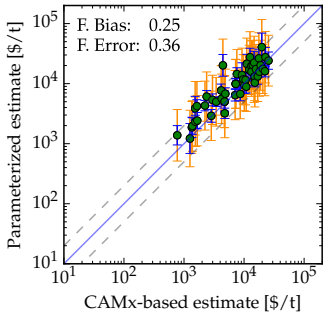

(b) Winter: Out-of-sample test

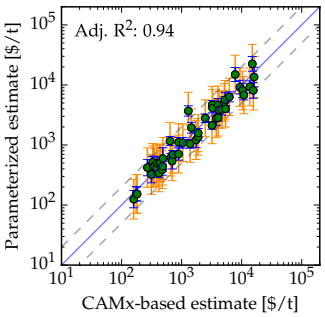

(c) Spring: Fitted values

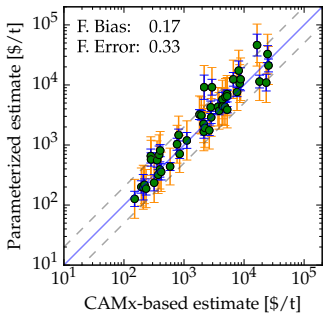

(d) Spring: Out-of-sample test

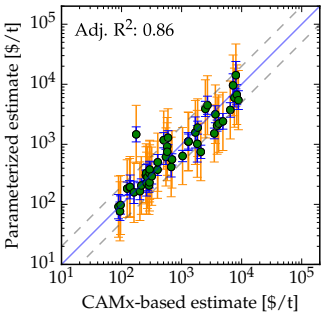

(e) Summer: Fitted values

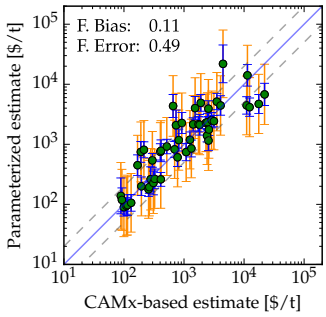

(f) Summer: Out-of-sample test

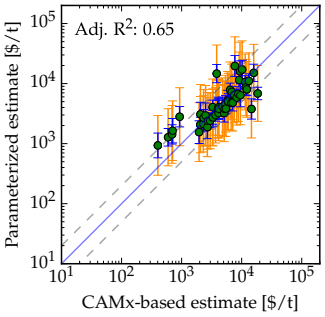

(g) Fall: Fitted values

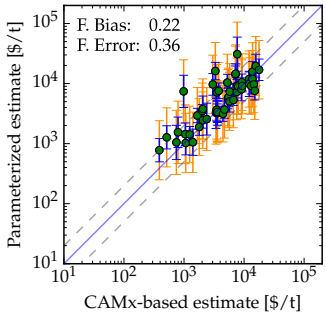

(h) Fall: Out-of-sample test

Figure C-26: Performance of NO_x social cost 'simple' model. Dashed lines indicate a factor of two and solid line indicates unbiased prediction. Orange bars show 95% prediction intervals and blue bars show 95% confidence intervals.

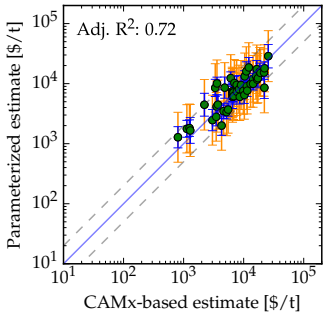

(a) Winter: Fitted values

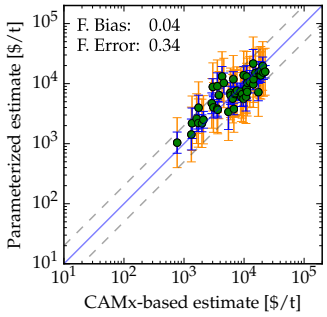

(b) Winter: Out-of-sample test

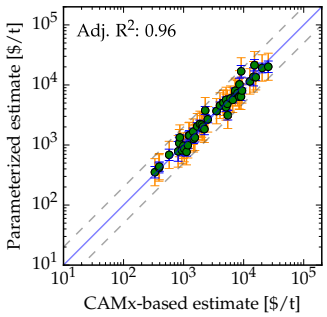

(c) Spring: Fitted values

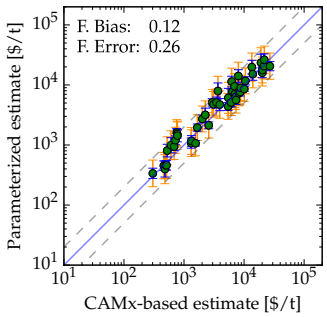

(d) Spring: Out-of-sample test

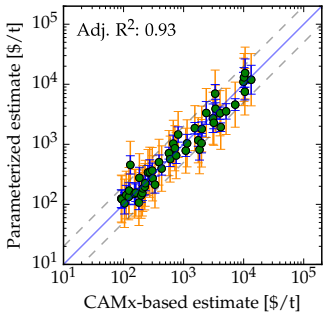

(e) Summer: Fitted values

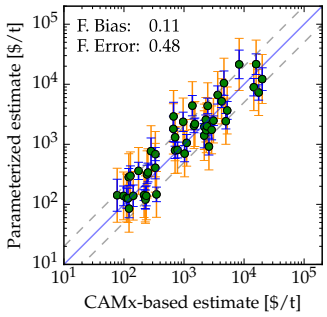

(f) Summer: Out-of-sample test

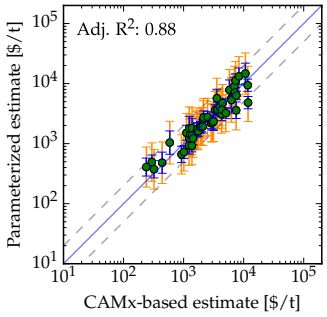

(g) Fall: Fitted values

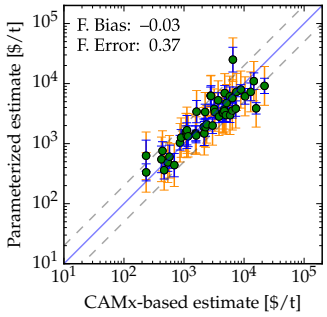

(h) Fall: Out-of-sample test

Figure C-27: Performance of NO_x social cost 'better-fit' model. Dashed lines indicate a factor of two and solid line indicates unbiased prediction. Orange bars show 95% prediction intervals and blue bars show 95% confidence intervals.

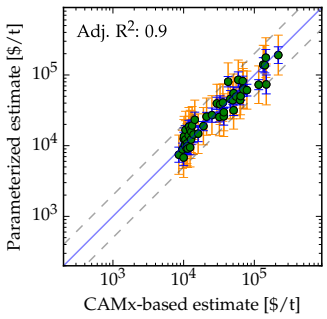

(a) Winter: Fitted values

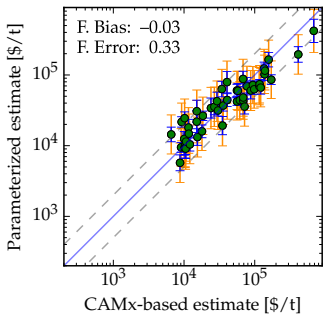

(b) Winter: Out-of-sample test

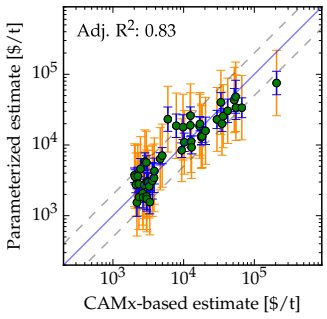

(c) Spring: Fitted values

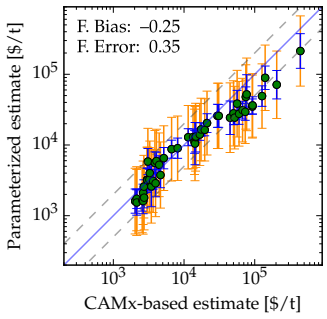

(d) Spring: Out-of-sample test

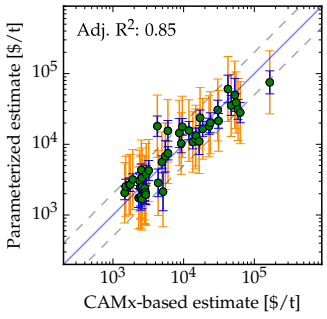

(e) Summer: Fitted values

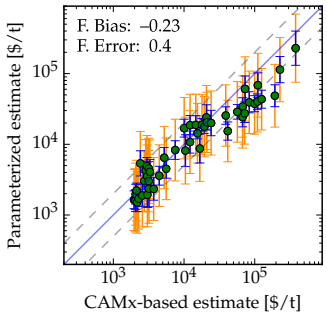

(f) Summer: Out-of-sample test

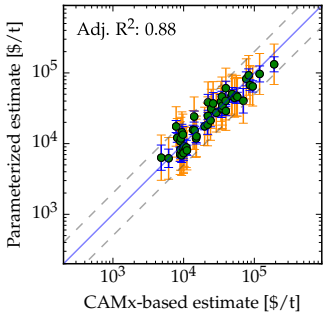

(g) Fall: Fitted values

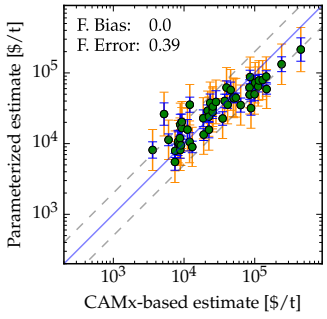

(h) Fall: Out-of-sample test

Figure C-28: Performance of NH_3 social cost 'simple' model. Dashed lines indicate a factor of two and solid line indicates unbiased prediction. Orange bars show 95% prediction intervals and blue bars show 95% confidence intervals.

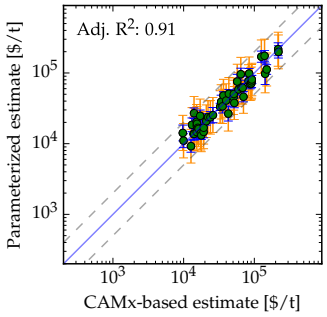

(a) Winter: Fitted values

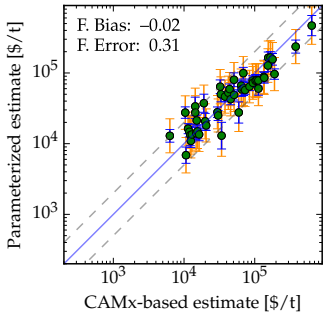

(b) Winter: Out-of-sample test

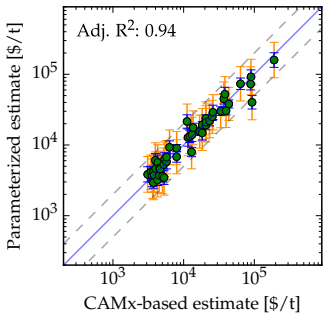

(c) Spring: Fitted values

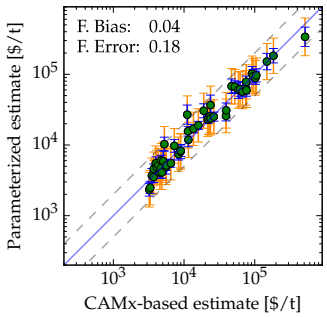

(d) Spring: Out-of-sample test

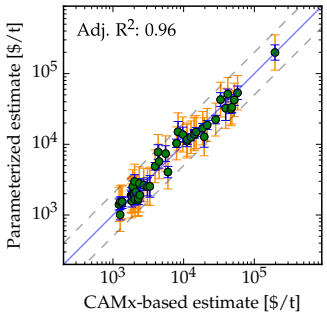

(e) Summer: Fitted values

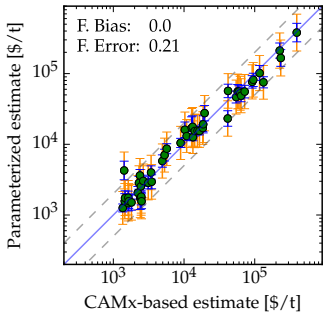

(f) Summer: Out-of-sample test

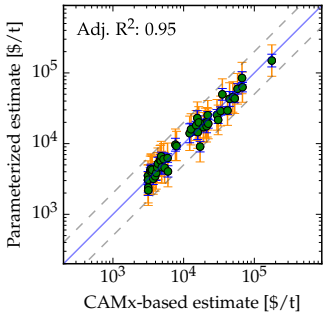

(g) Fall: Fitted values

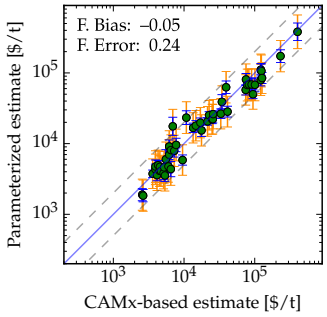

(h) Fall: Out-of-sample test

Figure C-29: Performance of NH_3 social cost 'better-fit' model. Dashed lines indicate a factor of two and solid line indicates unbiased prediction. Orange bars show 95% prediction intervals and blue bars show 95% confidence intervals.

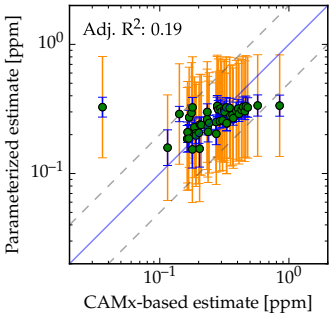

(a) Winter: Fitted values

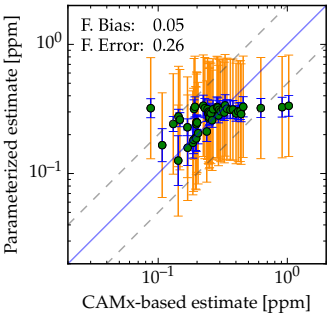

(b) Winter: Out-of-sample test

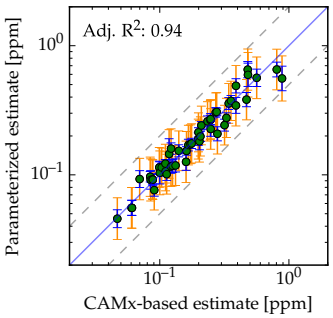

(c) Spring: Fitted values

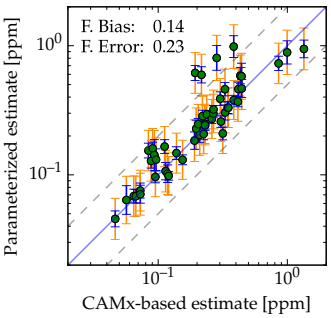

(d) Spring: Out-of-sample test

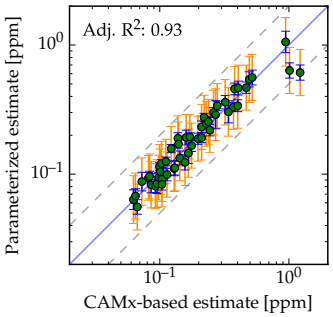

(e) Summer: Fitted values

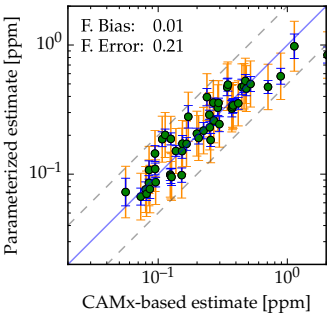

(f) Summer: Out-of-sample test

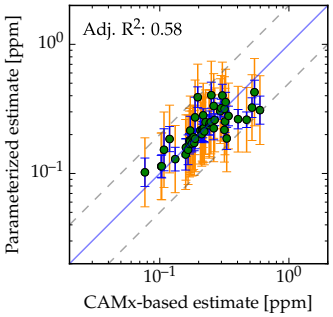

(g) Fall: Fitted values

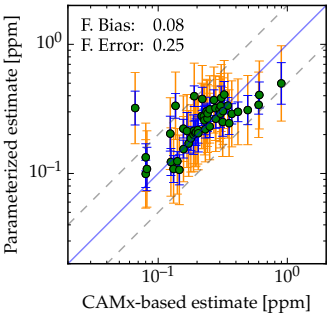

(h) Fall: Out-of-sample test

Figure C-30: Performance of SO_2 intake fraction 'simple' model. Dashed lines indicate a factor of two and solid line indicates unbiased prediction. Orange bars show 95% prediction intervals and blue bars show 95% confidence intervals.

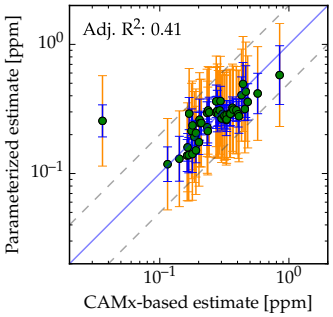

(a) Winter: Fitted values

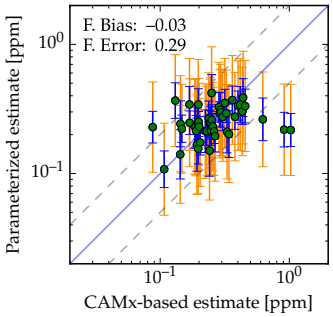

(b) Winter: Out-of-sample test

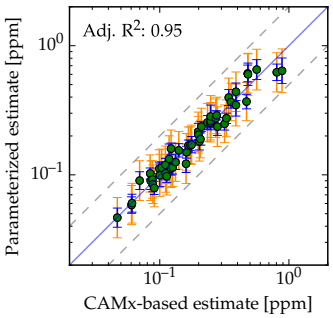

(c) Spring: Fitted values

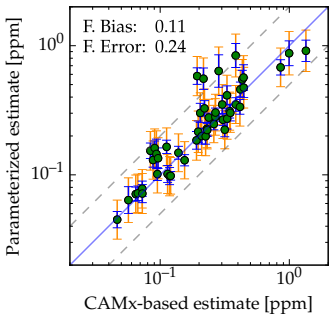

(d) Spring: Out-of-sample test

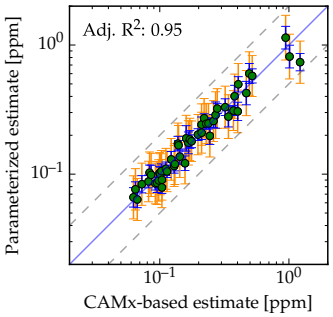

(e) Summer: Fitted values

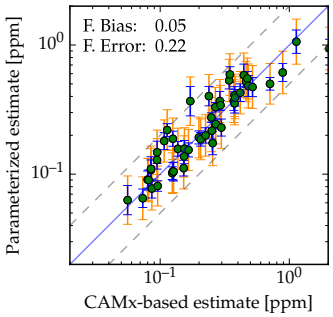

(f) Summer: Out-of-sample test

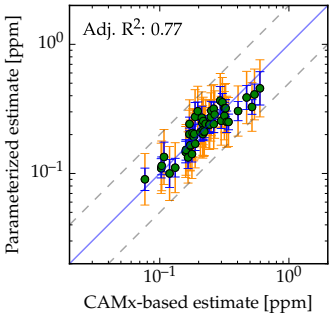

(g) Fall: Fitted values

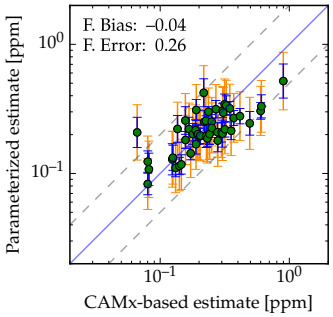

(h) Fall: Out-of-sample test

Figure C-31: Performance of SO_2 intake fraction 'better-fit' model. Dashed lines indicate a factor of two and solid line indicates unbiased prediction. Orange bars show 95% prediction intervals and blue bars show 95% confidence intervals.

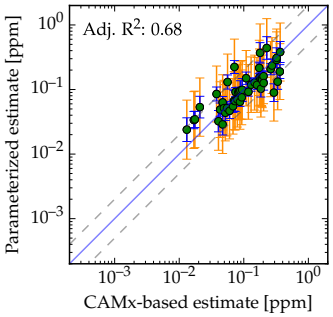

(a) Winter: Fitted values

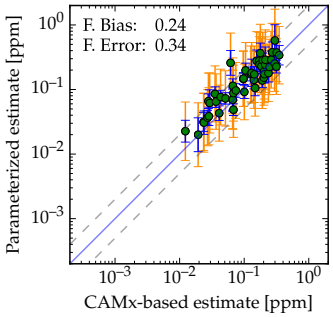

(b) Winter: Out-of-sample test

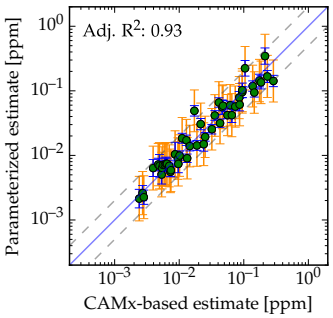

(c) Spring: Fitted values

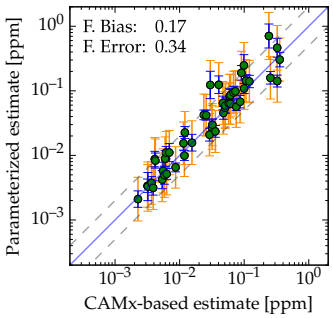

(d) Spring: Out-of-sample test

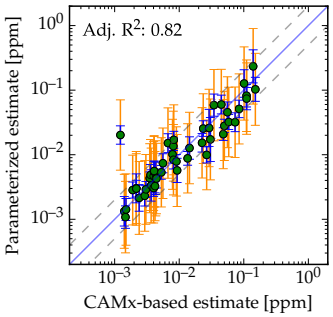

(e) Summer: Fitted values

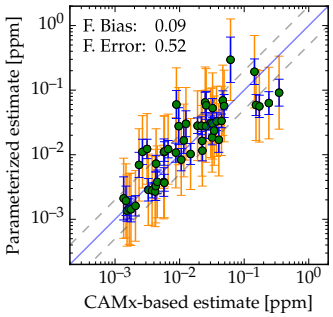

(f) Summer: Out-of-sample test

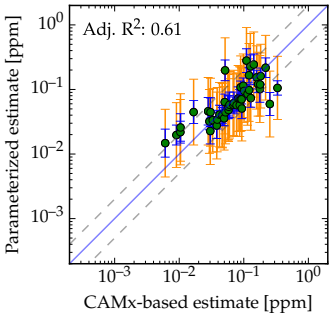

(g) Fall: Fitted values

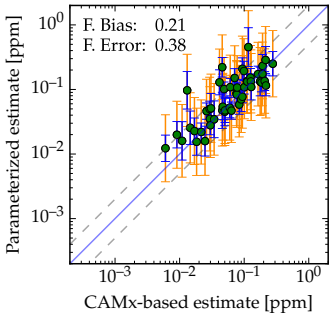

(h) Fall: Out-of-sample test

Figure C-32: Performance of NO_x intake fraction 'simple' model. Dashed lines indicate a factor of two and solid line indicates unbiased prediction. Orange bars show 95% prediction intervals and blue bars show 95% confidence intervals.

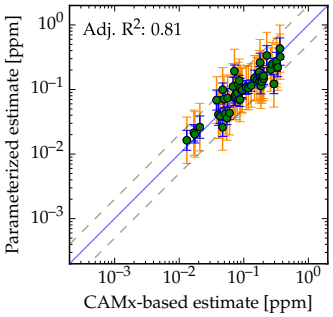

(a) Winter: Fitted values

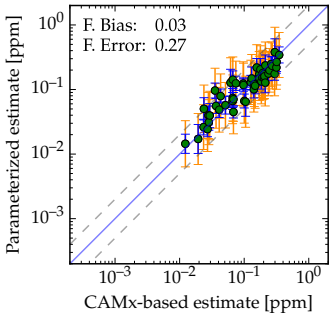

(b) Winter: Out-of-sample test

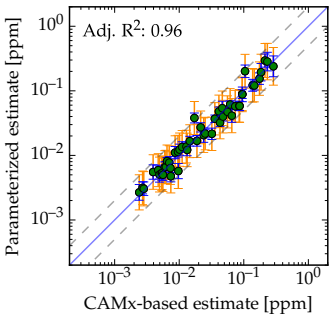

(c) Spring: Fitted values

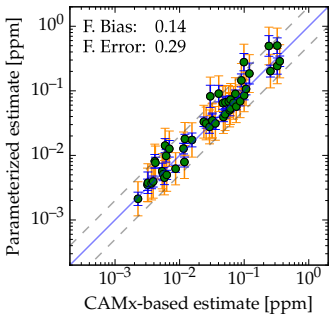

(d) Spring: Out-of-sample test

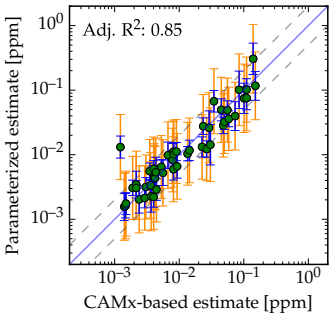

(e) Summer: Fitted values

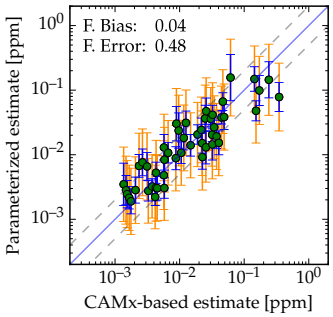

(f) Summer: Out-of-sample test

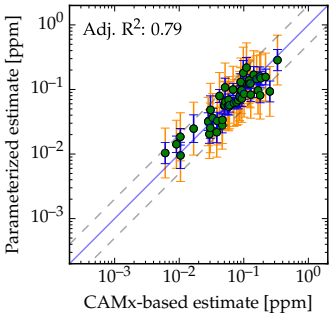

(g) Fall: Fitted values

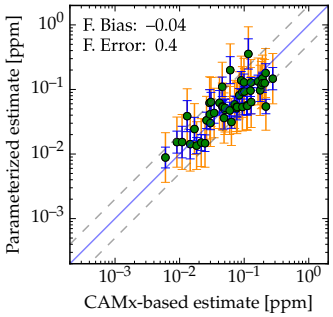

(h) Fall: Out-of-sample test

Figure C-33: Performance of NO_x intake fraction 'better-fit' model. Dashed lines indicate a factor of two and solid line indicates unbiased prediction. Orange bars show 95% prediction intervals and blue bars show 95% confidence intervals.

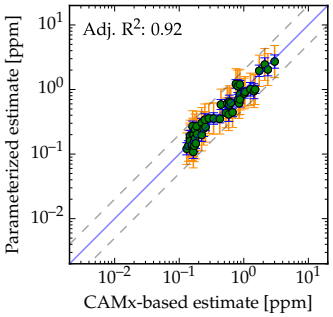

(a) Winter: Fitted values

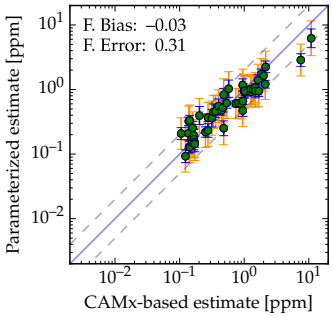

(b) Winter: Out-of-sample test

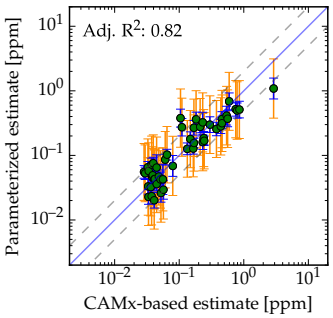

(c) Spring: Fitted values

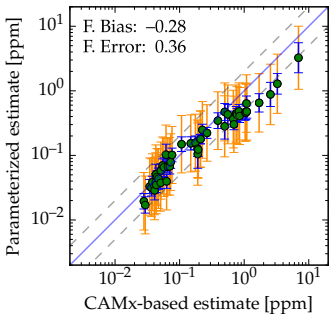

(d) Spring: Out-of-sample test

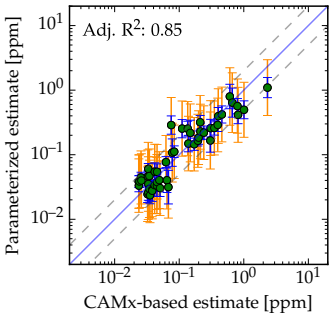

(e) Summer: Fitted values

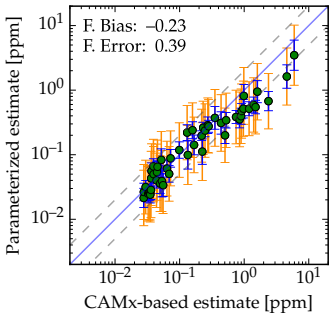

(f) Summer: Out-of-sample test

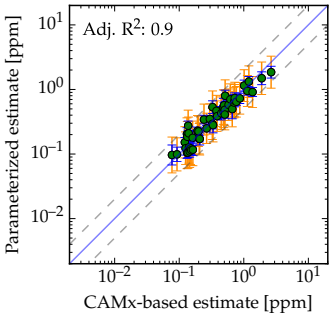

(g) Fall: Fitted values

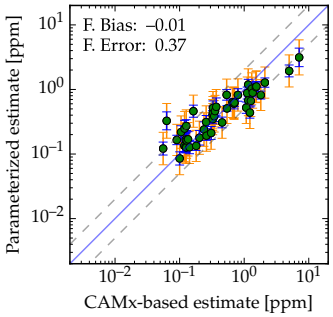

(h) Fall: Out-of-sample test

Figure C-34: Performance of NH_3 intake fraction 'simple' model. Dashed lines indicate a factor of two and solid line indicates unbiased prediction. Orange bars show 95% prediction intervals and blue bars show 95% confidence intervals.

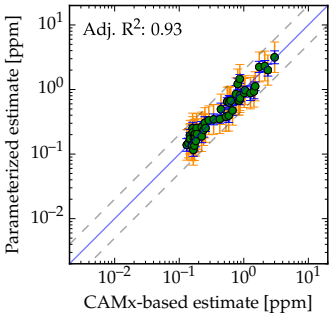

(a) Winter: Fitted values

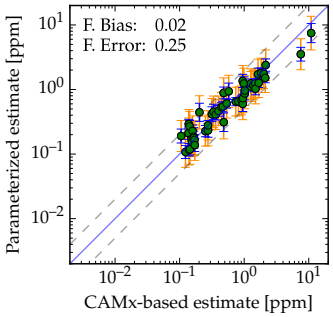

(b) Winter: Out-of-sample test

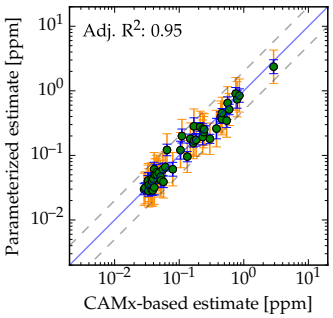

(c) Spring: Fitted values

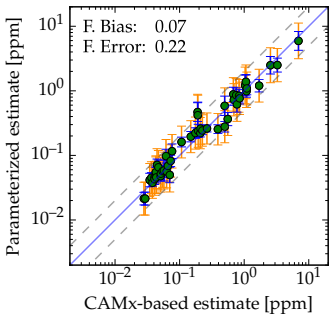

(d) Spring: Out-of-sample test

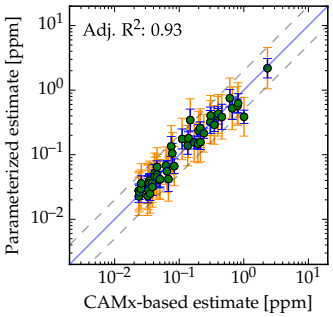

(e) Summer: Fitted values

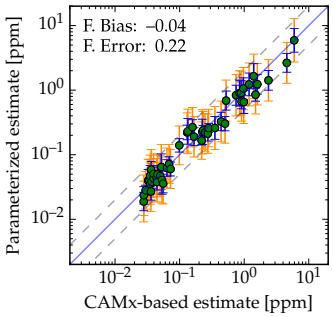

(f) Summer: Out-of-sample test

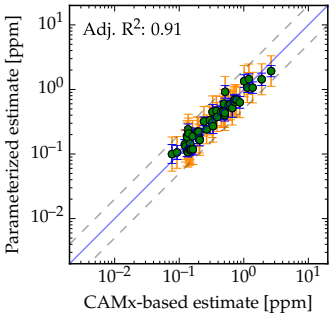

(g) Fall: Fitted values

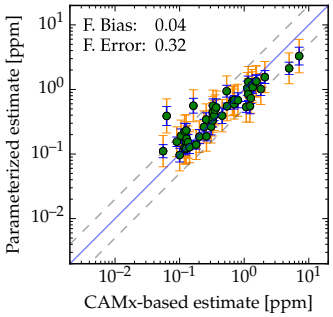

(h) Fall: Out-of-sample test

Figure C-35: Performance of NH_3 intake fraction 'better-fit' model. Dashed lines indicate a factor of two and solid line indicates unbiased prediction. Orange bars show 95% prediction intervals and blue bars show 95% confidence intervals.

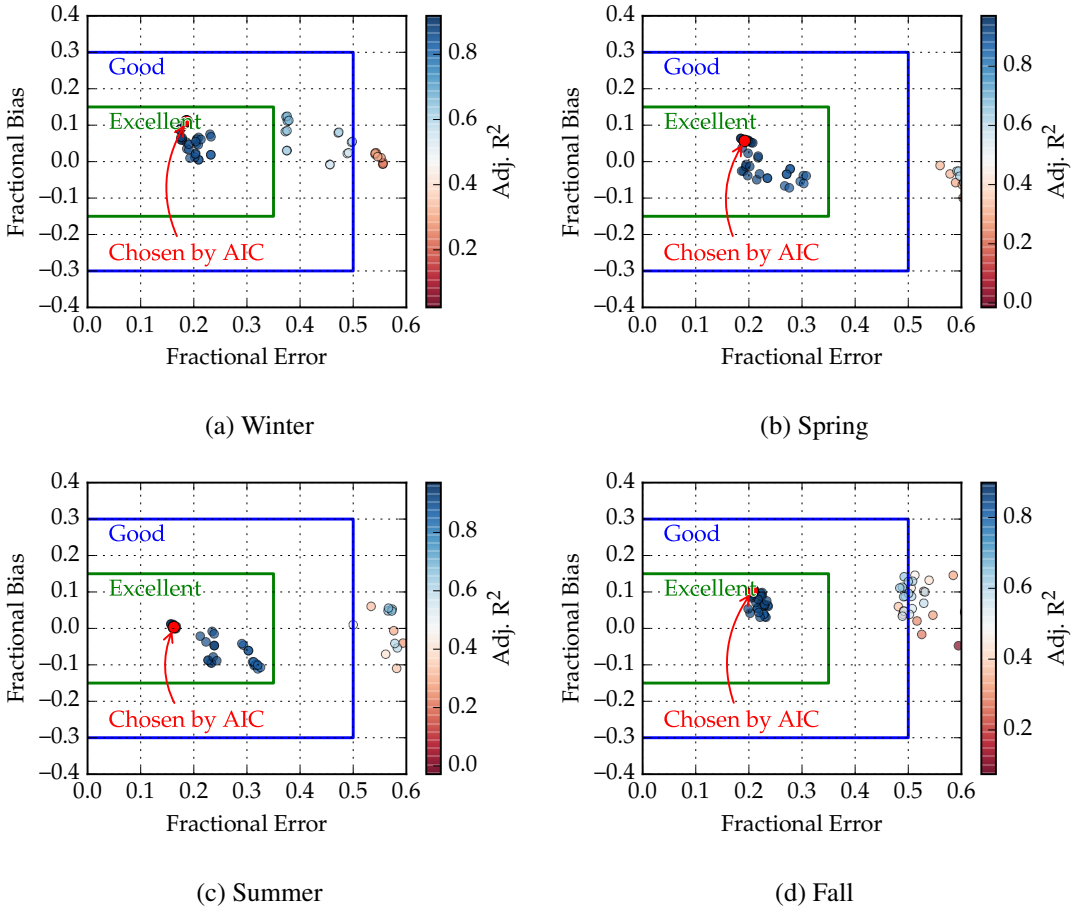

(a) Winter

(b) Spring

(c) Summer

(d) Fall

Figure C-36: Evaluations of EC social cost models. Each circle indicates a regression model. 'Excellent' and 'Good' model performance criteria are shown as suggested by Morris et al. (2005).

Table C-9: Evaluations of winter EC social cost models.

Model[†]	(1)[‡]	(2)	(3)	(4)	(5)	(6)	(7)
Intercept	$86^{\star\star}$	$91^{\star\star\star}$	$85^{\star\star}$	$90^{\star\star}$	$33^{\star\star\star}$	$32^{\star\star}$	$32^{\star\star}$
ln (Pop_w)	$0.61^{\star\star\star}$	$0.65^{\star\star\star}$	$0.61^{\star\star\star}$	$0.65^{\star\star\star}$	$0.63^{\star\star\star}$	$0.65^{\star\star\star}$	$0.63^{\star\star\star}$
ln (Pres)	$3.7^{\star\star\star}$	$3.5^{\star\star\star}$	$3.7^{\star\star\star}$	$3.6^{\star\star\star}$	$3.4^{\star\star\star}$	$3.3^{\star\star\star}$	$3.5^{\star\star\star}$
ln (Temp)	$-20^{\star\star\star}$	$-21^{\star\star\star}$	$-20^{\star\star\star}$	$-21^{\star\star\star}$	$-9.2^{\star\star\star}$	$-8.9^{\star\star\star}$	$-9.0^{\star\star\star}$
ln (Wind)	-	-	0.016	0.017	-	-	0.020
ln (Prec)	-	−0.10	-	−0.10	-	−0.062	-
ln (Humid)	$0.70^{\star}$	$0.79^{\star}$	$0.69^{\star}$	$0.78^{\star}$	-	-	-
AIC	−0.034	0.0046	1.8	1.9	3.5	4.8	5.3
Adj. R^2	0.92	0.92	0.92	0.92	0.91	0.91	0.91
F. Bias	0.11	0.10	0.11	0.10	0.095	0.088	0.094
F. Error	0.19	0.18	0.19	0.18	0.18	0.17	0.18

[†] Seven models with lowest AIC ordered by AIC, [‡] Chosen by AIC, *** $p < 0.001$, ** $p < 0.001$, * $p < 0.05$, $^{+}$ $p < 0.1$, Pop_w [# of people]: population (≥ age 30) weighted with average plume, Pres: pressure [hPa], Temp: temperature [K], Prec: precipitation + 0.0002 [$\mathrm{g/m^3}$] (shifted for log transformation), Wind: wind speed [$\mathrm{m/s}$], Humid: humidity [ppm], AIC: Akaike information criterion, Adj. R^2: adjusted R^2, F. Bias: fractional bias, F. Error: fractional error.

Table C-10: Evaluations of spring EC social cost models.

Model[†]	(1)[‡]	(2)	(3)	(4)	(5)	(6)	(7)
Intercept	$72^{\star\star\star}$	$70^{\star\star\star}$	$70^{\star\star\star}$	$72^{\star\star\star}$	$49^{\star\star\star}$	$46^{\star\star\star}$	$47^{\star\star\star}$
ln (Pop_w)	$0.72^{\star\star\star}$	$0.72^{\star\star\star}$	$0.72^{\star\star\star}$	$0.72^{\star\star\star}$	$0.72^{\star\star\star}$	$0.71^{\star\star\star}$	$0.71^{\star\star\star}$
ln (Pres)	$5.4^{\star\star\star}$	$5.3^{\star\star\star}$	$5.4^{\star\star\star}$	$5.2^{\star\star\star}$	$6.2^{\star\star\star}$	$6.2^{\star\star\star}$	$6.1^{\star\star\star}$
ln (Temp)	$-19^{\star\star\star}$	$-19^{\star\star\star}$	$-19^{\star\star\star}$	$-19^{\star\star\star}$	$-16^{\star\star\star}$	$-15^{\star\star\star}$	$-15^{\star\star\star}$
ln (Wind)	-	−0.037	-	−0.041	-	-	−0.040
ln (Prec)	-	-	0.0061	−0.0085	-	0.036	-
ln (Humid)	$0.37^{\star}$	$0.37^{\star}$	$0.36^{\star}$	$0.39^{\star}$	-	-	-
AIC	−21	−20	−19	−19	−17	−17	−16
Adj. R^2	0.97	0.97	0.97	0.97	0.97	0.97	0.97
F. Bias	0.057	0.063	0.057	0.064	0.051	0.052	0.058
F. Error	0.19	0.19	0.19	0.18	0.21	0.20	0.20

[†] Seven models with lowest AIC ordered by AIC, [‡] Chosen by AIC, *** $p < 0.001$, ** $p < 0.001$, * $p < 0.05$, $^{+}$ $p < 0.1$, Pop_w [# of people]: population (≥ age 30) weighted with average plume, Pres: pressure [hPa], Temp: temperature [K], Prec: precipitation + 0.0002 [$\mathrm{g/m^3}$] (shifted for log transformation), Wind: wind speed [$\mathrm{m/s}$], Humid: humidity [ppm], AIC: Akaike information criterion, Adj. R^2: adjusted R^2, F. Bias: fractional bias, F. Error: fractional error.

Table C-11: Evaluations of summer EC social cost models.

Model[†]	(1)[‡]	(2)	(3)	(4)	(5)	(6)	(7)
Intercept	73^{***}	74^{***}	67^{***}	73^{***}	68^{***}	62^{***}	74^{***}
ln (Pop_w)	0.74^{***}	0.73^{***}	0.74^{***}	0.74^{***}	0.73^{***}	0.74^{***}	0.73^{***}
ln (Pres)	6.0^{***}	5.9^{***}	6.2^{***}	6.0^{***}	6.2^{***}	6.5^{***}	5.9^{***}
ln (Temp)	-19^{***}	-19^{***}	-18^{***}	-19^{***}	-18^{***}	-18^{***}	-19^{***}
ln (Wind)	-	-0.034	-	-	-0.040	-	-0.036
ln (Prec)	-	-	-	0.0031	-	0.029	-0.0039
ln (Humid)	-	-	-0.090	-	-0.12	-0.22	-
AIC	-21	-20	-19	-19	-18	-18	-18
Adj. R^2	0.97	0.97	0.97	0.97	0.97	0.97	0.97
F. Bias	0.0034	0.012	-0.00079	0.0047	0.0083	0.0051	0.011
F. Error	0.16	0.16	0.17	0.16	0.16	0.17	0.16

[†] Seven models with lowest AIC ordered by AIC, [‡] Chosen by AIC, *** $p < 0.001$, ** $p < 0.001$, * $p < 0.05$, $^{+}$ $p < 0.1$, Pop_w [# of people]: population (≥ age 30) weighted with average plume, Pres: pressure [hPa], Temp: temperature [K], Prec: precipitation + 0.0002 [$\mathrm{g/m^3}$] (shifted for log transformation), Wind: wind speed [$\mathrm{m/s}$], Humid: humidity [ppm], AIC: Akaike information criterion, Adj. R^2: adjusted R^2, F. Bias: fractional bias, F. Error: fractional error.

Table C-12: Evaluations of fall EC social cost models.

Model[†]	(1)[‡]	(2)	(3)	(4)	(5)	(6)	(7)
Intercept	72^{***}	65^{**}	72^{**}	37^{**}	30^{*}	65^{*}	36^{**}
ln (Pop_w)	0.60^{***}	0.59^{***}	0.60^{***}	0.61^{***}	0.59^{***}	0.59^{***}	0.62^{***}
ln (Pres)	3.1^{***}	3.1^{***}	3.1^{***}	3.7^{***}	3.6^{***}	3.1^{***}	3.7^{***}
ln (Temp)	-17^{***}	-15^{**}	-17^{***}	-10^{***}	-8.7^{**}	-15^{**}	-9.9^{***}
ln (Wind)	-	-	-0.00056	-	-	-0.0030	0.029
ln (Prec)	-	0.029	-	-	0.062	0.030	-
ln (Humid)	0.64^{*}	0.57^{+}	0.64^{*}	-	-	0.57^{+}	-
AIC	5.3	6.9	7.3	8.0	8.3	8.9	9.8
Adj. R^2	0.90	0.90	0.90	0.89	0.89	0.89	0.89
F. Bias	0.10	0.10	0.10	0.089	0.097	0.11	0.084
F. Error	0.21	0.21	0.21	0.20	0.21	0.21	0.20

[†] Seven models with lowest AIC ordered by AIC, [‡] Chosen by AIC, *** $p < 0.001$, ** $p < 0.001$, * $p < 0.05$, $^{+}$ $p < 0.1$, Pop_w [# of people]: population (≥ age 30) weighted with average plume, Pres: pressure [hPa], Temp: temperature [K], Prec: precipitation + 0.0002 [$\mathrm{g/m^3}$] (shifted for log transformation), Wind: wind speed [$\mathrm{m/s}$], Humid: humidity [ppm], AIC: Akaike information criterion, Adj. R^2: adjusted R^2, F. Bias: fractional bias, F. Error: fractional error.

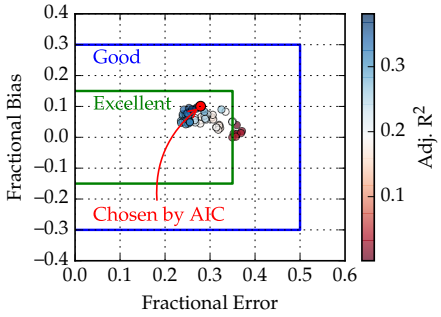

(a) Winter: ‘simple’ models

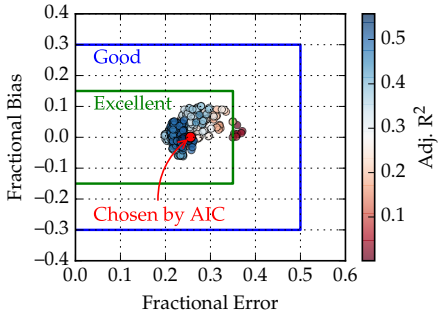

(b) Winter: ‘better-fit’ models

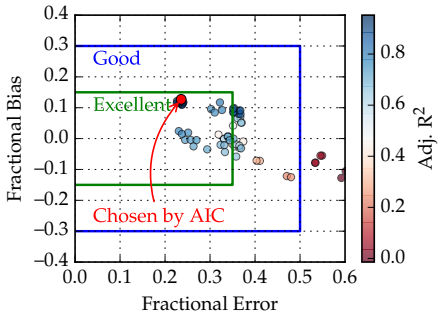

(c) Spring: ‘simple’ models

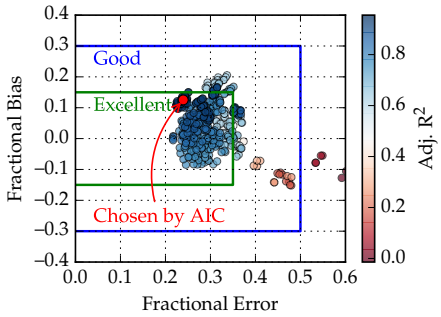

(d) Spring: ‘better-fit’ models

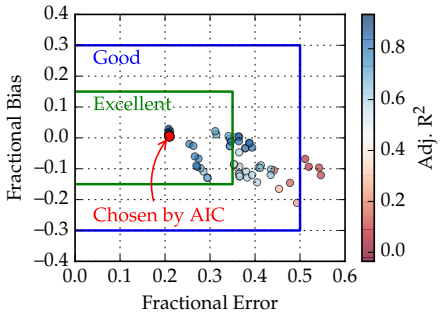

(e) Summer: ‘simple’ models

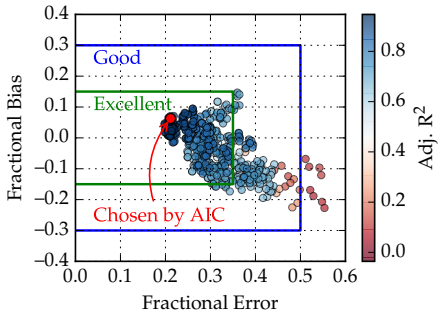

(f) Summer: ‘better-fit’ models

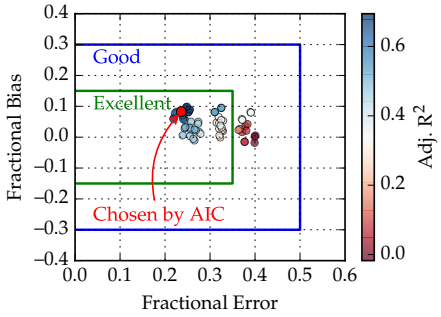

(g) Fall: ‘simple’ models

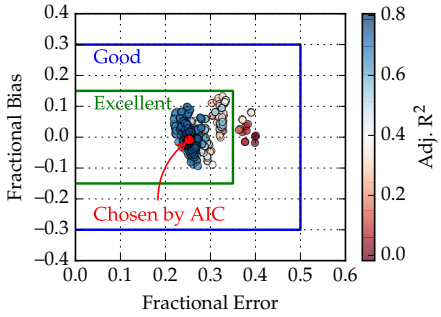

(h) Fall: ‘better-fit’ models

Figure C-37: Evaluations of SO_2 social cost models. Each circle indicates a regression model. ‘Excellent’ and ‘Good’ model performance criteria are shown as suggested by Morris et al. (2005).

Table C-13: Evaluations of winter SO_2 social cost 'simple' models.

Model[†]	(1)[‡]	(2)	(3)	(4)	(5)	(6)	(7)
Intercept	$86^{\star}$	$91^{\star}$	$86^{\star}$	72^{+}	$95^{\star}$	12	−6.7
ln (Pop_w)	-	-	0.0066	-	0.095	-	-
ln (Pres)	$3.0^{\star\star\star}$	$3.2^{\star\star\star}$	$3.0^{\star\star}$	$3.6^{\star\star\star}$	$2.8^{\star}$	$2.9^{\star\star}$	$2.4^{\star\star}$
ln (Temp)	$-19^{\star}$	$-20^{\star}$	$-19^{\star}$	$-17^{\star}$	$-20^{\star}$	−3.8	-
ln (Wind)	-0.14^{+}	-0.14^{+}	-0.14^{+}	-	-0.13^{+}	-0.13^{+}	−0.11
ln (Prec)	-	−0.092	-	-	−0.13	-	-
ln (Humid)	$0.96^{\star}$	$1.1^{\star}$	$0.96^{\star}$	0.92^{+}	$1.1^{\star}$	-	-
AIC	40	41	42	42	43	43	43
Adj. R^2	0.38	0.38	0.37	0.34	0.37	0.33	0.32
F. Bias	0.10	0.091	0.10	0.093	0.095	0.078	0.048
F. Error	0.28	0.26	0.28	0.27	0.25	0.25	0.26

[†] Seven models with lowest AIC ordered by AIC, [‡] Chosen by AIC, *** $p < 0.001$, ** $p < 0.001$, * $p < 0.05$, $^{+}$ $p < 0.1$, Pop_w [# of people]: population (≥ age 30) weighted with average plume, Pres: pressure [hPa], Temp: temperature [K], Prec: precipitation + 0.0002 [g/m^3] (shifted for log transformation), Wind: wind speed [m/s], Humid: humidity [ppm], AIC: Akaike information criterion, Adj. R^2: adjusted R^2, F. Bias: fractional bias, F. Error: fractional error.

Table C-14: Evaluations of winter SO_2 social cost 'better-fit' models.

Model[†]	(1)[‡]	(2)	(3)	(4)	(5)	(6)	(7)
Intercept	$77^{\star}$	$95^{\star}$	$80^{\star}$	$79^{\star}$	$96^{\star}$	$77^{\star}$	$8.5^{\star\star\star}$
ln (Pop_w)	-	0.23	-	0.029	0.23	-	-
ln (Pres)	-	-	-	-	0.35	−0.025	-
ln (Temp)	$-14^{\star}$	$-18^{\star}$	$-14^{\star}$	$-14^{\star}$	$-19^{\star}$	-14^{+}	-
ln (Wind)	$-0.15^{\star}$	$-0.19^{\star}$	$-0.16^{\star}$	$-0.16^{\star}$	$-0.19^{\star}$	$-0.15^{\star}$	$-0.16^{\star}$
ln (Prec)	-	-0.22^{+}	−0.081	-	-0.22^{+}	-	-
ln (Humid)	$1.0^{\star}$	$1.3^{\star\star}$	$1.1^{\star}$	$1.0^{\star}$	$1.3^{\star\star}$	$1.0^{\star}$	-
ln (TS)	$-0.25^{\star}$	$-0.37^{\star\star}$	$-0.26^{\star}$	$-0.27^{\star}$	$-0.38^{\star\star}$	$-0.25^{\star}$	−0.16
ln (TN)	$0.47^{\star\star\star}$	$0.45^{\star\star\star}$	$0.49^{\star\star\star}$	$0.46^{\star\star\star}$	$0.43^{\star\star}$	$0.48^{\star\star\star}$	$0.49^{\star\star\star}$
ln (TA)	$-0.24^{\star}$	$-0.25^{\star}$	$-0.26^{\star}$	$-0.24^{\star}$	-0.23^{+}	-0.24^{+}	$-0.34^{\star\star}$
AIC	27	27	28	29	29	29	29
Adj. R^2	0.54	0.56	0.54	0.53	0.55	0.53	0.50
F. Bias	0.00087	−0.0034	−0.012	0.0045	0.00089	0.00048	0.022
F. Error	0.26	0.24	0.25	0.26	0.24	0.26	0.24

[†] Seven models with lowest AIC ordered by AIC, [‡] Chosen by AIC, *** $p < 0.001$, ** $p < 0.001$, * $p < 0.05$, $^{+}$ $p < 0.1$, Pop_w [# of people]: population (≥ age 30) weighted with average plume, Pres: pressure [hPa], Temp: temperature [K], Prec: precipitation + 0.0002 [g/m^3] (shifted for log transformation), Wind: wind speed [m/s], Humid: humidity [ppm], TS: total sulfate (≡ $[SO_4{}^{2-}]$) [$\mu mol/m^3$], TN: total nitrate (≡ $[HNO_3]$ + $[NO_3{}^-]$) [$\mu mol/m^3$], TA: total ammonia (≡ $[NH_3]$ + $[NH_4{}^+]$) [$\mu mol/m^3$], AIC: Akaike information criterion, Adj. R^2: adjusted R^2, F. Bias: fractional bias, F. Error: fractional error.

Table C-15: Evaluations of spring SO_2 social cost 'simple' models.

Model[†]	(1)[‡]	(2)	(3)	(4)	(5)	(6)	(7)
Intercept	$120^{\star\star\star}$	$100^{\star\star\star}$	$110^{\star\star\star}$	$110^{\star\star\star}$	$81^{\star\star\star}$	$84^{\star\star\star}$	$81^{\star\star\star}$
ln (Pop_w)	$0.40^{\star\star\star}$	$0.39^{\star\star\star}$	$0.40^{\star\star\star}$	$0.41^{\star\star\star}$	$0.40^{\star\star\star}$	$0.41^{\star\star\star}$	$0.40^{\star\star\star}$
ln (Pres)	$6.3^{\star\star\star}$	$6.7^{\star\star\star}$	$6.8^{\star\star\star}$	$6.6^{\star\star\star}$	$7.4^{\star\star\star}$	$7.5^{\star\star\star}$	$7.4^{\star\star\star}$
ln (Temp)	$-28^{\star\star\star}$	$-26^{\star\star\star}$	$-26^{\star\star\star}$	$-28^{\star\star\star}$	$-22^{\star\star\star}$	$-23^{\star\star\star}$	$-22^{\star\star\star}$
ln (Wind)	$-0.070^{\star}$	-0.046	-	-	-0.048	-	-0.050
ln (Prec)	$-0.052^{\star}$	-	-	-0.028	-	-	-0.0056
ln (Humid)	$0.50^{\star\star\star}$	$0.36^{\star\star}$	$0.37^{\star\star}$	$0.44^{\star\star}$	-	-	-
AIC	-42	-39	-38	-38	-32	-32	-30
Adj. R^2	0.95	0.95	0.95	0.95	0.94	0.94	0.94
F. Bias	0.13	0.12	0.11	0.12	0.12	0.11	0.12
F. Error	0.24	0.23	0.23	0.23	0.24	0.24	0.24

[†] Seven models with lowest AIC ordered by AIC, [‡] Chosen by AIC, *** $p < 0.001$, ** $p < 0.001$, * $p < 0.05$, $^{+}$ $p < 0.1$, Pop_w [# of people]: population (≥ age 30) weighted with average plume, Pres: pressure [hPa], Temp: temperature [K], Prec: precipitation + 0.0002 [$\mathrm{g/m^3}$] (shifted for log transformation), Wind: wind speed [$\mathrm{m/s}$], Humid: humidity [ppm], AIC: Akaike information criterion, Adj. R^2: adjusted R^2, F. Bias: fractional bias, F. Error: fractional error.

Table C-16: Evaluations of spring SO_2 social cost 'better-fit' models.

Model[†]	(1)[‡]	(2)	(3)	(4)	(5)	(6)	(7)
Intercept	$89^{\star\star\star}$	$110^{\star\star\star}$	$98^{\star\star\star}$	$120^{\star\star\star}$	$89^{\star\star\star}$	$99^{\star\star\star}$	$110^{\star\star\star}$
ln (Pop_w)	$0.34^{\star\star\star}$	$0.41^{\star\star\star}$	$0.36^{\star\star\star}$	$0.40^{\star\star\star}$	$0.35^{\star\star\star}$	$0.41^{\star\star\star}$	$0.42^{\star\star\star}$
ln (Pres)	$6.2^{\star\star\star}$	$6.5^{\star\star\star}$	$6.2^{\star\star\star}$	$6.3^{\star\star\star}$	$6.2^{\star\star\star}$	$6.8^{\star\star\star}$	$6.5^{\star\star\star}$
ln (Temp)	$-23^{\star\star\star}$	$-27^{\star\star\star}$	$-24^{\star\star\star}$	$-28^{\star\star\star}$	$-23^{\star\star\star}$	$-25^{\star\star\star}$	$-27^{\star\star\star}$
ln (Wind)	$-0.074^{\star}$	$-0.083^{\star\star}$	$-0.081^{\star\star}$	$-0.070^{\star}$	$-0.074^{\star}$	$-0.066^{\star}$	$-0.084^{\star\star}$
ln (Prec)	-	-0.044^{+}	-0.025	$-0.052^{\star}$	-	-	-0.045^{+}
ln (Humid)	$0.30^{\star}$	$0.52^{\star\star\star}$	$0.39^{\star}$	$0.50^{\star\star\star}$	0.31^{+}	$0.41^{\star\star}$	$0.55^{\star\star}$
ln (TS)	-	-	-	-	-0.011	-	-0.026
ln (TN)	0.094^{+}	-	0.068	-	0.094^{+}	-	-
ln (TA)	$-0.092^{\star\star}$	-0.048	-0.077^{+}	-	$-0.091^{\star}$	-0.059^{+}	-0.046
AIC	-44	-43	-43	-42	-42	-42	-41
Adj. R^2	0.95	0.95	0.95	0.95	0.95	0.95	0.95
F. Bias	0.13	0.14	0.13	0.13	0.12	0.14	0.13
F. Error	0.24	0.24	0.24	0.24	0.24	0.24	0.24

[†] Seven models with lowest AIC ordered by AIC, [‡] Chosen by AIC, *** $p < 0.001$, ** $p < 0.001$, * $p < 0.05$, $^{+}$ $p < 0.1$, Pop_w [# of people]: population (≥ age 30) weighted with average plume, Pres: pressure [hPa], Temp: temperature [K], Prec: precipitation + 0.0002 [$\mathrm{g/m^3}$] (shifted for log transformation), Wind: wind speed [$\mathrm{m/s}$], Humid: humidity [ppm], TS: total sulfate (≡ $[{SO_4}^{2-}]$) [$\mathrm{\mu mol/m^3}$], TN: total nitrate (≡ $[HNO_3]$ + $[{NO_3}^{-}]$) [$\mathrm{\mu mol/m^3}$], TA: total ammonia (≡ $[NH_3]$ + $[{NH_4}^{+}]$) [$\mathrm{\mu mol/m^3}$], AIC: Akaike information criterion, Adj. R^2: adjusted R^2, F. Bias: fractional bias, F. Error: fractional error.

Table C-17: Evaluations of summer SO_2 social cost 'simple' models.

Model[†]	(1)[‡]	(2)	(3)	(4)	(5)	(6)	(7)
Intercept	$110^{\star\star\star}$	$100^{\star\star\star}$	$94^{\star\star\star}$	$110^{\star\star\star}$	$94^{\star\star\star}$	$100^{\star\star\star}$	$110^{\star\star\star}$
ln (Pop_w)	$0.54^{\star\star\star}$	$0.56^{\star\star\star}$	$0.57^{\star\star\star}$	$0.55^{\star\star\star}$	$0.58^{\star\star\star}$	$0.56^{\star\star\star}$	$0.52^{\star\star\star}$
ln (Pres)	$6.3^{\star\star\star}$	$6.5^{\star\star\star}$	$7.0^{\star\star\star}$	$6.3^{\star\star\star}$	$7.0^{\star\star\star}$	$6.6^{\star\star\star}$	$6.4^{\star\star\star}$
ln (Temp)	$-26^{\star\star\star}$	$-25^{\star\star\star}$	$-24^{\star\star\star}$	$-26^{\star\star\star}$	$-24^{\star\star\star}$	$-25^{\star\star\star}$	$-27^{\star\star\star}$
ln (Wind)	-	-	-	0.0055	0.031	0.012	-
ln (Prec)	$-0.064^{\star\star}$	−0.048	-	$-0.063^{\star}$	-	−0.045	-
ln (Humid)	-	−0.14	$-0.36^{\star}$	-	$-0.35^{\star}$	−0.15	-
AIC	−23	−22	−21	−21	−20	−20	−17
Adj. R^2	0.93	0.93	0.93	0.93	0.93	0.93	0.92
F. Bias	0.0051	0.0062	0.017	0.0043	0.011	0.0047	0.029
F. Error	0.21	0.21	0.21	0.21	0.21	0.21	0.21

[†] Seven models with lowest AIC ordered by AIC, [‡] Chosen by AIC, *** $p < 0.001$, ** $p < 0.001$, * $p < 0.05$, $^{+}$ $p < 0.1$, Pop_w [# of people]: population (≥ age 30) weighted with average plume, Pres: pressure [hPa], Temp: temperature [K], Prec: precipitation + 0.0002 [g/m^3] (shifted for log transformation), Wind: wind speed [m/s], Humid: humidity [ppm], AIC: Akaike information criterion, Adj. R^2: adjusted R^2, F. Bias: fractional bias, F. Error: fractional error.

Table C-18: Evaluations of summer SO_2 social cost 'better-fit' models.

Model[†]	(1)[‡]	(2)	(3)	(4)	(5)	(6)	(7)
Intercept	$76^{\star\star\star}$	$83^{\star\star\star}$	$76^{\star\star\star}$	$82^{\star\star\star}$	$91^{\star\star\star}$	$91^{\star\star\star}$	$79^{\star\star\star}$
ln (Pop_w)	$0.45^{\star\star\star}$	$0.44^{\star\star\star}$	$0.46^{\star\star\star}$	$0.50^{\star\star\star}$	$0.46^{\star\star\star}$	$0.49^{\star\star\star}$	$0.46^{\star\star\star}$
ln (Pres)	$6.8^{\star\star\star}$	$6.4^{\star\star\star}$	$6.7^{\star\star\star}$	$7.1^{\star\star\star}$	$6.7^{\star\star\star}$	$6.9^{\star\star\star}$	$7.0^{\star\star\star}$
ln (Temp)	$-19^{\star\star\star}$	$-20^{\star\star\star}$	$-19^{\star\star\star}$	$-21^{\star\star\star}$	$-22^{\star\star\star}$	$-22^{\star\star\star}$	$-20^{\star\star\star}$
ln (Wind)	-	-	0.041	0.063	-	0.052	-
ln (Prec)	-	−0.035	-	-	−0.045	−0.035	-
ln (Humid)	$-0.71^{\star\star}$	$-0.57^{\star}$	$-0.73^{\star\star}$	$-0.71^{\star\star}$	-0.51^{+}	$-0.56^{\star}$	$-0.70^{\star\star}$
ln (TS)	$0.32^{\star}$	$0.32^{\star}$	$0.34^{\star}$	$0.37^{\star\star}$	$0.34^{\star}$	$0.37^{\star\star}$	$0.32^{\star}$
ln (TN)	-	-	-	−0.057	−0.045	−0.066	−0.025
ln (TA)	$-0.10^{\star\star}$	$-0.098^{\star\star}$	$-0.11^{\star\star}$	$-0.098^{\star\star}$	$-0.090^{\star\star}$	$-0.090^{\star\star}$	$-0.10^{\star\star}$
AIC	−31	−30	−30	−30	−30	−30	−29
Adj. R^2	0.95	0.95	0.95	0.95	0.95	0.95	0.95
F. Bias	0.063	0.054	0.057	0.071	0.066	0.067	0.070
F. Error	0.21	0.21	0.21	0.22	0.21	0.21	0.21

[†] Seven models with lowest AIC ordered by AIC, [‡] Chosen by AIC, *** $p < 0.001$, ** $p < 0.001$, * $p < 0.05$, $^{+}$ $p < 0.1$, Pop_w [# of people]: population (≥ age 30) weighted with average plume, Pres: pressure [hPa], Temp: temperature [K], Prec: precipitation + 0.0002 [g/m^3] (shifted for log transformation), Wind: wind speed [m/s], Humid: humidity [ppm], TS: total sulfate (≡ $[SO_4{}^{2-}]$) [$\mu mol/m^3$], TN: total nitrate (≡ $[HNO_3]$ + $[NO_3{}^-]$) [$\mu mol/m^3$], TA: total ammonia (≡ $[NH_3]$ + $[NH_4{}^+]$) [$\mu mol/m^3$], AIC: Akaike information criterion, Adj. R^2: adjusted R^2, F. Bias: fractional bias, F. Error: fractional error.

Table C-19: Evaluations of fall SO_2 social cost 'simple' models.

Model[†]	(1)[‡]	(2)	(3)	(4)	(5)	(6)	(7)
Intercept	92^{***}	100^{***}	96^{***}	95^{***}	110^{***}	91^{***}	98^{***}
ln (Pop_w)	0.19^{*}	0.13	-	0.19^{*}	0.14	-	-
ln (Pres)	3.9^{***}	3.9^{***}	4.6^{***}	3.9^{***}	3.9^{***}	4.8^{***}	4.7^{***}
ln (Temp)	-21^{***}	-23^{***}	-22^{***}	-22^{***}	-23^{***}	-22^{***}	-23^{***}
ln (Wind)	0.10	-	-	0.10	-	0.040	-
ln (Prec)	-	-	-	−0.015	−0.016	-	−0.011
ln (Humid)	0.85^{**}	0.91^{**}	0.87^{**}	0.88^{**}	0.95^{**}	0.83^{**}	0.89^{**}
AIC	1.5	1.9	2.8	3.4	3.8	4.4	4.7
Adj. R^2	0.69	0.69	0.67	0.69	0.68	0.67	0.67
F. Bias	0.083	0.099	0.089	0.082	0.097	0.082	0.088
F. Error	0.24	0.25	0.26	0.23	0.25	0.25	0.25

[†] Seven models with lowest AIC ordered by AIC, [‡] Chosen by AIC, *** $p < 0.001$, ** $p < 0.001$, * $p < 0.05$, $^{+}$ $p < 0.1$, Pop_w [# of people]: population (≥ age 30) weighted with average plume, Pres: pressure [hPa], Temp: temperature [K], Prec: precipitation + 0.0002 [g/m^3] (shifted for log transformation), Wind: wind speed [m/s], Humid: humidity [ppm], AIC: Akaike information criterion, Adj. R^2: adjusted R^2, F. Bias: fractional bias, F. Error: fractional error.

Table C-20: Evaluations of fall SO_2 social cost 'better-fit' models.

Model[†]	(1)[‡]	(2)	(3)	(4)	(5)	(6)	(7)
Intercept	150^{***}	130^{***}	140^{***}	100^{***}	91^{***}	120^{***}	120^{***}
ln (Pop_w)	0.54^{***}	0.47^{***}	0.56^{***}	0.37^{***}	0.36^{***}	0.47^{***}	0.45^{***}
ln (Pres)	5.1^{***}	4.2^{***}	5.1^{***}	3.4^{***}	3.0^{**}	4.1^{***}	3.8^{**}
ln (Temp)	-35^{***}	-30^{***}	-34^{***}	-24^{***}	-21^{***}	-28^{***}	-27^{***}
ln (Wind)	-	-	0.045	-	-	0.056	-
ln (Prec)	-0.10^{*}	−0.074	-0.10^{*}	-	-	−0.066	−0.062
ln (Humid)	1.9^{***}	1.7^{***}	1.8^{***}	1.4^{***}	1.2^{***}	1.6^{***}	1.5^{***}
ln (TS)	-0.58^{***}	-0.54^{***}	-0.56^{***}	-0.45^{***}	-0.43^{***}	-0.51^{***}	-0.51^{***}
ln (TN)	-	0.067	-	0.12^{*}	0.20^{*}	0.076	0.13
ln (TA)	-	-	-	-	−0.084	-	−0.062
AIC	−20	−20	−19	−19	−19	−19	−19
Adj. R^2	0.81	0.81	0.80	0.80	0.80	0.81	0.81
F. Bias	−0.0084	−0.020	−0.012	−0.016	−0.013	−0.026	−0.017
F. Error	0.25	0.25	0.25	0.25	0.25	0.25	0.25

[†] Seven models with lowest AIC ordered by AIC, [‡] Chosen by AIC, *** $p < 0.001$, ** $p < 0.001$, * $p < 0.05$, $^{+}$ $p < 0.1$, Pop_w [# of people]: population (≥ age 30) weighted with average plume, Pres: pressure [hPa], Temp: temperature [K], Prec: precipitation + 0.0002 [g/m^3] (shifted for log transformation), Wind: wind speed [m/s], Humid: humidity [ppm], TS: total sulfate (≡ $[SO_4{}^{2-}]$) [$\mu mol/m^3$], TN: total nitrate (≡ $[HNO_3]$ + $[NO_3{}^-]$) [$\mu mol/m^3$], TA: total ammonia (≡ $[NH_3]$ + $[NH_4{}^+]$) [$\mu mol/m^3$], AIC: Akaike information criterion, Adj. R^2: adjusted R^2, F. Bias: fractional bias, F. Error: fractional error.

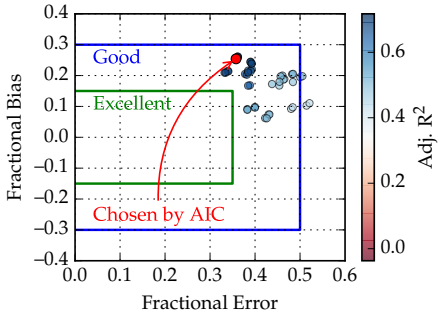

(a) Winter: 'simple' models

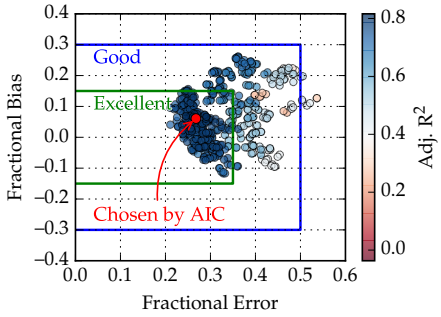

(b) Winter: 'better-fit' models

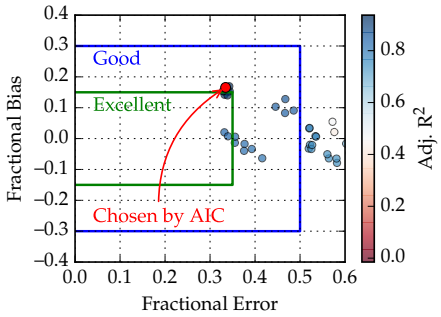

(c) Spring: 'simple' models

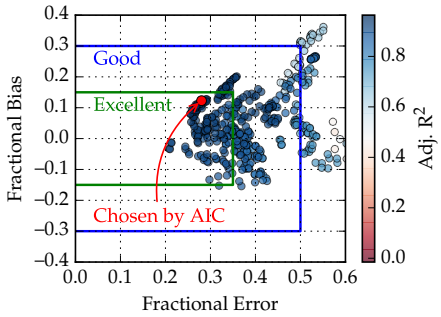

(d) Spring: 'better-fit' models

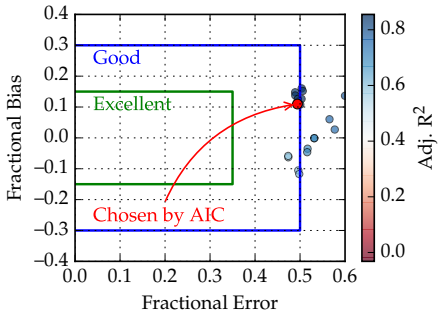

(e) Summer: 'simple' models

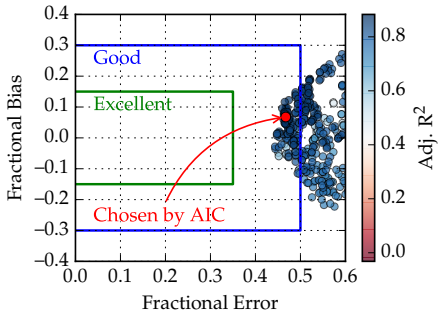

(f) Summer: 'better-fit' models

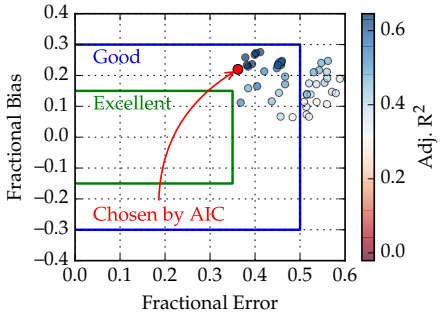

(g) Fall: 'simple' models

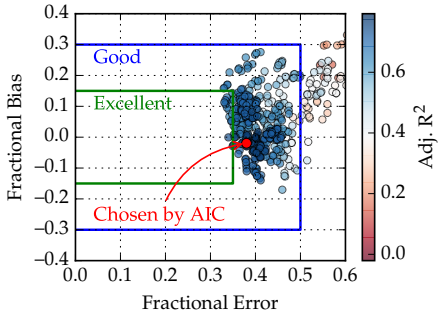

(h) Fall: 'better-fit' models

Figure C-38: Evaluations of NO_x social cost models. Each circle indicates a regression model. 'Excellent' and 'Good' model performance criteria are shown as suggested by Morris et al. (2005).

Table C-21: Evaluations of winter NO_x social cost 'simple' models.

Model[†]	(1)[‡]	(2)	(3)	(4)	(5)	(6)	(7)
Intercept	$55^{\star\star}$	$61^{\star\star}$	71	$55^{\star\star}$	79	$61^{\star\star}$	72
ln (Pop_w)	$0.37^{\star\star}$	$0.36^{\star\star}$	$0.37^{\star\star}$	$0.37^{\star}$	$0.36^{\star}$	$0.35^{\star}$	$0.38^{\star}$
ln (Pres)	$8.1^{\star\star\star}$	$7.8^{\star\star\star}$	$8.1^{\star\star\star}$	$8.0^{\star\star\star}$	$7.8^{\star\star\star}$	$7.8^{\star\star\star}$	$8.1^{\star\star\star}$
ln (Temp)	$-19^{\star\star\star}$	$-19^{\star\star\star}$	$-22^{\star}$	$-19^{\star\star\star}$	$-23^{\star}$	$-19^{\star\star\star}$	$-22^{\star}$
ln (Wind)	-	-0.077	-	-	-0.079	-0.078	-
ln (Prec)	-	-	-	-0.0036	-	0.010	-0.020
ln (Humid)	-	-	0.20	-	0.23	-	0.23
AIC	67	68	69	69	70	70	71
Adj. R^2	0.72	0.72	0.71	0.71	0.71	0.71	0.71
F. Bias	0.25	0.26	0.26	0.25	0.26	0.26	0.26
F. Error	0.36	0.36	0.36	0.36	0.36	0.36	0.36

[†] Seven models with lowest AIC ordered by AIC, [‡] Chosen by AIC, *** $p < 0.001$, ** $p < 0.001$, * $p < 0.05$, $^{+}$ $p < 0.1$, Pop_w [# of people]: population (≥ age 30) weighted with average plume, Pres: pressure [hPa], Temp: temperature [K], Prec: precipitation + 0.0002 [g/m^3] (shifted for log transformation), Wind: wind speed [m/s], Humid: humidity [ppm], AIC: Akaike information criterion, Adj. R^2: adjusted R^2, F. Bias: fractional bias, F. Error: fractional error.

Table C-22: Evaluations of winter NO_x social cost 'better-fit' models.

Model[†]	(1)[‡]	(2)	(3)	(4)	(5)	(6)	(7)
Intercept	$99^{\star}$	$32^{\star}$	82^{+}	$110^{\star}$	$37^{\star}$	$89^{\star}$	$33^{\star}$
ln (Pop_w)	$0.36^{\star\star}$	$0.34^{\star\star}$	$0.34^{\star\star}$	$0.37^{\star\star}$	$0.35^{\star\star}$	$0.35^{\star\star}$	$0.36^{\star\star}$
ln (Pres)	$4.1^{\star\star}$	$3.3^{\star}$	$3.5^{\star}$	$4.3^{\star\star}$	$3.4^{\star}$	$3.6^{\star}$	$4.2^{\star\star}$
ln (Temp)	$-23^{\star\star}$	$-9.1^{\star\star}$	$-19^{\star}$	$-25^{\star\star}$	$-10^{\star\star}$	$-21^{\star}$	$-10^{\star\star}$
ln (Wind)	-	-	-	-0.085	-0.089	-0.093	-
ln (Prec)	-	-	-	-	-	-	-
ln (Humid)	0.88^{+}	-	0.66	0.91^{+}	-	0.68	-
ln (TS)	$-0.48^{\star\star\star}$	$-0.38^{\star\star}$	$-0.44^{\star\star}$	$-0.53^{\star\star\star}$	$-0.43^{\star\star}$	$-0.49^{\star\star}$	$-0.43^{\star\star}$
ln (TN)	$0.50^{\star\star\star}$	$0.66^{\star\star\star}$	$0.62^{\star\star\star}$	$0.48^{\star\star\star}$	$0.65^{\star\star\star}$	$0.62^{\star\star\star}$	$0.45^{\star\star\star}$
ln (TA)	-	-0.22	-0.15	-	-0.24^{+}	-0.17	-
AIC	48	49	49	49	50	50	50
Adj. R^2	0.82	0.81	0.82	0.82	0.81	0.82	0.81
F. Bias	0.061	0.069	0.066	0.066	0.075	0.073	0.060
F. Error	0.27	0.25	0.26	0.29	0.26	0.29	0.24

[†] Seven models with lowest AIC ordered by AIC, [‡] Chosen by AIC, *** $p < 0.001$, ** $p < 0.001$, * $p < 0.05$, $^{+}$ $p < 0.1$, Pop_w [# of people]: population (≥ age 30) weighted with average plume, Pres: pressure [hPa], Temp: temperature [K], Prec: precipitation + 0.0002 [g/m^3] (shifted for log transformation), Wind: wind speed [m/s], Humid: humidity [ppm], TS: total sulfate (≡ $[SO_4{}^{2-}]$) [$\mu mol/m^3$], TN: total nitrate (≡ $[HNO_3]$ + $[NO_3{}^-]$) [$\mu mol/m^3$], TA: total ammonia (≡ $[NH_3]$ + $[NH_4{}^+]$) [$\mu mol/m^3$], AIC: Akaike information criterion, Adj. R^2: adjusted R^2, F. Bias: fractional bias, F. Error: fractional error.

Table C-23: Evaluations of spring NO_x social cost 'simple' models.

Model[†]	(1)[‡]	(2)	(3)	(4)	(5)	(6)	(7)
Intercept	$150^{\star\star\star}$	$150^{\star\star\star}$	$160^{\star\star\star}$	$160^{\star\star\star}$	$100^{\star\star\star}$	$98^{\star\star\star}$	$97^{\star\star\star}$
ln (Pop_w)	$0.98^{\star\star\star}$	$0.99^{\star\star\star}$	$0.99^{\star\star\star}$	$1.00^{\star\star\star}$	$1.00^{\star\star\star}$	$0.98^{\star\star\star}$	$0.99^{\star\star\star}$
ln (Pres)	$9.6^{\star\star\star}$	$9.7^{\star\star\star}$	$9.3^{\star\star\star}$	$9.7^{\star\star\star}$	$12^{\star\star\star}$	$11^{\star\star\star}$	$12^{\star\star\star}$
ln (Temp)	$-40^{\star\star\star}$	$-41^{\star\star\star}$	$-42^{\star\star\star}$	$-41^{\star\star\star}$	$-32^{\star\star\star}$	$-31^{\star\star\star}$	$-31^{\star\star\star}$
ln (Wind)	-0.084	-	-0.11	-	-	-0.090	-
ln (Prec)	-	-	-0.048	-0.011	-	-	0.062
ln (Humid)	$0.85^{\star\star}$	$0.86^{\star\star}$	$0.98^{\star\star}$	$0.89^{\star\star}$	-	-	-
AIC	40	40	41	42	48	48	48
Adj. R^2	0.94	0.94	0.94	0.93	0.92	0.92	0.92
F. Bias	0.17	0.15	0.17	0.15	0.14	0.15	0.14
F. Error	0.33	0.33	0.34	0.33	0.34	0.34	0.33

[†] Seven models with lowest AIC ordered by AIC, [‡] Chosen by AIC, *** $p < 0.001$, ** $p < 0.001$, * $p < 0.05$, $^{+}$ $p < 0.1$, Pop_w [# of people]: population (≥ age 30) weighted with average plume, Pres: pressure [hPa], Temp: temperature [K], Prec: precipitation + 0.0002 [g/m^3] (shifted for log transformation), Wind: wind speed [m/s], Humid: humidity [ppm], AIC: Akaike information criterion, Adj. R^2: adjusted R^2, F. Bias: fractional bias, F. Error: fractional error.

Table C-24: Evaluations of spring NO_x social cost 'better-fit' models.

Model[†]	(1)[‡]	(2)	(3)	(4)	(5)	(6)	(7)
Intercept	$76^{\star\star\star}$	$81^{\star\star\star}$	$73^{\star\star\star}$	$69^{\star}$	$86^{\star\star\star}$	$67^{\star}$	$79^{\star\star\star}$
ln (Pop_w)	$0.63^{\star\star\star}$	$0.64^{\star\star\star}$	$0.64^{\star\star\star}$	$0.62^{\star\star\star}$	$0.65^{\star\star\star}$	$0.62^{\star\star\star}$	$0.65^{\star\star\star}$
ln (Pres)	$6.9^{\star\star\star}$	$7.1^{\star\star\star}$	$7.0^{\star\star\star}$	$7.0^{\star\star\star}$	$7.0^{\star\star\star}$	$7.2^{\star\star\star}$	$7.1^{\star\star\star}$
ln (Temp)	$-21^{\star\star\star}$	$-23^{\star\star\star}$	$-21^{\star\star\star}$	$-20^{\star\star\star}$	$-23^{\star\star\star}$	$-20^{\star\star}$	$-22^{\star\star\star}$
ln (Wind)	-0.088	-	-0.089	-0.085	$-0.11^{\star}$	-	-
ln (Prec)	0.079^{+}	$0.096^{\star}$	0.083^{+}	0.089^{+}	-	$0.11^{\star}$	$0.099^{\star}$
ln (Humid)	-	-	-	-0.10	-	-0.19	-
ln (TS)	-	-	-0.048	-	-	-	-0.036
ln (TN)	$0.55^{\star\star\star}$	$0.54^{\star\star\star}$	$0.56^{\star\star\star}$	$0.57^{\star\star\star}$	$0.52^{\star\star\star}$	$0.58^{\star\star\star}$	$0.55^{\star\star\star}$
ln (TA)	$-0.20^{\star\star}$	$-0.18^{\star\star}$	$-0.20^{\star\star}$	$-0.21^{\star\star}$	$-0.16^{\star}$	$-0.19^{\star\star}$	$-0.18^{\star\star}$
AIC	14	16	16	16	17	17	17
Adj. R^2	0.96	0.96	0.96	0.96	0.96	0.96	0.96
F. Bias	0.12	0.11	0.11	0.12	0.12	0.10	0.099
F. Error	0.28	0.27	0.28	0.28	0.29	0.27	0.27

[†] Seven models with lowest AIC ordered by AIC, [‡] Chosen by AIC, *** $p < 0.001$, ** $p < 0.001$, * $p < 0.05$, $^{+}$ $p < 0.1$, Pop_w [# of people]: population (≥ age 30) weighted with average plume, Pres: pressure [hPa], Temp: temperature [K], Prec: precipitation + 0.0002 [g/m^3] (shifted for log transformation), Wind: wind speed [m/s], Humid: humidity [ppm], TS: total sulfate (≡ $[SO_4{}^{2-}]$) [$\mu mol/m^3$], TN: total nitrate (≡ $[HNO_3]$ + $[NO_3{}^-]$) [$\mu mol/m^3$], TA: total ammonia (≡ $[NH_3]$ + $[NH_4{}^+]$) [$\mu mol/m^3$], AIC: Akaike information criterion, Adj. R^2: adjusted R^2, F. Bias: fractional bias, F. Error: fractional error.

Table C-25: Evaluations of summer NO_x social cost 'simple' models.

Model[†]	(1)[‡]	(2)	(3)	(4)	(5)	(6)	(7)
Intercept	$200^{\star\star\star}$	$210^{\star\star\star}$	$210^{\star\star\star}$	$220^{\star\star\star}$	$230^{\star\star\star}$	$190^{\star\star\star}$	$210^{\star\star\star}$
ln (Pop_w)	$1.1^{\star\star\star}$	$1.0^{\star\star\star}$	$1.0^{\star\star\star}$	$1.1^{\star\star\star}$	$0.98^{\star\star\star}$	$1.1^{\star\star\star}$	$1.0^{\star\star\star}$
ln (Pres)	$12^{\star\star\star}$	$11^{\star\star\star}$	$12^{\star\star\star}$	$11^{\star\star\star}$	$11^{\star\star\star}$	$13^{\star\star\star}$	$12^{\star\star\star}$
ln (Temp)	$-51^{\star\star\star}$	$-51^{\star\star\star}$	$-52^{\star\star\star}$	$-53^{\star\star\star}$	$-54^{\star\star\star}$	$-48^{\star\star\star}$	$-52^{\star\star\star}$
ln (Wind)	-	-0.12	-	-	-0.13	-	-0.042
ln (Prec)	-0.12^{+}	$-0.14^{\star}$	-	-0.16	-0.19^{+}	-	-
ln (Humid)	-	-	-	0.32	0.45	-0.43	-
AIC	82	83	84	84	85	85	86
Adj. R^2	0.86	0.85	0.85	0.85	0.85	0.85	0.84
F. Bias	0.11	0.13	0.15	0.11	0.13	0.14	0.16
F. Error	0.49	0.50	0.51	0.50	0.50	0.49	0.50

[†] Seven models with lowest AIC ordered by AIC, [‡] Chosen by AIC, *** $p < 0.001$, ** $p < 0.001$, * $p < 0.05$, $^{+}$ $p < 0.1$, Pop_w [# of people]: population (≥ age 30) weighted with average plume, Pres: pressure [hPa], Temp: temperature [K], Prec: precipitation + 0.0002 [g/m^3] (shifted for log transformation), Wind: wind speed [m/s], Humid: humidity [ppm], AIC: Akaike information criterion, Adj. R^2: adjusted R^2, F. Bias: fractional bias, F. Error: fractional error.

Table C-26: Evaluations of summer NO_x social cost 'better-fit' models.

Model[†]	(1)[‡]	(2)	(3)	(4)	(5)	(6)	(7)
Intercept	$180^{\star\star\star}$	$170^{\star\star\star}$	$180^{\star\star\star}$	$180^{\star\star\star}$	$140^{\star\star\star}$	$180^{\star\star\star}$	$140^{\star\star\star}$
ln (Pop_w)	$0.65^{\star\star}$	$0.66^{\star\star}$	$0.64^{\star\star}$	$0.65^{\star\star}$	$0.70^{\star\star}$	$0.84^{\star\star\star}$	$0.85^{\star\star\star}$
ln (Pres)	$7.1^{\star\star\star}$	$7.4^{\star\star\star}$	$7.1^{\star\star\star}$	$7.1^{\star\star\star}$	$8.6^{\star\star\star}$	$8.0^{\star\star\star}$	$9.1^{\star\star\star}$
ln (Temp)	$-41^{\star\star\star}$	$-38^{\star\star\star}$	$-40^{\star\star\star}$	$-41^{\star\star\star}$	$-32^{\star\star\star}$	$-42^{\star\star\star}$	$-35^{\star\star\star}$
ln (Wind)	$-0.24^{\star}$	-0.24^{+}	$-0.24^{\star}$	-0.24^{+}	-0.19	-	-
ln (Prec)	$-0.17^{\star\star}$	-0.15	$-0.17^{\star}$	$-0.17^{\star}$	-	$-0.13^{\star}$	-
ln (Humid)	-	-0.22	-	-	$-0.94^{\star}$	-	-0.81^{+}
ln (TS)	-	-	-	$-2.3 \cdot 10^{-5}$	-	-	-
ln (TN)	$0.38^{\star\star}$	$0.40^{\star\star}$	$0.39^{\star\star}$	$0.38^{\star\star}$	$0.42^{\star\star}$	$0.31^{\star\star}$	$0.36^{\star\star}$
ln (TA)	-	-	-0.019	-	-	-	-
AIC	74	75	75	76	76	76	77
Adj. R^2	0.88	0.88	0.88	0.88	0.88	0.87	0.87
F. Bias	0.068	0.066	0.070	0.068	0.079	0.046	0.056
F. Error	0.47	0.47	0.47	0.47	0.47	0.47	0.47

[†] Seven models with lowest AIC ordered by AIC, [‡] Chosen by AIC, *** $p < 0.001$, ** $p < 0.001$, * $p < 0.05$, $^{+}$ $p < 0.1$, Pop_w [# of people]: population (≥ age 30) weighted with average plume, Pres: pressure [hPa], Temp: temperature [K], Prec: precipitation + 0.0002 [g/m^3] (shifted for log transformation), Wind: wind speed [m/s], Humid: humidity [ppm], TS: total sulfate (≡ $[SO_4{}^{2-}]$) [$\mu mol/m^3$], TN: total nitrate (≡ $[HNO_3]$ + $[NO_3{}^-]$) [$\mu mol/m^3$], TA: total ammonia (≡ $[NH_3]$ + $[NH_4{}^+]$) [$\mu mol/m^3$], AIC: Akaike information criterion, Adj. R^2: adjusted R^2, F. Bias: fractional bias, F. Error: fractional error.

Table C-27: Evaluations of fall NO_x social cost 'simple' models.

Model[†]	(1)[‡]	(2)	(3)	(4)	(5)	(6)	(7)
Intercept	100^{***}	120^{***}	130^{**}	97^{***}	160^{**}	110^{***}	120^{*}
ln (Pop_w)	0.59^{**}	0.47^{**}	0.59^{**}	0.58^{**}	0.49^{**}	0.47^{**}	0.59^{**}
ln (Pres)	8.8^{***}	8.7^{***}	8.1^{***}	8.5^{***}	7.9^{***}	8.4^{***}	8.1^{***}
ln (Temp)	-29^{***}	-31^{***}	-34^{***}	-27^{***}	-37^{***}	-29^{***}	-31^{**}
ln (Wind)	0.24	-	0.23	0.24	-	-	0.23
ln (Prec)	-	-	-	0.072	-	0.078	0.052
ln (Humid)	-	-	0.51	-	0.65	-	0.38
AIC	81	82	82	82	83	83	84
Adj. R^2	0.65	0.63	0.64	0.64	0.63	0.63	0.64
F. Bias	0.22	0.26	0.23	0.23	0.27	0.27	0.24
F. Error	0.36	0.38	0.38	0.38	0.40	0.40	0.39

[†] Seven models with lowest AIC ordered by AIC, [‡] Chosen by AIC, *** $p < 0.001$, ** $p < 0.001$, * $p < 0.05$, $^{+}$ $p < 0.1$, Pop_w [# of people]: population (≥ age 30) weighted with average plume, Pres: pressure [hPa], Temp: temperature [K], Prec: precipitation + 0.0002 [g/m^3] (shifted for log transformation), Wind: wind speed [m/s], Humid: humidity [ppm], AIC: Akaike information criterion, Adj. R^2: adjusted R^2, F. Bias: fractional bias, F. Error: fractional error.

Table C-28: Evaluations of fall NO_x social cost 'better-fit' models.

Model[†]	(1)[‡]	(2)	(3)	(4)	(5)	(6)	(7)
Intercept	170^{***}	150^{***}	150^{***}	130^{**}	200^{***}	160^{***}	180^{***}
ln (Pop_w)	0.95^{***}	0.81^{***}	0.89^{***}	0.84^{***}	0.92^{***}	0.84^{***}	0.96^{***}
ln (Pres)	8.1^{***}	6.3^{**}	6.9^{**}	6.2^{**}	8.4^{***}	6.8^{**}	8.2^{***}
ln (Temp)	-45^{***}	-37^{***}	-39^{***}	-34^{***}	-49^{***}	-41^{***}	-46^{***}
ln (Wind)	0.21^{+}	-	0.18	0.12	-	-	0.20
ln (Prec)	-	-	-	-	-	-	−0.021
ln (Humid)	1.9^{**}	1.5^{**}	1.7^{**}	1.4^{*}	2.1^{***}	1.7^{**}	2.0^{**}
ln (TS)	-0.95^{***}	-0.93^{***}	-0.92^{***}	-0.89^{***}	-1.0^{***}	-0.97^{***}	-0.97^{***}
ln (TN)	-	0.34^{**}	0.16	0.35^{**}	-	0.22	-
ln (TA)	0.31^{**}	-	0.20	-	0.26^{**}	0.12	0.30^{**}
AIC	56	57	57	58	58	58	58
Adj. R^2	0.79	0.79	0.79	0.79	0.78	0.79	0.79
F. Bias	−0.020	−0.00051	−0.030	−0.016	0.016	−0.0040	−0.022
F. Error	0.38	0.40	0.38	0.38	0.41	0.40	0.38

[†] Seven models with lowest AIC ordered by AIC, [‡] Chosen by AIC, *** $p < 0.001$, ** $p < 0.001$, * $p < 0.05$, $^{+}$ $p < 0.1$, Pop_w [# of people]: population (≥ age 30) weighted with average plume, Pres: pressure [hPa], Temp: temperature [K], Prec: precipitation + 0.0002 [g/m^3] (shifted for log transformation), Wind: wind speed [m/s], Humid: humidity [ppm], TS: total sulfate (≡ $[SO_4{}^{2-}]$) [$\mu mol/m^3$], TN: total nitrate (≡ $[HNO_3]$ + $[NO_3{}^-]$) [$\mu mol/m^3$], TA: total ammonia (≡ $[NH_3]$ + $[NH_4{}^+]$) [$\mu mol/m^3$], AIC: Akaike information criterion, Adj. R^2: adjusted R^2, F. Bias: fractional bias, F. Error: fractional error.

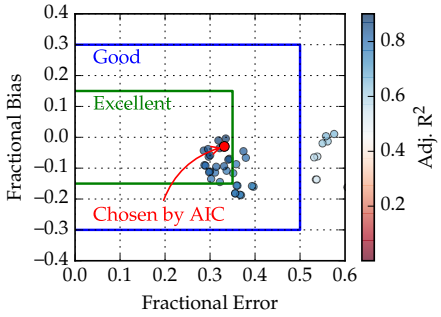

(a) Winter: ‘simple’ models

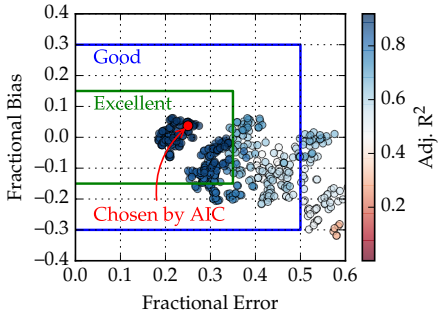

(b) Winter: ‘better-fit’ models

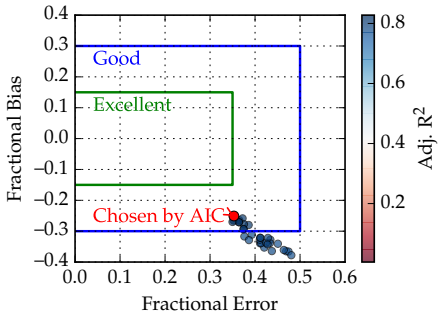

(c) Spring: ‘simple’ models

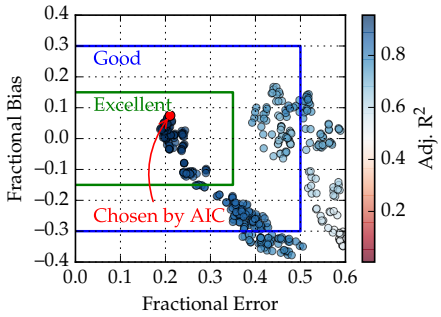

(d) Spring: ‘better-fit’ models

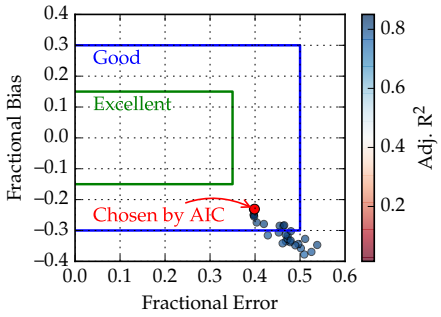

(e) Summer: ‘simple’ models

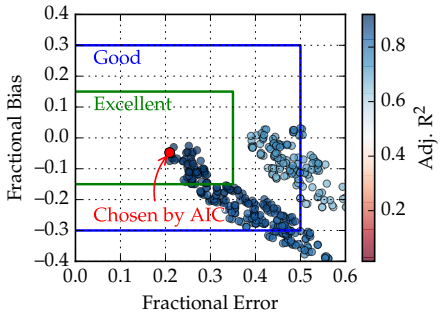

(f) Summer: ‘better-fit’ models

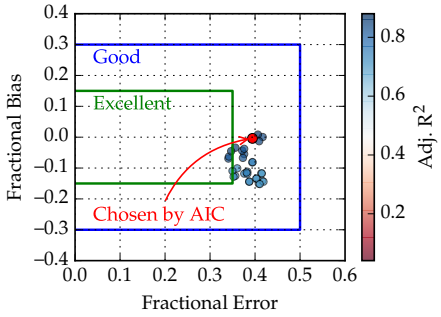

(g) Fall: ‘simple’ models

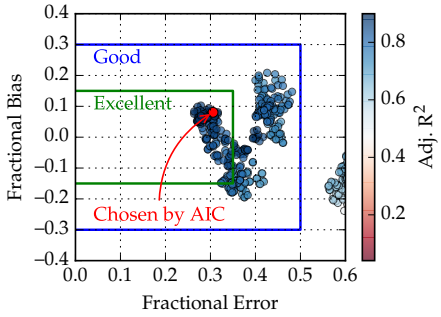

(h) Fall: ‘better-fit’ models

Figure C-39: Evaluations of NH_3 social cost models. Each circle indicates a regression model. ‘Excellent’ and ‘Good’ model performance criteria are shown as suggested by Morris et al. (2005).

Table C-29: Evaluations of winter NH_3 social cost 'simple' models.

Model[†]	(1)[‡]	(2)	(3)	(4)	(5)	(6)	(7)
Intercept	190^{***}	180^{***}	180^{***}	170^{***}	58^{***}	50^{***}	62^{***}
ln (Pop_w)	0.81^{***}	0.80^{***}	0.69^{***}	0.69^{***}	0.80^{***}	0.80^{***}	0.72^{***}
ln (Pres)	4.0^{***}	4.6^{***}	4.4^{***}	5.0^{***}	3.6^{**}	4.1^{***}	3.9^{***}
ln (Temp)	-41^{***}	-40^{***}	-39^{***}	-37^{***}	-14^{***}	-13^{***}	-15^{***}
ln (Wind)	-0.11^{+}	-	-0.11^{+}	-	-0.10	-	-0.10
ln (Prec)	-0.26^{*}	-0.27^{*}	-	-	-0.17	-0.18	-
ln (Humid)	1.7^{***}	1.7^{***}	1.5^{***}	1.5^{**}	-	-	-
AIC	25	27	31	33	42	42	42
Adj. R^2	0.90	0.90	0.89	0.88	0.86	0.86	0.86
F. Bias	-0.030	-0.035	-0.0041	-0.010	-0.058	-0.063	-0.038
F. Error	0.33	0.32	0.33	0.32	0.30	0.30	0.30

[†] Seven models with lowest AIC ordered by AIC, [‡] Chosen by AIC, *** $p < 0.001$, ** $p < 0.001$, * $p < 0.05$, $^{+}$ $p < 0.1$, Pop_w [# of people]: population (≥ age 30) weighted with average plume, Pres: pressure [hPa], Temp: temperature [K], Prec: precipitation + 0.0002 [g/m^3] (shifted for log transformation), Wind: wind speed [m/s], Humid: humidity [ppm], AIC: Akaike information criterion, Adj. R^2: adjusted R^2, F. Bias: fractional bias, F. Error: fractional error.

Table C-30: Evaluations of winter NH_3 social cost 'better-fit' models.

Model[†]	(1)[‡]	(2)	(3)	(4)	(5)	(6)	(7)
Intercept	160^{***}	170^{***}	180^{***}	160^{***}	160^{***}	170^{***}	160^{***}
ln (Pop_w)	0.77^{***}	0.76^{***}	0.73^{***}	0.78^{***}	0.77^{***}	0.66^{***}	0.67^{***}
ln (Pres)	3.4^{***}	4.0^{***}	3.1^{**}	3.4^{***}	3.6^{**}	3.0^{**}	3.3^{***}
ln (Temp)	-34^{***}	-37^{***}	-37^{***}	-34^{***}	-34^{***}	-35^{***}	-32^{***}
ln (Wind)	-	-	-	-0.048	-	-	-
ln (Prec)	-0.19^{+}	-0.19^{+}	-0.16	-0.21^{*}	-0.20^{+}	-	-
ln (Humid)	1.2^{**}	1.4^{***}	1.5^{***}	1.2^{**}	1.2^{**}	1.3^{***}	1.1^{**}
ln (TS)	0.37^{***}	0.35^{***}	0.28^{**}	0.34^{**}	0.37^{***}	0.33^{***}	0.40^{***}
ln (TN)	-	-0.11	-	-	-0.026	-	-
ln (TA)	-0.12^{+}	-	-	-0.13^{+}	-0.098	-	-0.086
AIC	16	17	18	18	18	18	19
Adj. R^2	0.92	0.92	0.92	0.92	0.92	0.91	0.91
F. Bias	0.037	0.035	-0.00084	0.039	0.040	0.018	0.049
F. Error	0.25	0.26	0.26	0.26	0.25	0.25	0.25

[†] Seven models with lowest AIC ordered by AIC, [‡] Chosen by AIC, *** $p < 0.001$, ** $p < 0.001$, * $p < 0.05$, $^{+}$ $p < 0.1$, Pop_w [# of people]: population (≥ age 30) weighted with average plume, Pres: pressure [hPa], Temp: temperature [K], Prec: precipitation + 0.0002 [g/m^3] (shifted for log transformation), Wind: wind speed [m/s], Humid: humidity [ppm], TS: total sulfate (≡ $[{SO_4}^{2-}]$) [$\mu mol/m^3$], TN: total nitrate (≡ $[HNO_3]$ + $[{NO_3}^{-}]$) [$\mu mol/m^3$], TA: total ammonia (≡ $[NH_3]$ + $[{NH_4}^{+}]$) [$\mu mol/m^3$], AIC: Akaike information criterion, Adj. R^2: adjusted R^2, F. Bias: fractional bias, F. Error: fractional error.

Table C-31: Evaluations of spring NH_3 social cost 'simple' models.

Model[†]	(1)[‡]	(2)	(3)	(4)	(5)	(6)	(7)
Intercept	$99^{\star\star}$	$110^{\star\star}$	$110^{\star\star}$	$120^{\star\star}$	$93^{\star}$	$110^{\star\star}$	$97^{\star}$
ln (Pop_w)	$0.90^{\star\star\star}$	$0.98^{\star\star\star}$	$0.91^{\star\star\star}$	$1.0^{\star\star\star}$	$0.90^{\star\star\star}$	$0.98^{\star\star\star}$	$0.90^{\star\star\star}$
ln (Pres)	2.4	-	2.6	-	3.0	-	2.5
ln (Temp)	$-22^{\star\star}$	$-21^{\star\star}$	$-23^{\star\star\star}$	$-23^{\star\star}$	$-21^{\star\star}$	$-22^{\star\star}$	$-21^{\star\star}$
ln (Wind)	-0.13	-0.13	-	-	-	-0.15	-0.12
ln (Prec)	-	-	-	-	0.051	-0.032	0.0089
ln (Humid)	$0.93^{\star}$	$1.2^{\star\star\star}$	$0.95^{\star}$	$1.3^{\star\star\star}$	0.81^{+}	$1.3^{\star\star}$	0.91^{+}
AIC	77	77	77	77	79	79	79
Adj. R^2	0.83	0.82	0.82	0.82	0.82	0.82	0.82
F. Bias	-0.25	-0.27	-0.27	-0.29	-0.27	-0.27	-0.25
F. Error	0.35	0.35	0.36	0.37	0.36	0.35	0.35

[†] Seven models with lowest AIC ordered by AIC, [‡] Chosen by AIC, *** $p < 0.001$, ** $p < 0.001$, * $p < 0.05$, $^{+}$ $p < 0.1$, Pop_w [# of people]: population (≥ age 30) weighted with average plume, Pres: pressure [hPa], Temp: temperature [K], Prec: precipitation + 0.0002 [g/m^3] (shifted for log transformation), Wind: wind speed [m/s], Humid: humidity [ppm], AIC: Akaike information criterion, Adj. R^2: adjusted R^2, F. Bias: fractional bias, F. Error: fractional error.

Table C-32: Evaluations of spring NH_3 social cost 'better-fit' models.

Model[†]	(1)[‡]	(2)	(3)	(4)	(5)	(6)	(7)
Intercept	$89^{\star\star\star}$	$82^{\star\star\star}$	$97^{\star\star\star}$	$84^{\star\star}$	$90^{\star\star\star}$	$84^{\star\star\star}$	$100^{\star\star\star}$
ln (Pop_w)	$0.81^{\star\star\star}$	$0.80^{\star\star\star}$	$0.82^{\star\star\star}$	$0.81^{\star\star\star}$	$0.81^{\star\star\star}$	$0.83^{\star\star\star}$	$0.82^{\star\star\star}$
ln (Pres)	$2.7^{\star}$	$2.7^{\star}$	$2.6^{\star}$	$2.7^{\star}$	$2.9^{\star}$	-	$2.9^{\star}$
ln (Temp)	$-18^{\star\star\star}$	$-17^{\star\star\star}$	$-20^{\star\star\star}$	$-17^{\star\star}$	$-18^{\star\star\star}$	$-14^{\star\star\star}$	$-21^{\star\star\star}$
ln (Wind)	$-0.13^{\star}$	$-0.12^{\star}$	$-0.14^{\star}$	$-0.12^{\star}$	-	$-0.14^{\star\star}$	-
ln (Prec)	-	0.042	-	0.039	0.064	-	-
ln (Humid)	-	-	0.18	0.033	-	-	-
ln (TS)	$1.3^{\star\star\star}$	$1.3^{\star\star\star}$	$1.3^{\star\star\star}$	$1.3^{\star\star\star}$	$1.3^{\star\star\star}$	$1.4^{\star\star\star}$	$1.4^{\star\star\star}$
ln (TN)	$-0.24^{\star\star}$	$-0.22^{\star}$	$-0.26^{\star\star}$	$-0.22^{\star}$	$-0.23^{\star\star}$	-0.14^{+}	$-0.28^{\star\star}$
ln (TA)	$-0.33^{\star\star\star}$	$-0.35^{\star\star\star}$	$-0.33^{\star\star\star}$	$-0.35^{\star\star\star}$	$-0.32^{\star\star\star}$	$-0.36^{\star\star\star}$	$-0.28^{\star\star\star}$
AIC	12	12	13	14	17	17	17
Adj. R^2	0.95	0.95	0.95	0.95	0.95	0.95	0.95
F. Bias	0.075	0.067	0.070	0.066	0.047	0.059	0.057
F. Error	0.21	0.20	0.21	0.20	0.20	0.20	0.21

[†] Seven models with lowest AIC ordered by AIC, [‡] Chosen by AIC, *** $p < 0.001$, ** $p < 0.001$, * $p < 0.05$, $^{+}$ $p < 0.1$, Pop_w [# of people]: population (≥ age 30) weighted with average plume, Pres: pressure [hPa], Temp: temperature [K], Prec: precipitation + 0.0002 [g/m^3] (shifted for log transformation), Wind: wind speed [m/s], Humid: humidity [ppm], TS: total sulfate (≡ $[SO_4{}^{2-}]$) [$\mu mol/m^3$], TN: total nitrate (≡ $[HNO_3]$ + $[NO_3{}^-]$) [$\mu mol/m^3$], TA: total ammonia (≡ $[NH_3]$ + $[NH_4{}^+]$) [$\mu mol/m^3$], AIC: Akaike information criterion, Adj. R^2: adjusted R^2, F. Bias: fractional bias, F. Error: fractional error.

Table C-33: Evaluations of summer NH_3 social cost 'simple' models.

Model[†]	(1)[‡]	(2)	(3)	(4)	(5)	(6)	(7)
Intercept	$54^{\star}$	$82^{\star}$	$120^{\star\star\star}$	$110^{\star\star}$	$110^{\star\star}$	45	$-20^{\star}$
ln (Pop_w)	$0.78^{\star\star\star}$	$0.77^{\star\star\star}$	$0.83^{\star\star\star}$	$0.76^{\star\star\star}$	$0.86^{\star\star\star}$	$0.85^{\star\star\star}$	$0.82^{\star\star\star}$
ln (Pres)	$4.8^{\star\star\star}$	3.6^{+}	-	2.0	-	$5.2^{\star\star\star}$	$3.3^{\star}$
ln (Temp)	$-15^{\star\star}$	$-19^{\star\star}$	$-24^{\star\star\star}$	$-24^{\star\star\star}$	$-22^{\star\star}$	$-14^{\star}$	-
ln (Wind)	$-0.31^{\star\star}$	$-0.32^{\star\star}$	$-0.37^{\star\star}$	$-0.37^{\star\star\star}$	$-0.34^{\star\star}$	-	$-0.28^{\star}$
ln (Prec)	$0.21^{\star\star}$	0.15	-	-	0.057	$0.27^{\star\star\star}$	$0.20^{\star\star}$
ln (Humid)	-	0.54	$1.4^{\star\star\star}$	$1.2^{\star\star}$	$1.2^{\star\star}$	-	-
AIC	73	74	75	75	76	80	80
Adj. R^2	0.85	0.85	0.84	0.84	0.84	0.83	0.83
F. Bias	−0.23	−0.23	−0.25	−0.25	−0.25	−0.28	−0.30
F. Error	0.40	0.40	0.40	0.40	0.40	0.46	0.48

[†] Seven models with lowest AIC ordered by AIC, [‡] Chosen by AIC, *** $p < 0.001$, ** $p < 0.001$, * $p < 0.05$, $^{+}$ $p < 0.1$, Pop_w [# of people]: population (≥ age 30) weighted with average plume, Pres: pressure [hPa], Temp: temperature [K], Prec: precipitation + 0.0002 [g/m^3] (shifted for log transformation), Wind: wind speed [m/s], Humid: humidity [ppm], AIC: Akaike information criterion, Adj. R^2: adjusted R^2, F. Bias: fractional bias, F. Error: fractional error.

Table C-34: Evaluations of summer NH_3 social cost 'better-fit' models.

Model[†]	(1)[‡]	(2)	(3)	(4)	(5)	(6)	(7)
Intercept	$75^{\star\star}$	46	41	−12	$79^{\star\star}$	−13	−8.7
ln (Pop_w)	$0.81^{\star\star\star}$	$0.78^{\star\star\star}$	$0.82^{\star\star\star}$	$0.75^{\star\star\star}$	$0.85^{\star\star\star}$	$0.78^{\star\star\star}$	$0.72^{\star\star\star}$
ln (Pres)	$4.5^{\star\star}$	$4.9^{\star\star}$	$5.3^{\star\star\star}$	$4.6^{\star\star}$	$4.8^{\star\star}$	$5.0^{\star\star}$	$3.8^{\star}$
ln (Temp)	$-18^{\star\star\star}$	-12^{+}	−11	-	$-19^{\star\star\star}$	-	-
ln (Wind)	$-0.17^{\star}$	-0.15^{+}	-	−0.14	-	-	$-0.20^{\star}$
ln (Prec)	$0.16^{\star\star}$	$0.21^{\star\star}$	$0.23^{\star\star}$	$0.27^{\star\star\star}$	$0.17^{\star\star}$	$0.29^{\star\star\star}$	$0.27^{\star\star\star}$
ln (Humid)	-	−0.66	−0.86	$-1.4^{\star\star\star}$	-	$-1.5^{\star\star\star}$	$-1.2^{\star\star}$
ln (TS)	$0.84^{\star\star\star}$	$1.0^{\star\star\star}$	$1.2^{\star\star\star}$	$1.2^{\star\star\star}$	$0.97^{\star\star\star}$	$1.3^{\star\star\star}$	$0.91^{\star\star\star}$
ln (TN)	$-0.24^{\star}$	$-0.23^{\star}$	$-0.28^{\star\star}$	-0.15^{+}	$-0.32^{\star\star}$	$-0.21^{\star}$	-
ln (TA)	$-0.32^{\star\star\star}$	$-0.33^{\star\star\star}$	$-0.34^{\star\star\star}$	$-0.37^{\star\star\star}$	$-0.32^{\star\star\star}$	$-0.37^{\star\star\star}$	$-0.37^{\star\star\star}$
AIC	45	45	47	47	48	48	48
Adj. R^2	0.92	0.92	0.92	0.92	0.91	0.91	0.91
F. Bias	−0.048	−0.030	−0.026	−0.045	−0.048	−0.040	−0.083
F. Error	0.21	0.22	0.25	0.25	0.25	0.27	0.26

[†] Seven models with lowest AIC ordered by AIC, [‡] Chosen by AIC, *** $p < 0.001$, ** $p < 0.001$, * $p < 0.05$, $^{+}$ $p < 0.1$, Pop_w [# of people]: population (≥ age 30) weighted with average plume, Pres: pressure [hPa], Temp: temperature [K], Prec: precipitation + 0.0002 [g/m^3] (shifted for log transformation), Wind: wind speed [m/s], Humid: humidity [ppm], TS: total sulfate (≡ $[SO_4{}^{2-}]$) [$\mu mol/m^3$], TN: total nitrate (≡ $[HNO_3]$ + $[NO_3{}^-]$) [$\mu mol/m^3$], TA: total ammonia (≡ $[NH_3]$ + $[NH_4{}^+]$) [$\mu mol/m^3$], AIC: Akaike information criterion, Adj. R^2: adjusted R^2, F. Bias: fractional bias, F. Error: fractional error.

Table C-35: Evaluations of fall NH_3 social cost 'simple' models.

Model[†]	(1)[‡]	(2)	(3)	(4)	(5)	(6)	(7)
Intercept	$210^{\star\star\star}$	$170^{\star\star\star}$	$180^{\star\star\star}$	$150^{\star\star\star}$	$230^{\star\star\star}$	$200^{\star\star\star}$	$210^{\star\star\star}$
ln (Pop_w)	$0.64^{\star\star\star}$	$0.58^{\star\star\star}$	$0.69^{\star\star\star}$	$0.64^{\star\star\star}$	$0.75^{\star\star\star}$	$0.70^{\star\star\star}$	$0.84^{\star\star\star}$
ln (Pres)	$3.5^{\star\star}$	$3.6^{\star\star}$	$3.8^{\star\star\star}$	$4.0^{\star\star\star}$	-	-	-
ln (Temp)	$-43^{\star\star\star}$	$-37^{\star\star\star}$	$-39^{\star\star\star}$	$-32^{\star\star\star}$	$-44^{\star\star\star}$	$-38^{\star\star\star}$	$-40^{\star\star\star}$
ln (Wind)	$-0.21^{\star}$	$-0.23^{\star}$	-	-	$-0.26^{\star\star}$	$-0.27^{\star\star}$	-
ln (Prec)	$-0.14^{\star}$	-	$-0.15^{\star}$	-	$-0.15^{\star}$	-	$-0.16^{\star}$
ln (Humid)	$1.9^{\star\star\star}$	$1.6^{\star\star\star}$	$1.8^{\star\star\star}$	$1.4^{\star\star}$	$2.5^{\star\star\star}$	$2.2^{\star\star\star}$	$2.3^{\star\star\star}$
AIC	29	32	34	37	40	42	45
Adj. R^2	0.88	0.87	0.87	0.85	0.85	0.84	0.83
F. Bias	−0.0039	0.0082	−0.045	−0.034	−0.013	0.00047	−0.067
F. Error	0.39	0.41	0.35	0.36	0.41	0.42	0.37

[†] Seven models with lowest AIC ordered by AIC, [‡] Chosen by AIC, *** $p < 0.001$, ** $p < 0.001$, * $p < 0.05$, $^{+}$ $p < 0.1$, Pop_w [# of people]: population (≥ age 30) weighted with average plume, Pres: pressure [hPa], Temp: temperature [K], Prec: precipitation + 0.0002 [g/m^3] (shifted for log transformation), Wind: wind speed [m/s], Humid: humidity [ppm], AIC: Akaike information criterion, Adj. R^2: adjusted R^2, F. Bias: fractional bias, F. Error: fractional error.

Table C-36: Evaluations of fall NH_3 social cost 'better-fit' models.

Model[†]	(1)[‡]	(2)	(3)	(4)	(5)	(6)	(7)
Intercept	$160^{\star\star\star}$	$140^{\star\star\star}$	$170^{\star\star\star}$	$160^{\star\star\star}$	$160^{\star\star\star}$	$150^{\star\star\star}$	$160^{\star\star\star}$
ln (Pop_w)	$0.50^{\star\star\star}$	$0.52^{\star\star\star}$	$0.53^{\star\star\star}$	$0.54^{\star\star\star}$	$0.50^{\star\star\star}$	$0.51^{\star\star\star}$	$0.50^{\star\star\star}$
ln (Pres)	2.0^{+}	1.9^{+}	$2.1^{\star}$	2.1^{+}	1.8	1.6	2.0
ln (Temp)	$-31^{\star\star\star}$	$-28^{\star\star\star}$	$-34^{\star\star\star}$	$-31^{\star\star\star}$	$-31^{\star\star\star}$	$-28^{\star\star\star}$	$-31^{\star\star\star}$
ln (Wind)	−0.12	-	−0.13	-	−0.12	-	−0.12
ln (Prec)	-	-	−0.060	−0.051	-	-	-
ln (Humid)	$1.2^{\star\star}$	$1.00^{\star\star}$	$1.3^{\star\star}$	$1.1^{\star\star}$	$1.2^{\star\star}$	$1.1^{\star\star}$	$1.2^{\star\star}$
ln (TS)	$0.44^{\star\star\star}$	$0.50^{\star\star\star}$	$0.39^{\star\star}$	$0.46^{\star\star\star}$	$0.44^{\star\star\star}$	$0.48^{\star\star\star}$	$0.44^{\star\star\star}$
ln (TN)	-	-	-	-	-	-	−0.0040
ln (TA)	-	-	-	-	0.018	0.043	-
AIC	20	21	21	22	22	22	22
Adj. R^2	0.90	0.90	0.90	0.90	0.90	0.90	0.90
F. Bias	0.081	0.070	0.067	0.058	0.074	0.056	0.082
F. Error	0.31	0.28	0.31	0.27	0.30	0.28	0.31

[†] Seven models with lowest AIC ordered by AIC, [‡] Chosen by AIC, *** $p < 0.001$, ** $p < 0.001$, * $p < 0.05$, $^{+}$ $p < 0.1$, Pop_w [# of people]: population (≥ age 30) weighted with average plume, Pres: pressure [hPa], Temp: temperature [K], Prec: precipitation + 0.0002 [g/m^3] (shifted for log transformation), Wind: wind speed [m/s], Humid: humidity [ppm], TS: total sulfate (≡ $[SO_4{}^{2-}]$) [$\mu mol/m^3$], TN: total nitrate (≡ $[HNO_3]$ + $[NO_3{}^-]$) [$\mu mol/m^3$], TA: total ammonia (≡ $[NH_3]$ + $[NH_4{}^+]$) [$\mu mol/m^3$], AIC: Akaike information criterion, Adj. R^2: adjusted R^2, F. Bias: fractional bias, F. Error: fractional error.

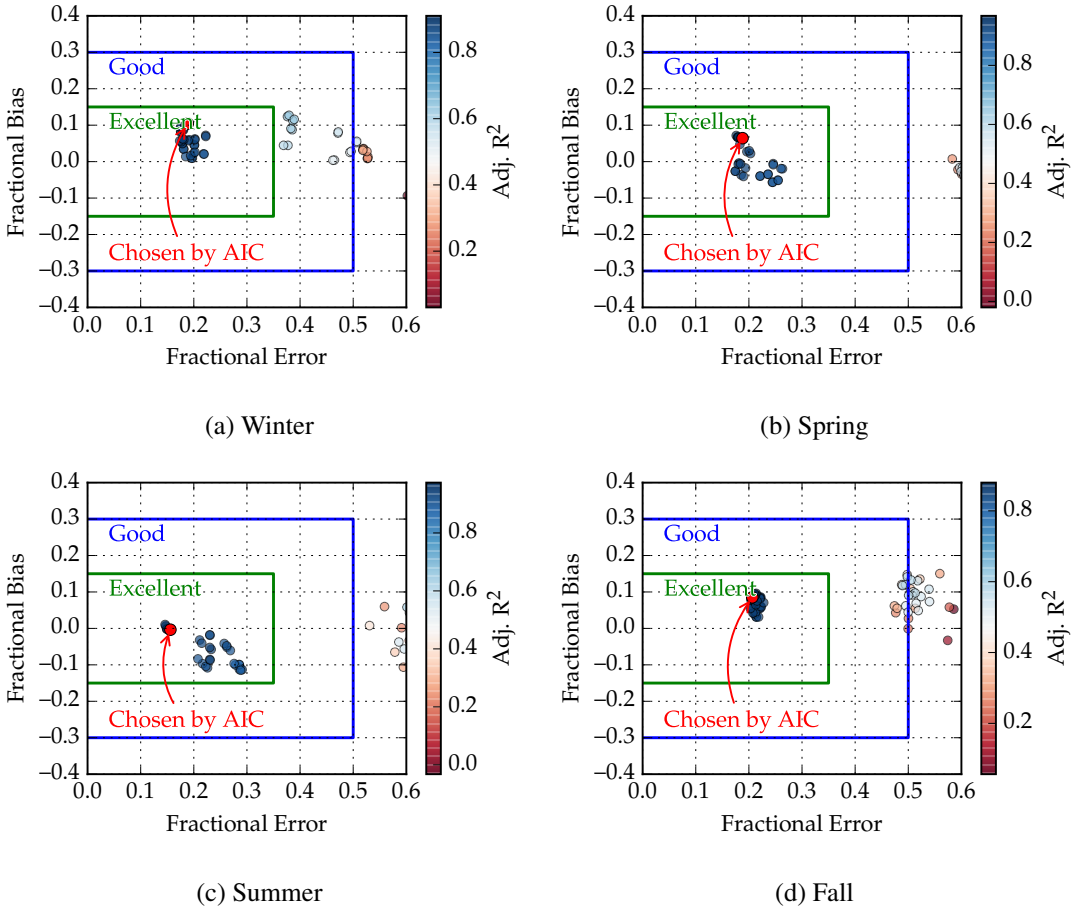

(a) Winter

(b) Spring

(c) Summer

(d) Fall

Figure C-40: Evaluations of EC intake fraction models. Each circle indicates a regression model. 'Excellent' and 'Good' model performance criteria are shown as suggested by Morris et al. (2005).

Table C-37: Evaluations of winter EC intake fraction models.

Model[†]	(1)[‡]	(2)	(3)	(4)	(5)	(6)	(7)
Intercept	$74^{\star\star}$	$78^{\star\star}$	$69^{\star}$	$74^{\star\star}$	$20^{\star}$	17	$20^{\star}$
ln (Pop_w)	$0.65^{\star\star\star}$	$0.69^{\star\star\star}$	$0.65^{\star\star\star}$	$0.69^{\star\star\star}$	$0.67^{\star\star\star}$	$0.67^{\star\star\star}$	$0.69^{\star\star\star}$
ln (Pres)	$2.9^{\star\star\star}$	$2.8^{\star\star\star}$	$3.1^{\star\star\star}$	$3.0^{\star\star\star}$	$2.7^{\star\star\star}$	$2.9^{\star\star\star}$	$2.6^{\star\star\star}$
ln (Temp)	$-19^{\star\star\star}$	$-20^{\star\star\star}$	$-18^{\star\star}$	$-19^{\star\star\star}$	$-8.1^{\star\star\star}$	$-7.7^{\star\star\star}$	$-7.9^{\star\star\star}$
ln (Wind)	-	-	0.041	0.042	-	0.045	-
ln (Prec)	-	−0.094	-	−0.095	-	-	−0.051
ln (Humid)	$0.70^{\star}$	$0.78^{\star}$	$0.69^{\star}$	$0.77^{\star}$	-	-	-
AIC	3.0	3.5	4.2	4.6	6.2	7.3	7.8
Adj. R^2	0.91	0.91	0.91	0.91	0.90	0.90	0.90
F. Bias	0.10	0.096	0.10	0.093	0.089	0.086	0.083
F. Error	0.19	0.18	0.19	0.17	0.18	0.18	0.18

[†] Seven models with lowest AIC ordered by AIC, [‡] Chosen by AIC, *** $p < 0.001$, ** $p < 0.001$, * $p < 0.05$, $^{+}$ $p < 0.1$, Pop_w [# of people]: population weighted with average plume, Pres: pressure [hPa], Temp: temperature [K], Prec: precipitation + 0.0002 [$\mathrm{g/m^3}$] (shifted for log transformation), Wind: wind speed [$\mathrm{m/s}$], Humid: humidity [ppm], AIC: Akaike information criterion, Adj. R^2: adjusted R^2, F. Bias: fractional bias, F. Error: fractional error.

Table C-38: Evaluations of spring EC intake fraction models.

Model[†]	(1)[‡]	(2)	(3)	(4)	(5)	(6)	(7)
Intercept	$46^{\star\star\star}$	$69^{\star\star\star}$	$57^{\star\star\star}$	$48^{\star\star\star}$	$70^{\star\star\star}$	$46^{\star\star\star}$	$57^{\star\star\star}$
ln (Pop_w)	$0.76^{\star\star\star}$	$0.77^{\star\star\star}$	$0.77^{\star\star\star}$	$0.76^{\star\star\star}$	$0.77^{\star\star\star}$	$0.76^{\star\star\star}$	$0.77^{\star\star\star}$
ln (Pres)	$5.5^{\star\star\star}$	$4.8^{\star\star\star}$	$5.1^{\star\star\star}$	$5.5^{\star\star\star}$	$4.7^{\star\star\star}$	$5.5^{\star\star\star}$	$5.1^{\star\star\star}$
ln (Temp)	$-16^{\star\star\star}$	$-20^{\star\star\star}$	$-18^{\star\star\star}$	$-16^{\star\star\star}$	$-20^{\star\star\star}$	$-16^{\star\star\star}$	$-18^{\star\star\star}$
ln (Wind)	-	-	-	-	−0.023	0.00062	0.0020
ln (Prec)	-	−0.044	-	−0.018	−0.052	-	-
ln (Humid)	-	0.31^{+}	0.18	-	0.33^{+}	-	0.18
AIC	−18	−18	−17	−16	−16	−16	−15
Adj. R^2	0.97	0.97	0.97	0.97	0.97	0.97	0.97
F. Bias	0.064	0.068	0.067	0.064	0.072	0.064	0.067
F. Error	0.19	0.18	0.18	0.19	0.18	0.19	0.18

[†] Seven models with lowest AIC ordered by AIC, [‡] Chosen by AIC, *** $p < 0.001$, ** $p < 0.001$, * $p < 0.05$, $^{+}$ $p < 0.1$, Pop_w [# of people]: population weighted with average plume, Pres: pressure [hPa], Temp: temperature [K], Prec: precipitation + 0.0002 [$\mathrm{g/m^3}$] (shifted for log transformation), Wind: wind speed [$\mathrm{m/s}$], Humid: humidity [ppm], AIC: Akaike information criterion, Adj. R^2: adjusted R^2, F. Bias: fractional bias, F. Error: fractional error.

Table C-39: Evaluations of summer EC intake fraction models.

Model[†]	(1)[‡]	(2)	(3)	(4)	(5)	(6)	(7)
Intercept	54^{***}	52^{***}	54^{***}	72^{***}	70^{***}	52^{***}	71^{***}
ln (Pop_w)	0.80^{***}	0.80^{***}	0.80^{***}	0.79^{***}	0.79^{***}	0.80^{***}	0.80^{***}
ln (Pres)	5.8^{***}	5.9^{***}	5.8^{***}	5.1^{***}	5.1^{***}	5.9^{***}	5.1^{***}
ln (Temp)	-17^{***}	-17^{***}	-17^{***}	-20^{***}	-20^{***}	-17^{***}	-20^{***}
ln (Wind)	-	-	0.00014	-	-	0.0047	0.016
ln (Prec)	-	0.011	-	-	−0.030	0.012	-
ln (Humid)	-0.30^{*}	-0.35^{+}	-0.30^{*}	-	-	-0.35^{+}	-
AIC	−25	−24	−23	−22	−22	−22	−20
Adj. R^2	0.97	0.97	0.97	0.97	0.97	0.97	0.97
F. Bias	−0.0036	−0.0013	−0.0036	0.011	−0.0019	−0.0021	0.0064
F. Error	0.16	0.16	0.16	0.15	0.15	0.16	0.15

[†] Seven models with lowest AIC ordered by AIC, [‡] Chosen by AIC, *** $p < 0.001$, ** $p < 0.001$, * $p < 0.05$, $^{+}$ $p < 0.1$, Pop_w [# of people]: population weighted with average plume, Pres: pressure [hPa], Temp: temperature [K], Prec: precipitation + 0.0002 [$\mathrm{g/m^3}$] (shifted for log transformation), Wind: wind speed [$\mathrm{m/s}$], Humid: humidity [ppm], AIC: Akaike information criterion, Adj. R^2: adjusted R^2, F. Bias: fractional bias, F. Error: fractional error.

Table C-40: Evaluations of fall EC intake fraction models.

Model[†]	(1)[‡]	(2)	(3)	(4)	(5)	(6)	(7)
Intercept	25^{*}	49^{*}	20	23^{+}	45^{+}	47^{+}	19
ln (Pop_w)	0.66^{***}	0.65^{***}	0.64^{***}	0.66^{***}	0.65^{***}	0.66^{***}	0.65^{***}
ln (Pres)	2.9^{***}	2.5^{**}	2.9^{***}	3.0^{***}	2.5^{**}	2.5^{**}	2.9^{***}
ln (Temp)	-9.2^{***}	-14^{**}	-8.3^{**}	-8.8^{**}	-13^{*}	-13^{**}	-8.0^{**}
ln (Wind)	-	-	-	0.038	-	0.019	0.031
ln (Prec)	-	-	0.039	-	0.016	-	0.036
ln (Humid)	-	0.43	-	-	0.39	0.41	-
AIC	14	14	15	15	16	16	17
Adj. R^2	0.88	0.88	0.88	0.88	0.88	0.88	0.87
F. Bias	0.085	0.095	0.090	0.079	0.096	0.091	0.085
F. Error	0.21	0.21	0.21	0.20	0.21	0.21	0.21

[†] Seven models with lowest AIC ordered by AIC, [‡] Chosen by AIC, *** $p < 0.001$, ** $p < 0.001$, * $p < 0.05$, $^{+}$ $p < 0.1$, Pop_w [# of people]: population weighted with average plume, Pres: pressure [hPa], Temp: temperature [K], Prec: precipitation + 0.0002 [$\mathrm{g/m^3}$] (shifted for log transformation), Wind: wind speed [$\mathrm{m/s}$], Humid: humidity [ppm], AIC: Akaike information criterion, Adj. R^2: adjusted R^2, F. Bias: fractional bias, F. Error: fractional error.

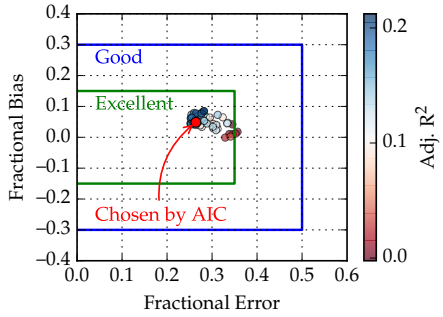

(a) Winter: ‘simple’ models

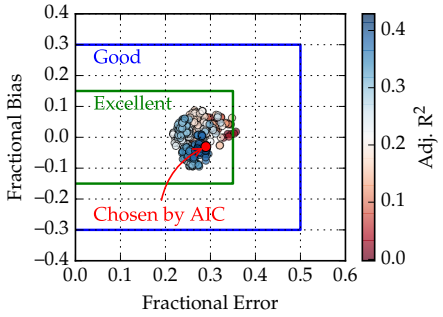

(b) Winter: ‘better-fit’ models

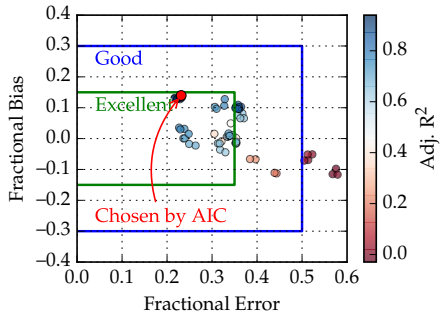

(c) Spring: ‘simple’ models

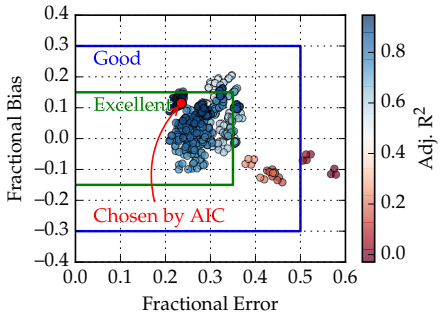

(d) Spring: ‘better-fit’ models

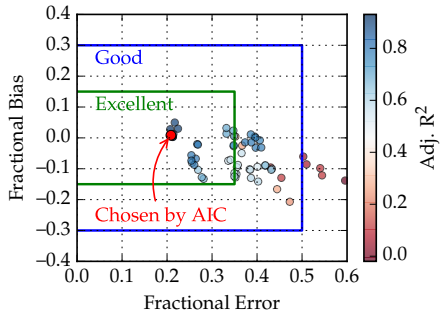

(e) Summer: ‘simple’ models

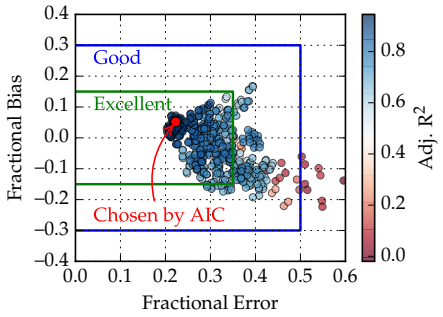

(f) Summer: ‘better-fit’ models

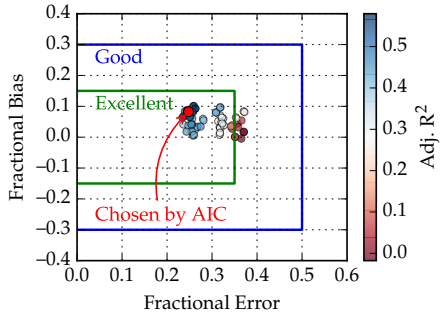

(g) Fall: ‘simple’ models

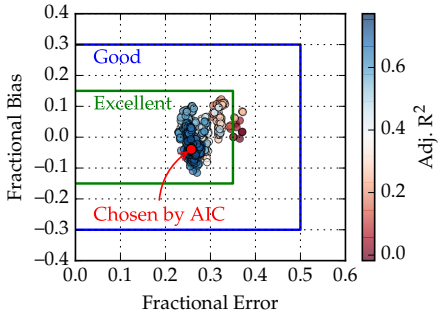

(h) Fall: ‘better-fit’ models

Figure C-41: Evaluations of SO_2 intake fraction models. Each circle indicates a regression model. ‘Excellent’ and ‘Good’ model performance criteria are shown as suggested by Morris et al. (2005).

Table C-41: Evaluations of winter SO_2 intake fraction 'simple' models.

Model[†]	(1)[‡]	(2)	(3)	(4)	(5)	(6)	(7)
Intercept	$-20^{\star\star\star}$	$-15^{\star}$	63	50	-4.4	-15	$-21^{\star\star}$
ln (Pop_w)	-	-	-	-	-	-	-
ln (Pres)	$2.7^{\star\star}$	$2.0^{\star}$	$2.4^{\star}$	$3.0^{\star\star}$	$2.3^{\star}$	$2.9^{\star\star}$	$2.8^{\star\star}$
ln (Temp)	-	-	-16	-14	-2.2	-1.1	-
ln (Wind)	-	-0.11	-0.13	-	-0.13	-	-
ln (Prec)	-	-	-	-	-	-	-0.033
ln (Humid)	-	-	0.87	0.83	-	-	-
AIC	62	62	63	64	64	64	64
Adj. R^2	0.19	0.20	0.21	0.19	0.19	0.17	0.17
F. Bias	0.049	0.047	0.085	0.077	0.064	0.057	0.045
F. Error	0.26	0.26	0.28	0.28	0.26	0.26	0.26

[†] Seven models with lowest AIC ordered by AIC, [‡] Chosen by AIC, *** $p < 0.001$, ** $p < 0.001$, * $p < 0.05$, $^{+}$ $p < 0.1$, Pop_w [# of people]: population weighted with average plume, Pres: pressure [hPa], Temp: temperature [K], Prec: precipitation + 0.0002 [g/m^3] (shifted for log transformation), Wind: wind speed [m/s], Humid: humidity [ppm], AIC: Akaike information criterion, Adj. R^2: adjusted R^2, F. Bias: fractional bias, F. Error: fractional error.

Table C-42: Evaluations of winter SO_2 intake fraction 'better-fit' models.

Model[†]	(1)[‡]	(2)	(3)	(4)	(5)	(6)	(7)
Intercept	59	81^{+}	$-5.8^{\star\star}$	$-3.3^{\star\star\star}$	61	61	84^{+}
ln (Pop_w)	-	0.30	-	-	-	0.052	-
ln (Pres)	-	-	-	-	-	-	-
ln (Temp)	-13	-18^{+}	-	-	-13	-13	$-18^{\star}$
ln (Wind)	$-0.20^{\star}$	$-0.24^{\star}$	$-0.19^{\star}$	$-0.23^{\star}$	$-0.21^{\star}$	$-0.21^{\star}$	-0.18^{+}
ln (Prec)	-	-0.26^{+}	-	-	-0.090	-	-
ln (Humid)	1.0^{+}	$1.4^{\star}$	0.27	-	1.1^{+}	1.1^{+}	$1.4^{\star\star}$
ln (TS)	$-0.42^{\star\star}$	$-0.57^{\star\star}$	$-0.38^{\star}$	$-0.31^{\star}$	$-0.43^{\star\star}$	$-0.44^{\star\star}$	$-0.47^{\star\star}$
ln (TN)	$0.51^{\star\star\star}$	$0.48^{\star\star\star}$	$0.53^{\star\star\star}$	$0.52^{\star\star\star}$	$0.53^{\star\star\star}$	$0.49^{\star\star\star}$	$0.35^{\star\star\star}$
ln (TA)	-0.26^{+}	-0.26^{+}	$-0.32^{\star}$	$-0.36^{\star\star}$	-0.27^{+}	-0.25^{+}	-
AIC	50	50	50	51	51	52	52
Adj. R^2	0.41	0.43	0.40	0.38	0.41	0.40	0.38
F. Bias	-0.030	-0.036	-0.037	0.0043	-0.044	-0.024	-0.065
F. Error	0.29	0.27	0.28	0.28	0.29	0.29	0.29

[†] Seven models with lowest AIC ordered by AIC, [‡] Chosen by AIC, *** $p < 0.001$, ** $p < 0.001$, * $p < 0.05$, $^{+}$ $p < 0.1$, Pop_w [# of people]: population weighted with average plume, Pres: pressure [hPa], Temp: temperature [K], Prec: precipitation + 0.0002 [g/m^3] (shifted for log transformation), Wind: wind speed [m/s], Humid: humidity [ppm], TS: total sulfate (≡ $[SO_4{}^{2-}]$) [μmol/m^3], TN: total nitrate (≡ $[HNO_3]$ + $[NO_3{}^{-}]$) [μmol/m^3], TA: total ammonia (≡ $[NH_3]$ + $[NH_4{}^{+}]$) [μmol/m^3], AIC: Akaike information criterion, Adj. R^2: adjusted R^2, F. Bias: fractional bias, F. Error: fractional error.

Table C-43: Evaluations of spring SO_2 intake fraction 'simple' models.

Model[†]	(1)[‡]	(2)	(3)	(4)	(5)	(6)	(7)
Intercept	$110^{\star\star\star}$	$100^{\star\star\star}$	$81^{\star\star\star}$	$77^{\star\star\star}$	$87^{\star\star\star}$	$80^{\star\star\star}$	$76^{\star\star\star}$
ln (Pop_w)	$0.44^{\star\star\star}$	$0.45^{\star\star\star}$	$0.44^{\star\star\star}$	$0.43^{\star\star\star}$	$0.43^{\star\star\star}$	$0.44^{\star\star\star}$	$0.43^{\star\star\star}$
ln (Pres)	$6.4^{\star\star\star}$	$6.6^{\star\star\star}$	$7.4^{\star\star\star}$	$7.4^{\star\star\star}$	$7.0^{\star\star\star}$	$7.3^{\star\star\star}$	$7.4^{\star\star\star}$
ln (Temp)	$-28^{\star\star\star}$	$-28^{\star\star\star}$	$-24^{\star\star\star}$	$-24^{\star\star\star}$	$-25^{\star\star\star}$	$-24^{\star\star\star}$	$-23^{\star\star\star}$
ln (Wind)	-0.047	-	-	-	-	-0.031	-0.0089
ln (Prec)	$-0.082^{\star\star}$	$-0.065^{\star}$	-0.037	-	-	-0.046^{+}	-
ln (Humid)	$0.39^{\star}$	$0.35^{\star}$	-	-	0.16	-	-
AIC	-30	-30	-27	-26	-26	-26	-24
Adj. R^2	0.94	0.94	0.93	0.93	0.93	0.93	0.93
F. Bias	0.14	0.13	0.13	0.13	0.13	0.13	0.13
F. Error	0.23	0.23	0.23	0.22	0.22	0.23	0.22

[†] Seven models with lowest AIC ordered by AIC, [‡] Chosen by AIC, *** $p < 0.001$, ** $p < 0.001$, * $p < 0.05$, $^{+}$ $p < 0.1$, Pop_w [# of people]: population weighted with average plume, Pres: pressure [hPa], Temp: temperature [K], Prec: precipitation + 0.0002 [g/m^3] (shifted for log transformation), Wind: wind speed [m/s], Humid: humidity [ppm], AIC: Akaike information criterion, Adj. R^2: adjusted R^2, F. Bias: fractional bias, F. Error: fractional error.

Table C-44: Evaluations of spring SO_2 intake fraction 'better-fit' models.

Model[†]	(1)[‡]	(2)	(3)	(4)	(5)	(6)	(7)
Intercept	$88^{\star\star\star}$	$63^{\star\star\star}$	$110^{\star\star\star}$	$67^{\star\star\star}$	$59^{\star\star\star}$	$110^{\star\star\star}$	$69^{\star\star\star}$
ln (Pop_w)	$0.46^{\star\star\star}$	$0.34^{\star\star\star}$	$0.54^{\star\star\star}$	$0.35^{\star\star\star}$	$0.36^{\star\star\star}$	$0.53^{\star\star\star}$	$0.41^{\star\star\star}$
ln (Pres)	$6.3^{\star\star\star}$	$6.3^{\star\star\star}$	$6.6^{\star\star\star}$	$6.4^{\star\star\star}$	$6.4^{\star\star\star}$	$6.7^{\star\star\star}$	$6.3^{\star\star\star}$
ln (Temp)	$-25^{\star\star\star}$	$-20^{\star\star\star}$	$-30^{\star\star\star}$	$-20^{\star\star\star}$	$-19^{\star\star\star}$	$-29^{\star\star\star}$	$-21^{\star\star\star}$
ln (Wind)	$-0.068^{\star}$	-0.045	-0.064^{+}	-	-0.050	$-0.071^{\star}$	-0.052
ln (Prec)	-0.050	-	$-0.084^{\star\star}$	-	-	$-0.076^{\star\star}$	-
ln (Humid)	0.41^{+}	-	$0.62^{\star\star}$	-	-	$0.59^{\star\star}$	0.20
ln (TS)	-0.17^{+}	-	$-0.21^{\star}$	-	-0.093	-0.18^{+}	-0.15
ln (TN)	0.096	$0.16^{\star\star}$	-	$0.15^{\star\star}$	$0.17^{\star\star}$	-	$0.15^{\star\star}$
ln (TA)	-0.079^{+}	$-0.13^{\star\star}$	-	$-0.11^{\star\star}$	$-0.12^{\star\star}$	-0.038	$-0.11^{\star\star}$
AIC	-35	-34	-34	-34	-34	-34	-34
Adj. R^2	0.95	0.94	0.95	0.94	0.95	0.95	0.95
F. Bias	0.11	0.13	0.11	0.12	0.11	0.13	0.11
F. Error	0.24	0.24	0.23	0.23	0.24	0.23	0.23

[†] Seven models with lowest AIC ordered by AIC, [‡] Chosen by AIC, *** $p < 0.001$, ** $p < 0.001$, * $p < 0.05$, $^{+}$ $p < 0.1$, Pop_w [# of people]: population weighted with average plume, Pres: pressure [hPa], Temp: temperature [K], Prec: precipitation + 0.0002 [g/m^3] (shifted for log transformation), Wind: wind speed [m/s], Humid: humidity [ppm], TS: total sulfate (≡ $[SO_4{}^{2-}]$) [μmol/m^3], TN: total nitrate (≡ $[HNO_3]$ + $[NO_3{}^-]$) [μmol/m^3], TA: total ammonia (≡ $[NH_3]$ + $[NH_4{}^+]$) [μmol/m^3], AIC: Akaike information criterion, Adj. R^2: adjusted R^2, F. Bias: fractional bias, F. Error: fractional error.

Table C-45: Evaluations of summer SO_2 intake fraction 'simple' models.

Model[†]	(1)[‡]	(2)	(3)	(4)	(5)	(6)	(7)
Intercept	100^{***}	91^{***}	100^{***}	88^{***}	76^{***}	75^{***}	110^{***}
ln (Pop_w)	0.60^{***}	0.62^{***}	0.62^{***}	0.65^{***}	0.68^{***}	0.64^{***}	0.62^{***}
ln (Pres)	5.9^{***}	6.4^{***}	5.9^{***}	6.5^{***}	7.1^{***}	7.1^{***}	6.1^{***}
ln (Temp)	-26^{***}	-25^{***}	-26^{***}	-24^{***}	-22^{***}	-22^{***}	-27^{***}
ln (Wind)	-	-	0.040	0.051	0.080^{+}	-	0.097^{+}
ln (Prec)	-0.11^{***}	$-0.079^{\star}$	-0.099^{***}	-0.065^{+}	-	-	-
ln (Humid)	-	−0.24	-	−0.28	-0.57^{***}	-0.60^{***}	-
AIC	−18	−17	−17	−17	−15	−14	−3.6
Adj. R^2	0.93	0.93	0.93	0.93	0.93	0.92	0.91
F. Bias	0.0085	0.010	0.0029	0.0036	0.013	0.028	0.030
F. Error	0.21	0.21	0.21	0.21	0.21	0.21	0.22

[†] Seven models with lowest AIC ordered by AIC, [‡] Chosen by AIC, *** $p < 0.001$, ** $p < 0.001$, * $p < 0.05$, $^{+}$ $p < 0.1$, Pop_w [# of people]: population weighted with average plume, Pres: pressure [hPa], Temp: temperature [K], Prec: precipitation + 0.0002 [g/m^3] (shifted for log transformation), Wind: wind speed [m/s], Humid: humidity [ppm], AIC: Akaike information criterion, Adj. R^2: adjusted R^2, F. Bias: fractional bias, F. Error: fractional error.

Table C-46: Evaluations of summer SO_2 intake fraction 'better-fit' models.

Model[†]	(1)[‡]	(2)	(3)	(4)	(5)	(6)	(7)
Intercept	66^{***}	58^{***}	71^{***}	72^{***}	60^{***}	72^{***}	96^{***}
ln (Pop_w)	0.56^{***}	0.58^{***}	0.58^{***}	0.53^{***}	0.59^{***}	0.53^{***}	0.62^{***}
ln (Pres)	6.5^{***}	7.0^{***}	6.7^{***}	6.4^{***}	7.1^{***}	6.4^{***}	6.3^{***}
ln (Temp)	-19^{***}	-18^{***}	-21^{***}	-20^{***}	-19^{***}	-20^{***}	-26^{***}
ln (Wind)	0.070^{+}	$0.089^{\star}$	0.081^{+}	-	$0.096^{\star}$	-	-
ln (Prec)	−0.044	-	−0.048	-0.064^{+}	-	-0.063^{+}	-0.089^{***}
ln (Humid)	$-0.71^{\star}$	-0.89^{***}	$-0.68^{\star}$	$-0.60^{\star}$	-0.89^{***}	$-0.60^{\star}$	-
ln (TS)	$0.30^{\star}$	$0.30^{\star}$	$0.32^{\star}$	0.27^{+}	$0.31^{\star}$	0.27^{+}	-
ln (TN)	-	-	−0.033	-	−0.020	0.00047	-
ln (TA)	-0.11^{**}	-0.12^{***}	-0.11^{**}	-0.11^{**}	-0.12^{***}	-0.11^{**}	$-0.084^{\star}$
AIC	−27	−27	−26	−26	−25	−24	−23
Adj. R^2	0.95	0.94	0.94	0.94	0.94	0.94	0.94
F. Bias	0.052	0.059	0.059	0.057	0.064	0.057	0.030
F. Error	0.22	0.23	0.23	0.22	0.23	0.22	0.21

[†] Seven models with lowest AIC ordered by AIC, [‡] Chosen by AIC, *** $p < 0.001$, ** $p < 0.001$, * $p < 0.05$, $^{+}$ $p < 0.1$, Pop_w [# of people]: population weighted with average plume, Pres: pressure [hPa], Temp: temperature [K], Prec: precipitation + 0.0002 [g/m^3] (shifted for log transformation), Wind: wind speed [m/s], Humid: humidity [ppm], TS: total sulfate (≡ $[SO_4{}^{2-}]$) [μmol/m^3], TN: total nitrate (≡ $[HNO_3]$ + $[NO_3{}^-]$) [μmol/m^3], TA: total ammonia (≡ $[NH_3]$ + $[NH_4{}^+]$) [μmol/m^3], AIC: Akaike information criterion, Adj. R^2: adjusted R^2, F. Bias: fractional bias, F. Error: fractional error.

Table C-47: Evaluations of fall SO_2 intake fraction 'simple' models.

Model[†]	(1)[‡]	(2)	(3)	(4)	(5)	(6)	(7)
Intercept	$64^{\star}$	$68^{\star\star}$	$74^{\star\star}$	$61^{\star}$	$65^{\star}$	24^{+}	$30^{\star}$
ln (Pop_w)	0.20^{+}	-	0.13	-	0.20^{+}	0.19	-
ln (Pres)	$3.9^{\star\star\star}$	$4.6^{\star\star\star}$	$3.8^{\star\star\star}$	$4.8^{\star\star\star}$	$3.9^{\star\star\star}$	$4.7^{\star\star\star}$	$5.3^{\star\star\star}$
ln (Temp)	$-18^{\star\star\star}$	$-19^{\star\star\star}$	$-20^{\star\star\star}$	$-18^{\star\star\star}$	$-18^{\star\star}$	$-11^{\star\star\star}$	$-12^{\star\star\star}$
ln (Wind)	0.12	-	-	0.052	0.12	0.14	-
ln (Prec)	-	-	-	-	−0.0067	-	-
ln (Humid)	0.67^{+}	0.68^{+}	$0.73^{\star}$	0.64^{+}	0.69^{+}	-	-
AIC	19	20	20	21	21	21	22
Adj. R^2	0.58	0.56	0.57	0.56	0.57	0.55	0.54
F. Bias	0.083	0.093	0.10	0.083	0.082	0.064	0.078
F. Error	0.25	0.26	0.26	0.26	0.25	0.23	0.25

[†] Seven models with lowest AIC ordered by AIC, [‡] Chosen by AIC, *** $p < 0.001$, ** $p < 0.001$, * $p < 0.05$, $^{+}$ $p < 0.1$, Pop_w [# of people]: population weighted with average plume, Pres: pressure [hPa], Temp: temperature [K], Prec: precipitation + 0.0002 [g/m^3] (shifted for log transformation), Wind: wind speed [m/s], Humid: humidity [ppm], AIC: Akaike information criterion, Adj. R^2: adjusted R^2, F. Bias: fractional bias, F. Error: fractional error.

Table C-48: Evaluations of fall SO_2 intake fraction 'better-fit' models.

Model[†]	(1)[‡]	(2)	(3)	(4)	(5)	(6)	(7)
Intercept	$59^{\star\star}$	$83^{\star}$	$130^{\star\star\star}$	$57^{\star}$	$110^{\star\star\star}$	$81^{\star}$	$120^{\star\star\star}$
ln (Pop_w)	$0.44^{\star\star\star}$	$0.52^{\star\star\star}$	$0.65^{\star\star\star}$	$0.45^{\star\star\star}$	$0.56^{\star\star\star}$	$0.53^{\star\star\star}$	$0.66^{\star\star\star}$
ln (Pres)	$2.9^{\star\star}$	$3.6^{\star\star}$	$5.4^{\star\star\star}$	$2.9^{\star\star}$	$4.5^{\star\star\star}$	$3.6^{\star\star}$	$5.4^{\star\star\star}$
ln (Temp)	$-17^{\star\star\star}$	$-23^{\star\star}$	$-35^{\star\star\star}$	$-17^{\star\star}$	$-30^{\star\star\star}$	$-23^{\star\star}$	$-33^{\star\star\star}$
ln (Wind)	-	-	-	0.029	-	0.025	0.049
ln (Prec)	-	−0.058	$-0.11^{\star}$	-	−0.084	−0.056	$-0.11^{\star}$
ln (Humid)	$1.1^{\star\star}$	$1.4^{\star\star}$	$1.9^{\star\star\star}$	$1.1^{\star\star}$	$1.7^{\star\star\star}$	$1.4^{\star\star}$	$1.9^{\star\star\star}$
ln (TS)	$-0.55^{\star\star\star}$	$-0.63^{\star\star\star}$	$-0.73^{\star\star\star}$	$-0.55^{\star\star\star}$	$-0.69^{\star\star\star}$	$-0.62^{\star\star\star}$	$-0.72^{\star\star\star}$
ln (TN)	$0.28^{\star\star}$	$0.22^{\star}$	-	$0.27^{\star\star}$	0.072	0.21^{+}	-
ln (TA)	$-0.15^{\star}$	-0.13^{+}	-	-0.14^{+}	-	−0.12	-
AIC	−9.4	−8.7	−7.7	−7.6	−6.9	−6.9	−6.4
Adj. R^2	0.77	0.77	0.76	0.77	0.76	0.77	0.76
F. Bias	−0.039	−0.043	−0.036	−0.043	−0.048	−0.046	−0.041
F. Error	0.26	0.26	0.26	0.26	0.25	0.26	0.25

[†] Seven models with lowest AIC ordered by AIC, [‡] Chosen by AIC, *** $p < 0.001$, ** $p < 0.001$, * $p < 0.05$, $^{+}$ $p < 0.1$, Pop_w [# of people]: population weighted with average plume, Pres: pressure [hPa], Temp: temperature [K], Prec: precipitation + 0.0002 [g/m^3] (shifted for log transformation), Wind: wind speed [m/s], Humid: humidity [ppm], TS: total sulfate (≡ $[SO_4{}^{2-}]$) [μmol/m^3], TN: total nitrate (≡ $[HNO_3]$ + $[NO_3{}^-]$) [μmol/m^3], TA: total ammonia (≡ $[NH_3]$ + $[NH_4{}^+]$) [μmol/m^3], AIC: Akaike information criterion, Adj. R^2: adjusted R^2, F. Bias: fractional bias, F. Error: fractional error.

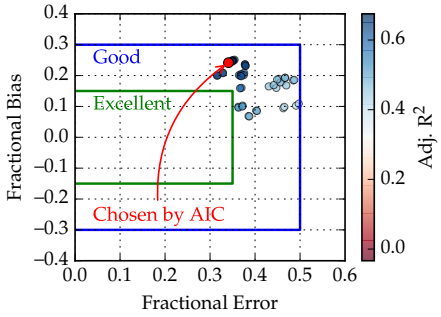

(a) Winter: 'simple' models

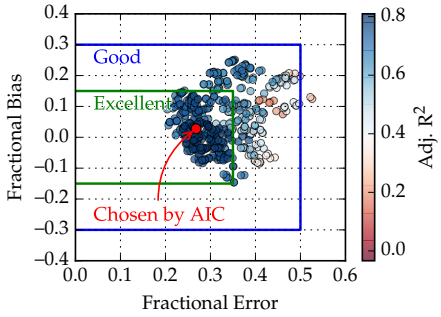

(b) Winter: 'better-fit' models

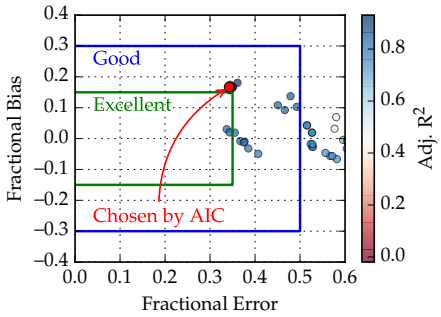

(c) Spring: 'simple' models

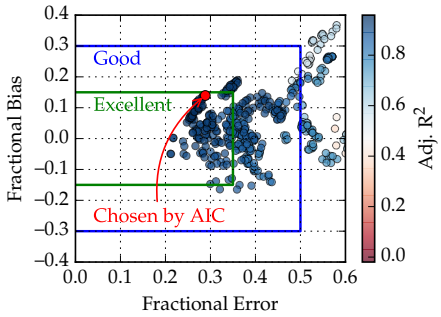

(d) Spring: 'better-fit' models

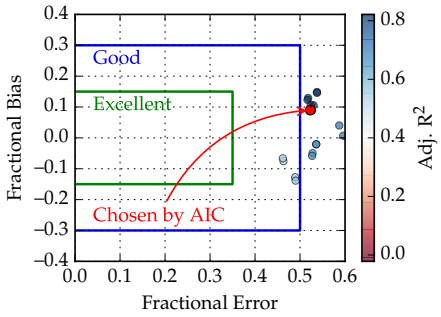

(e) Summer: 'simple' models

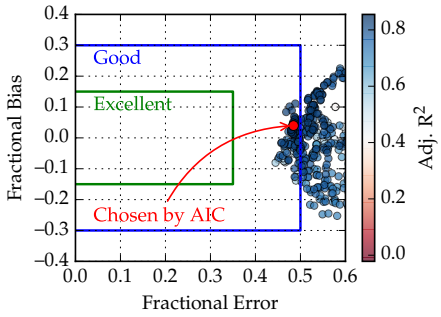

(f) Summer: 'better-fit' models

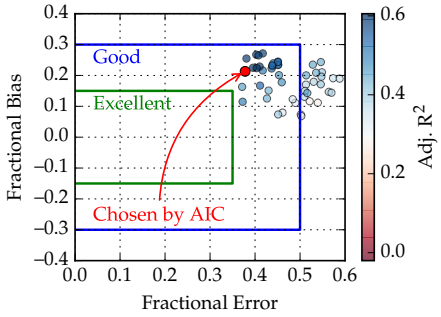

(g) Fall: 'simple' models

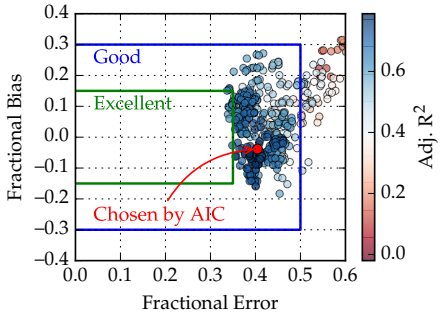

(h) Fall: 'better-fit' models

Figure C-42: Evaluations of NO_x intake fraction models. Each circle indicates a regression model. 'Excellent' and 'Good' model performance criteria are shown as suggested by Morris et al. (2005).

Table C-49: Evaluations of winter NO_x intake fraction 'simple' models.

Model[†]	(1)[‡]	(2)	(3)	(4)	(5)	(6)	(7)
Intercept	$38^{\star}$	$42^{\star}$	57	$38^{\star}$	63	$43^{\star}$	55
ln (Pop_w)	$0.39^{\star\star}$	$0.39^{\star\star}$	$0.39^{\star\star}$	$0.37^{\star}$	$0.38^{\star\star}$	$0.35^{\star}$	$0.38^{\star}$
ln (Pres)	$7.4^{\star\star\star}$	$7.2^{\star\star\star}$	$7.5^{\star\star\star}$	$7.5^{\star\star\star}$	$7.3^{\star\star\star}$	$7.3^{\star\star\star}$	$7.5^{\star\star\star}$
ln (Temp)	$-17^{\star\star\star}$	$-17^{\star\star\star}$	-21^{+}	$-17^{\star\star\star}$	$-21^{\star}$	$-17^{\star\star\star}$	-20^{+}
ln (Wind)	-	-0.056	-	-	-0.058	-0.060	-
ln (Prec)	-	-	-	0.039	-	0.050	0.022
ln (Humid)	-	-	0.25	-	0.27	-	0.23
AIC	72	74	74	74	76	76	76
Adj. R^2	0.68	0.67	0.67	0.67	0.66	0.66	0.66
F. Bias	0.24	0.24	0.25	0.24	0.25	0.25	0.25
F. Error	0.34	0.34	0.35	0.35	0.35	0.35	0.35

[†] Seven models with lowest AIC ordered by AIC, [‡] Chosen by AIC, *** $p < 0.001$, ** $p < 0.001$, * $p < 0.05$, $^{+}$ $p < 0.1$, Pop_w [# of people]: population weighted with average plume, Pres: pressure [hPa], Temp: temperature [K], Prec: precipitation + 0.0002 [g/m^3] (shifted for log transformation), Wind: wind speed [m/s], Humid: humidity [ppm], AIC: Akaike information criterion, Adj. R^2: adjusted R^2, F. Bias: fractional bias, F. Error: fractional error.

Table C-50: Evaluations of winter NO_x intake fraction 'better-fit' models.

Model[†]	(1)[‡]	(2)	(3)	(4)	(5)	(6)	(7)
Intercept	$86^{\star}$	$95^{\star}$	76^{+}	68	9.1	16	$-8.8^{\star\star\star}$
ln (Pop_w)	$0.40^{\star\star\star}$	$0.41^{\star\star\star}$	$0.40^{\star\star}$	$0.39^{\star\star}$	$0.38^{\star\star}$	$0.39^{\star\star}$	$0.39^{\star\star\star}$
ln (Pres)	$3.8^{\star}$	$4.0^{\star}$	$3.3^{\star}$	3.1^{+}	2.9^{+}	3.0^{+}	-
ln (Temp)	$-23^{\star\star}$	$-25^{\star\star}$	$-20^{\star}$	$-19^{\star}$	-6.6^{+}	$-8.0^{\star}$	-
ln (Wind)	-	-0.11	-0.12	-	-	-0.11	-
ln (Prec)	-	-	-	-	-	-	-
ln (Humid)	$1.0^{\star}$	$1.1^{\star}$	0.81	0.78	-	-	-
ln (TS)	$-0.62^{\star\star\star}$	$-0.68^{\star\star\star}$	$-0.63^{\star\star\star}$	$-0.57^{\star\star\star}$	$-0.51^{\star\star\star}$	$-0.57^{\star\star\star}$	$-0.53^{\star\star\star}$
ln (TN)	$0.53^{\star\star\star}$	$0.50^{\star\star\star}$	$0.66^{\star\star\star}$	$0.67^{\star\star\star}$	$0.71^{\star\star\star}$	$0.70^{\star\star\star}$	$0.92^{\star\star\star}$
ln (TA)	-	-	-0.18	-0.17	-0.25^{+}	-0.27^{+}	$-0.35^{\star}$
AIC	49	50	50	50	50	50	51
Adj. R^2	0.81	0.81	0.81	0.81	0.80	0.80	0.79
F. Bias	0.028	0.034	0.041	0.034	0.037	0.044	-0.039
F. Error	0.27	0.30	0.29	0.26	0.24	0.27	0.26

[†] Seven models with lowest AIC ordered by AIC, [‡] Chosen by AIC, *** $p < 0.001$, ** $p < 0.001$, * $p < 0.05$, $^{+}$ $p < 0.1$, Pop_w [# of people]: population weighted with average plume, Pres: pressure [hPa], Temp: temperature [K], Prec: precipitation + 0.0002 [g/m^3] (shifted for log transformation), Wind: wind speed [m/s], Humid: humidity [ppm], TS: total sulfate (≡ $[SO_4{}^{2-}]$) [μmol/m^3], TN: total nitrate (≡ $[HNO_3]$ + $[NO_3{}^-]$) [μmol/m^3], TA: total ammonia (≡ $[NH_3]$ + $[NH_4{}^+]$) [μmol/m^3], AIC: Akaike information criterion, Adj. R^2: adjusted R^2, F. Bias: fractional bias, F. Error: fractional error.

Table C-51: Evaluations of spring NO_x intake fraction 'simple' models.

Model[†]	(1)[‡]	(2)	(3)	(4)	(5)	(6)	(7)
Intercept	140^{***}	150^{***}	150^{***}	130^{***}	95^{***}	92^{***}	94^{***}
ln (Pop_w)	1.1^{***}	1.1^{***}	1.1^{***}	1.0^{***}	1.0^{***}	1.0^{***}	1.0^{***}
ln (Pres)	9.7^{***}	9.4^{***}	9.1^{***}	9.6^{***}	11^{***}	11^{***}	11^{***}
ln (Temp)	-39^{***}	-42^{***}	-42^{***}	-39^{***}	-33^{***}	-32^{***}	-32^{***}
ln (Wind)	-	-	-0.089	-0.049	-	-0.054	-
ln (Prec)	-	-0.051	-0.082	-	-	-	0.016
ln (Humid)	0.67^{*}	0.82^{*}	0.89^{**}	0.67^{*}	-	-	-
AIC	44	45	45	45	48	49	50
Adj. R^2	0.93	0.93	0.93	0.93	0.92	0.92	0.92
F. Bias	0.17	0.17	0.18	0.17	0.16	0.16	0.16
F. Error	0.34	0.35	0.36	0.35	0.35	0.35	0.34

[†] Seven models with lowest AIC ordered by AIC, [‡] Chosen by AIC, *** $p < 0.001$, ** $p < 0.001$, * $p < 0.05$, $^{+}$ $p < 0.1$, Pop_w [# of people]: population weighted with average plume, Pres: pressure [hPa], Temp: temperature [K], Prec: precipitation + 0.0002 [g/m^3] (shifted for log transformation), Wind: wind speed [m/s], Humid: humidity [ppm], AIC: Akaike information criterion, Adj. R^2: adjusted R^2, F. Bias: fractional bias, F. Error: fractional error.

Table C-52: Evaluations of spring NO_x intake fraction 'better-fit' models.

Model[†]	(1)[‡]	(2)	(3)	(4)	(5)	(6)	(7)
Intercept	77^{***}	69^{***}	60^{**}	85^{***}	65^{**}	73^{***}	77^{***}
ln (Pop_w)	0.71^{***}	0.74^{***}	0.74^{***}	0.72^{***}	0.75^{***}	0.70^{***}	0.71^{***}
ln (Pres)	6.6^{***}	6.8^{***}	6.8^{***}	6.8^{***}	7.0^{***}	6.6^{***}	6.8^{***}
ln (Temp)	-23^{***}	-22^{***}	-21^{***}	-25^{***}	-22^{***}	-23^{***}	-24^{***}
ln (Wind)	-0.086	-0.095^{+}	-0.079	-	-	-0.074	-
ln (Prec)	-	-	0.054	-	0.069	0.034	0.049
ln (Humid)	-	-	-	-	-	-	-
ln (TS)	-	-0.15	-0.20	-	-0.19	-	-
ln (TN)	0.53^{***}	0.56^{***}	0.59^{***}	0.51^{***}	0.57^{***}	0.54^{***}	0.53^{***}
ln (TA)	-0.19^{**}	-0.18^{**}	-0.21^{**}	-0.16^{*}	-0.18^{**}	-0.21^{**}	-0.19^{**}
AIC	20	21	21	21	21	21	21
Adj. R^2	0.96	0.96	0.96	0.96	0.96	0.96	0.96
F. Bias	0.14	0.11	0.098	0.12	0.086	0.14	0.13
F. Error	0.29	0.28	0.27	0.28	0.26	0.28	0.27

[†] Seven models with lowest AIC ordered by AIC, [‡] Chosen by AIC, *** $p < 0.001$, ** $p < 0.001$, * $p < 0.05$, $^{+}$ $p < 0.1$, Pop_w [# of people]: population weighted with average plume, Pres: pressure [hPa], Temp: temperature [K], Prec: precipitation + 0.0002 [g/m^3] (shifted for log transformation), Wind: wind speed [m/s], Humid: humidity [ppm], TS: total sulfate (≡ $[SO_4{}^{2-}]$) [$\mu mol/m^3$], TN: total nitrate (≡ $[HNO_3]$ + $[NO_3{}^-]$) [$\mu mol/m^3$], TA: total ammonia (≡ $[NH_3]$ + $[NH_4{}^+]$) [$\mu mol/m^3$], AIC: Akaike information criterion, Adj. R^2: adjusted R^2, F. Bias: fractional bias, F. Error: fractional error.

Table C-53: Evaluations of summer NO_x intake fraction 'simple' models.

Model[†]	(1)[‡]	(2)	(3)	(4)	(5)	(6)	(7)
Intercept	$200^{\star\star\star}$	$200^{\star\star\star}$	$210^{\star\star\star}$	$210^{\star\star\star}$	$170^{\star\star\star}$	$220^{\star\star\star}$	$170^{\star\star\star}$
ln (Pop_w)	$1.1^{\star\star\star}$	$1.0^{\star\star\star}$	$1.1^{\star\star\star}$	$1.0^{\star\star\star}$	$1.1^{\star\star\star}$	$1.0^{\star\star\star}$	$1.1^{\star\star\star}$
ln (Pres)	$11^{\star\star\star}$	$11^{\star\star\star}$	$11^{\star\star\star}$	$12^{\star\star\star}$	$13^{\star\star\star}$	$11^{\star\star\star}$	$13^{\star\star\star}$
ln (Temp)	$-52^{\star\star\star}$	$-52^{\star\star\star}$	$-53^{\star\star\star}$	$-53^{\star\star\star}$	$-47^{\star\star\star}$	$-54^{\star\star\star}$	$-47^{\star\star\star}$
ln (Wind)	-	-0.11	-	-	-	-0.12	-0.033
ln (Prec)	$-0.16^{\star}$	$-0.18^{\star}$	-0.18	-	-	-0.21^{+}	-
ln (Humid)	-	-	0.19	-	-0.68	0.30	-0.69
AIC	94	95	96	97	97	97	99
Adj. R^2	0.82	0.82	0.82	0.81	0.81	0.82	0.81
F. Bias	0.090	0.11	0.089	0.15	0.12	0.11	0.13
F. Error	0.52	0.52	0.53	0.54	0.52	0.53	0.52

[†] Seven models with lowest AIC ordered by AIC, [‡] Chosen by AIC, *** $p < 0.001$, ** $p < 0.001$, * $p < 0.05$, $^{+}$ $p < 0.1$, Pop_w [# of people]: population weighted with average plume, Pres: pressure [hPa], Temp: temperature [K], Prec: precipitation + 0.0002 [g/m^3] (shifted for log transformation), Wind: wind speed [m/s], Humid: humidity [ppm], AIC: Akaike information criterion, Adj. R^2: adjusted R^2, F. Bias: fractional bias, F. Error: fractional error.

Table C-54: Evaluations of summer NO_x intake fraction 'better-fit' models.

Model[†]	(1)[‡]	(2)	(3)	(4)	(5)	(6)	(7)
Intercept	$180^{\star\star\star}$	$150^{\star\star}$	$170^{\star\star\star}$	$170^{\star\star\star}$	$180^{\star\star\star}$	$110^{\star}$	$120^{\star\star}$
ln (Pop_w)	$0.61^{\star}$	$0.63^{\star}$	$0.60^{\star}$	$0.64^{\star}$	$0.80^{\star\star\star}$	$0.67^{\star\star}$	$0.82^{\star\star\star}$
ln (Pres)	$6.3^{\star\star}$	$6.9^{\star\star}$	$6.4^{\star\star}$	$6.6^{\star\star}$	$7.3^{\star\star}$	$8.3^{\star\star\star}$	$8.8^{\star\star\star}$
ln (Temp)	$-40^{\star\star\star}$	$-36^{\star\star\star}$	$-39^{\star\star\star}$	$-40^{\star\star\star}$	$-42^{\star\star\star}$	$-29^{\star\star}$	$-32^{\star\star\star}$
ln (Wind)	-0.25^{+}	-0.24^{+}	-0.25^{+}	-0.26^{+}	-	-0.19	-
ln (Prec)	$-0.22^{\star\star}$	-0.16	$-0.21^{\star\star}$	$-0.20^{\star}$	$-0.17^{\star}$	-	-
ln (Humid)	-	-0.48	-	-	-	$-1.3^{\star}$	$-1.1^{\star}$
ln (TS)	-	-	-	-0.12	-	-	-
ln (TN)	$0.43^{\star\star}$	$0.46^{\star\star}$	$0.46^{\star\star}$	$0.46^{\star\star}$	$0.36^{\star\star}$	$0.50^{\star\star\star}$	$0.43^{\star\star}$
ln (TA)	-	-	-0.058	-	-	-	-
AIC	85	87	87	87	87	88	88
Adj. R^2	0.85	0.85	0.85	0.85	0.85	0.85	0.84
F. Bias	0.040	0.036	0.047	0.026	0.018	0.050	0.027
F. Error	0.48	0.48	0.49	0.48	0.48	0.48	0.48

[†] Seven models with lowest AIC ordered by AIC, [‡] Chosen by AIC, *** $p < 0.001$, ** $p < 0.001$, * $p < 0.05$, $^{+}$ $p < 0.1$, Pop_w [# of people]: population weighted with average plume, Pres: pressure [hPa], Temp: temperature [K], Prec: precipitation + 0.0002 [g/m^3] (shifted for log transformation), Wind: wind speed [m/s], Humid: humidity [ppm], TS: total sulfate (≡ $[SO_4{}^{2-}]$) [$\mu mol/m^3$], TN: total nitrate (≡ $[HNO_3]$ + $[NO_3{}^-]$) [$\mu mol/m^3$], TA: total ammonia (≡ $[NH_3]$ + $[NH_4{}^+]$) [$\mu mol/m^3$], AIC: Akaike information criterion, Adj. R^2: adjusted R^2, F. Bias: fractional bias, F. Error: fractional error.

Table C-55: Evaluations of fall NO_x intake fraction 'simple' models.

Model[†]	(1)[‡]	(2)	(3)	(4)	(5)	(6)	(7)
Intercept	$83^{\star\star}$	$98^{\star\star\star}$	$75^{\star}$	$110^{\star}$	$89^{\star\star}$	$130^{\star\star}$	91
ln (Pop_w)	$0.61^{\star\star}$	$0.48^{\star}$	$0.61^{\star\star}$	$0.62^{\star\star}$	$0.48^{\star}$	$0.50^{\star\star}$	$0.61^{\star\star}$
ln (Pres)	$8.4^{\star\star\star}$	$8.4^{\star\star\star}$	$8.0^{\star\star\star}$	$7.9^{\star\star\star}$	$8.0^{\star\star\star}$	$7.6^{\star\star\star}$	$7.8^{\star\star\star}$
ln (Temp)	$-27^{\star\star\star}$	$-29^{\star\star\star}$	$-25^{\star\star\star}$	$-31^{\star\star}$	$-27^{\star\star\star}$	$-35^{\star\star\star}$	$-28^{\star}$
ln (Wind)	0.26	-	0.26	0.25	-	-	0.25
ln (Prec)	-	-	0.085	-	0.090	-	0.072
ln (Humid)	-	-	-	0.43	-	0.57	0.25
AIC	86	87	87	88	88	88	89
Adj. R^2	0.61	0.59	0.60	0.60	0.59	0.59	0.59
F. Bias	0.21	0.25	0.22	0.22	0.27	0.27	0.23
F. Error	0.38	0.38	0.40	0.40	0.41	0.40	0.41

[†] Seven models with lowest AIC ordered by AIC, [‡] Chosen by AIC, *** $p < 0.001$, ** $p < 0.001$, * $p < 0.05$, $^{+}$ $p < 0.1$, Pop_w [# of people]: population weighted with average plume, Pres: pressure [hPa], Temp: temperature [K], Prec: precipitation + 0.0002 [g/m^3] (shifted for log transformation), Wind: wind speed [m/s], Humid: humidity [ppm], AIC: Akaike information criterion, Adj. R^2: adjusted R^2, F. Bias: fractional bias, F. Error: fractional error.

Table C-56: Evaluations of fall NO_x intake fraction 'better-fit' models.

Model[†]	(1)[‡]	(2)	(3)	(4)	(5)	(6)	(7)
Intercept	$130^{\star\star}$	$110^{\star\star}$	$110^{\star}$	$140^{\star\star}$	$130^{\star\star}$	$160^{\star\star\star}$	87
ln (Pop_w)	$0.89^{\star\star\star}$	$0.92^{\star\star\star}$	$0.84^{\star\star\star}$	$0.90^{\star\star\star}$	$0.95^{\star\star\star}$	$1.0^{\star\star\star}$	$0.85^{\star\star\star}$
ln (Pres)	$6.4^{\star\star}$	$6.3^{\star\star}$	$5.8^{\star}$	$6.7^{\star\star}$	$6.8^{\star\star}$	$8.5^{\star\star\star}$	$5.5^{\star}$
ln (Temp)	$-36^{\star\star\star}$	$-33^{\star\star\star}$	$-31^{\star}$	$-38^{\star\star\star}$	$-37^{\star\star\star}$	$-45^{\star\star\star}$	$-27^{\star}$
ln (Wind)	-	0.12	-	-	0.16	0.20	0.13
ln (Prec)	-	-	0.049	-	-	-	0.068
ln (Humid)	$1.6^{\star\star}$	$1.5^{\star}$	$1.4^{\star}$	$1.7^{\star\star}$	$1.7^{\star\star}$	$2.0^{\star\star\star}$	1.2
ln (TS)	$-1.1^{\star\star\star}$	$-1.0^{\star\star\star}$	$-1.0^{\star\star\star}$	$-1.1^{\star\star\star}$	$-1.1^{\star\star\star}$	$-1.1^{\star\star\star}$	$-0.97^{\star\star\star}$
ln (TN)	$0.35^{\star\star}$	$0.36^{\star\star}$	$0.39^{\star\star}$	0.30	0.24	-	$0.41^{\star\star}$
ln (TA)	-	-	-	0.060	0.13	$0.28^{\star\star}$	-
AIC	56	57	58	58	58	58	59
Adj. R^2	0.79	0.79	0.79	0.79	0.79	0.78	0.79
F. Bias	−0.038	−0.054	−0.036	−0.040	−0.063	−0.048	−0.052
F. Error	0.40	0.39	0.40	0.40	0.39	0.39	0.39

[†] Seven models with lowest AIC ordered by AIC, [‡] Chosen by AIC, *** $p < 0.001$, ** $p < 0.001$, * $p < 0.05$, $^{+}$ $p < 0.1$, Pop_w [# of people]: population weighted with average plume, Pres: pressure [hPa], Temp: temperature [K], Prec: precipitation + 0.0002 [g/m^3] (shifted for log transformation), Wind: wind speed [m/s], Humid: humidity [ppm], TS: total sulfate (≡ $[SO_4{}^{2-}]$) [μmol/m^3], TN: total nitrate (≡ $[HNO_3]$ + $[NO_3{}^-]$) [μmol/m^3], TA: total ammonia (≡ $[NH_3]$ + $[NH_4{}^+]$) [μmol/m^3], AIC: Akaike information criterion, Adj. R^2: adjusted R^2, F. Bias: fractional bias, F. Error: fractional error.

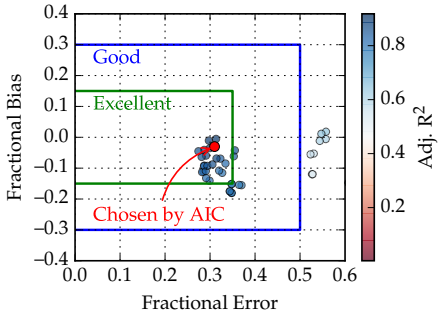

(a) Winter: ‘simple’ models

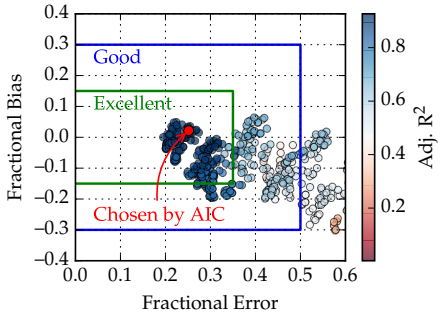

(b) Winter: ‘better-fit’ models

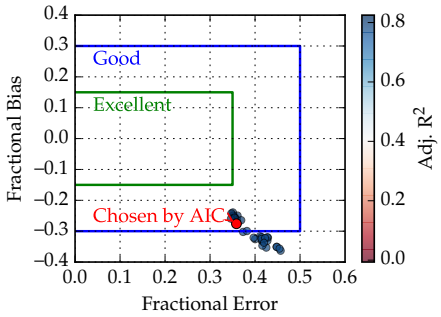

(c) Spring: ‘simple’ models

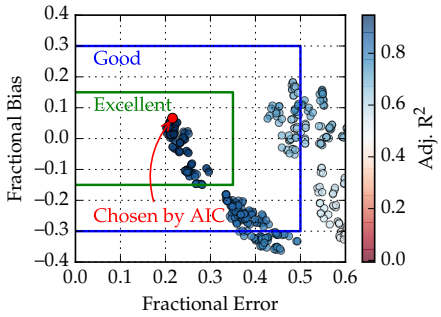

(d) Spring: ‘better-fit’ models

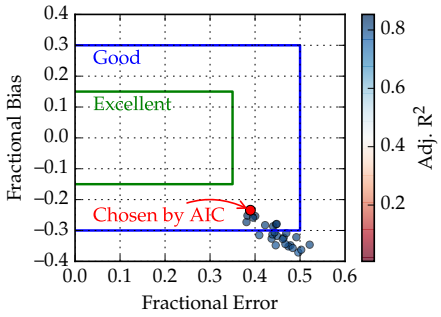

(e) Summer: ‘simple’ models

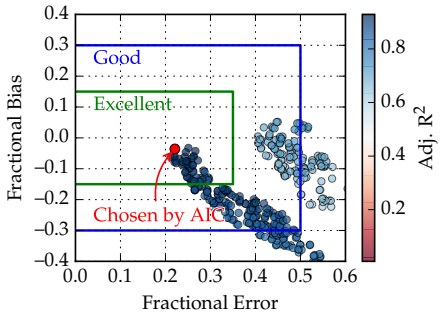

(f) Summer: ‘better-fit’ models

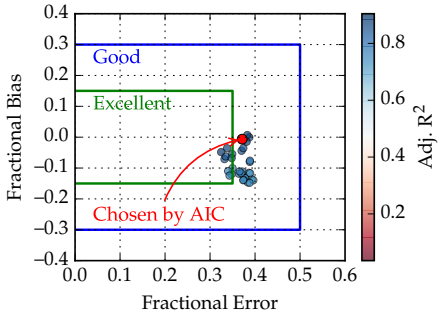

(g) Fall: ‘simple’ models

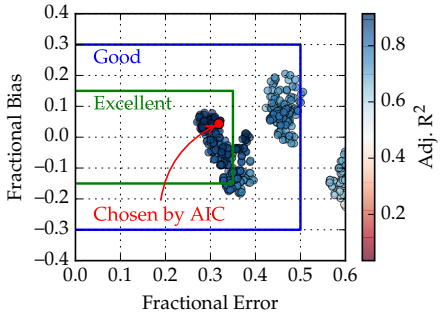

(h) Fall: ‘better-fit’ models

Figure C-43: Evaluations of NH_3 intake fraction models. Each circle indicates a regression model. ‘Excellent’ and ‘Good’ model performance criteria are shown as suggested by Morris et al. (2005).

Table C-57: Evaluations of winter NH_3 intake fraction 'simple' models.

Model[†]	(1)[‡]	(2)	(3)	(4)	(5)	(6)	(7)
Intercept	180^{***}	170^{***}	170^{***}	160^{***}	170^{***}	38^{**}	45^{**}
ln (Pop_w)	0.83^{***}	0.83^{***}	0.72^{***}	0.72^{***}	1.0^{***}	0.83^{***}	0.83^{***}
ln (Pres)	3.5^{***}	3.9^{***}	3.8^{***}	4.2^{***}	-	3.5^{***}	3.1^{**}
ln (Temp)	-41^{***}	-39^{***}	-38^{***}	-37^{***}	-35^{***}	-13^{***}	-13^{***}
ln (Wind)	-0.094^{+}	-	-0.097^{+}	-	-0.17^{**}	-	-0.085
ln (Prec)	-0.25^{**}	-0.25^{**}	-	-	-0.31^{**}	-0.16	-0.15
ln (Humid)	1.8^{***}	1.7^{***}	1.6^{***}	1.5^{***}	1.6^{***}	-	-
AIC	13	15	20	21	31	34	34
Adj. R^2	0.92	0.91	0.91	0.90	0.88	0.87	0.87
F. Bias	-0.030	-0.035	-0.0053	-0.011	-0.069	-0.064	-0.059
F. Error	0.31	0.30	0.31	0.30	0.31	0.28	0.29

[†] Seven models with lowest AIC ordered by AIC, [‡] Chosen by AIC, *** $p < 0.001$, ** $p < 0.001$, * $p < 0.05$, $^{+}$ $p < 0.1$, Pop_w [# of people]: population weighted with average plume, Pres: pressure [hPa], Temp: temperature [K], Prec: precipitation + 0.0002 [g/m^3] (shifted for log transformation), Wind: wind speed [m/s], Humid: humidity [ppm], AIC: Akaike information criterion, Adj. R^2: adjusted R^2, F. Bias: fractional bias, F. Error: fractional error.

Table C-58: Evaluations of winter NH_3 intake fraction 'better-fit' models.

Model[†]	(1)[‡]	(2)	(3)	(4)	(5)	(6)	(7)
Intercept	150^{***}	170^{***}	160^{***}	160^{***}	150^{***}	170^{***}	160^{***}
ln (Pop_w)	0.81^{***}	0.78^{***}	0.83^{***}	0.80^{***}	0.81^{***}	0.79^{***}	0.70^{***}
ln (Pres)	3.1^{***}	2.8^{**}	3.1^{***}	3.4^{**}	2.9^{*}	2.8^{**}	2.8^{**}
ln (Temp)	-35^{***}	-37^{***}	-36^{***}	-37^{***}	-34^{***}	-38^{***}	-35^{***}
ln (Wind)	-	-	-0.061	-	-	-0.031	-
ln (Prec)	-0.21^{*}	-0.17^{+}	-0.23^{*}	-0.20^{*}	-0.20^{*}	-0.18^{+}	-
ln (Humid)	1.4^{***}	1.6^{***}	1.4^{***}	1.5^{***}	1.4^{***}	1.6^{***}	1.4^{***}
ln (TS)	0.28^{**}	0.20^{*}	0.24^{*}	0.24^{**}	0.27^{**}	0.18^{+}	0.25^{**}
ln (TN)	-	-	-	-0.068	0.029	-	-
ln (TA)	-0.098	-	-0.12^{+}	-	-0.12	-	-
AIC	8.5	9.2	9.3	10	10	11	11
Adj. R^2	0.93	0.92	0.93	0.92	0.92	0.92	0.92
F. Bias	0.022	-0.0097	0.024	0.013	0.019	-0.011	0.011
F. Error	0.25	0.26	0.27	0.26	0.25	0.27	0.25

[†] Seven models with lowest AIC ordered by AIC, [‡] Chosen by AIC, *** $p < 0.001$, ** $p < 0.001$, * $p < 0.05$, $^{+}$ $p < 0.1$, Pop_w [# of people]: population weighted with average plume, Pres: pressure [hPa], Temp: temperature [K], Prec: precipitation + 0.0002 [g/m^3] (shifted for log transformation), Wind: wind speed [m/s], Humid: humidity [ppm], TS: total sulfate (≡ $[SO_4{}^{2-}]$) [μmol/m^3], TN: total nitrate (≡ $[HNO_3]$ + $[NO_3{}^{-}]$) [μmol/m^3], TA: total ammonia (≡ $[NH_3]$ + $[NH_4{}^{+}]$) [μmol/m^3], AIC: Akaike information criterion, Adj. R^2: adjusted R^2, F. Bias: fractional bias, F. Error: fractional error.

Table C-59: Evaluations of spring NH_3 intake fraction 'simple' models.

Model[†]	(1)[‡]	(2)	(3)	(4)	(5)	(6)	(7)
Intercept	$110^{\star\star}$	$97^{\star\star}$	$100^{\star\star}$	$92^{\star}$	$110^{\star\star}$	$110^{\star\star}$	$96^{\star}$
ln (Pop_w)	$1.0^{\star\star\star}$	$0.95^{\star\star\star}$	$1.0^{\star\star\star}$	$0.94^{\star\star\star}$	$1.0^{\star\star\star}$	$1.0^{\star\star\star}$	$0.95^{\star\star\star}$
ln (Pres)	-	2.2	-	2.1	-	-	2.2
ln (Temp)	$-23^{\star\star\star}$	$-23^{\star\star\star}$	$-21^{\star\star}$	$-22^{\star\star}$	$-24^{\star\star}$	$-24^{\star\star}$	$-23^{\star\star}$
ln (Wind)	-	-	-0.097	-0.087	-	-0.12	-
ln (Prec)	-	-	-	-	-0.026	-0.063	0.0029
ln (Humid)	$1.1^{\star\star}$	$0.84^{\star}$	$1.1^{\star\star}$	$0.83^{\star}$	$1.2^{\star\star}$	$1.2^{\star\star}$	0.84^{+}
AIC	75	75	75	76	77	77	77
Adj. R^2	0.82	0.82	0.82	0.82	0.82	0.82	0.82
F. Bias	-0.28	-0.26	-0.26	-0.24	-0.27	-0.25	-0.26
F. Error	0.36	0.35	0.35	0.35	0.36	0.35	0.35

[†] Seven models with lowest AIC ordered by AIC, [‡] Chosen by AIC, *** $p < 0.001$, ** $p < 0.001$, * $p < 0.05$, $^{+}$ $p < 0.1$, Pop_w [# of people]: population weighted with average plume, Pres: pressure [hPa], Temp: temperature [K], Prec: precipitation + 0.0002 [g/m^3] (shifted for log transformation), Wind: wind speed [m/s], Humid: humidity [ppm], AIC: Akaike information criterion, Adj. R^2: adjusted R^2, F. Bias: fractional bias, F. Error: fractional error.

Table C-60: Evaluations of spring NH_3 intake fraction 'better-fit' models.

Model[†]	(1)[‡]	(2)	(3)	(4)	(5)	(6)	(7)
Intercept	$80^{\star\star\star}$	$76^{\star\star\star}$	$83^{\star\star\star}$	$79^{\star\star\star}$	$70^{\star\star\star}$	$91^{\star\star\star}$	$82^{\star\star\star}$
ln (Pop_w)	$0.86^{\star\star\star}$	$0.87^{\star\star\star}$	$0.86^{\star\star\star}$	$0.86^{\star\star\star}$	$0.83^{\star\star\star}$	$0.86^{\star\star\star}$	$0.88^{\star\star\star}$
ln (Pres)	1.9^{+}	-	1.8	1.9^{+}	-	2.0^{+}	-
ln (Temp)	$-18^{\star\star\star}$	$-15^{\star\star\star}$	$-18^{\star\star\star}$	$-17^{\star\star\star}$	$-14^{\star\star\star}$	$-20^{\star\star\star}$	$-16^{\star\star\star}$
ln (Wind)	-0.11^{+}	$-0.11^{\star}$	-0.11^{+}	-0.10^{+}	$-0.13^{\star}$	-	$-0.12^{\star}$
ln (Prec)	-	-	-	0.0073	-	-	-
ln (Humid)	-	-	0.065	-	-	-	0.11
ln (TS)	$1.2^{\star\star\star}$	$1.2^{\star\star\star}$	$1.2^{\star\star\star}$	$1.2^{\star\star\star}$	$1.1^{\star\star\star}$	$1.3^{\star\star\star}$	$1.2^{\star\star\star}$
ln (TN)	$-0.18^{\star}$	-0.11	$-0.19^{\star}$	$-0.18^{\star}$	-	$-0.21^{\star}$	-0.12
ln (TA)	$-0.35^{\star\star\star}$	$-0.38^{\star\star\star}$	$-0.35^{\star\star\star}$	$-0.36^{\star\star\star}$	$-0.41^{\star\star\star}$	$-0.31^{\star\star\star}$	$-0.37^{\star\star\star}$
AIC	17	19	19	19	19	20	20
Adj. R^2	0.95	0.95	0.95	0.95	0.94	0.94	0.94
F. Bias	0.066	0.055	0.065	0.065	0.036	0.052	0.052
F. Error	0.22	0.21	0.21	0.21	0.21	0.23	0.21

[†] Seven models with lowest AIC ordered by AIC, [‡] Chosen by AIC, *** $p < 0.001$, ** $p < 0.001$, * $p < 0.05$, $^{+}$ $p < 0.1$, Pop_w [# of people]: population weighted with average plume, Pres: pressure [hPa], Temp: temperature [K], Prec: precipitation + 0.0002 [g/m^3] (shifted for log transformation), Wind: wind speed [m/s], Humid: humidity [ppm], TS: total sulfate (≡ $[SO_4{}^{2-}]$) [μmol/m^3], TN: total nitrate (≡ $[HNO_3]$ + $[NO_3{}^-]$) [μmol/m^3], TA: total ammonia (≡ $[NH_3]$ + $[NH_4{}^+]$) [μmol/m^3], AIC: Akaike information criterion, Adj. R^2: adjusted R^2, F. Bias: fractional bias, F. Error: fractional error.

Table C-61: Evaluations of summer NH_3 intake fraction 'simple' models.

Model[†]	(1)[‡]	(2)	(3)	(4)	(5)	(6)	(7)
Intercept	50^{+}	70^{+}	$110^{\star\star}$	$99^{\star\star}$	$100^{\star\star}$	43	56
ln (Pop_w)	$0.84^{\star\star\star}$	$0.84^{\star\star\star}$	$0.88^{\star\star\star}$	$0.91^{\star\star\star}$	$0.82^{\star\star\star}$	$0.90^{\star\star\star}$	$0.90^{\star\star\star}$
ln (Pres)	$4.1^{\star\star}$	3.2^{+}	-	-	1.5	$4.5^{\star\star}$	$3.9^{\star}$
ln (Temp)	$-16^{\star\star}$	$-19^{\star\star}$	$-24^{\star\star\star}$	$-21^{\star\star}$	$-24^{\star\star\star}$	$-15^{\star\star}$	$-17^{\star}$
ln (Wind)	$-0.27^{\star}$	$-0.27^{\star}$	$-0.33^{\star\star}$	$-0.30^{\star\star}$	$-0.33^{\star\star}$	-	-
ln (Prec)	$0.21^{\star\star}$	0.16^{+}	-	0.080	-	$0.26^{\star\star\star}$	$0.23^{\star}$
ln (Humid)	-	0.38	$1.2^{\star\star\star}$	$1.0^{\star}$	$1.1^{\star\star}$	-	0.26
AIC	70	71	72	73	73	75	77
Adj. R^2	0.85	0.85	0.84	0.84	0.84	0.83	0.83
F. Bias	−0.23	−0.23	−0.26	−0.25	−0.25	−0.28	−0.28
F. Error	0.39	0.39	0.40	0.38	0.40	0.45	0.45

[†] Seven models with lowest AIC ordered by AIC, [‡] Chosen by AIC, *** $p < 0.001$, ** $p < 0.001$, * $p < 0.05$, $^{+}$ $p < 0.1$, Pop_w [# of people]: population weighted with average plume, Pres: pressure [hPa], Temp: temperature [K], Prec: precipitation + 0.0002 [g/m^3] (shifted for log transformation), Wind: wind speed [m/s], Humid: humidity [ppm], AIC: Akaike information criterion, Adj. R^2: adjusted R^2, F. Bias: fractional bias, F. Error: fractional error.

Table C-62: Evaluations of summer NH_3 intake fraction 'better-fit' models.

Model[†]	(1)[‡]	(2)	(3)	(4)	(5)	(6)	(7)
Intercept	23	$-19^{\star}$	19	$-20^{\star}$	-17^{+}	$65^{\star\star}$	1.4
ln (Pop_w)	$0.83^{\star\star\star}$	$0.81^{\star\star\star}$	$0.85^{\star\star\star}$	$0.83^{\star\star\star}$	$0.78^{\star\star\star}$	$0.87^{\star\star\star}$	$0.79^{\star\star\star}$
ln (Pres)	$4.2^{\star\star}$	$4.0^{\star\star}$	$4.6^{\star\star}$	$4.4^{\star\star}$	$3.4^{\star}$	$3.7^{\star\star}$	$3.4^{\star}$
ln (Temp)	−8.8	-	−8.2	-	-	$-17^{\star\star\star}$	−3.7
ln (Wind)	−0.12	−0.11	-	-	$-0.15^{\star}$	-0.15^{+}	$-0.17^{\star}$
ln (Prec)	$0.24^{\star\star\star}$	$0.28^{\star\star\star}$	$0.26^{\star\star\star}$	$0.30^{\star\star\star}$	$0.28^{\star\star\star}$	$0.17^{\star\star}$	$0.27^{\star\star\star}$
ln (Humid)	-0.95^{+}	$-1.5^{\star\star\star}$	$-1.1^{\star}$	$-1.6^{\star\star\star}$	$-1.3^{\star\star\star}$	-	$-1.1^{\star}$
ln (TS)	$1.0^{\star\star\star}$	$1.1^{\star\star\star}$	$1.1^{\star\star\star}$	$1.2^{\star\star\star}$	$0.93^{\star\star\star}$	$0.76^{\star\star\star}$	$0.85^{\star\star\star}$
ln (TN)	-0.17^{+}	−0.12	$-0.22^{\star}$	$-0.16^{\star}$	-	$-0.20^{\star}$	-
ln (TA)	$-0.36^{\star\star\star}$	$-0.39^{\star\star\star}$	$-0.37^{\star\star\star}$	$-0.39^{\star\star\star}$	$-0.39^{\star\star\star}$	$-0.33^{\star\star\star}$	$-0.38^{\star\star\star}$
AIC	37	38	38	38	38	39	40
Adj. R^2	0.93	0.93	0.93	0.93	0.93	0.92	0.92
F. Bias	−0.036	−0.046	−0.033	−0.043	−0.076	−0.061	−0.077
F. Error	0.22	0.25	0.25	0.27	0.25	0.21	0.24

[†] Seven models with lowest AIC ordered by AIC, [‡] Chosen by AIC, *** $p < 0.001$, ** $p < 0.001$, * $p < 0.05$, $^{+}$ $p < 0.1$, Pop_w [# of people]: population weighted with average plume, Pres: pressure [hPa], Temp: temperature [K], Prec: precipitation + 0.0002 [g/m^3] (shifted for log transformation), Wind: wind speed [m/s], Humid: humidity [ppm], TS: total sulfate (≡ $[SO_4{}^{2-}]$) [μmol/m^3], TN: total nitrate (≡ $[HNO_3]$ + $[NO_3{}^{-}]$) [μmol/m^3], TA: total ammonia (≡ $[NH_3]$ + $[NH_4{}^{+}]$) [μmol/m^3], AIC: Akaike information criterion, Adj. R^2: adjusted R^2, F. Bias: fractional bias, F. Error: fractional error.

Table C-63: Evaluations of fall NH_3 intake fraction 'simple' models.

Model[†]	(1)[‡]	(2)	(3)	(4)	(5)	(6)	(7)
Intercept	190^{***}	150^{***}	170^{***}	210^{***}	130^{***}	180^{***}	190^{***}
ln (Pop_w)	0.67^{***}	0.62^{***}	0.73^{***}	0.77^{***}	0.68^{***}	0.72^{***}	0.86^{***}
ln (Pres)	3.0^{**}	3.1^{**}	3.3^{***}	-	3.4^{***}	-	-
ln (Temp)	-42^{***}	-35^{***}	-38^{***}	-43^{***}	-30^{***}	-36^{***}	-39^{***}
ln (Wind)	-0.21^{**}	-0.23^{**}	-	-0.25^{**}	-	-0.26^{**}	-
ln (Prec)	-0.15^{**}	-	-0.16^{**}	-0.16^{*}	-	-	-0.17^{*}
ln (Humid)	1.8^{***}	1.5^{***}	1.7^{***}	2.3^{***}	1.3^{**}	2.0^{***}	2.2^{***}
AIC	15	21	22	25	27	30	33
Adj. R^2	0.90	0.89	0.89	0.88	0.87	0.87	0.86
F. Bias	−0.0064	0.0069	−0.048	−0.015	−0.036	−0.00058	−0.068
F. Error	0.37	0.38	0.32	0.38	0.34	0.39	0.35

[†] Seven models with lowest AIC ordered by AIC, [‡] Chosen by AIC, *** $p < 0.001$, ** $p < 0.001$, * $p < 0.05$, $^{+}$ $p < 0.1$, Pop_w [# of people]: population weighted with average plume, Pres: pressure [hPa], Temp: temperature [K], Prec: precipitation + 0.0002 [g/m^3] (shifted for log transformation), Wind: wind speed [m/s], Humid: humidity [ppm], AIC: Akaike information criterion, Adj. R^2: adjusted R^2, F. Bias: fractional bias, F. Error: fractional error.

Table C-64: Evaluations of fall NH_3 intake fraction 'better-fit' models.

Model[†]	(1)[‡]	(2)	(3)	(4)	(5)	(6)	(7)
Intercept	170^{***}	140^{***}	180^{***}	170^{***}	140^{***}	150^{***}	140^{***}
ln (Pop_w)	0.60^{***}	0.55^{***}	0.63^{***}	0.61^{***}	0.54^{***}	0.62^{***}	0.55^{***}
ln (Pres)	2.0^{*}	1.8^{+}	2.6^{+}	2.2^{*}	-	1.9^{*}	1.3
ln (Temp)	-36^{***}	-30^{***}	-38^{***}	-36^{***}	-27^{***}	-31^{***}	-29^{***}
ln (Wind)	-0.15^{*}	-0.14^{+}	-0.16^{*}	-0.16^{*}	-0.13^{+}	-	-0.14^{+}
ln (Prec)	-0.099^{+}	-	-0.12^{+}	-0.11^{+}	-	−0.089	-
ln (Humid)	1.4^{***}	1.1^{**}	1.5^{***}	1.4^{***}	1.1^{**}	1.2^{**}	1.1^{**}
ln (TS)	0.27^{*}	0.35^{**}	0.26^{*}	0.27^{*}	0.38^{***}	0.35^{**}	0.35^{**}
ln (TN)	-	-	−0.045	-	0.085	-	0.035
ln (TA)	-	-	-	−0.025	-	-	-
AIC	11	12	12	12	13	13	14
Adj. R^2	0.91	0.91	0.91	0.91	0.91	0.91	0.91
F. Bias	0.044	0.066	0.053	0.051	0.044	0.032	0.055
F. Error	0.32	0.31	0.32	0.32	0.30	0.28	0.31

[†] Seven models with lowest AIC ordered by AIC, [‡] Chosen by AIC, *** $p < 0.001$, ** $p < 0.001$, * $p < 0.05$, $^{+}$ $p < 0.1$, Pop_w [# of people]: population weighted with average plume, Pres: pressure [hPa], Temp: temperature [K], Prec: precipitation + 0.0002 [g/m^3] (shifted for log transformation), Wind: wind speed [m/s], Humid: humidity [ppm], TS: total sulfate (≡ $[SO_4{}^{2-}]$) [$\mu mol/m^3$], TN: total nitrate (≡ $[HNO_3]$ + $[NO_3{}^-]$) [$\mu mol/m^3$], TA: total ammonia (≡ $[NH_3]$ + $[NH_4{}^+]$) [$\mu mol/m^3$], AIC: Akaike information criterion, Adj. R^2: adjusted R^2, F. Bias: fractional bias, F. Error: fractional error.

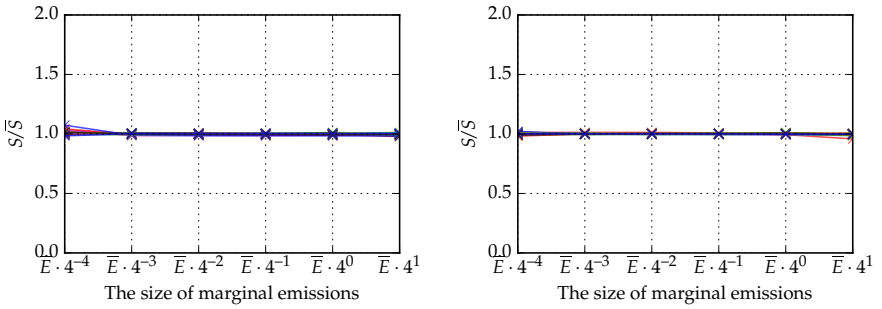

(a) EC: January

(b) EC: July

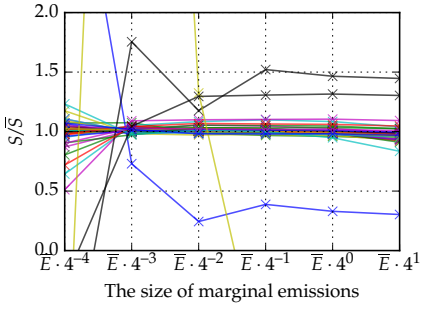

(c) SO_2: January

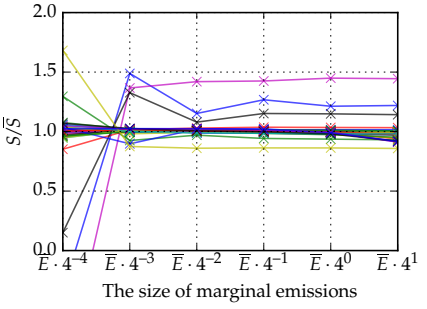

(d) SO_2: July

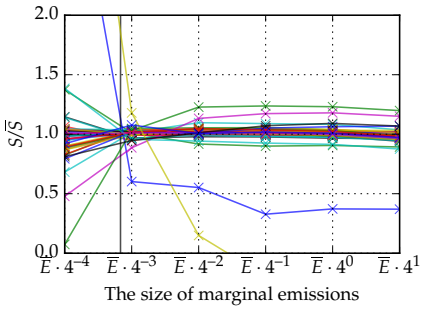

(e) NO_x: January

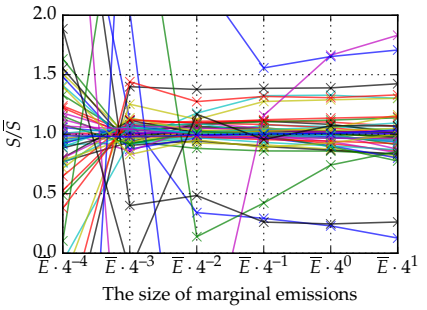

(f) NO_x: July

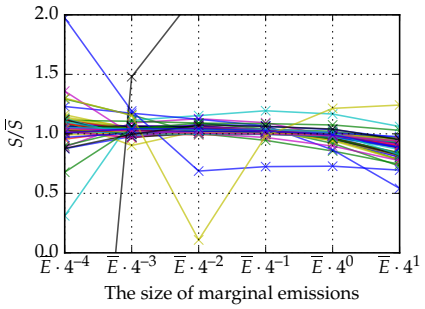

(g) NH_3: January

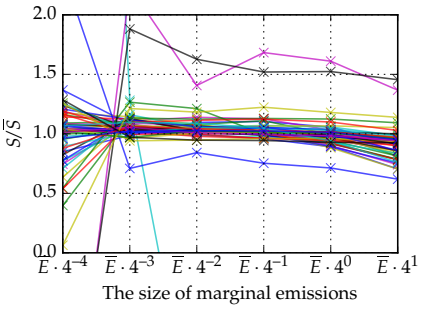

(h) NH_3: July

Figure C-44: Social costs over a range of marginal emissions. For the 50 training samples, the per-tonne social costs were calculated over a range of $\overline{E}\cdot 4^k (k = -4, ..., 1)$, where $\overline{E}$ is the average emissions of area and point sources in the CAMx grid. The ratios of S, the per-tonne social cost for given emissions, over $\overline{S}$, the average of S over all $\overline{E}\cdot 4^k$, are on the y-axis.

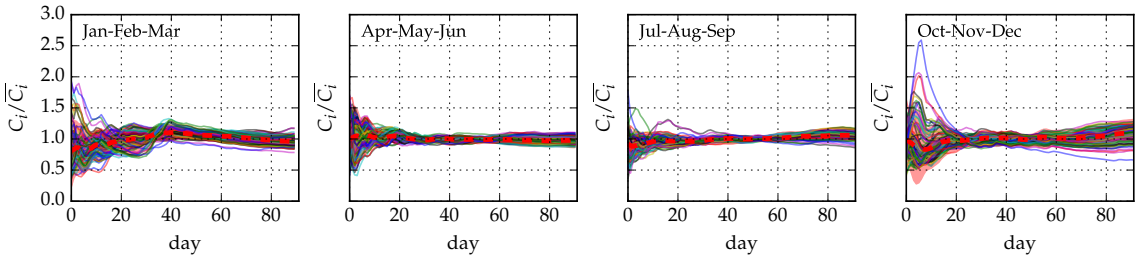

(a) EC

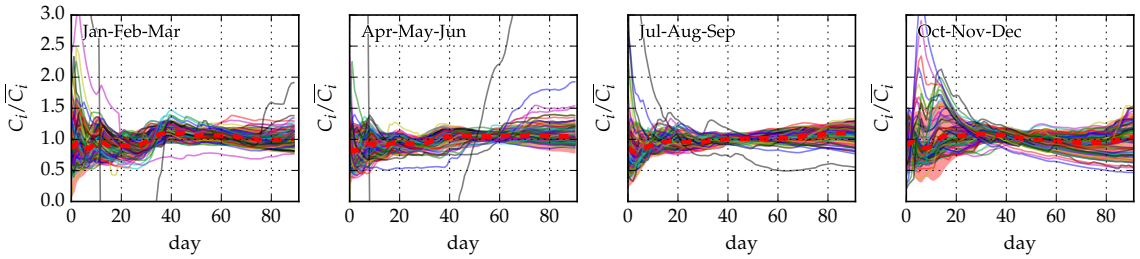

(b) SO_2

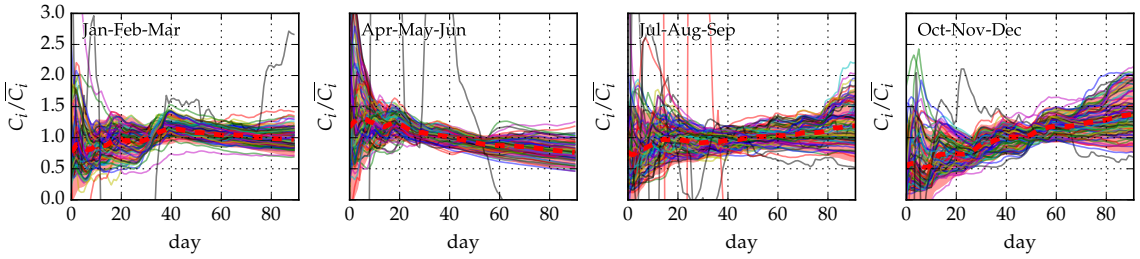

(c) NO_x

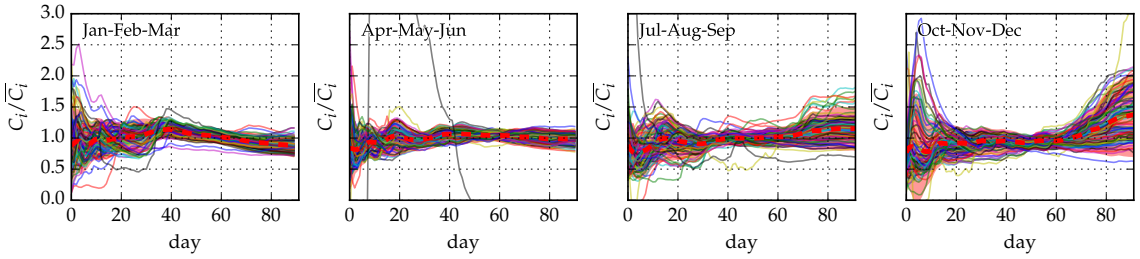

(d) NH_3

Figure C-45: Changes in $PM_{2.5}$ concentrations over a range of simulation period. Each line indicates each sample location. C_i is the sum of the CAMx grid of the changes in average $PM_{2.5}$ concentrations created by the marginal emissions ($\overline{E}\cdot 4^{-2}$) for a given day. $\overline{C_i}$ is the average of C_i's over the whole season time period. The red dashed line indicates the 2.5% truncated means and the shaded area covers the 95% confidence intervals of the means.

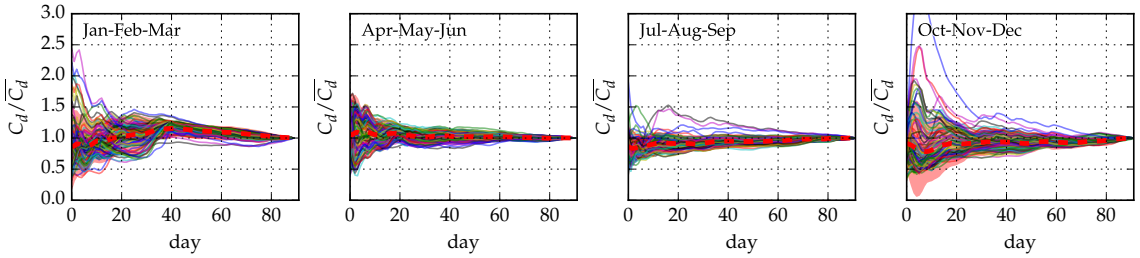

(a) EC

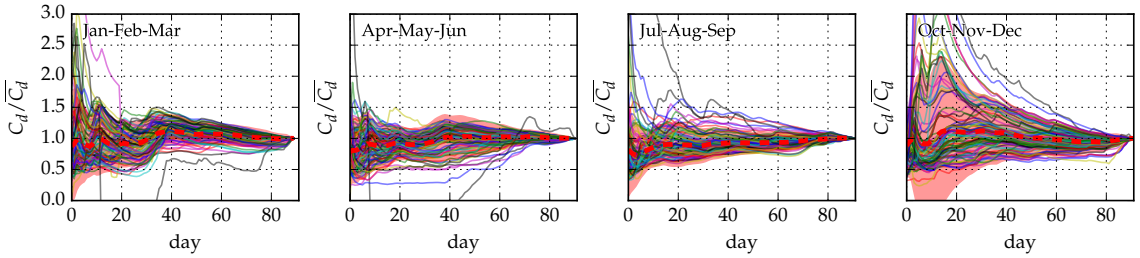

(b) SO_2

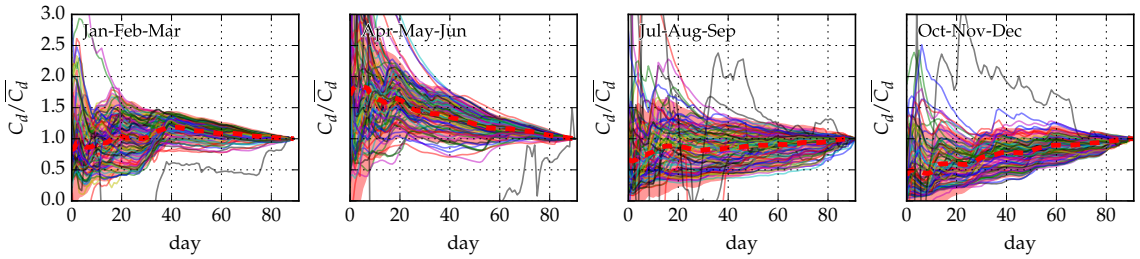

(c) NO_x

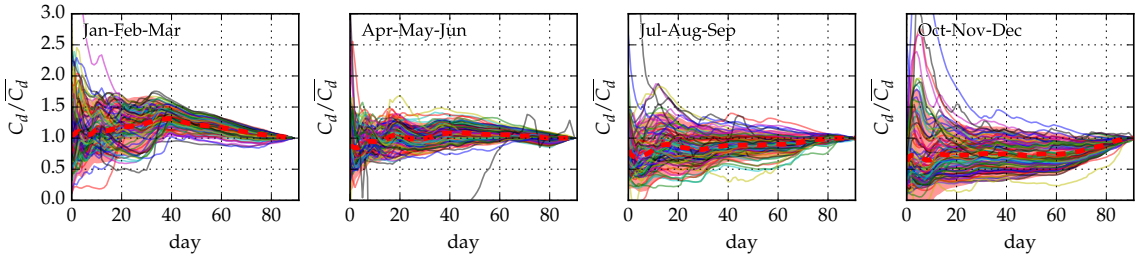

(d) NH_3

Figure C-46: Average changes in $PM_{2.5}$ concentrations over different lengths of simulation. Each line indicates each sample location. C_d is the sum of the CAMx grid of the average changes in $PM_{2.5}$ concentrations created by the marginal emissions ($\overline{E} \cdot 4^{-2}$) for a given simulation period (e.g. from day one to day d). $\overline{C_d}$ is the sum of the average changes in $PM_{2.5}$ concentrations for the entire season period. The red dashed line indicates the 2.5% truncated means and the shaded area covers the 95% confidence intervals of the means.

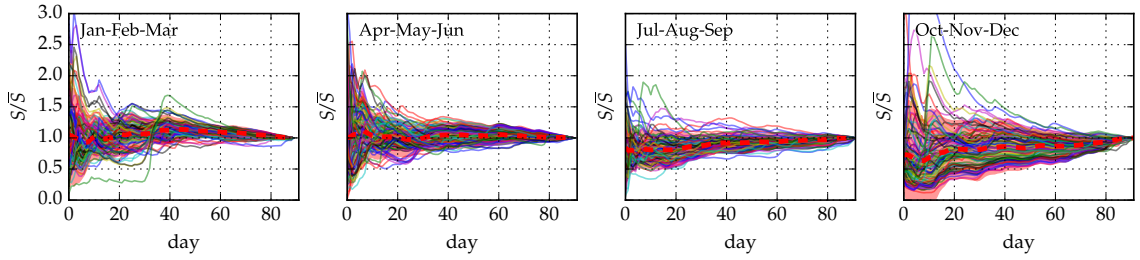

(a) EC

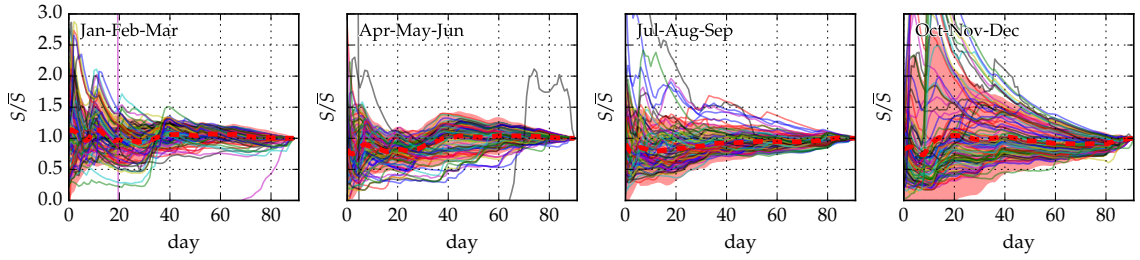

(b) SO_2

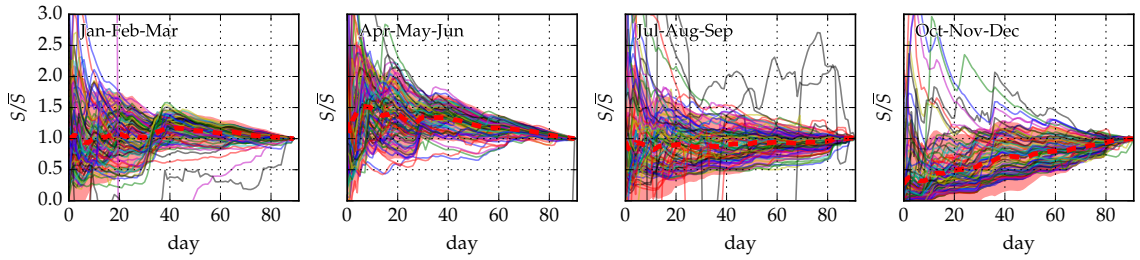

(c) NO_x

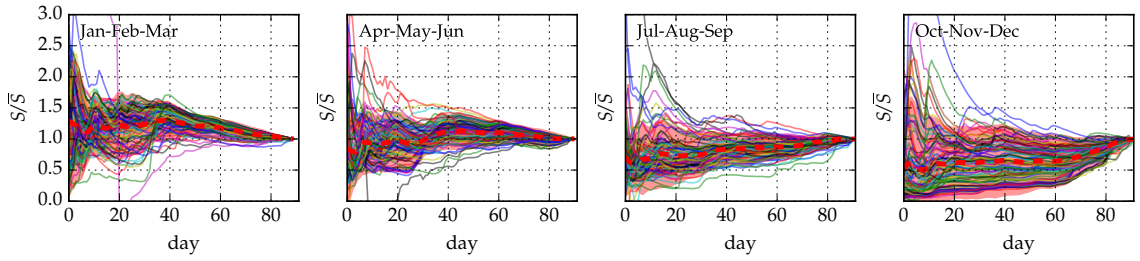

(d) NH_3

Figure C-47: Social costs over different lengths of simulation. Each line indicates each sample location. S is the per-tonne social cost calculated for a given simulation period. $\overline{S}$ is the per-tonne social cost for the whole season simulation. The red dashed line indicates the 2.5% truncated means and the shaded area covers the 95% confidence intervals of the means.

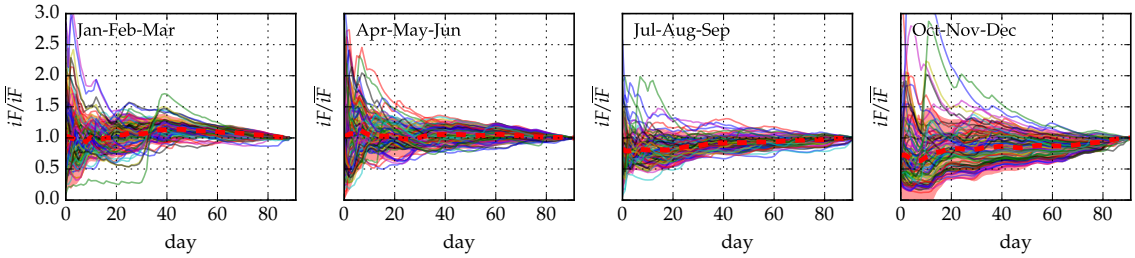

(a) EC

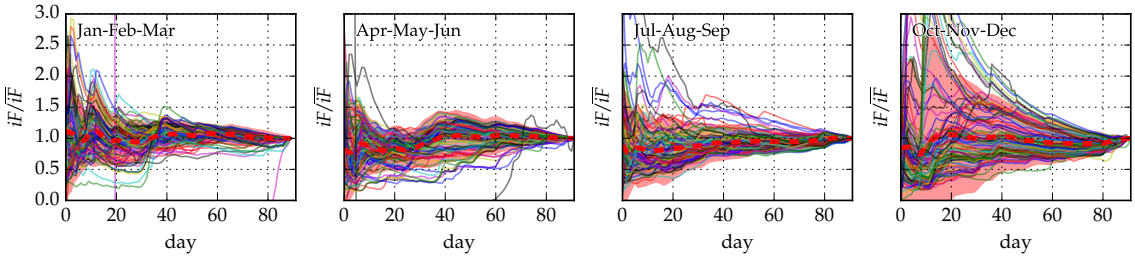

(b) SO_2

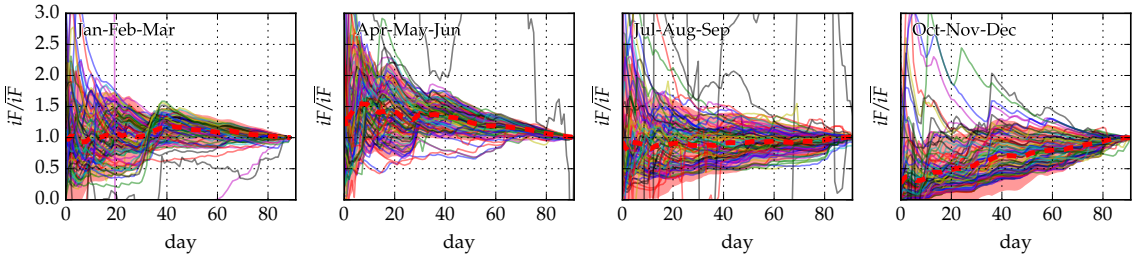

(c) NO_x

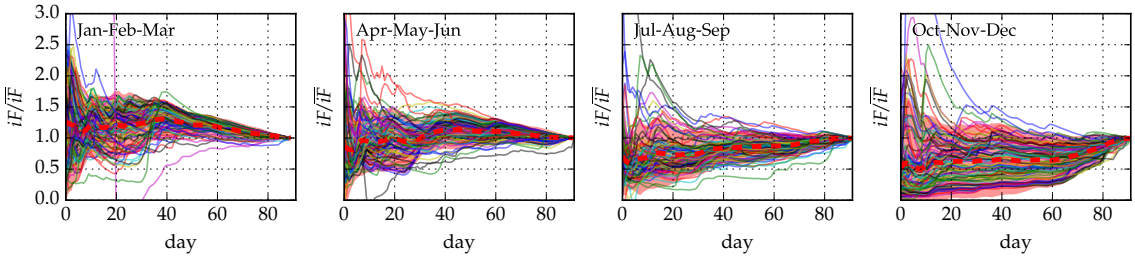

(d) NH_3

Figure C-48: Intake fractions over different lengths of simulation. Each line indicates each sample location. iF is the intake fraction calculated for a given simulation period. $\overline{iF}$ is the intake fraction for the whole season simulation. The red dashed line indicates the 2.5% truncated means and the shaded area covers the 95% confidence intervals of the means.

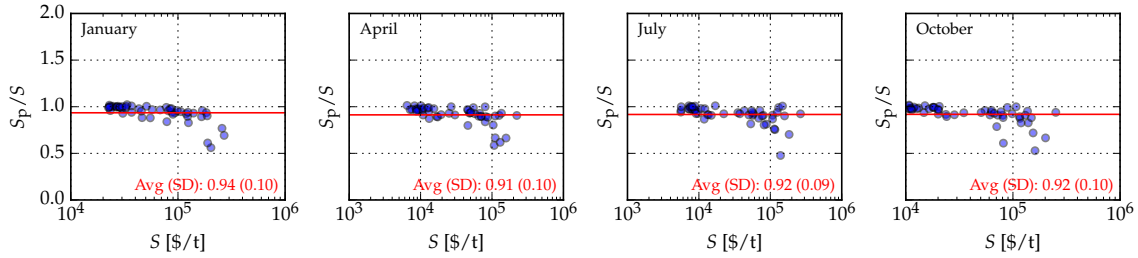

(a) EC

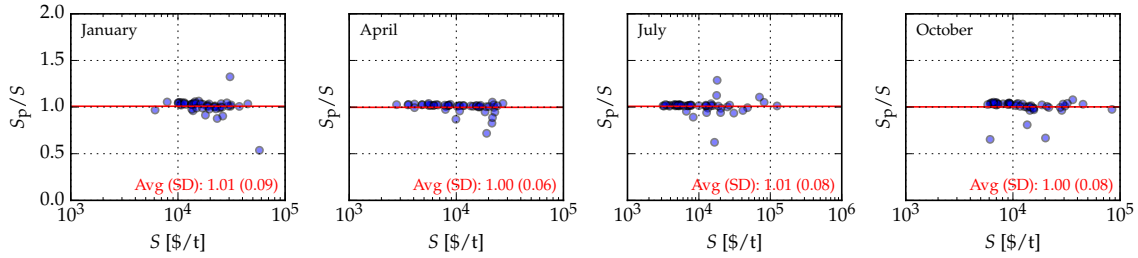

(b) SO_2

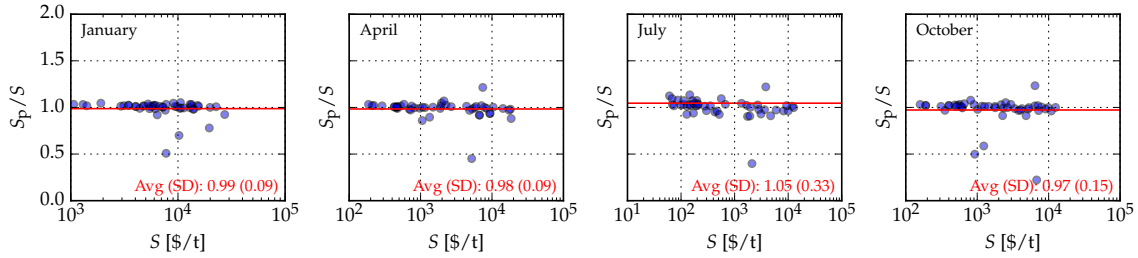

(c) NO_x

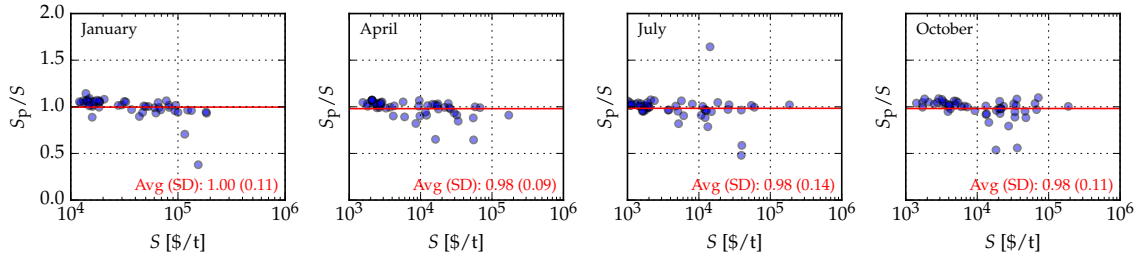

(d) NH_3

Figure C-49: Sensitivity of social cost to elevated point sources for the 50 training samples. S and S_p are the per-tonne social cost of area emissions and point emissions, respectively.

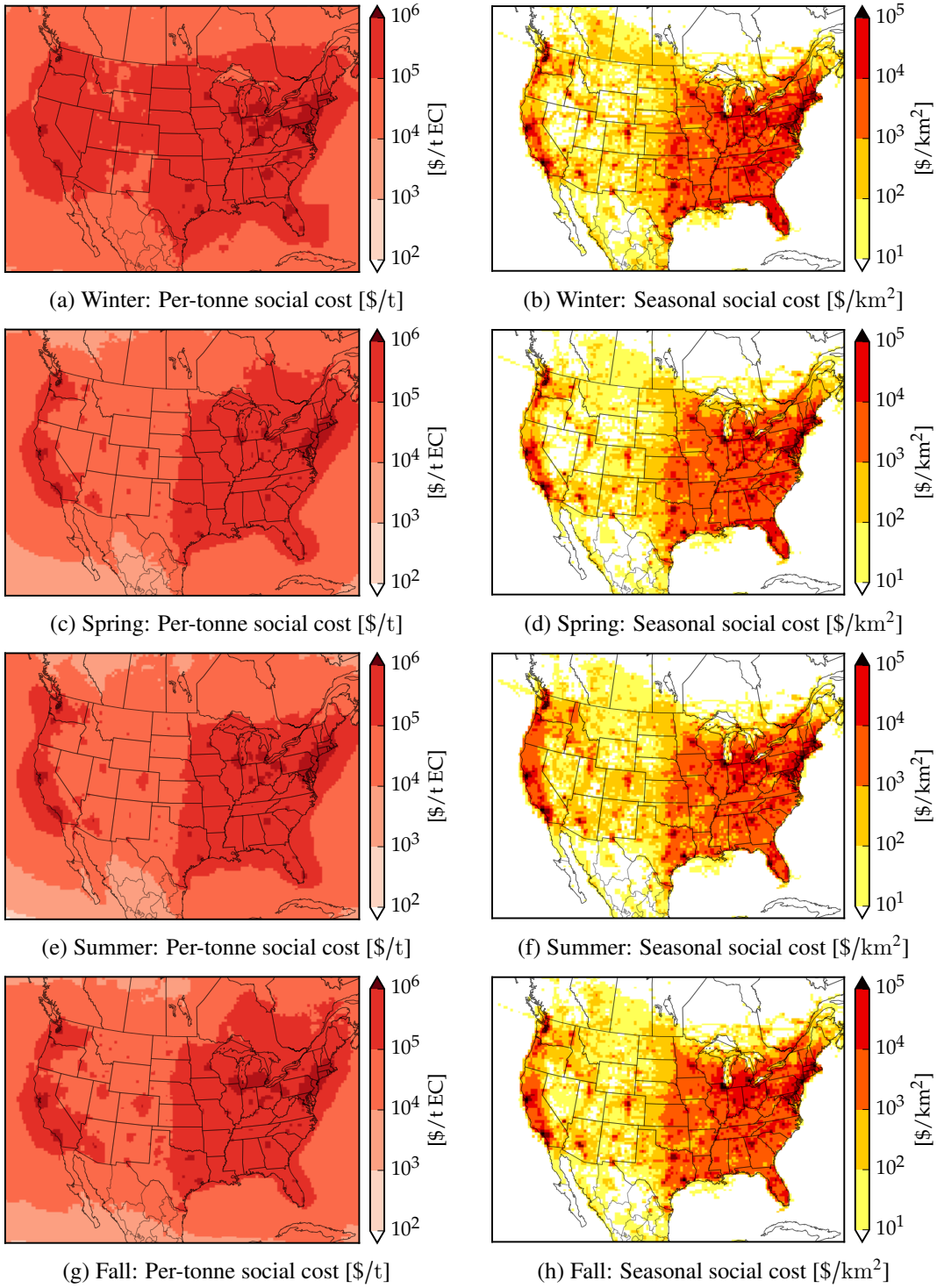

(a) Winter: Per-tonne social cost [$/t]

(b) Winter: Seasonal social cost [$/km^2]

(c) Spring: Per-tonne social cost [$/t]

(d) Spring: Seasonal social cost [$/km^2]

(e) Summer: Per-tonne social cost [$/t]

(f) Summer: Seasonal social cost [$/km^2]

(g) Fall: Per-tonne social cost [$/t]

(h) Fall: Seasonal social cost [$/km^2]

Figure C-50: Map of EC social cost at the point of emissions estimated using the relative risk of 1.06 and the VSL of $8.8M. The right-hand side figures show the seasonal social costs calculated by multiplying the left-hand side values with season emissions.

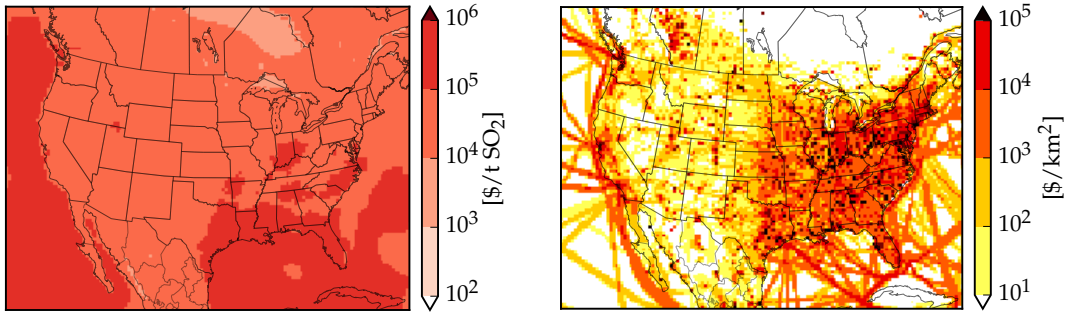

(a) Winter: Per-tonne social cost [$/t]

(b) Winter: Seasonal social cost [$/km^2]

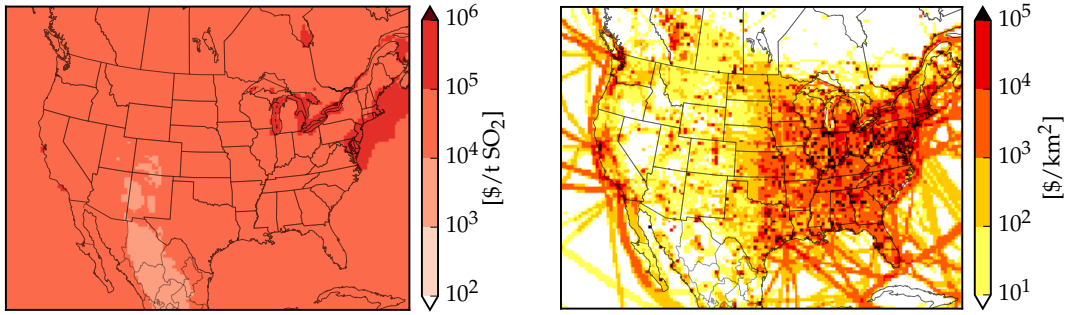

(c) Spring: Per-tonne social cost [$/t]

(d) Spring: Seasonal social cost [$/km^2]

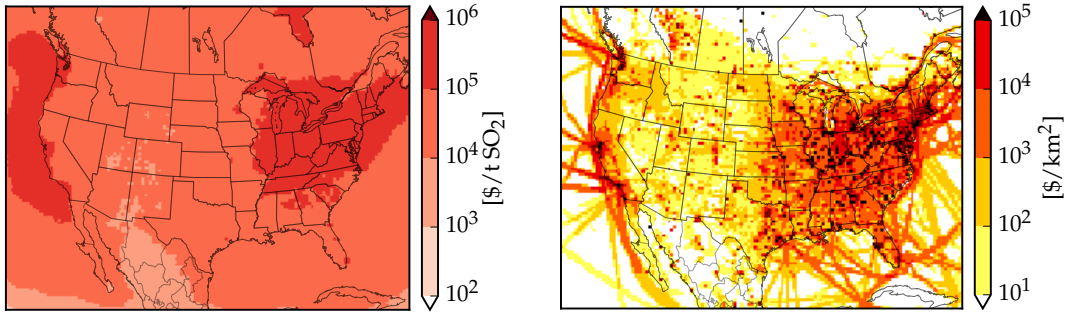

(e) Summer: Per-tonne social cost [$/t]

(f) Summer: Seasonal social cost [$/km^2]

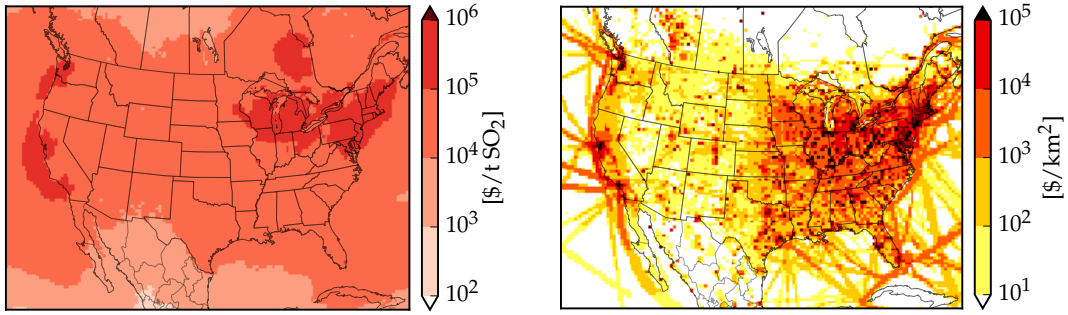

(g) Fall: Per-tonne social cost [$/t]

(h) Fall: Seasonal social cost [$/km^2]

Figure C-51: Map of SO_2 social cost at the point of emissions estimated using the relative risk of 1.06 and the VSL of $8.8M. The right-hand side figures show the seasonal social costs calculated by multiplying the left-hand side values with season emissions.

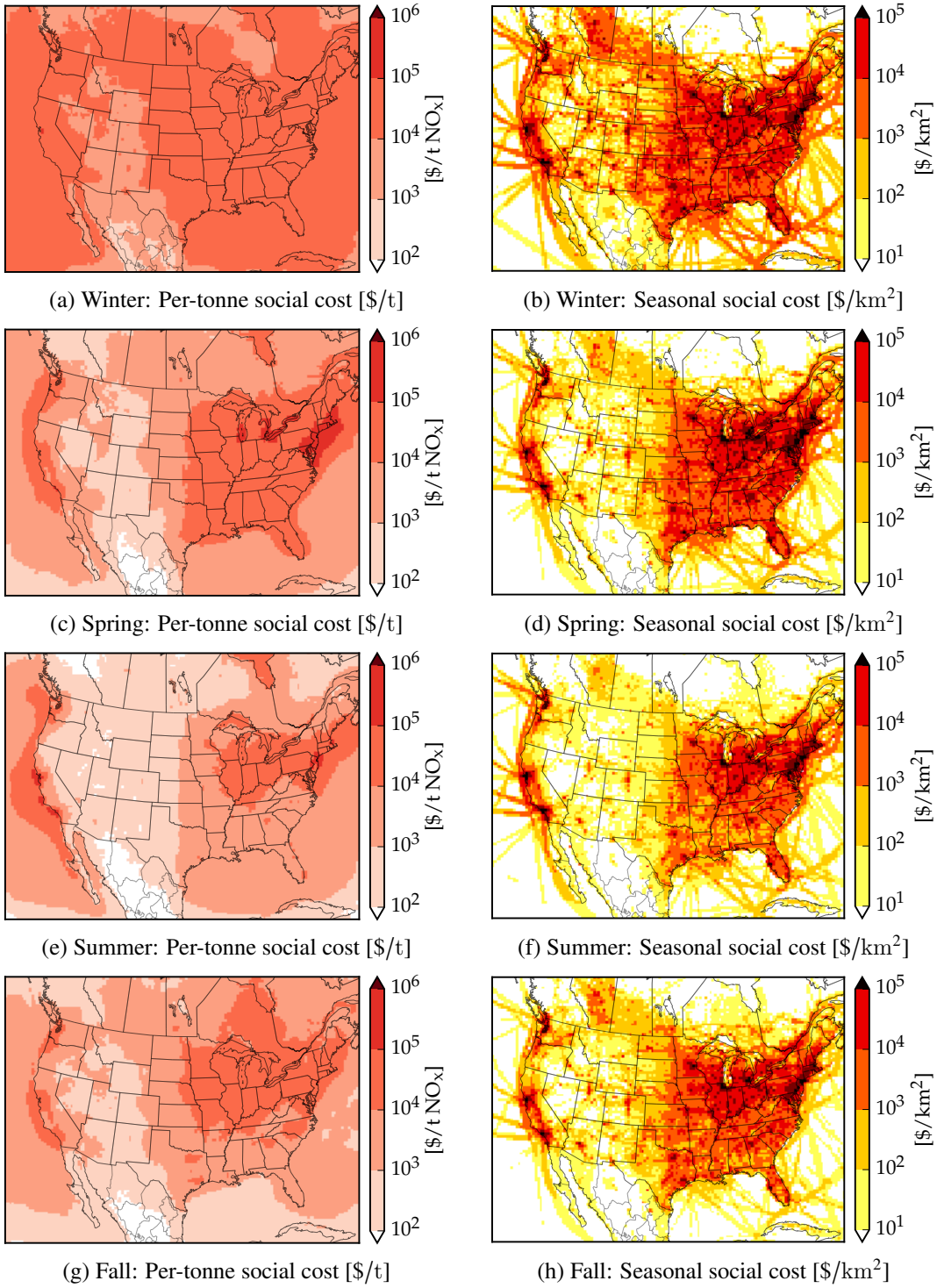

(a) Winter: Per-tonne social cost [$/t]

(b) Winter: Seasonal social cost [$/km^2]

(c) Spring: Per-tonne social cost [$/t]

(d) Spring: Seasonal social cost [$/km^2]

(e) Summer: Per-tonne social cost [$/t]

(f) Summer: Seasonal social cost [$/km^2]

(g) Fall: Per-tonne social cost [$/t]

(h) Fall: Seasonal social cost [$/km^2]

Figure C-52: Map of NO_x social cost at the point of emissions estimated using the relative risk of 1.06 and the VSL of $8.8M. The right-hand side figures show the seasonal social costs calculated by multiplying the left-hand side values with season emissions.

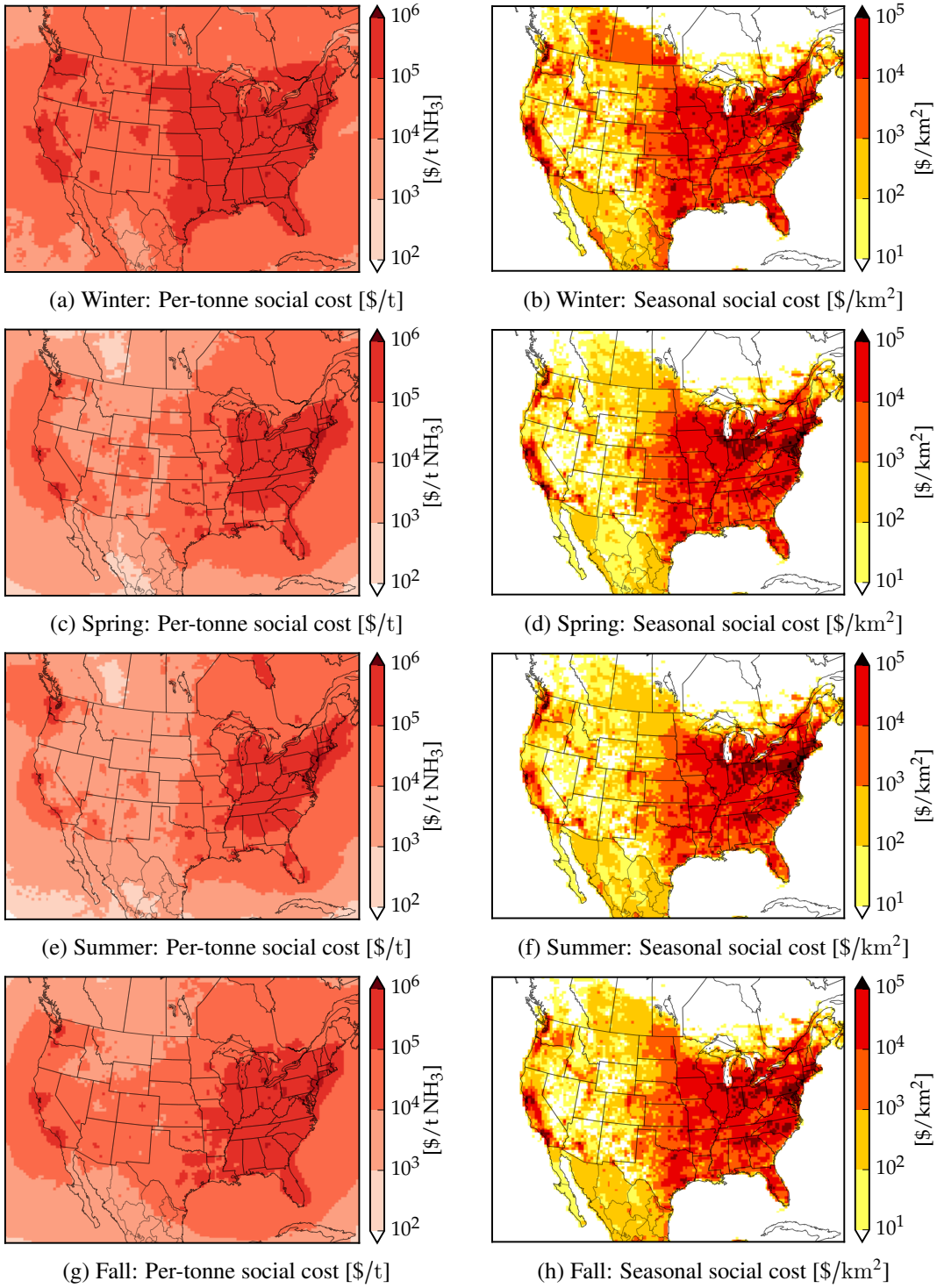

(a) Winter: Per-tonne social cost [$/t]

(b) Winter: Seasonal social cost [$/km^2]

(c) Spring: Per-tonne social cost [$/t]

(d) Spring: Seasonal social cost [$/km^2]

(e) Summer: Per-tonne social cost [$/t]

(f) Summer: Seasonal social cost [$/km^2]

(g) Fall: Per-tonne social cost [$/t]

(h) Fall: Seasonal social cost [$/km^2]

Figure C-53: Map of NH_3 social cost at the point of emissions estimated using the relative risk of 1.06 and the VSL of $8.8M. The right-hand side figures show the seasonal social costs calculated by multiplying the left-hand side values with season emissions.

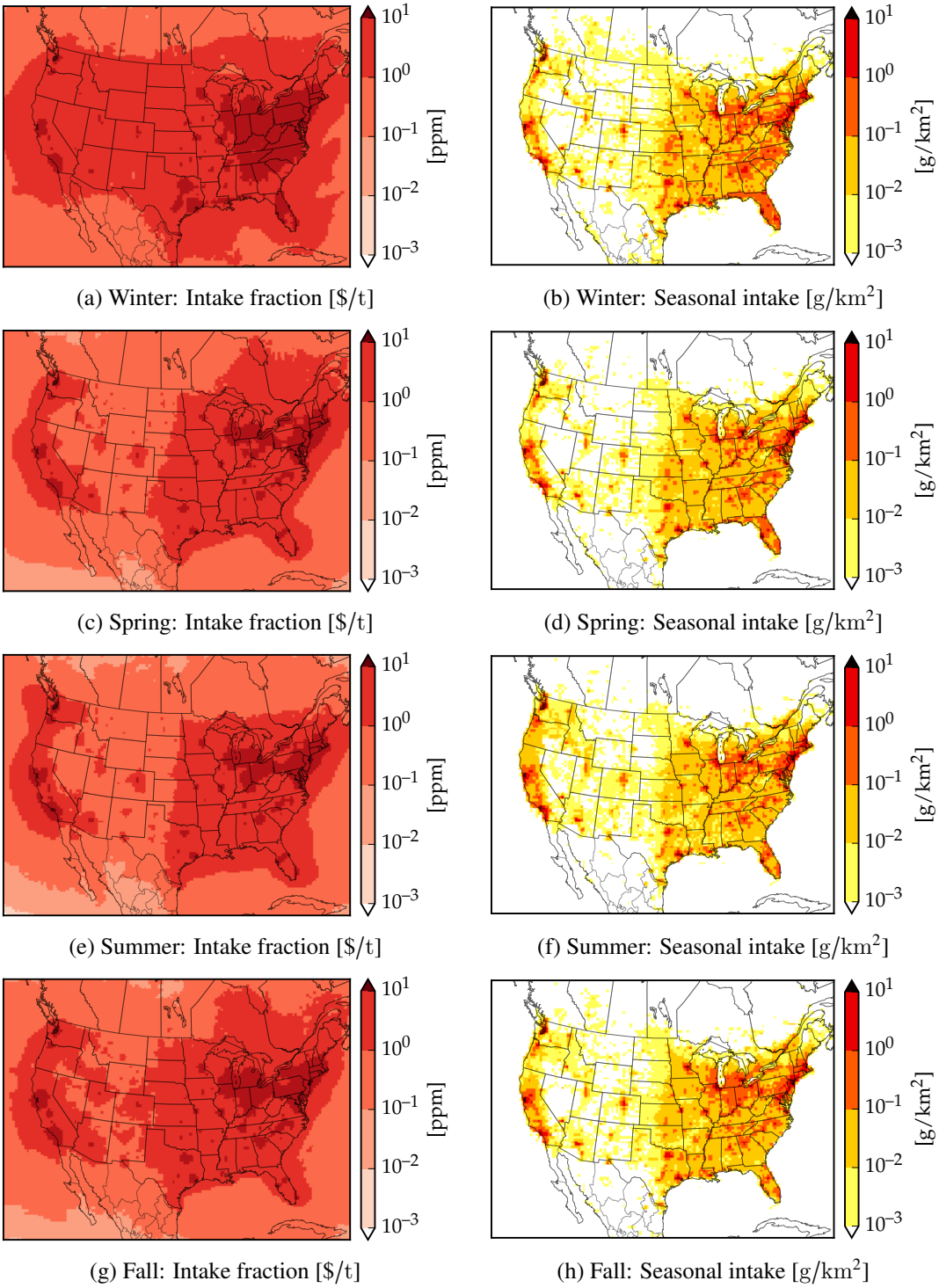

(a) Winter: Intake fraction [$/t]

(b) Winter: Seasonal intake [g/km^2]

(c) Spring: Intake fraction [$/t]

(d) Spring: Seasonal intake [g/km^2]

(e) Summer: Intake fraction [$/t]

(f) Summer: Seasonal intake [g/km^2]

(g) Fall: Intake fraction [$/t]

(h) Fall: Seasonal intake [g/km^2]

Figure C-54: Map of EC intake fraction at the point of emissions. The right-hand side figures show the seasonal intake values calculated by multiplying the left-hand side values with season emissions.

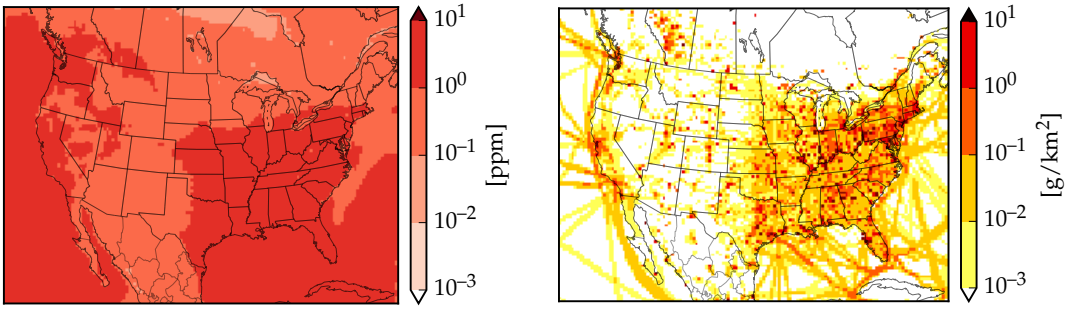

(a) Winter: Intake fraction [$/t]

(b) Winter: Seasonal intake [g/km^2]

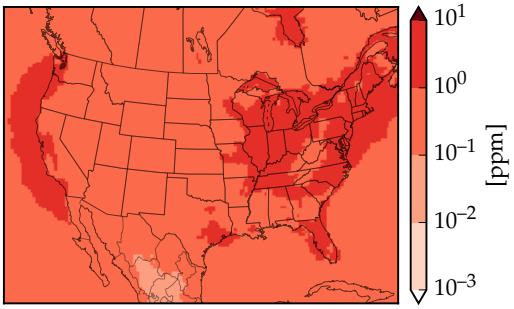

(c) Spring: Intake fraction [$/t]

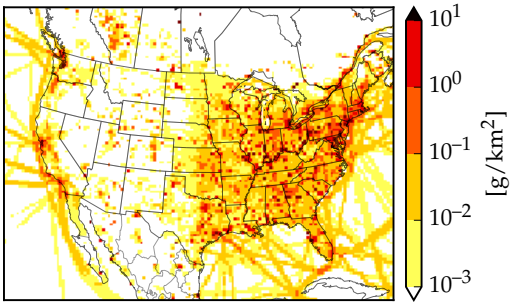

(d) Spring: Seasonal intake [g/km^2]

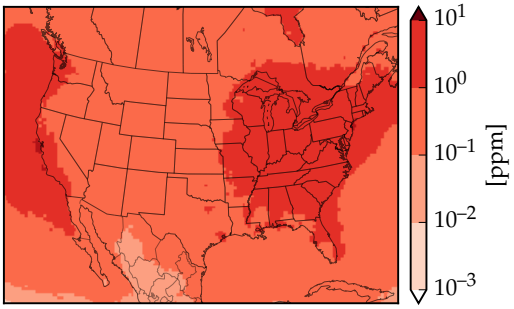

(e) Summer: Intake fraction [$/t]

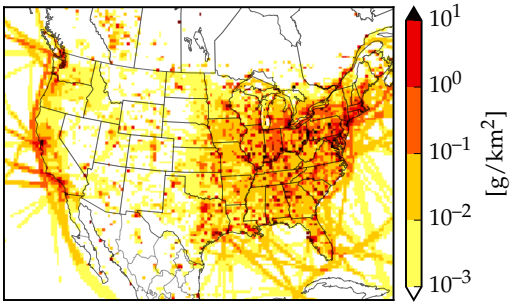

(f) Summer: Seasonal intake [g/km^2]

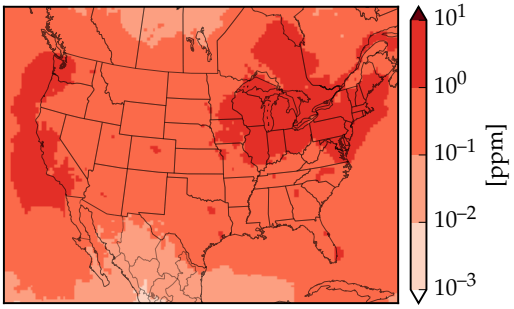

(g) Fall: Intake fraction [$/t]

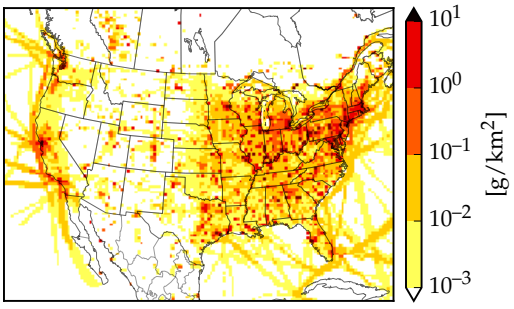

(h) Fall: Seasonal intake [g/km^2]

Figure C-55: Map of SO_2 intake fraction at the point of emissions. The right-hand side figures show the seasonal intake values calculated by multiplying the left-hand side values with season emissions.

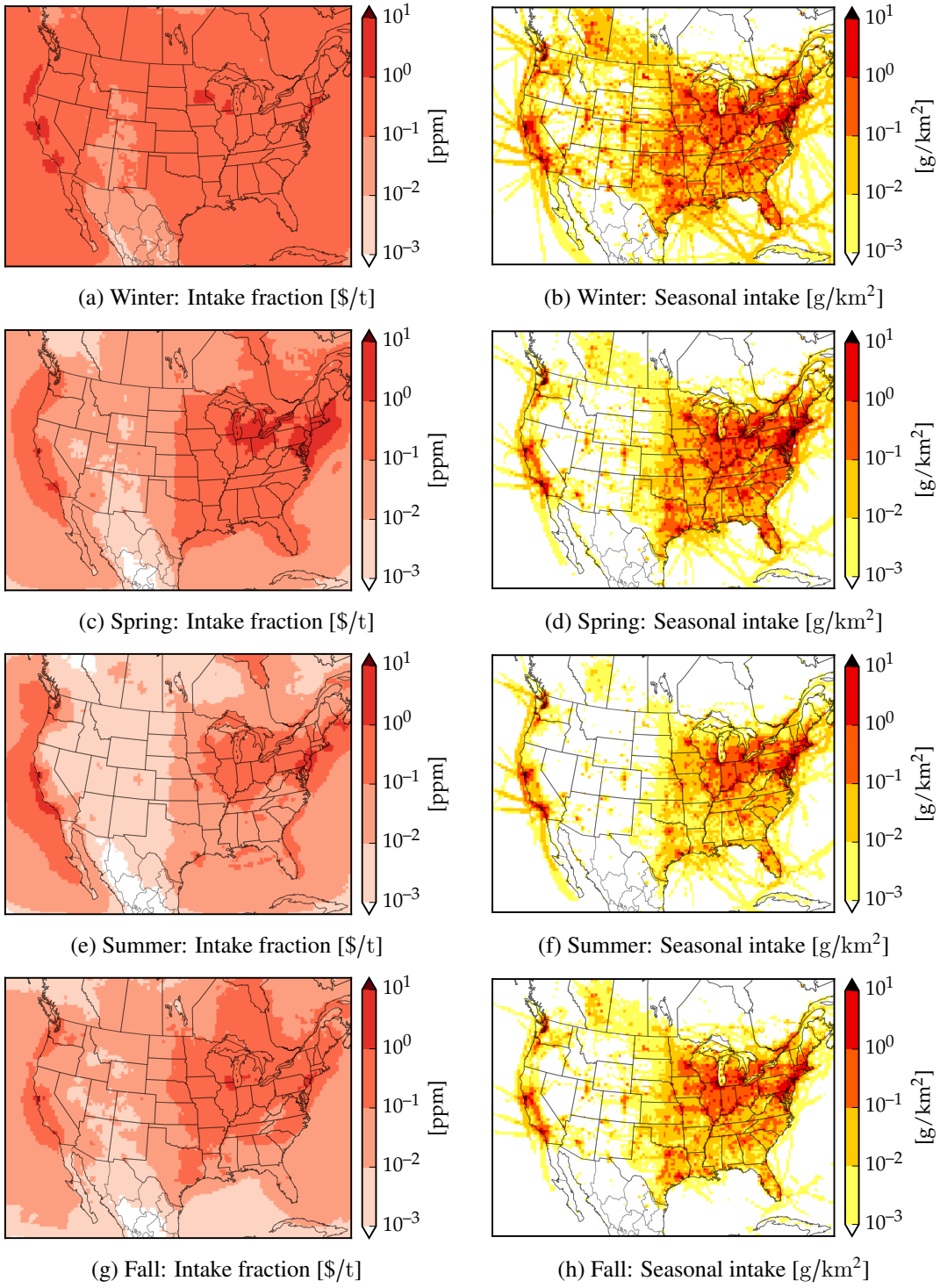

(a) Winter: Intake fraction [$/t]

(b) Winter: Seasonal intake [g/km^2]

(c) Spring: Intake fraction [$/t]

(d) Spring: Seasonal intake [g/km^2]

(e) Summer: Intake fraction [$/t]

(f) Summer: Seasonal intake [g/km^2]

(g) Fall: Intake fraction [$/t]

(h) Fall: Seasonal intake [g/km^2]

Figure C-56: Map of NO_x intake fraction at the point of emissions. The right-hand side figures show the seasonal intake values calculated by multiplying the left-hand side values with season emissions.

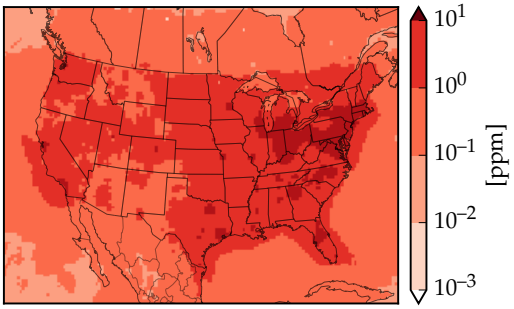

(a) Winter: Intake fraction [$/t]

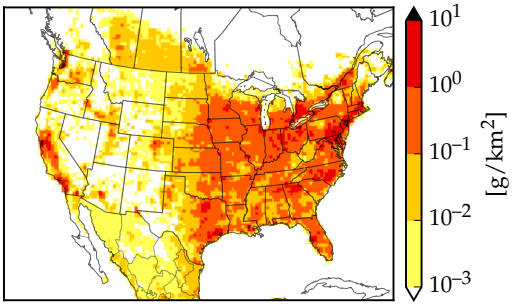

(b) Winter: Seasonal intake [g/km^2]

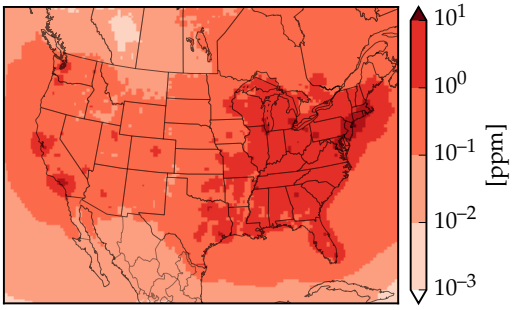

(c) Spring: Intake fraction [$/t]

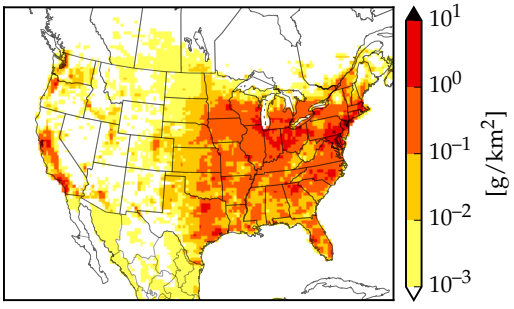

(d) Spring: Seasonal intake [g/km^2]

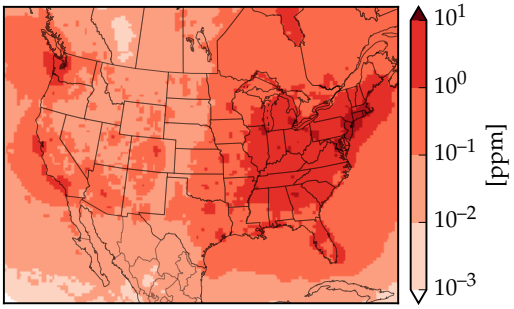

(e) Summer: Intake fraction [$/t]

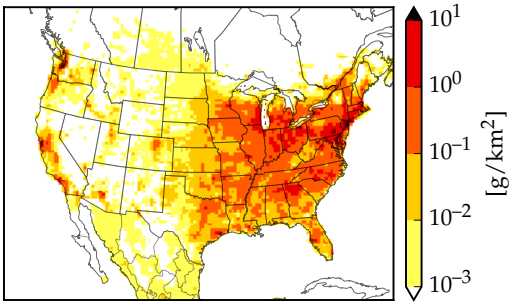

(f) Summer: Seasonal intake [g/km^2]

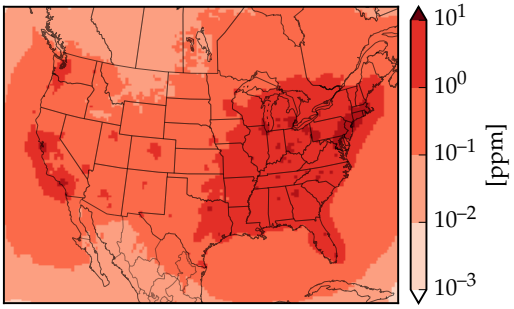

(g) Fall: Intake fraction [$/t]

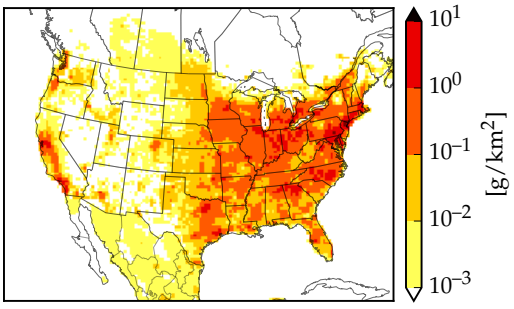

(h) Fall: Seasonal intake [g/km^2]

Figure C-57: Map of NH_3 intake fraction at the point of emissions. The right-hand side figures show the seasonal intake values calculated by multiplying the left-hand side values with season emissions.

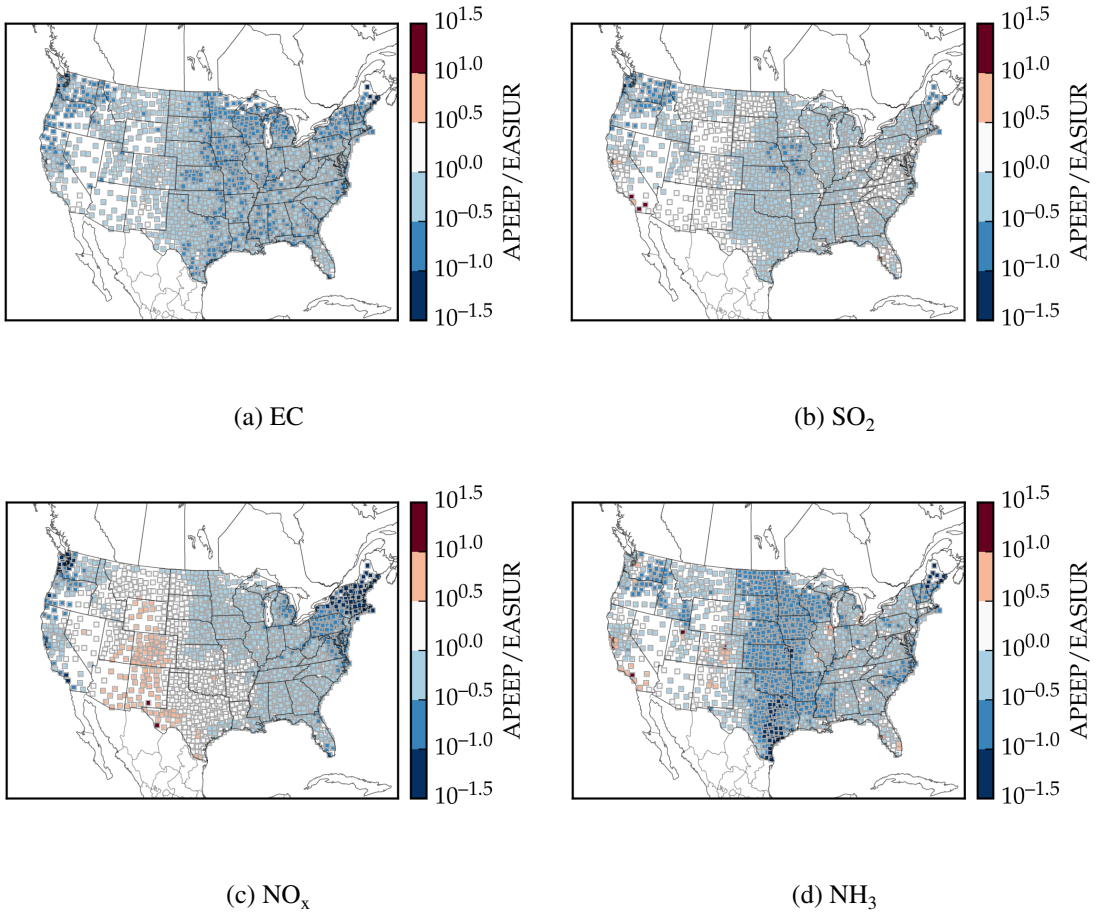

(a) EC

(b) SO_2

(c) NO_x

(d) NH_3

Figure C-58: Spatial comparison between EASIUR and APEEP. The APEEP values are based on Muller et al (2011). EASIUR estimates are calculated for the centroid location of each county and matched to corresponding APEEP values. All the values are further adjusted to match dollar year, income growth, VSL, and tonne unit with the EASIUR.

Table C-65: Annual emissions from the life cycle of electricity generation in 2005. (Unit: [metric ton/year])

Sector	EC	SO_2	NO_x	NH_3
Coal mining	10,000	1,900	2,300	410
Energy pipelines	7,600	40,000	410,000	470
Oil and gas extraction	6,300	70,000	330,000	91
Petroleum refineries	30,000	250,000	150,000	4,700
Power generation	530,000	10,000,000	3,800,000	29,000
Total	590,000	11,000,000	4,600,000	35,000

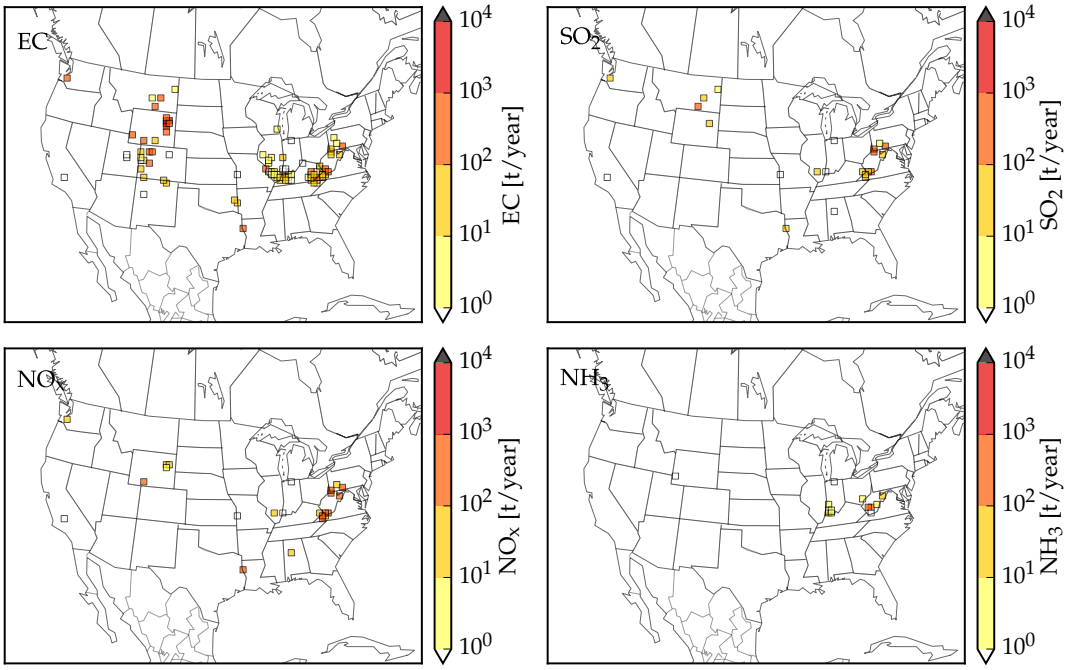

Figure C-59: Emissions from Coal Mining

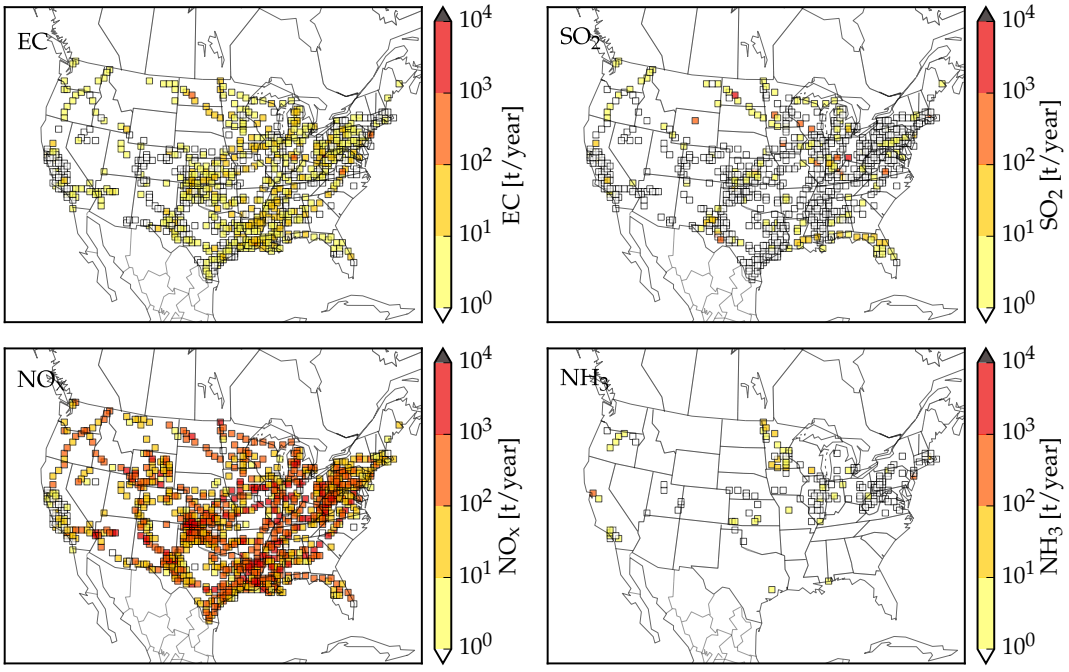

Figure C-60: Emissions from Energy Pipelines

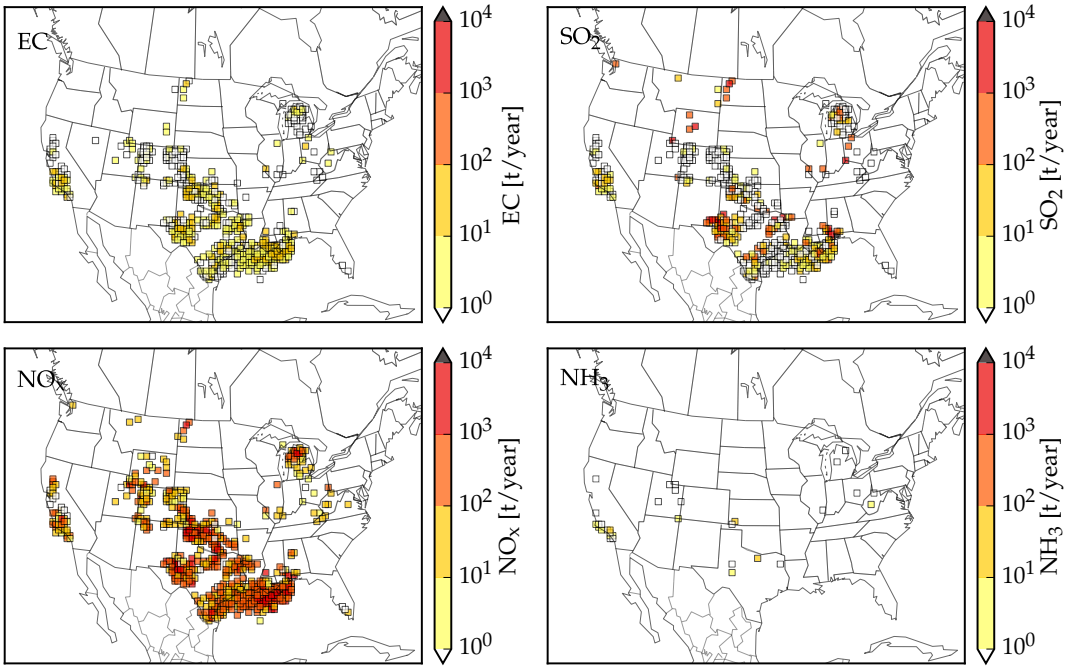

Figure C-61: Emissions from Oil & Gas extraction

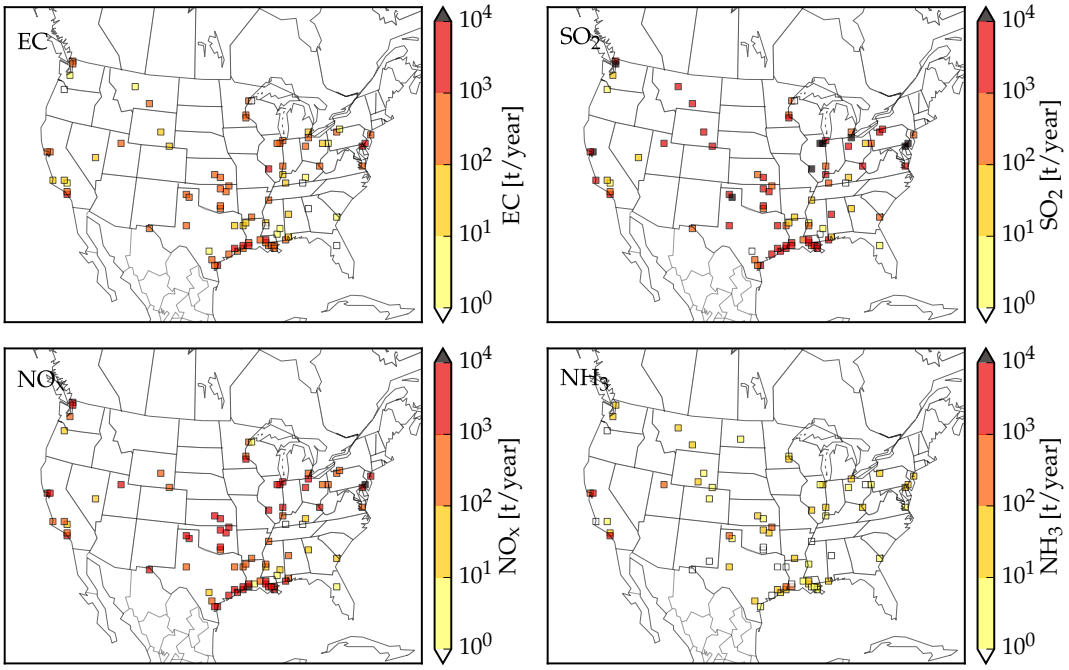

Figure C-62: Emissions from Petroleum refineries

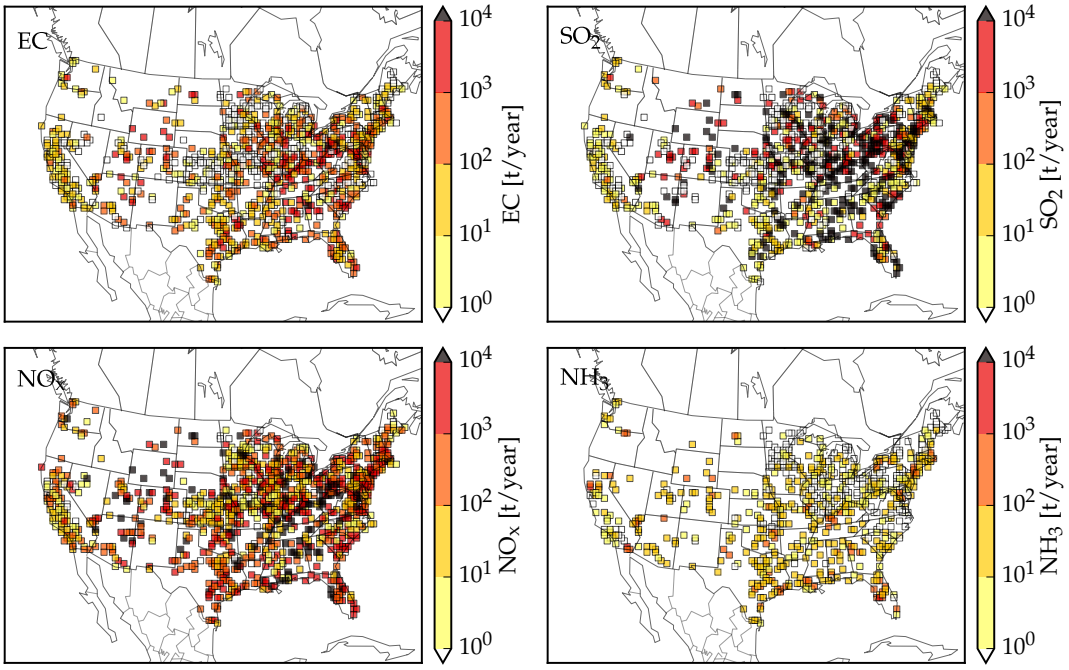

Figure C-63: Emissions from Power generation

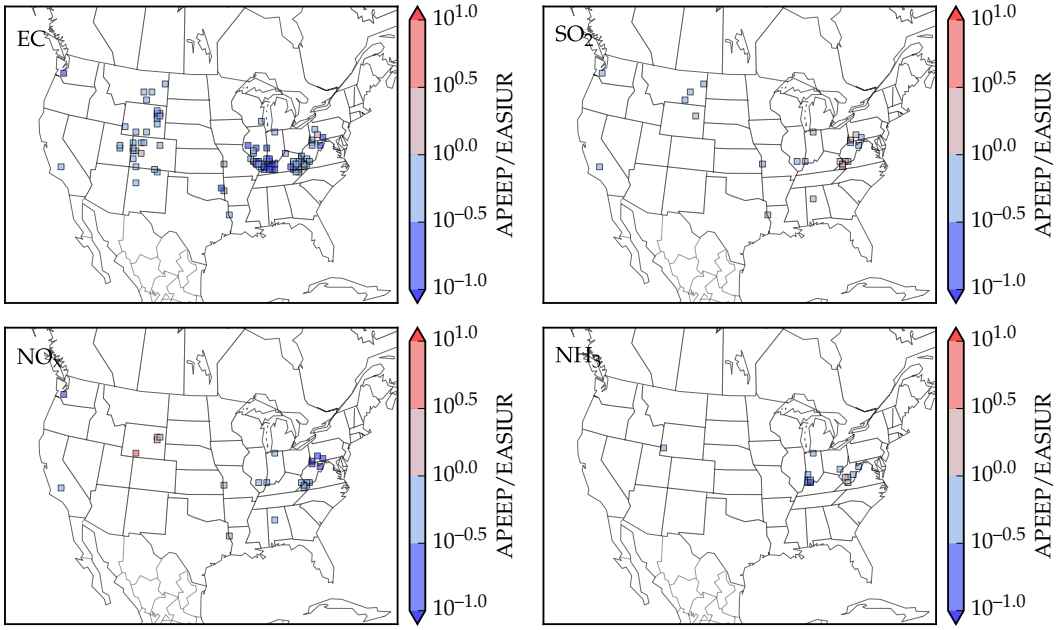

Figure C-64: Comparison between EASIUR and APEEP for Coal Mining. Marginal damages for area sources from APEEP are used for comparison.

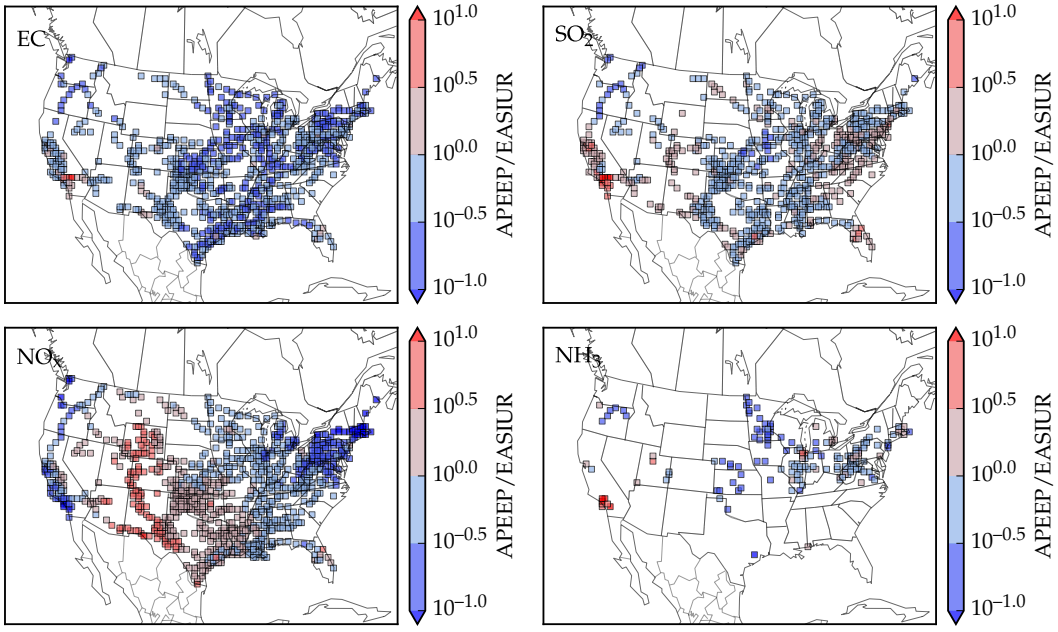

Figure C-65: Comparison between EASIUR and APEEP for Energy Pipelines. Marginal damages for area sources from APEEP are used for comparison.

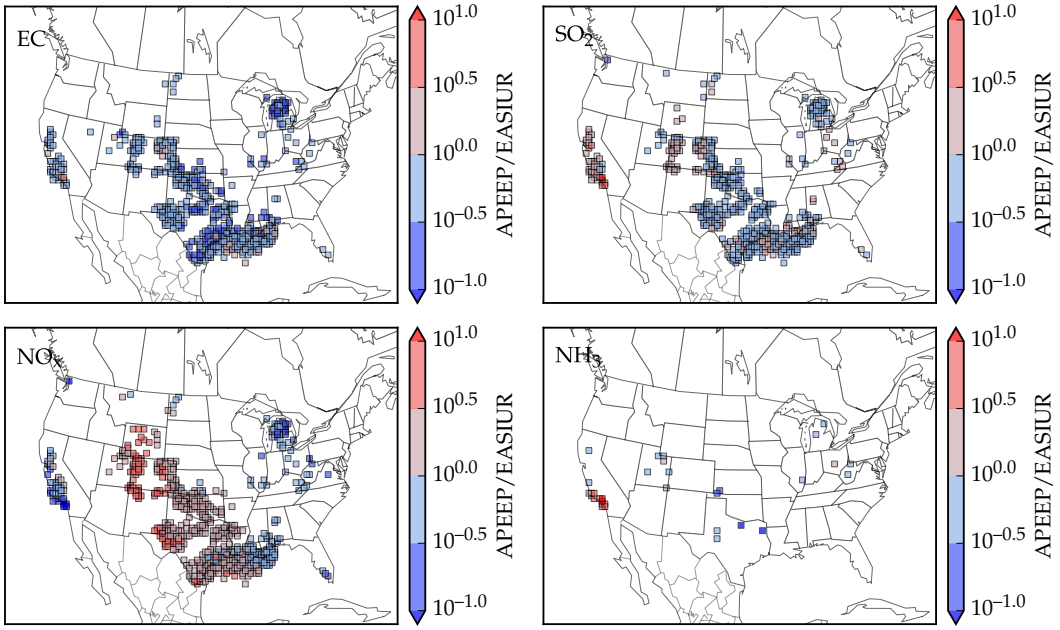

Figure C-66: Comparison between EASIUR and APEEP for Oil & Gas extraction. Marginal damages for area sources from APEEP are used for comparison.

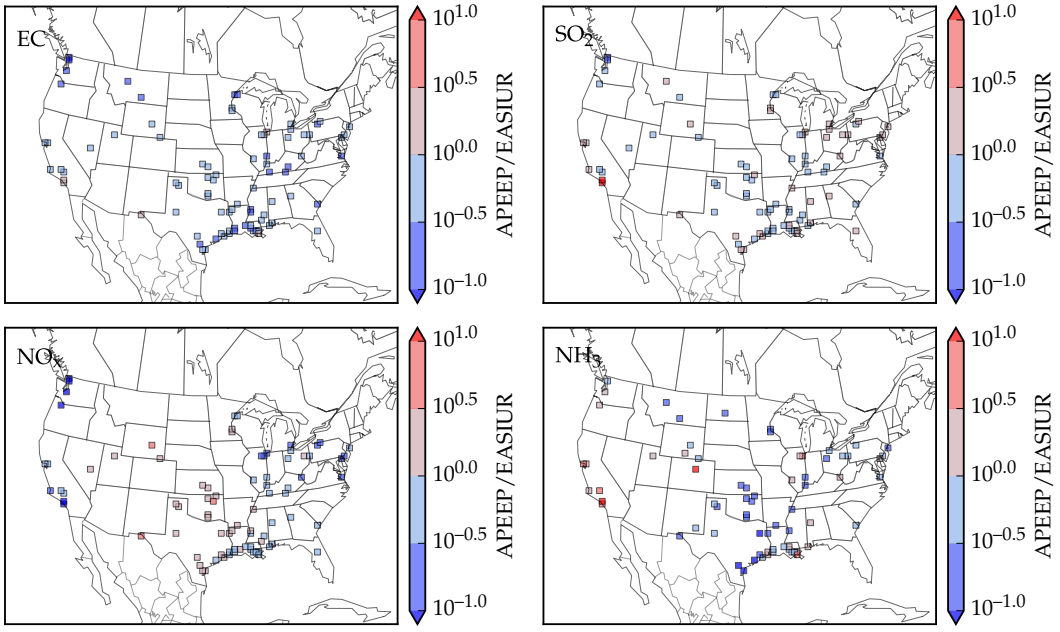

Figure C-67: Comparison between EASIUR and APEEP for Petroleum refineries. Marginal damages for area sources from APEEP are used for comparison.

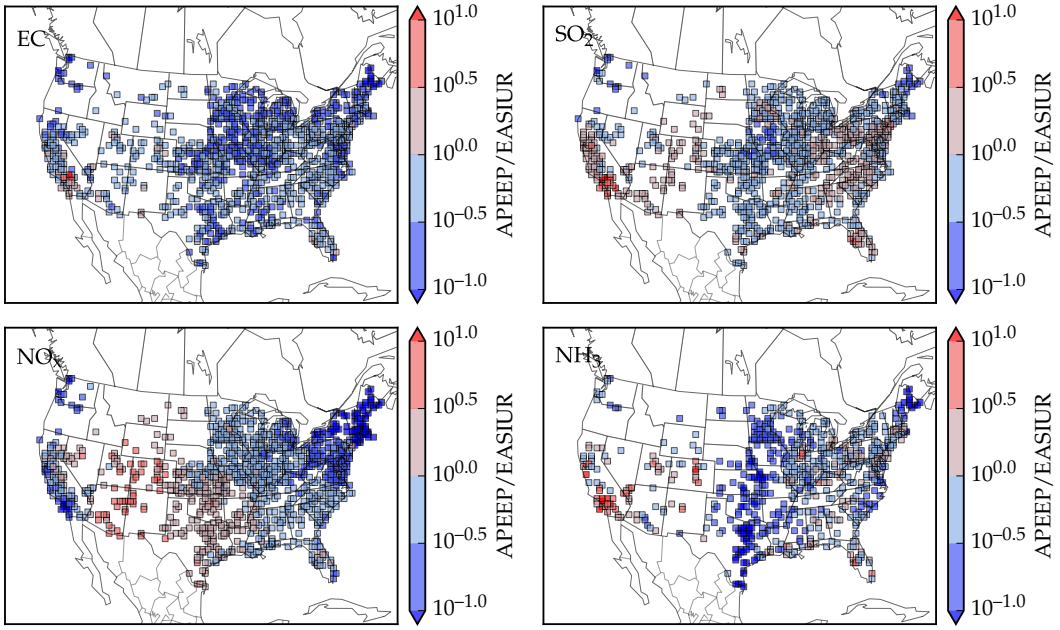

Figure C-68: Comparison between EASIUR and APEEP for Power generation. Marginal damages for area sources from APEEP are used for comparison.

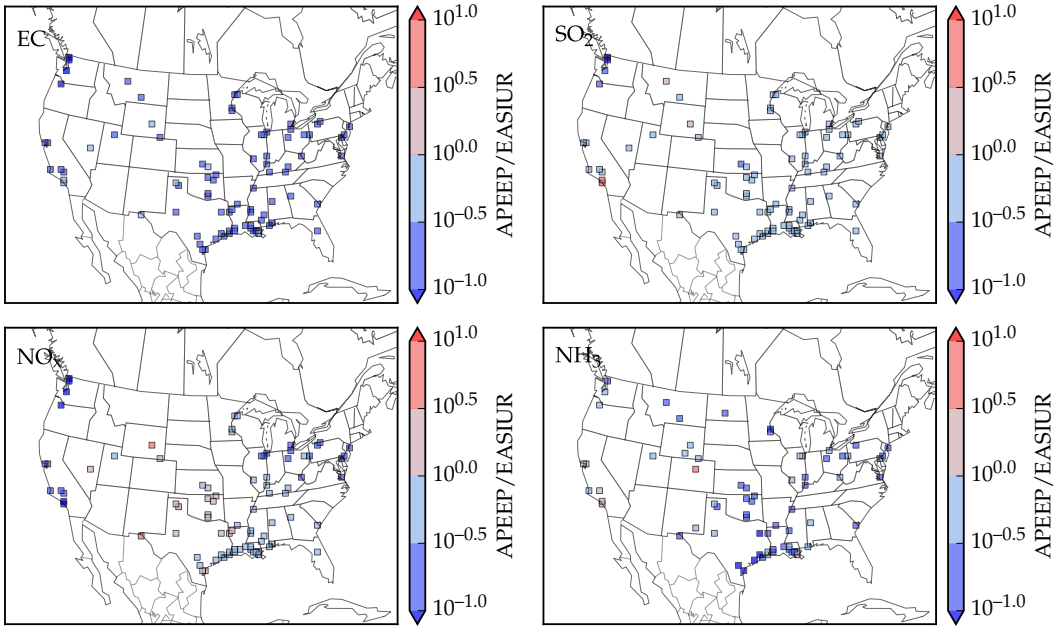

Figure C-69: Comparison between EASIUR and APEEP for Petroleum refineries. Marginal damages for mid-height (250-500 m) point sources from APEEP are used for comparison.

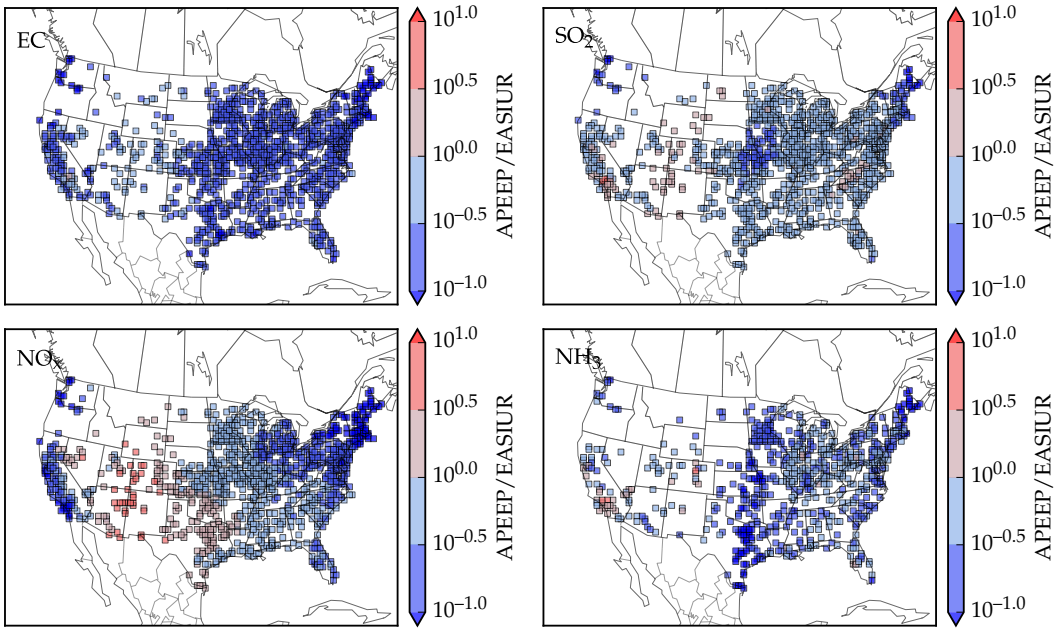

Figure C-70: Comparison between EASIUR and APEEP for Power generation. Marginal damages for mid-height (250-500 m) point sources from APEEP are used for comparison.

D Appendix II: EASIUR User's Guide

EASIUR User's Guide Version 0.1

Jinhyok Heo

Feb 2014

1. Introduction

The Estimating Air pollution Social Impacts Using Regression (EASIUR) model predicts marginal social costs for air pollutants [$/t] emitted anywhere in the United States and from nearby areas of neighboring countries (Canada and Mexico) and oceans. The EASIUR's social costs include only the impact of $PM_{2.5}$ on premature death, which usually accounts for more than 90% of social costs. It estimates the monetized impacts of $PM_{2.5}$ from a certain emissions affecting over a large (~thousands km) area downwind.

Currently, EASIUR predicts marginal damages of four major species: elemental carbon (EC), sulfur dioxide (SO_2), nitrogen oxides (NO_x), and ammonia (NH_3). EC represents directly emitted $PM_{2.5}$ and, therefore, is called direct or "primary" $PM_{2.5}$. The other three species (SO_2, NO_x, and NH_3) are emitted as gas and produce $PM_{2.5}$ chemically in the atmosphere, and are called "secondary" $PM_{2.5}$. Volatile organic compounds (VOCs), which form secondary organic $PM_{2.5}$, are not modeled yet. In addition, EASIUR is derived based on ground-level area emissions. Though EASIUR estimates were tested and found valid for low-height (~20 m) point sources, they may not represent marginal damages for highly (100-200m or higher) elevated point sources.

The marginal damages are derived based on the meteorology and emissions of 2005. They should be valid in the near future or past (e.g. 2005 ± 10 years), though rigorous analyses need to be done. The estimates, however, may change substantially in the longer term (e.g. 30-50 years) because large changes in SO_2, NO_x, and NH_3 emissions may change the chemical environment in the atmosphere that affects secondary $PM_{2.5}$ formation. To the contrary, the marginal damages of primary species (or EC) will not change.

2. Where to get EASIUR

EASIUR is distributed through its website: <http://barney.ce.cmu.edu/~jinhyok/easiur/>.

3. How to use EASIUR

The EASIUR model estimates marginal damages over the United States in a 148×112 grid, where one cell covers area of 36 km × 36 km, as shown in Figure D-1 (c). Accordingly, the marginal damage estimates from the EASIUR model are presented as two-dimensional arrays of size 148×112, where each cell points to a specific location in the U.S. domain. Sixteen arrays are provided because each species has one array per season (16 arrays = 1 array/species/season × 4 species × 4 seasons). Winter is defined as a period from January to March, spring from April to June, summer from July to September, and fall from October and December.

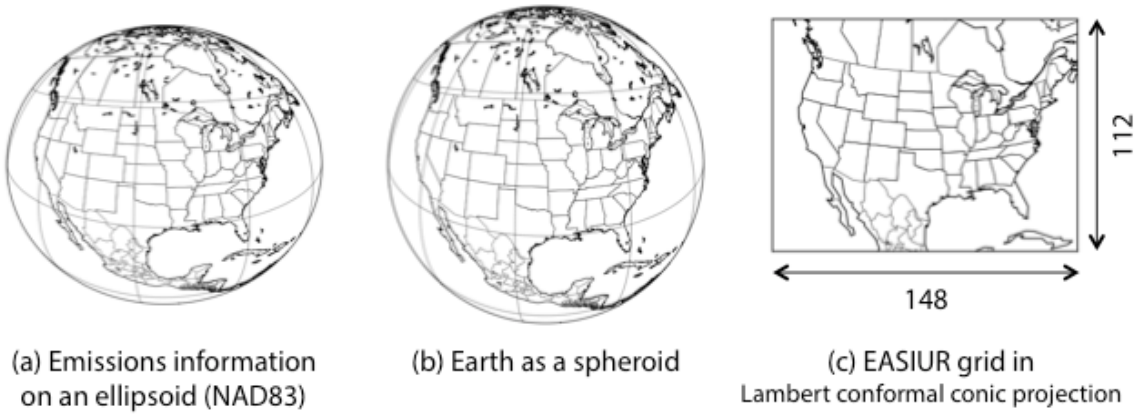

Figure D-1. Converting geodetic location to EASIUR grid. Emission location usually given in an ellipsoid datum (NAD83) needs to be converted to one on a spheroid and to the EASIUR grid (148×112).

Three pieces of information are needed to estimate the social cost of emissions: (1) the amount (*E*) of emissions, (2) the location (longitude and latitude) of emissions, and (3) the season of the emissions.

An important step is to convert the location (longitude and latitude) to the EASIUR grid coordinate system (or to a location (x, y) in the EASIUR's 148×112 grid). The EASIUR website provides an on-line conversion tool for a single or batch conversion.

The conversion is a bit complicated because the geodetic system (or datum) of a location needs to be converted. Usually, the location of emissions in the U.S. is provided in an ellipsoid, the NAD83 datum (Figure D-1 (a)) while CAMx (EASIUR's underlying chemical transport model) relies on a Lambert Conformal Conic projection (Figure D-1 (c)) on a spherical Earth (Figure D-1 (b)). The coordinate conversion is done in two steps:

1. The location in NAD83 datum needs to be converted to one in a spherical datum of Earth's radius 6,370 km. (Figure D-1 (a) to Figure D-1 (b))

2. The location in the spherical Earth needs to be converted with a Lambert Conformal Conic projection. (Figure D-1 (b) to Figure D-1 (c))

After conversion, you will have the position of emissions (x, y) in the EASIUR grid. Then, you can find marginal emissions [$/t] from a pollutant- and season-specific EASIUR array and multiply the marginal emissions by the amount of emissions [t] to calculate the social cost of the emissions [$]. If emissions do not have season information, averages of four seasonal estimates would be used.

4. Adjusting EASIUR estimates

The EASIUR marginal damages can be adjusted for a different choice of the value of a statistical life (VSL) and a concentration-response (CR) relation. EASIUR is published with $8.8M in 2010 USD for VSL and a relative risk of 1.06 for CR.

4.1 Adjusting VSL for Inflation and Income Growth

An adjusted EASIUR marginal damage (S') for a different VSL can be calculated as follows:

$$S' = S \cdot \frac{\text{VSL}}{\$8.8M} \quad (1)$$

where S is the default EASIUR marginal damages.

Usually, U.S. EPA's official VSL will be used, which is $4.8M in 1990 USD and 1990 income level. This VSL is the central estimate from a Weibull distribution that U.S. EPA built based on 26 value-of-life studies (U.S. EPA, 2010). U.S. EPA recommends that this $4.8M be used in benefit analyses (U.S. EPA, 2010).

This $4.8M often needs to be adjusted for a different dollar year to account for inflation. It also needs to be adjusted for income level since people are willing to pay more to avoid the mortality risk from $PM_{2.5}$ as their income grows. The U.S. EPA's official adjustment factors for these two factors are included in Table D-2.

For example, $4.8M in 1990 USD can be converted to a VSL (V') in 2000 USD and 2000 income level as follows:

$$V' = \$4.8M \cdot \frac{G_{2000}}{G_{1990}} \cdot \frac{I_{2000}}{I_{1990}}$$

$$= \$4.8M \cdot \frac{1.00}{0.76} \cdot \frac{1.04}{1.0}$$

$$= \$6.6M$$

where G_{2000} and G_{1990} are GDP deflators and I_{2000} and I_{1990} are income level adjustment factor for year 2000 and 1990 from Table D-2. Then, EASIUR's marginal damage with the default $8.8M VSL ($S'$) can be converted to this $6.6M using Eq. (1):

$$S' = S \cdot \frac{\$6.6\text{M}}{\$8.8\text{M}} = 0.75 \cdot S$$

4.2 Adjusting Concentration-Response relation

The EASIUR default estimates are based on a relative risk of 1.06 for the concentration response relation, which is reported by a recent American Cancer Society cohort study (Krewski et al., 2009). The relative risk is usually defined as increased mortality per each increase of 10 $\mu g\ PM_{2.5}/m^3$.

Though concentration-response relations have a log-linear form, marginal damages are almost linear to the size of relative risk. The base EASIUR estimates can be adjusted for a different relative risk (R) with the following factor, (F_R):

$$F_R = -15.1 + 15.2R \quad (2)$$

Derivation can be found in Section 4.3.7. For example, an adjusted EASIUR estimate can be obtained for a relative risk of 1.14 from Lepeule et al. (2012), the other important $PM_{2.5}$ epidemiological study, by multiplying the following factor to the base value:

$$F_R = -15.1 + 15.2 \cdot 1.14 = 2.2$$

5. Uncertainties

Here we summarize the major uncertainties surrounding EASIUR's marginal damages.

5.1 Air Quality Modeling

Multipliers to estimate the 95th prediction intervals of EASIUR estimates are presented in Table D-1. If you multiply 2.5% and 97.5% factors to EASIUR marginal damages, you would get the 95% prediction intervals of the damages, which represent the uncertainty originated from air quality simulations.

5.2 Value of a Statistical Life

There is one official distribution of the value of a statistical life that U.S. EPA built based on 26 value-of-life studies (U.S. EPA, 2010). It is a Weibull distribution (scale parameter $= 5.32\times10^6$, shape parameter $= 1.51$). Therefore, uncertainty analysis can be done with the Weibull distribution. The mean value of this distribution is \$4.8M in 1990 dollar. The 95% confidence intervals are [\$0.46M, \$12.6M] in 1990 USD.

5.3 Concentration-Response Relations

Epidemiological studies of $PM_{2.5}$ on mortality publish 95% confidence intervals for the relative risk of $PM_{2.5}$. The two most important series of cohort-based $PM_{2.5}$ epidemiological studies are the American Cancer Society (ACS) study and Harvard Six Cities (H6C) study. The most recent follow-up studies as of now are Krewski et al. (2009) for ACS and Lepeule et al. (2012) for H6C. Here are the reported relative risks with 95% confidence intervals in parentheses:

- Krewski et al. (2009): 1.06 (1.04-1.08)
- Lepeule et al. (2012): 1.14 (1.07-1.22)

Uncertainties from CR relations can be explored for these confidence intervals with Eq. (2).

References

Krewski, D., Jerrett, M., Burnett, R. T., Ma, R., Hughes, E., Shi, Y., Turner, M. C., Pope, C. A., III, Thurston, G., Calle, E. E., Thun, M. J., Beckerman, B., DeLuca, P., Finkelstein, N., Ito, K., Moore, D. K., Newbold, K. B., Ramsay, T., Ross, Z., Shin, H. and Tempalski, B.: Extended follow-up and spatial analysis of the American Cancer Society study linking particulate air pollution and mortality, Health Effects Institute, Boston, MA., 2009.

Lepeule, J., Laden, F., Dockery, D. and Schwartz, J.: Chronic Exposure to Fine Particles and Mortality: An Extended Follow-up of the Harvard Six Cities Study from 1974 to 2009, Environ. Health Perspect., 120(7), 965–970, doi:10.1289/ehp.1104660, 2012.

U.S. EPA: Guidelines for Preparing Economic Analyses, National Center for Environmental Economics, Office of Policy, U.S. Environmental Protection Agency., 2010.

Table D-1: Multipliers for EASIUR 95% prediction intervals.

	Winter		Spring		Summer		Fall	
	2.5%	97.5%	2.5%	97.5%	2.5%	97.5%	2.5%	97.5%
EC	0.61	1.64	0.67	1.49	0.67	1.49	0.60	1.68
SO_2	0.53	1.90	0.73	1.38	0.69	1.44	0.67	1.50
NO_x	0.45	2.23	0.57	1.77	0.35	2.86	0.41	2.42
NH_3	0.56	1.79	0.57	1.75	0.46	2.19	0.54	1.84

Table D-2: U.S. EPA standard GDP deflator and income growth adjustment factors (extracted from BenMAP (U.S. EPA, 2014))

Year	GDP Deflator	Income Growth Adj.
1980	0.479	-
1981	0.528	-
1982	0.560	-
1983	0.578	-
1984	0.603	-
1985	0.625	-
1986	0.636	-
1987	0.660	-
1988	0.687	-
1989	0.720	-
1990	0.759	1.000
1991	0.791	0.992
1992	0.815	0.998
1993	0.839	1.003
1994	0.861	1.013
1995	0.885	1.017
1996	0.911	1.024
1997	0.932	1.034
1998	0.947	1.039
1999	0.967	1.043
2000	1.000	1.039
2001	1.028	1.044
2002	1.045	1.050
2003	1.069	1.056
2004	1.097	1.063
2005	1.134	1.069
2006	1.171	1.075
2007	1.204	1.081
2008	1.250	1.087
2009	1.246	1.093
2010	1.266	1.100
2011	-	1.112
2012	-	1.123
2013	-	1.134
2014	-	1.144
2015	-	1.155
2016	-	1.164
2017	-	1.174
2018	-	1.183
2019	-	1.192
2020	-	1.201
2021	-	1.209
2022	-	1.217
2023	-	1.225
2024	-	1.233

Chapter 5. Conclusions

5.1 Summary of Work

The main theme of this thesis is air quality and its impact on public health. This work is focused on the use of rigorous state-of-the-science tools to characterize the potential risk of an emerging technology and to develop a general method of employing a complex up-to-date air quality modeling platform without high computational costs. The key results and conclusions from each chapter are summarized in the following.

First, I explored the potential air quality risk of a post-combustion carbon capture and storage (CCS) technology from a public health point of view with a state-of-the-science chemical transport model (Chapter 2). It was found that amine scrubbing, the most mature post-combustion technology (IPCC, 2005; Rochelle, 2009), could emit a substantial amount of ammonia under an aggressive deployment scenario. Using CAMx, a state-of-the-science chemical transport model, I found that ammonia emissions from CCS could increase a $PM_{2.5}$ to a worrisome level, imposing significant public health costs ($31-68/t CO_2) — comparable to the social cost of mitigating carbon dioxide considered in government regulatory agencies (U.S. IAWG, 2010, 2013). Sensitivity analyses addressed the uncertainty, most importantly, surrounding the amount of CCS ammonia emissions as well as the amount of co-pollutants (SO_2, NO_x, and NH_3) that may interact with CCS ammonia in a complicated nonlinear manner. The findings could guide the potential air quality risk of CCS ammonia for a wide range of possible future scenarios. Though ammonia is highly soluble in water and, therefore, not difficult to control, this requires the increase of capital and operation costs in CCS plants. The impact

assessment performed in Chapter 2 therefore provides quantitative regulatory guidance for what level of control is appropriate.

In Chapter 3, I developed a new method called the Estimating Air pollution Social Impacts Using Regression (EASIUR). Though a chemical transport model is the most realistic and rigorous way of simulating air quality, running a CTM comes at the cost of high computational burden. As computer systems get faster and more affordable, a CTM has been getting more popular in assisting air quality policy research as well as in understanding atmospheric science in recent years. But running a CTM requires expensive computational costs as well as expertise in sophisticated computer systems and advanced atmospheric science. Therefore, many policy researchers cannot afford to employ a CTM. Even U.S. EPA runs a CTM only for limited policy scenarios for their regulatory impact assessments.

The EASIUR method that I developed can derive simple equations to predict the public health impacts of air quality with the prediction performance of a state-of-the-science CTM but without high computational burdens. The basic idea of the EASIUR method is to derive parameterizations from CTM simulation results. The method describes the size of the population exposed to $PM_{2.5}$, which is directly emitted or chemically produced in the atmosphere, using 'population ring' and 'average plume' methods. The 'population ring' method defines exposed population as the size of population within a certain distance from an emissions source while the 'average plume' method uses a generic plume shape built from CTM results to weight people in large receptor areas around an emissions source. Because of the more detailed nature, the average plume method worked better, though both methods worked quite well. The EASIUR parameterizations derive from running linear regressions on per-tonne social cost or intake fraction, with population described by either 'population ring' or 'average plume' methods, and

common atmospheric variables such as temperature, atmospheric pressure, precipitation, wind speed, and humidity. For a limited simulation period and two air pollutants for method development, it was shown that the parameterizations could tremendously reduce the computational burden of running a CTM while estimating the public health impacts very similarly to a CTM.

Finally, using the method developed in Chapter 3, I built a set of parameterizations that predict per-tonne social cost and intake fraction quickly but accurately. They can predict the public health impacts anywhere in the United States (including nearby areas in the oceans and neighboring countries, Canada and Mexico) at a high spatial resolution (36 km×36 km) for every season for four major air pollutants: elemental carbon, sulfur dioxide, nitrogen oxides, and ammonia. They have simple intuitive functional forms, from which model users can gain useful insight on underlying key mechanisms. They are also generalized for different choices of concentration-response relation that epidemiological studies provide, as well as for different choices of the value of statistical life that economists estimate for people's willingness to pay to avoid the risk of premature death. The EASIUR models will be of great use to policy research that involves changes in emissions.

In sum, this work provides a useful guideline for the appropriate level of control on CCS ammonia emissions from a public health point of view. The development of the EASIUR method will provide a novel way of deriving simple and easy-to-use parameterizations from the most realistic but computationally expensive simulation model for air quality. The EASIUR parameterizations built for the United States domain will be of great use to policy research.

5.2 Future work

An important part of the development of the EASIUR parameterizations is done in this work. However, there are the important areas to investigate for further improvements. A few directions for future work are proposed here.

One important missing part in the EASIUR parameterizations is organic $PM_{2.5}$, the science of which is much more complicated than inorganic $PM_{2.5}$. Despite the complexity, the understanding of organic $PM_{2.5}$ has progressed substantially in recent years, making traditional views obsolete (Goldstein and Galbally, 2007; Robinson et al., 2007; Zhang et al., 2007). The main reason we did not develop the EASIUR parameterizations for organic $PM_{2.5}$ was that even the best chemical transport models are not ready for parameterizations. In particular, though a new method of describing the complex organic $PM_{2.5}$ systematically in a manageable manner is developed (Donahue et al., 2006, 2011, 2012) and implemented in CTMs (Koo et al., 2014; Murphy and Pandis, 2009), the emissions inventory still needs to be revised properly to address organic $PM_{2.5}$ properly (Jathar et al., 2014). Once CTMs are ready to fully address organic $PM_{2.5}$, at least consistent with current understanding, the EASIUR parameterization could be derived in the same manner done for inorganic species in this work. Developing the EASIUR parameterizations for organic $PM_{2.5}$ will be especially important for the transportation sector, which is the most important emissions source of organic $PM_{2.5}$ precursors.

There are important sources of uncertainty that need to be addressed. One is the inter-annual variability of meteorology. It is still not clear how the per-ton social cost and intake fraction might change for different years. Though this may be small, the manner in which inter-annual variability affects public health impacts should be investigated by analyzing sensitivity to meteorological data for multiple years. Probably sensitivity analysis for inter-annual

meteorology would provide the insight for "representative meteorology" for public health impacts as well as the uncertainty and variability from meteorological data.

Changing emissions is also a concern. In particular, the emissions of sulfur dioxide and nitrogen oxides have been decreasing substantially in recent years and are expected to decrease further in the future (Pinder et al., 2008; U.S. EPA, 2011). Considering the complex interaction between inorganic species (SO_2, NO_x, and NH_3), the changing future emissions will have an impact on associated public health effects. For example, if SO_2 emissions are substantially reduced in the future, the social costs of NO_x and NH_3 will increase because they will form more ammonium nitrate $PM_{2.5}$. Therefore, the sensitivity over different emissions environments of inorganic species needs to be investigated.

Last but not least, one potential merit of the EAISUR method is the possibility that it could be ported to outside of the United States. It would be possible to build the EASIUR parameterizations by running a CTM for a domain of interest anywhere in the world. However, it relies on a CTM, which requires detailed emissions inventory to simulate air quality. Especially in many non-western parts of the world, such information will not always be available, rendering the derivation of the EASIUR parameterization impossible. However, the EASIUR models could be further abstracted not including factors currently tuned to the United States domain so that the parameterizations can be applied reasonably to other places. For example, EC parameterizations would work decently only with temperature and population. Considering the inert nature of elemental carbon, the EC average plume derived from the U.S. domain may work well to describe the exposed population in other parts of the world. Probably, building the EASIUR models for other domains where a CTM can be run, for example, the European Union domain, and comparing them with the U.S. ones will provide an useful insight

for the abstraction. A strategy for the mitigation of global climate change may require maximizing co-benefits from improving air quality (IPCC, 2014). The EASIUR model may help with quantifying the co-benefits of improving air quality and designing optimal policy not only in the U.S. but also in many parts of the world, especially where information is lacking.

5.3 References

Donahue, N. M., Epstein, S. A., Pandis, S. N. and Robinson, A. L.: A two-dimensional volatility basis set: 1. organic-aerosol mixing thermodynamics, Atmos Chem Phys, 11(7), 3303–3318, 2011.

Donahue, N. M., Kroll, J. H., Pandis, S. N. and Robinson, A. L.: A two-dimensional volatility basis set–Part 2: Diagnostics of organic-aerosol evolution, [online] Available from: http://dspace.mit.edu/handle/1721.1/71793 (Accessed 22 March 2013), 2012.

Donahue, N. M., Robinson, A. L., Stanier, C. O. and Pandis, S. N.: Coupled Partitioning, Dilution, and Chemical Aging of Semivolatile Organics, Environ. Sci. Technol., 40(8), 2635–2643, doi:10.1021/es052297c, 2006.

Goldstein, A. H. and Galbally, I. E.: Known and Unexplored Organic Constituents in the Earth's Atmosphere, Environ. Sci. Technol., 41(5), 1514–1521, doi:10.1021/es072476p, 2007.

IPCC: IPCC Special Report on Carbon Dioxide Capture and Storage. Prepared by Working Group III of the Intergovernmental Panel on Climate Change., edited by B. Metz, O. Davidson, H. C. de Coninck, M. Loos, and L. A. Meyer, Cambridge University Press, Cambridge, UK and New York, NY, USA., 2005.

IPCC: Climate Change 2014, Mitigation of Climate Change. Contribution of Working Group III to the Fifth Assessment Report of the Intergovernmental Panel on Climate Change, Cambridge University Press, Cambridge, United Kingdom and New York, NY, USA., 2014.

Jathar, S. H., Gordon, T. D., Hennigan, C. J., Pye, H. O. T., Pouliot, G., Adams, P. J., Donahue, N. M. and Robinson, A. L.: Unspeciated organic emissions from combustion sources and their influence on the secondary organic aerosol budget in the United States, Proc. Natl. Acad. Sci., 201323740, doi:10.1073/pnas.1323740111, 2014.

Koo, B., Knipping, E. and Yarwood, G.: 1.5-Dimensional volatility basis set approach for modeling organic aerosol in CAMx and CMAQ, Atmos. Environ., 95, 158–164, doi:10.1016/j.atmosenv.2014.06.031, 2014.

Murphy, B. N. and Pandis, S. N.: Simulating the Formation of Semivolatile Primary and Secondary Organic Aerosol in a Regional Chemical Transport Model, Environ. Sci. Technol., 43(13), 4722–4728, doi:10.1021/es803168a, 2009.

Pinder, R. W., Gilliland, A. B. and Dennis, R. L.: Environmental impact of atmospheric NH3 emissions under present and future conditions in the eastern United States, Geophys. Res. Lett., 35(12), L12808, doi:10.1029/2008GL033732, 2008.

Robinson, A. L., Donahue, N. M., Shrivastava, M. K., Weitkamp, E. A., Sage, A. M., Grieshop, A. P., Lane, T. E., Pierce, J. R. and Pandis, S. N.: Rethinking Organic Aerosols: Semivolatile Emissions and Photochemical Aging, Science, 315(5816), 1259–1262, doi:10.1126/science.1133061, 2007.

Rochelle, G. T.: Amine Scrubbing for CO2 Capture, Science, 325(5948), 1652 –1654, doi:10.1126/science.1176731, 2009.

U.S. EPA: Regulatory Impact Analysis for the Federal Implementation Plans to Reduce Interstate Transport of Fine Particulate Matter and Ozone in 27 States; Correction of SIP Approvals for 22 States, U.S. Environmental Protection Agency, Office of Air and Radiation. [online] Available from: http://www.epa.gov/airtransport/pdfs/FinalRIA.pdf, 2011.

U.S. IAWG: Technical Support Document: Social Cost of Carbon for Regulatory Impact Analysis Under Executive Order 12866, Interagency Working Group on Social Cost of Carbon, United States Government, Washington, DC., 2010.

U.S. IAWG: Technical Support Document: Technical Update of the Social Cost of Carbon for Regulatory Impact Analysis - Under Executive Order 12866, Interagency Working Group on Social Cost of Carbon, United States Government, Washington, DC., 2013.

Zhang, Q., Jimenez, J. L., Canagaratna, M. R., Allan, J. D., Coe, H., Ulbrich, I., Alfarra, M. R., Takami, A., Middlebrook, A. M., Sun, Y. L., Dzepina, K., Dunlea, E., Docherty, K., DeCarlo, P. F., Salcedo, D., Onasch, T., Jayne, J. T., Miyoshi, T., Shimono, A., Hatakeyama, S., Takegawa, N., Kondo, Y., Schneider, J., Drewnick, F., Borrmann, S., Weimer, S., Demerjian, K., Williams, P., Bower, K., Bahreini, R., Cottrell, L., Griffin, R. J., Rautiainen, J., Sun, J. Y., Zhang, Y. M. and Worsnop, D. R.: Ubiquity and dominance of oxygenated species in organic aerosols in anthropogenically-influenced Northern Hemisphere midlatitudes, Geophys. Res. Lett., 34(13), L13801, doi:10.1029/2007GL029979, 2007.